Drained Residual Strength of Expansive Soils Causing Pavement Distress along Alabama Highway 5

by

Lydia Pauline Kennedy

A thesis submitted to the Graduate Faculty of
Auburn University
in partial fulfillment of the
requirements for the Degree of
Master of Science

Auburn, Alabama
December 14, 2019

Keywords: expansive clays, ring shear, drained residual strength

Approved by

J. Brian Anderson, Ph.D., P.E., Chair, Associate Professor of Civil Engineering
Jack Montgomery, Ph.D., Assistant Professor of Civil Engineering
David Timm, Ph.D, P.E., Brasfield & Gorrie Professor of Civil Engineering

ABSTRACT

A segment of Alabama Highway 5 (AL-5) located in Perry County, Alabama has been experiencing severe pavement distress that is mostly caused by the behavior of soil beneath the roadway. AL-5 is a farm-to-market road that was built directly on the subgrade which consists of expansive clays with no compacted base. Previous laboratory tests confirmed shrink-swell behavior in the soil with swell pressures of up to 1500 psf. Five remediation techniques were investigated on sections of AL-5 in an attempt to identify a method that would increase the span between resurfacing. These remediation techniques included a sand blanket, vertical moisture barriers, lime columns, paved shoulders, and edge drains. Sensors were installed to remotely monitor the subgrade and asphalt conditions for the duration of the project. To further characterize the subgrade behavior, torsional ring shear tests were completed to determine the drained residual strength of the soil. Specimens from each remediation section were consolidated and then subjected to torsional shear in the ring shear device to determine the shear strength of the subgrade soils which may have contributed to pavement distress.

Continuous monitoring of the pavement and subgrade instrumentation has shown improvement in the pavement distress over the past few years with the lime column test section as the most improved. The torsional ring shear tests resulted in very low angles of peak and residual resistance for the subgrade; therefore, the material was very weak and likely has contributed to the pavement distress. Slope stability analyses concluded the roadway embankments were stable at the end of construction, but quickly began to fail as the peak and residual shear strength values were reached.

ACKNOWLEDGEMENTS

I would like to thank Auburn University and Alabama Department of Transportation for their support on this research project during the previous few years. Also, thank you to my committee chair, Dr. J. Brian Anderson for his continued support and help. Dr. Jack Montgomery and Dr. David Timm have also been very influential, and I would like the thank them as well. I would like to thank the previous students who have also worked hard on this project including Dylan Jones, Elizabeth Stallings, Jeremy Herman, Dan Jackson, Pavlo Voitenko, Justin McLaughlin, Jonathan Hogan, Matt Barr, and Mengwei Xuan. I would like to thank Andy Weldon in the aerospace engineering machine shop for helping us modify the ring shear apparatus. I would also like to thank my friends and family for continuing to support me during my graduate studies.

TABLE OF CONTENTS

LIST OF TABLES

LIST OF FIGURES

LIST OF ABBREVIATIONS AND SYMBOLS

AADT	Average Annual Daily Traffic
AC	Asphalt Concrete
AL	Alabama
AL-5	Alabama Highway 5
ALDOT	Alabama Department of Transportation
a_m	Coefficient of Compressibility with Respect to Change in Matric Suction
ASGs	Asphalt Strain Gages
ASTM	American Society for Testing and Materials
a_t	Coefficient of Compressibility with Respect to Change in Net Normal Stress
b_m	Coefficient of Water Content Change with Respect to Change in matric Suction
b_t	Coefficient of Water Content Change with Respect to Change in Net Normal Stress
c'	Effective Cohesive Intercept
CO	Control
de	Incremental Change in Void Ratio
deg	Degrees
d_f	Estimated Shear Displacement at Failure
d_h	Shear Displacement Rate
d_r	Displacement Rate

dw	Incremental Change in Water Content (Gravimetric)
$d(u_a - u_w)$	Incremental Change in Matric Suction
e	Void Ratio
E_i	Normal Forces on Side of Slice
EC	Electrical Conductivity
ED	Edge Drains
F_1	Load on the Load Cell 1
F_2	Load on the Load Cell 2
FHWA	Federal Highway Administration
ft	Feet
GWC	Gravimetric Water Content
Hr	Hour
In	Inches
IRI	International Roughness Index
IWP	Inside Wheel Path
kg	Kilograms
kN	Kilonewtons
kPa	Kilopascals
L	Torque Arm Length
LC	Lime Columns
LL	Liquid Limit
Min	Minutes
mm	Millimeters

MP	Mile Point
MPa	Megapascals
M_o	Driving Moment
M_r	Resisting Moment
mS/m	Millisemens per Meter
N	Newton
N_i	Normal Effective Force on Slice
NCAT	National Center for Asphalt Technology
NOAA	National Oceanic and Atmospheric Administration
OWP	Outside Wheel Path
P	Normal Vertical Force Acting on the Specimen
Pcf	Pounds per Cubic Foot
PI	Plasticity Index
PS	Paved Shoulders
Psf	Pounds per Square Foot
R_1	Inner Specimen Radii
R_2	Outer Specimen Radii
R	Radius of Failure Arc
r	Radius of Curvature
S	Degree of Saturation
S_i	Shear Force on Side of Slice
SB	Sand Blankets
SWCC	Soil Water Characteristic Curve

t_{50}	Time Required for the Specimen to Achieve 50% Consolidation under the Maximum Normal Stress Increment
t_{90}	Time Required for the Specimen to Achieve 90% Consolidation under the Maximum Normal Stress Increment
t_e	Elapsed Time of Test
t_f	Total estimated elapsed time to failure
T_i	Shear Force on Bottom of Slice
T_s	Surface Tension
τ	Shear Strength
u_a	Pore Air Pressure
u_w	Pore Water Pressure
$(u_a - u_w)$	Matric Suction
U_i	Water Pressure Force for Vertical Slice
UIUC	University of Illinois At Urbana-Champaign
USCS	Unified Soil Classification System
USDA	United States Department of Agriculture
VB	Vertical Barriers
VMC	Volumetric Moisture Content
w	Gravimetric Water Content
W_i	Weight of Slice
α_i	Inclination of Slice Failure Plane
^{o}	Degree
ΔL_i	Length of Slice Failure Plane

Δx_i	Width of Slice
φ'	Effective Angle of internal Friction
π	Osmotic Suction
ρ_d	Dry Density
ρ_w	Density of Water
σ'	Effective Normal Stress
σ	Total Normal Stress
$\sigma' n$	Normal Stress
σ_{mean}	Average Normal Stress
$(\sigma - u_a)$	Net Normal Stress
$\surd$	Square Root
ψ	Total Suction

CHAPTER 1: INTRODUCTION

1.1 Background

Roadways in many parts of the United States and around the world experience pavement distress due to expansive clays. Expansive clays undergo large volume changes primarily occurring due to fluctuating moisture contents attributable to seasonal changes in precipitation. In the United States, damage from expansive clays has exceeded $10 billion in 1984, likely closer to $25 billion today, with half of the damages involving highways, streets, and roadways. (Steinberg 1985).

Alabama Highway 5 (AL-5) is a heavy traffic roadway connecting Mobile to Birmingham in Alabama. AL-5 is a farm-to-market road and it was constructed by pavement directly on the subgrade with little or no aggregate base. In the segment studied in this research project, the subgrade consists of expansive clay that has caused significant pavement distress over many years. The distress includes large patches, rutting, and longitudinal cracks located along the majority of the roadway as shown in Figure 1 and Figure 2. In order to maintain safe roadway conditions, patching, levelling, and resurfacing is needed often on AL-5 and similar roads over expansive clay, which has been very expensive for the state of Alabama.

Figure 1: Distress Pavement at AL-5 (Herman 2015)

Figure 2: Longitudinal Cracking along AL-5 (Herman 2015)

The Alabama Department of Transportation (ALDOT) sponsored research project that this thesis contributes to consists of a four-mile segment of AL-5 located in Perry County, Alabama. Several remediation techniques were implemented along a four-mile length section of AL-5 to identify designs that could extend the life of the pavement. Instruments were installed into the subgrade and pavement to monitor the changes of the soil conditions and pavement

distress over an extended period of time to evaluate the performance of each remediation technique.

Field observations have concluded possible slope stability problems on the roadway embankments. These slope failures at AL-5 could have occurred due to the drained fully soften strength of the clays.

1.2 Objective

The primary objective of this investigation was to determine the drained residual shear strength of the subgrade and the impact of the shear strength on the stability of AL-5 embankments. A secondary objective was to continue monitoring the test section instrumentation and report the observations and conclusions of the performance of the test sections.

1.3 Scope

Eighteen ring shear tests were performed using the Bromhead Ring Shear Device (Bromhead 1979). The results of the tests were used to develop failure envelopes to determine the drained residual shear strength of the clay. The results were used on slope stability calculations to investigate the impact of the clay strength on the performance of the embankments sections of AL-5. Periodic data collection was conducted on AL-5 sensors along with quarterly IRI tests completed by The National Center of Asphalt Technology (NCAT). Data collection occurred remotely and through site visits. Data was reduced and plotted to observe potential trends in each section.

CHAPTER 2: BACKGROUND AND LITERATURE REVIEW

Shrink-swell behavior of soils is generally related to fluctuations in water content in soils and minerology. Therefore, saturated and unsaturated soil mechanics principles should be reviewed along with the minerology of expansive clays.

2.1 Saturated Soils

Saturated soil is known as a two-phase system consisting of water and soil particles. This system allows soil to be completely saturated meaning no air in the voids. If the material is below the water table, then the soil is most likely fully saturated. However, if the soil is located above the water table, the material will generally be in an unsaturated state.

2.2 Unsaturated Soils

Unsaturated soil is generally known to be a three-phase system consisting of air, water, and soil particles. This system allows soil to be completely dry meaning no water in the voids. This assumption is rarely found in the field; therefore, soil is normally in an unsaturated state located somewhere in between being completely dry or completely saturated.

2.2.1 Soil as a Four Phase System

Instead of characterizing soil as a three-phase system, unsaturated soil can be considered a four-phase system for stress analysis. The fourth phase consists of the air-water interface also known as the *contractile skin* (Fredlund and Morgenstern 1977). There can be changes in the stress state of the contractile skin resulting in changes in water content, volume, or shear strength (Fredlund et al. 2012). Figure 3 shows an unsaturated element of soil with the four phases labeled.

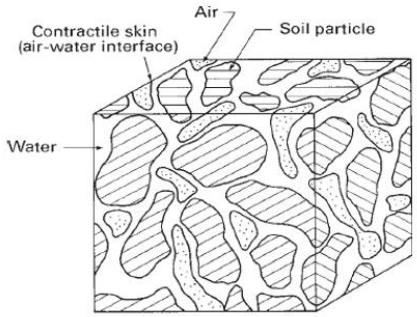

Figure 3: Unsaturated Soil Element with Four Phases Labeled (Fredlund et al. 2012)

Figure 4 shows the free body diagram for the contractile skin. The air pressure is greater than the water pressure in the unsaturated soil; therefore, the contractile skin will show a concave curvature towards the air pressure and tension will be applied to the contractile skin in order to maintain equilibrium (Fredlund et al. 2012). Using Figure 4, an equilibrium equation is computed and is given by Equation 1 (Nelson and Miller 1992). Equation 1 is known as Kelvin's capillary model in which the surface tension of the contractile skin varies with temperature (Fredlund and Rahardjo 1993). The matric suction can be defined as the pressure difference $u_a - u_w$ in Equation 1. The matric suction and radius of curvature are inversely related because when the matric suction increases, the radius of curvature of the contractile skin decreases.

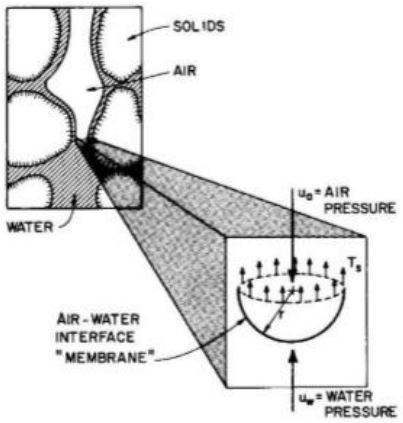

Figure 4: Free Body Diagram of Contractile Skin (Nelson and Miller 1992)

$$u_a - u_w = \frac{2T_s}{r} \qquad \text{Equation 1}$$

Where u_a = air pressure

u_w = water pressure

T_s = surface tension

r = radius of curvature

2.2.2 States of Stress for Unsaturated Soils

The state of stress must be considered when characterizing the behavior of a given soil. A state variable is a "non-material variable required for the characterization of a system" (Fredlund and Rahardjo 1993). A state variable can be a stress state variable or a deformation state variable. A stress state variable characterizes stress equilibrium conditions; whereas, a deformation state variable characterizes deviations from an initial state. A relationship between different state variables generate unique empirical mathematical relationships called *constitutive relations* (Fredlund and Rahardjo 1993).

The soil behavior of saturated soils can be described by the state of the effective stress on the soil shown in Equation 2. Changes in volume and shear strength are governed by the changes in effective stress (Fredlund et al. 2012).

$$\sigma' = \sigma - u_w \qquad \text{Equation 2}$$

Where σ' = effective normal stress

σ = total normal stress

u_w = pore water pressure

Adding the fourth phase for an unsaturated soil increases the complexity for describing the behavior of the soil. An effective stress concept like the one used for saturated soil was created for unsaturated soil; however, it is much more difficult (Fredlund and Rahardjo 1993). Efforts were made to produce a single effective stress relationship for unsaturated soils (Croney et al. 1958, Bishop 1959, Aitchison 1961, Jennings 1961), but all the relationships incorporate soil properties; therefore, the relationships are considered to be constitutive rather than stress state descriptions (Fredlund and Rahardjo 1993).

An idea using two independent stress state variables to describe an unsaturated soil was proposed by Fredlund and Morgenstern (1977). They based their analysis on multi-phase continuum mechanics and included the fourth phase for unsaturated soils (Fredlund and Rahardjo 1993). Three stress state variables were generated, but the most common ones used are the net normal stress $(\sigma - u_a)$ and the matric suction $(u_a - u_w)$. These stress state variables were experimentally tested (Fredlund 1973) and are commonly accepted and used (Fredlund et al. 2012). This is important because it describes the volume change responsible for the shrink-swell behavior beneath pavements.

To define the volume change of unsaturated soils, there are three common deformation state variables that are widely used. These deformation state variables include void ratio (e), gravimetric water content (w), and degree of saturation (S). There are other deformation state

variables possible if continuum mechanics notation is used (Fredlund et al. 2012). When combined with the stress state variables in mentioned above, two constitutive relationships are created and are shown in Equation 3 and Equation 4 .

$$de = a_t d(\sigma_{mean} - u_a) + a_m d(u_a - u_w) \quad \text{Equation 3}$$

$$dw = b_t d(\sigma_{mean} - u_a) + b_m d(u_a - u_w) \quad \text{Equation 4}$$

where de = incremental change in void ratio

dw = incremental change in water content (gravimetric)

`$d(\sigma_{mean} - u_a)$ = incremental change in net normal stress

$d(u_a - u_w)$ = incremental change in matric suction

a_t= coefficient of compressibility with respect to change in net normal stress

a_m = coefficient of compressibility with respect to change in matric suction

b_t = coefficient of water content change with respect to change in net normal stress

b_m= coefficient of water content change with respect to change in matric suction

$$\sigma_{mean} = \frac{\sigma_1 + \sigma_2 + \sigma_3}{3}$$

u_a = pore air pressure

u_w = pore water pressure

Since volume change uses two stress state variables, the plot of Equation 3 and Equation 4 must take the form of a three dimensional shape. Figure 5 shows an example of the three-dimensional shape for the void ratio and water content. As shown in Figure 5, the void ratio and water content are affected by a change in net normal stress and matric suction. It is a good assumption to assume the net normal stress will remain constant for an existing structure or underneath the pavement; therefore, volume change is solely controlled by the changes in matric suction.

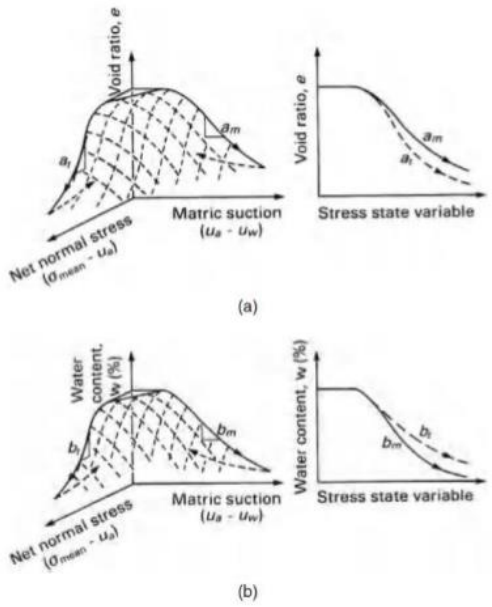

Figure 5: Constitutive Surfaces for an Unsaturated Soil: (a) Void Ratio Constitutive Surface; (b) Water Content Constitutive Surface (Fredlund et al. 2012)

2.3 Minerology

Montmorillonite is a very common and important mineral found in clays. Montmorillonite crystals can be very small in size, but the crystals have a strong attraction for water. Shrink-swell potential of soils containing montmorillonite is very high. Swelling pressures

develop and have caused damage to structures and pavements (Holtz et al. 2011). Holtz et al. (2011) suggest using Atterberg limits to classify active clay minerology. Clays containing montmorillonite generally plot near the U-line on Casagrande's plasticity chart shown in Figure 6.

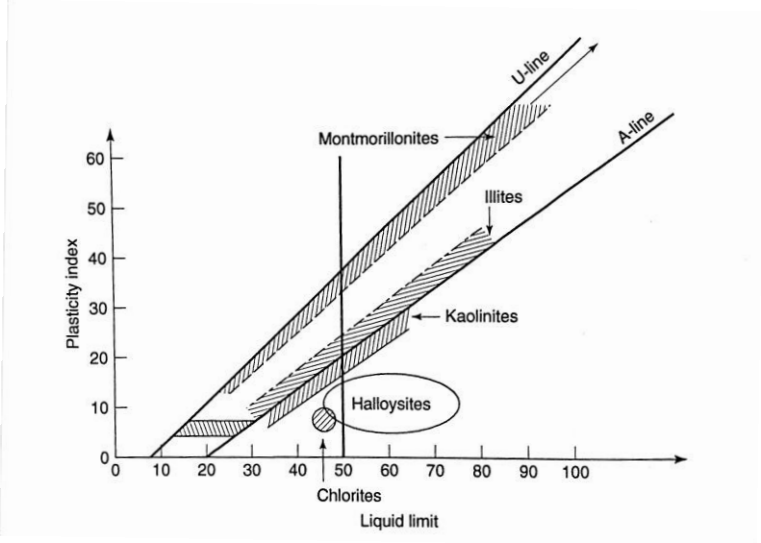

Figure 6: Location of Common Clay minerals on Casagrande's plasticity chart (developed from Casagrande, 1948, and data in Mitchell and Soga, 2005) (Holtz et al. 2011)

Specific surface is an important concept in soil minerology. Specific surface is the surface area of the soil divided by the unit volume. Therefore, the specific surface of a soil is inversely proportional to its grain size. Clay, made up of small soil particles, will have a larger specific surface than the same amount of coarse-grained soil (Holtz et al. 2011).

Water naturally is attracted to clay particles because of the polar nature of water. A water molecule is electrostatically attracted to the surface of a clay crystal because of a positive and negative separate center of charge for each molecule. Hydrogen bonding creates the bond between the water and clay particle. Hydrogen bonding occurs when the hydrogen atom of the

water is attracted to the oxygen atoms on the surface of the clay. The cations in a water molecule can contribute to the hydration of clay minerals since the surface of a clay is negatively charged (Holtz et al. 2011). The cation in the water molecules are generally more concentrated near the surface of the clay crystals. The cations thermally diffuse away from the clay surfaces in order to achieve equilibrium on the surface of the clay. However, the diffusion is counterbalanced by the electrical attraction the cation has to the negatively charged surface of the clay which creates the diffuse double layer (Holtz et al. 2011).

2.4 Soil Suction

2.4.1 Soil Suction Components

As explained above, volume change in expansive soils is primarily caused by a change in matric suction. Another type of soil suction includes *osmotic suction* which is commonly found in soils. Osmotic suction is caused by the presence of salts and cations as they dissolve in the pore water of the soil. Osmotic suction is fairly constant and is not considered in this investigation because the ground and pore water are assumed to be homogenous. In soils with very low water contents, osmotic suction can affect the soil and Equation 5 should be used. Equation 5 shows the relationship between matric and osmotic suction to create total suction.

$$\psi = (u_a - u_w) + \pi \qquad \text{Equation 5}$$

where ψ = total suction

$(u_a - u_w)$ = matric suction

π = osmotic suction

2.4.2 Active Zone

As mentioned previously, the water content; therefore, the soil suction, is a primary cause of the shrink-swell behavior of expansive unsaturated clays. In the upper few meters of soil, the water content fluctuates because of environmental factors. These environmental factors include vegetation and trees along with rainfall and temperature changes. The upper few meters of soil which experience seasonal suction changes is called the *active zone* (Nelson and Miller 1992). Figure 7 illustrates the active zone for a ground profile.

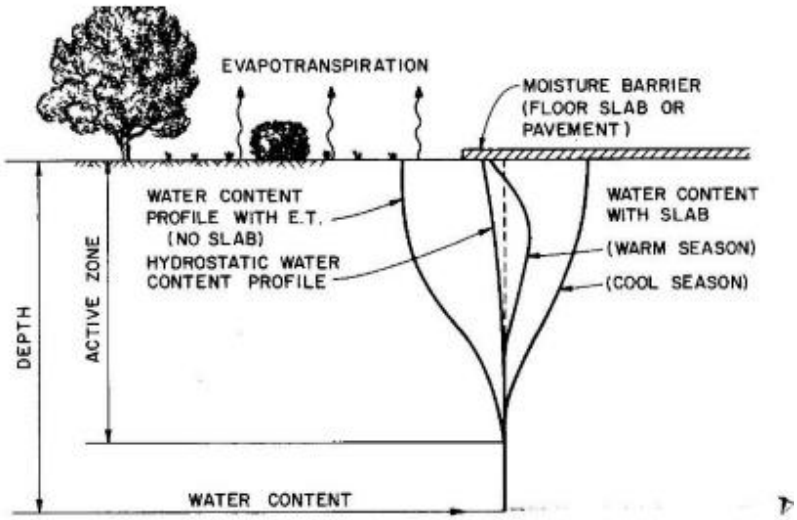

Figure 7: Water Content Profiles in the Active Zone (Nelson and Miller 1992)

2.5 Shear Strength

2.5.1 Mohr-Coulomb Failure Criterion

For saturated soil, the Mohr-Coulomb failure criterion can be used to calculate the shear strength of a given soil specimen using Terzaghi's effective stress equation shown in Equation 2. Equation 6 shows the Mohr-Coulomb failure criterion.

$$\tau = c' + \sigma' tan\varphi' \qquad \text{Equation 6}$$

where τ = shear strength

c'= effective cohesive intercept

σ'= effective normal stress

φ' = effective angle of internal friction

The slope of the failure envelope is the effective angle of internal friction and the y-intercept is the effective cohesion of the soil. For most non-cemented soils, the effective cohesion is zero. Figure 8 shows a general Mohr-Coulomb failure criterion for a saturated soil.

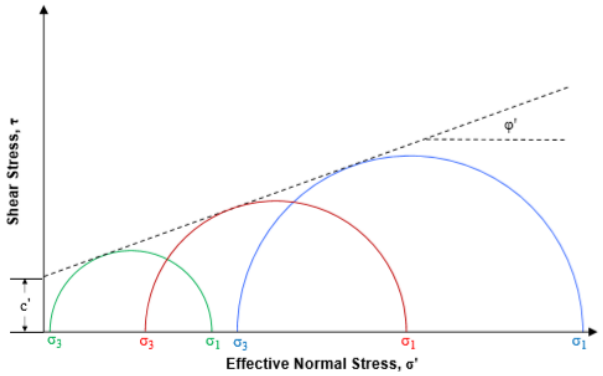

Figure 8: Mohr-Coulomb Failure Criterion for Saturated Soil (Burrage 2016)

2.5.2 Typical and Correlated Values for Soil and Asphalt Concrete

Lambe and Whitman (1969) provide typical values for the drained shear strength of soil based on the Atterberg limits using data by Kenney (1959). Figure 9 shows the correlation

between sin of the peak friction angle and the plasticity index for normally consolidated soils. As the plasticity index increases, the drained shear strength decreases. Table 1 shows the summary of friction angle data from Lambe and Whitman (1969) for preliminary design depending on soil type.

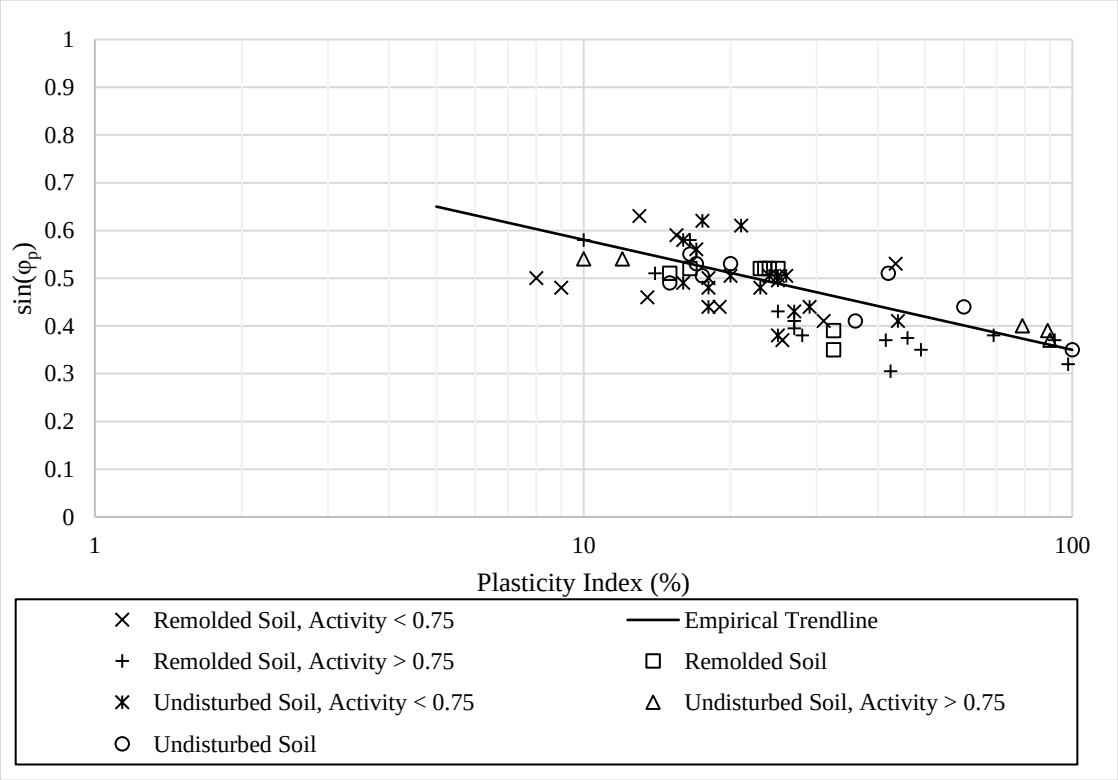

Figure 9: Relationship between sin ϕ_p and plasticity index for normally consolidated soils (After Lambe and Whitman 1969, Kenney 1959)

Table 1: Summary of Friction Angle Data for Use in Preliminary Design (Lambe and Whitman 1969)

	Friction Angles							
	Slope Angle of Repose		At Ultimate Strength		At Peak Strength			
					Medium Dense		Dense	
Classification	$i(^\circ)$	Slope (vert. to hor.)	$\phi_{cv}(^\circ)$	$\tan \phi_{cv}$	$\phi(^\circ)$	$\tan \phi$	$\phi(^\circ)$	$\tan \phi$
Silt (nonplastic)	26	1 on 2	26	0.488	28	0.532	30	0.577
	to		to		to		to	
	30	1 on 1.75	30	0.577	32	0.625	34	0.675
Uniform fine to medium sand	26	1 on 2	26	0.488	30	0.577	32	0.675
	to		to		to		to	
	30	1 on 1.75	30	0.577	34	0.675	36	0.726
Well-graded sand	30	1 on 1.75	30	0.577	34	0.675	38	0.839
	to		to		to		to	
	34	1 on 1.50	34	0.675	40	0.839	46	1.030
Sand and gravel	32	1 on 1.60	32	0.625	36	0.726	40	0.900
	to		to		to		to	
	36	1 on 1.40	36	0.726	42	0.900	48	1.110

Mitchell and Soga (2005) plotted residual friction angles as a function of effective normal stress raised to the minus one third power. This plot is shown in Figure 10 using data from Chattopadhyay (1972). In this figure, the residual friction angles are not affected when the normal stress is less than roughly 200 kPa. However, at higher stresses, the friction angle is independent of the stress and increases with larger stress values.

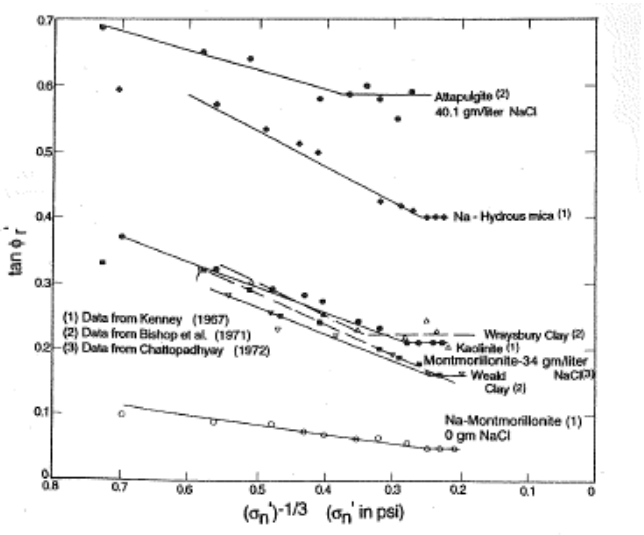

Figure 10: Residual Friction Angle versus Effective Normal Stress Raised to the Minus One Third Power (Data from Chattopadhyay 1972) (Mitchel and Soga 2005)

The EPRI Manual uses several methods to estimate the undrained shear strength of a clay by correlating the strength to the plasticity index based on vane shear tests. These correlations provided in Figure 11 show an approximation of the undrained shear strength.

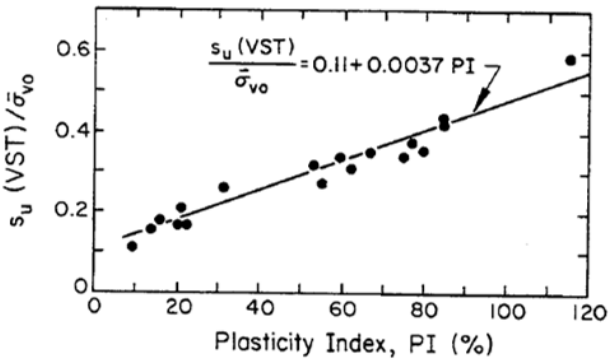

Figure 11: Undrained Shear Strength Ratio versus Plasticity Index based on Vane Shear Tests (Kulhawy and Mayne 1990)

A case study completed by Pennsylvania State University evaluated triaxial strength tests of asphalt concrete mixtures to better understand rut resistance. The Mohr-Coulomb criteria was used to determine the cohesion and internal angle of friction for the different types of asphalt concrete tested (Christensen et al. 2000). Table 2 shows the values of the cohesion and internal angle of friction for the different asphalt concrete mixes.

Table 2: c- and ϕ- Values from Triaxial Testing on Asphalt Concrete (Christensen et al. 2000)

Mixture	c (kPa)	ϕ (degrees)
ID2/AC20	664	39.8
ID3/AC20	685	34.1
ID2/SB	814	39.3
ID3/SB	838	36.3
ID3/AC20/MF+	665	36.8
ID3/AC20/MF++	537	41.8
NY76	369	41.4
NY96	480	42.5
NY109	471	36.7

Mixture	c (kPa)	ϕ (degrees)
NY126	534	38.1

2.5.3 Effect of Swelling on Clay Strength

Case studies have proven that when a clay swells, the shear strength is negatively affected; therefore, the shear strength is variable depending on the swell potential of the material. Sixty triaxial tests were performed on expansive shale which was classified as a fat clay by the Unified Soil Classification System (USCS) (Al-Mhaidib and Al-Shamrani 2006). The samples consisted of material 100% passing the No. 40 sieve and were remolded to form uniform remolded specimens at a predetermined water content (Al-Mhaidib and Al-Shamrani, 2006). The specimens were consolidated for approximately 24 hours under an isotropic confining pressure. After 24 hours had passed, water was introduced to the specimen and allowed to swell. The specimens could swell to 0%, 25%, 50%, 75%, and 100% of the ultimate vertical swell. When the predetermined percent swell value was achieved, the specimen was sheared to calculate the shear strength of the soil. The results were calculated in terms of the *shear ratio* which is the ratio of the shear strength of the swelled specimen and the non-swelled specimen (Al-Mhaidib and Al-Shamrani 2006), as shown in Equation 7.

$$Shear\ Ratio = \frac{Shear\ Strength\ of\ swelled\ specimen}{Shear\ Strength\ of\ non-swelled\ specimen} \qquad \text{Equation 7}$$

Table 3 expresses the shear ratio values calculated for each of the swelled triaxial tests completed. The data agrees with the conclusion that the swelling of expansive clays has a large negative impact on the shear strength of the soil. Much of the shear strength was not present

when the specimen could swell to the ultimate vertical swell value. As shown in Table 3, as the percentage in vertical swell increased for each specimen, the shear ratio rapidly decreased. As the shear ratio approaches zero, the strength of the swelled specimen is also approaching zero as the strength of the non-swelled specimen remains constant for each specimen.

Table 3: Calculated Values for Shear Ratio for all Tested Specimens (Al-Mhaidib and Al-Shamrani 2006)

		% Vertical Swell Before Shearing			
Initial Water Content (%)	Confining Pressure (kPa)	25	50	75	100
14	25	0.32	0.09	0.07	0.04
	50	0.33	0.17	0.09	0.06
	100	0.35	0.20	0.15	0.08
	150	0.37	0.20	0.15	0.07
	Average	0.34	0.17	0.12	0.05
18	25	0.26	0.11	0.08	0.05
	50	0.26	0.16	0.11	0.08
	100	0.28	0.20	0.17	0.10
	150	0.33	0.22	0.18	0.11
	Average	0.28	0.17	0.14	0.09
22	25	0.36	0.27	0.18	0.11
	50	0.37	0.3	0.22	0.14
	100	0.39	0.32	0.27	0.20
	150	0.44	0.35	0.30	0.22
	Average	0.39	0.31	0.24	0.17
Average		0.34	0.22	0.16	0.11

2.6 Torsional Ring Shear Device

The torsional ring shear device tests specimens under drained conditions to determine the residual shear strength of cohesive soils. The remolded specimen is consolidated and sheared at a predetermined water content. Generally, three phases of testing are conducted with three different normal stress levels.

2.6.1 Bromhead Ring Shear Test Procedure

In a paper by Stark and Vettel (1992), four different test procedures were applied to soil specimens in a Bromhead Ring Shear Device (Bromhead 1979) to illustrate the effect the procedure has on the measured shear strength. The specimen is confined radially; therefore, wall friction is introduced to the inner and outer circumferences of the specimen from the top porous stone. The main concern for measuring the residual strength is the magnitude of wall friction that is developed. The further the top porous stone settles into the specimen, the more wall friction; therefore, a higher residual strength will be measured. Currently, there are four test procedures used to measure the drained residual strength including single stage, preshearing, multistage, and the "flush" procedure (Stark and Vettel 1992).

The single stage test procedure includes loading the remolded specimen to the desired normal stress and then shearing the specimen. The preshearing procedure includes preshearing the specimen prior to shearing at a rapid displacement rate of approximately 25 degrees per minute. The rapid displacement rate generally allows the specimen to rotate up to five revolutions. The multistage procedure reduces test duration by allowing all stages of testing to be performed on one specimen. The "flush" procedure ensures the top porous stone remains near or flush with the surface of the specimen container. Only one test is performed for each specimen (Stark and Vettel 1992).

Ring shear tests were performed on remolded Pierre shale material classified as a clay of high plasticity according to USCS. Each testing procedure was tested to determine the residual shear strength. Figure 12 shows the effects of the testing procedure on measured residual strength of the material.

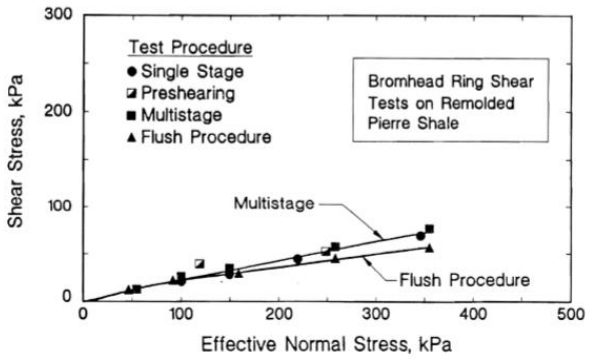

Figure 12: Effect of Test Procedure on Measured Residual Strength of Pierre Shale (Stark and Vettel 1992)

Based on the results of the study shown in Figure 12, the flush procedure resulted in the lowest residual strength since the wall friction was minimized. A sensitivity study was completed to determine how much settlement the top porous stone could move before the wall friction started effecting the residual strength. It was determined the specimen could endure a total settlement of 0.75 mm or 15% of the initial height during consolidation and shearing and still produce reasonable strength values. If the top porous stone settles more than 0.75 mm or 15% of the initial height, the addition of soil and reconsolidation of the specimen is required (Stark and Vettel 1992). Therefore, the recommended test procedure used in this investigation is the "flush" procedure.

2.6.2 Porous Stones

The specimen setup for a ring shear test includes two porous stones with the soil specimen in between the porous stones confined by the specimen container. The specimen and porous stone interface is important as the porous stone should not slide across the surface of the soil. A discussion by Stark (2016) criticizes research work from other researchers using the ring shear device specifically referencing the porous stones. Stark criticizes the work by (Castellanos

et al. 2016) where their paper claims the torsional ring shear device "results in very conservative fully softened shear strength envelopes." It has been determined that the conservative strength values are a result of the upper porous stone sliding over the soil and/or the sliding between the upper and lower porous stones (Stark 2016). Figure 13 shows a typical photograph of the ring shear specimen and container after testing according to Castellanos (2014).

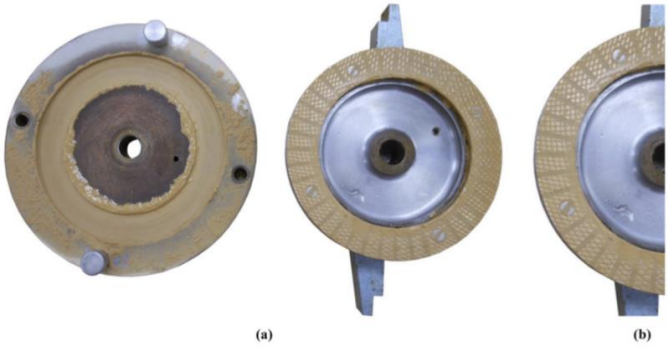

Figure 13: Photographs of Ring Shear Specimen (a) After Shearing (b) Close-up of Top Porous Stone After Shearing Showing the Smooth and Large Flat Areas (Castellanos 2014)

Figure 13a shows the sliding effect of the top porous stone on the specimen. Figure 13b shows the insufficient serration pattern on the porous stone to create an interlocking between the soil and the upper porous stone. A better serration pattern is needed to create a shear surface within the soil instead of at the upper porous stone and soil interface (Stark 2016).

A serration pattern was developed at the University of Illinois at Urbana-Champaign (UIUC) to increase the interlocking between the porous stone and the specimen. The new design results in only approximately 25% of the soil being in contact with the tips of the porous stone. Figure 14 shows the serration pattern developed at UIUC and the serration pattern used in this research.

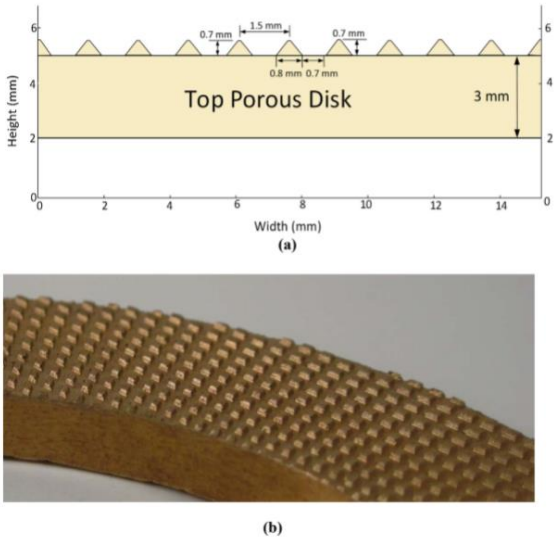

Figure 14: Serration Pattern (a) developed at UIUC (b) Photograph of Serrated Porous Stone (Stark 2016)

2.6.3 Case History

Stark and Eid (1992) conducted a field case history to investigate the effect of the test specimen and testing apparatus on the measured residual strength of the soil. A location in southern California was selected because there had been three previous landslides at the site prior to the slide that was investigated. The specimens were remolded and placed in the ring shear apparatus where the specimen was consolidated for one or two days and sheared for four days at a displacement rate of 0.018 mm/minute. A reverse direct shear test was also performed on samples from the same site. The shear box was reversed manually at the end of each horizontal travel of 0.5 centimeters. Two different types of specimens were used for the direct shear test which include remolded and precut, remolded specimens. The remolded specimens were consolidated to a desired normal stress and then sheared using a displacement rate of 0.0034 mm/minute. The consolidation test required two to six days of testing while the direct shear test ran for 15 to 17 days in order to obtain a residual strength for the remolded specimens (Stark and

Eid 1992). The precut, remolded specimens were consolidated and then sheared at a displacement rate of 0.0034 mm/minute also. A precut specimen was prepared by following a special procedure developed by Mesri and Cepeda-Diaz (1986). Each half of the shear box was filled with material and then consolidated separately. After the material was consolidated, the material is precut using a razor blade in order to obtain a smooth and polished surface. The two precut specimens are then attached together and consolidated again before shearing. These shearing tests ran for approximately 10 to 11 days to acquire a residual strength. Figure 15 shows the results from the ring shear and direct shear tests.

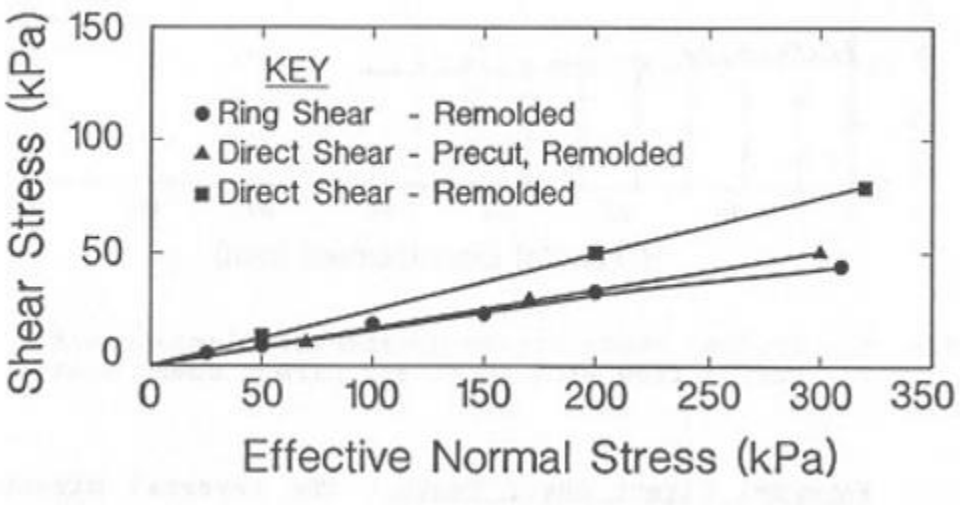

Figure 15: Drained Residual Failure Envelopes for Case History (Stark and Eid 1992)

The remolded specimens in the direct shear test resulted in a failure envelope much higher than the other tests. Since the duration of the direct shear tests are longer than the duration of a ring shear test, this direct shear method should not be used to measure the residual strength of the soil in order to save time if a ring shear apparatus is available (Stark and Eid 1992). The precut, remolded specimens used in the direct shear testing generally had good agreement with the ring shear testing. However, the ring shear apparatus better illustrates the slow decrease in strength after the peak strength is obtained as shown in Figure 16 (Stark and Eid 1992).

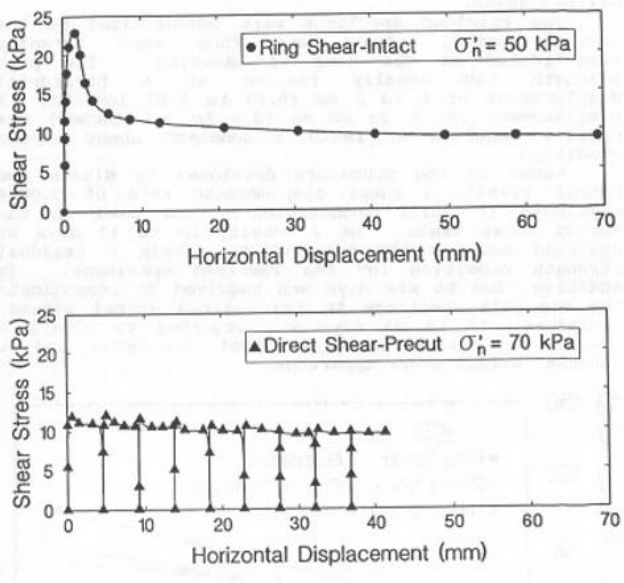

Figure 16: Shear Stress versus Horizontal Displacement Curves for Ring Shear and Direct Shear Tests (Stark and Eid 1992)

Based on this case history, Stark and Eid (1992) recommend using a torsional ring shear apparatus and remolded specimens to determine the residual strength of soil specimens. The precut, remolded direct shear tests did show good agreement with the ring shear tests, but in an interest of time, the ring shear test can be performed in 4 to 6 days; whereas, the direct shear tests on a precut, remolded specimen takes approximately 18 to 20 days (Stark and Eid 1992).

2.7 Slope Stability

Slope stability is an important issue when embankments are built over soft soils such as expansive clays. Adequate design is needed to prevent slope failures and stabilize the embankment. Figure 17 shows the different types of embankment slope failures AL-5 could possibly experience.

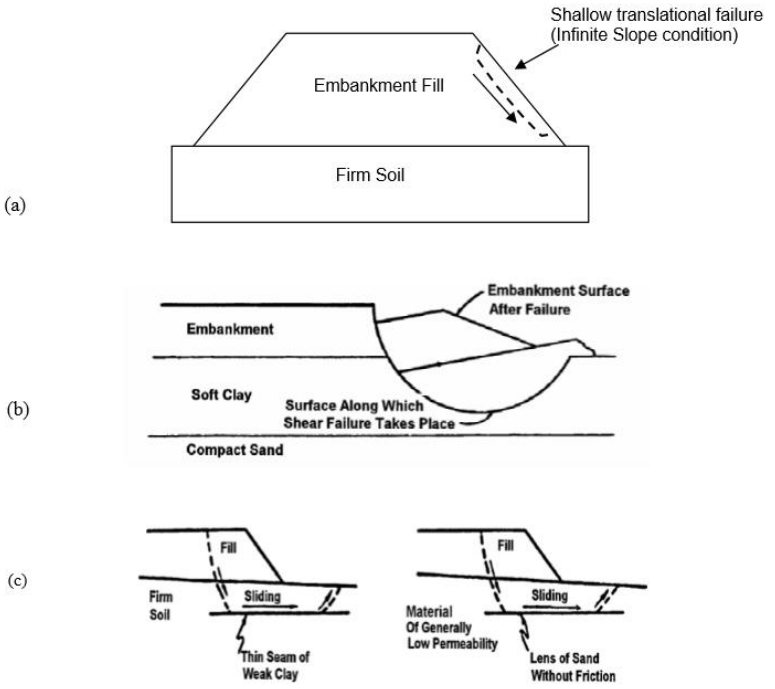

Figure 17: Embankment Failures: (a) Infinite slope failure in embankment fill, (b) Circular arc failure in embankment fill and foundation soil, (c) Sliding block failure in embankment fill and foundation soil (FHWA 2001a)

There are multiple slope stability analysis methods available to determine the factor of safety of an embankment or slope. Embankment and slope failures located over soft soils generally show signs that the embankment has sunk down into the soft soil. As the embankment sinks, the adjacent ground at the toe of the embankment or slope heaves up causing the failure surface to follow a circular arc. Figure 18 shows a typical circular arc failure.

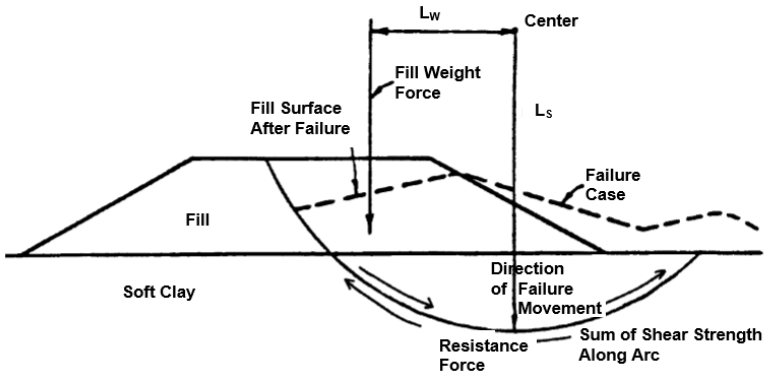

Figure 18: Typical Circular Arc Failure (FHWA 2001a)

At failure, there are driving and resisting forces occurring. The driving force includes the weight of the embankment and the resisting force includes the total shear strength acting along the failure arc as shown in Figure 18. The factor of safety of the embankment can be computed by dividing the sum of the resisting movements by the sum of the driving movements. Failure will occur when the factor of safety is less than 1 or when the driving forces are greater than the resisting forces (FHWA 2001a).

A common analysis method for determining the factor of safety of an embankment or slope is the Ordinary Method of Slices (Fellenius 1927). This method allows there to be some variability in the soil properties. For this method, the failure mass is divided into series of vertical slices which intersects a circular failure surface. Each slice contains one type of soil and the bottom of the slice will be a straight line. Figure 19 shows an example of the geometry of the ordinary method of slices. A free body diagram of one slice with different water conditions can be seen in Figure 20.

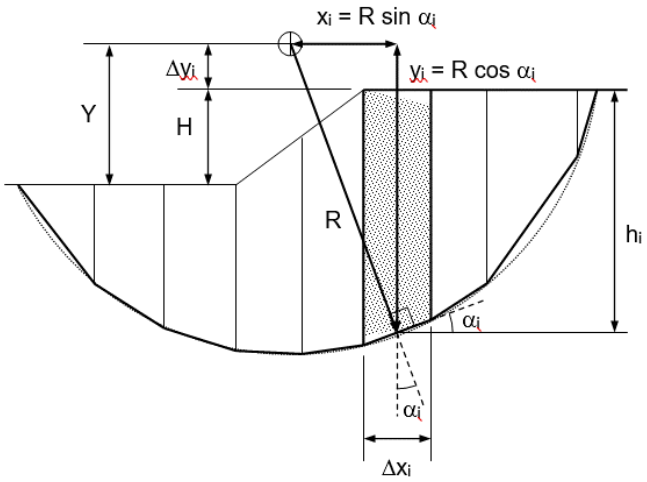

Figure 19: Geometry of Ordinary Method of Slices

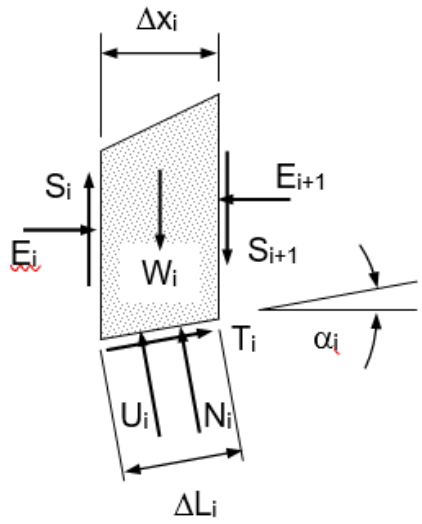

where:
- U_i = Water pressure force
- T_i = Shear force
- N_i = Normal effective force
- E_i = Normal forces on side
- S_i = Shear force on sides
- W_i = Weight of slice
- α_i = Inclination of slice failure plane
- Δx_i = Width of slice
- ΔL_i = Length of slice failure plane

Figure 20: Free Body Diagram for a Slice

The factor of safety can be determined using Equation 8. However, there are too many unknowns in the free body diagram of the slice to solve for the factor of safety. Some assumptions must be made in order to compute the factor of safety. Fellinius (1927) assumed the side shear and normal forces were equal and opposite; therefore, the forces cancel each other out. This simplifies the equations for the factor of safety. Figure 21 shows an example of a slope

embankment with the forces labeled. The resisting moment can be calculated by Equation 9. The driving moment can be determined from Equation 10.

$$FS = \frac{Resisting\ Moment}{Driving\ Moment}$$ Equation 8

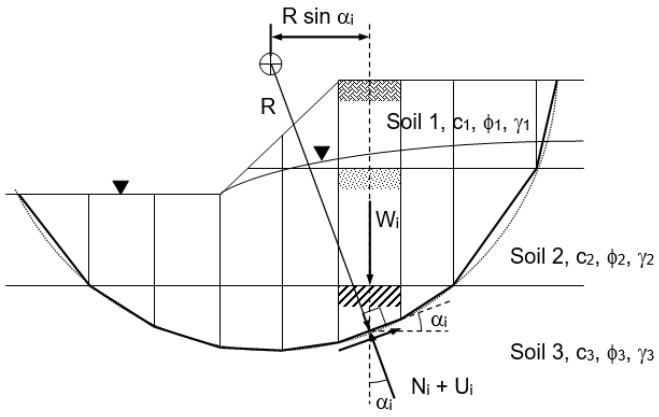

Figure 21: Ordinary Method of Slices Example

$$M_R = R\sum c_i \Delta L_i + R\sum (W_i \cos a_i - u_i \Delta L_i)\tan \varphi_i$$ Equation 9

Where M_R = Resisting Moment

R = Radius of failure arc

c_i = Soil cohesion

$\Delta L_i = \Delta x_i \sec a_i$

W_i = Weight of slice

a_i = Inclination of slice failure plane

u_i = Water pressure force of slice

φ_i = Angle of internal friction for soil

$$M_O = R \sum W_i \sin a_i \qquad \text{Equation 10}$$

where M_O = Driving Moment

As previously stated, the Ordinary Method of Slices ignores the shear and normal forces on each slice; therefore, it is a conservative method for analyzing slope stability. Bishop's Method (Bishop 1955) is common method used to determine the factor of safety and is less conservative than the Ordinary Method of Slices. Bishop's Method does include the normal forces on each slice but ignores the shear force on each slice. Figure 22 shows the free body diagram of a slice using Bishop's Method. This method will change how the resisting moment is calculated. The equations for the resisting moment and the normal force on the slice is shown in Equation 11 and Equation 12. As shown in the following equation, Bishop's Method is an iterative process. A factor of safety must be assumed to start the calculations. Since Bishop's Method is a commonly used method, Bishop's Method will be used in a slope stability software, SLIDE, to determine the factors of safety for AL-5 at the end of construction, peak strength, and residual strength.

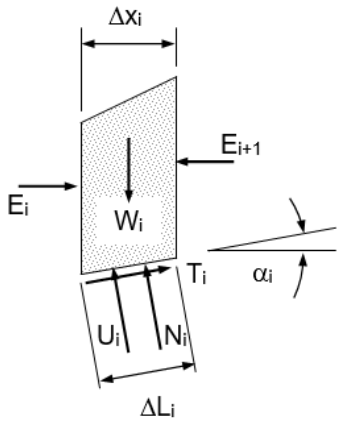

Figure 22: Free Body Diagram of Slice using Bishop's Method

$$M_R = R\sum c_i \Delta x_i \sec a_i + R\sum N_i \tan \varphi_i \qquad \text{Equation 11}$$

$$N_i = \frac{W_i - u_i \Delta x_i - \frac{c_i \Delta x_i \tan a_i}{FS}}{\cos a_i + \frac{\tan \varphi_i \sin a_i}{FS}} \qquad \text{Equation 12}$$

where N_i = Normal force on each slice

The critical slip surface of a slope will result in a minimum factor of safety. To find the most critical slip surface, multiple circular failure surfaces must be evaluated using different center points or circles with a variety of radii values. A contour map is developed showing the factor of safety for each failure slip surface. An example of the process of determining the critical slip surface is shown in Figure 23.

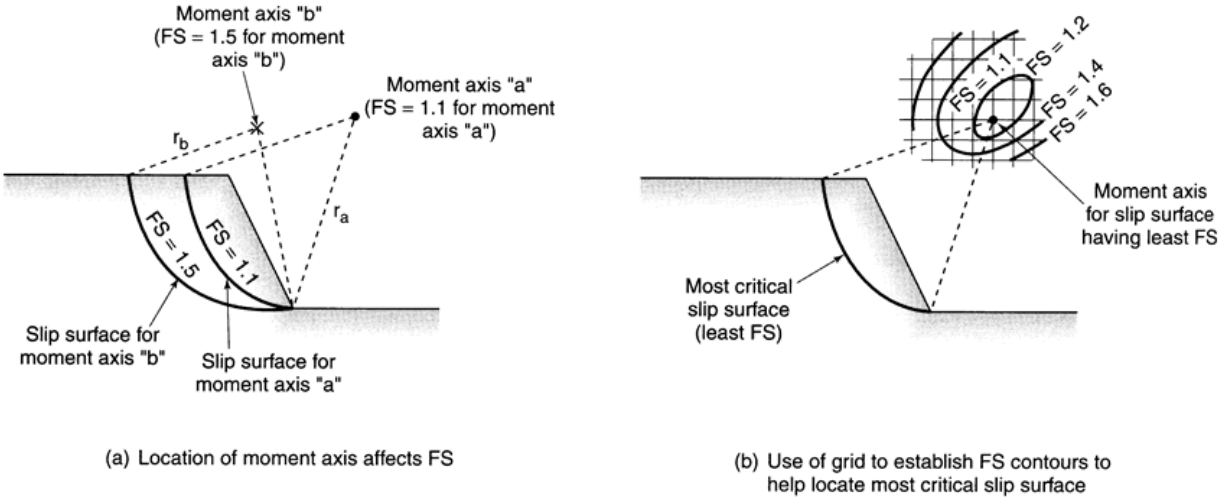

Figure 23: Determining Critical Slip Surface of an Embankment (McCarthy 2007)

CHAPTER 3: PROJECT OVERVIEW

3.1 Site Description

The research site for this study is located west of Selma, AL in Perry County. The four-mile section of Alabama Highway 5 is located between mile marker 50.85 to mile marker 54.85. This section of roadway is generally flat with the surrounding land being both wooded and farming land. The site is divided into eight half-mile sections as shown in Figure 24 and Table 4.

Table 4: Test Sections

Test Section	Remediation Technique	Milepost
1	Control (CO) Sand Blanket (SB) Control (CO)	50.85 – 50.95 50.95 – 51.25 51.25 – 51.35
2	Vertical Moisture Barriers (VB)	51.35 – 51.85
3	Lime Columns (LC)	51.85 – 52.35
4	6’ Paved Shoulders (PS)	52.35 – 52.85
5	Edge Drains (ED)	52.85 – 53.35
6	Control (CO)	53.35 – 53.85
7	Deep Mixing – Canceled	53.85 – 54.35
8	Control (CO)	54.35 – 54.85

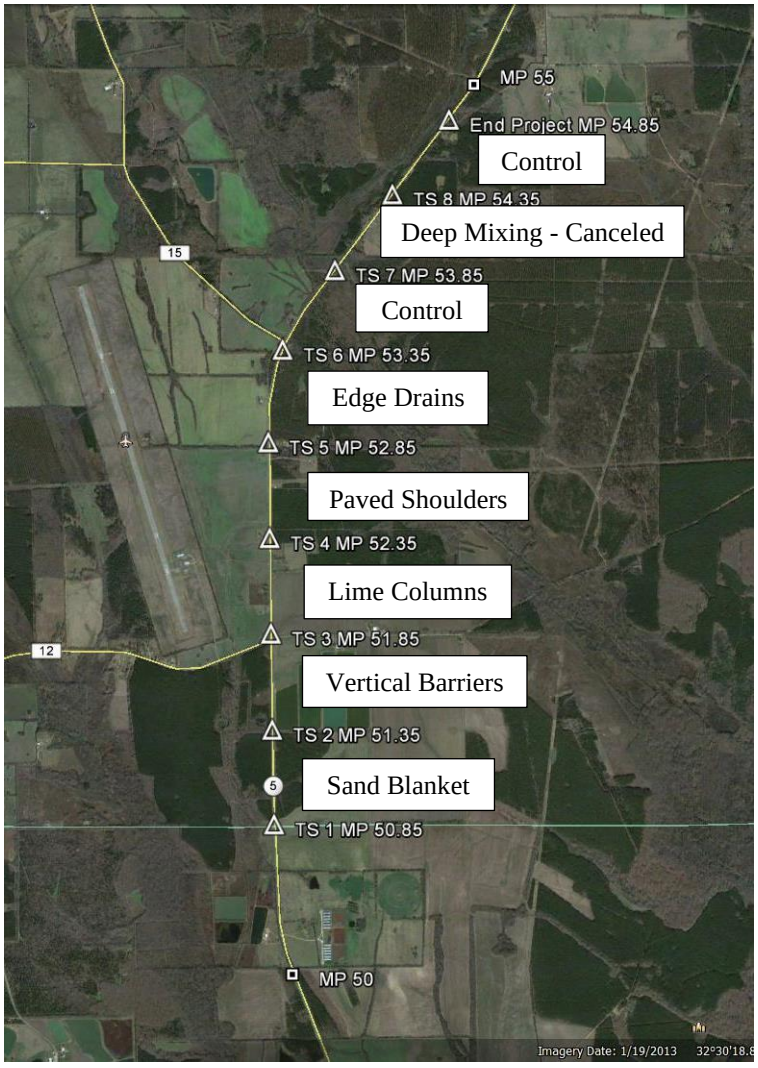

Figure 24: Layout of Research Site (Google Earth)

The original plans for the research site included a different remediation technique for each half mile section of roadway. However, after the initial site exploration was complete, it was noted that the clay layer in Test Section 8 was much thinner than other Test Sections. Therefore, no remediation was implemented in Test Section 8 and it was used as an additional control section. Test Section 7 was canceled due to the complexity of construction and therefore became another control section for the project. Due to more construction constraints and traffic control requirements, the sand blanket was only constructed in the center of the half mile long

section of Test Section 1. The first and last 500 feet of Test Section 1 has no remediation and serves as additional control sections for the project. Construction of the test sections and resurfacing were finished in August 2016.

3.2 Site Characterization

3.2.1 Site Geology

Much of the research site lies in the Mooreville Chalk formation as illustrated in Figure 25. There are also some sections of roadway located near Washington Creek which consist of low terrace and alluvial deposits from the Quaternary age. Mooreville Chalk can be described as "yellowish-gray to olive-gray compact fossiliferous clayey chalk and chalky marl." (Osborne et al. 1989). The upper and lower sections of the Mooreville Chalk formation can vary with the upper ten feet being comprised of interbedded clay and limestone and the lower couple of feet comprised of calcareous sand (Raymond et al. 1988). Site investigation during the research project did not encounter any evidence of varying upper and lower sections of the Mooreville Chalk.

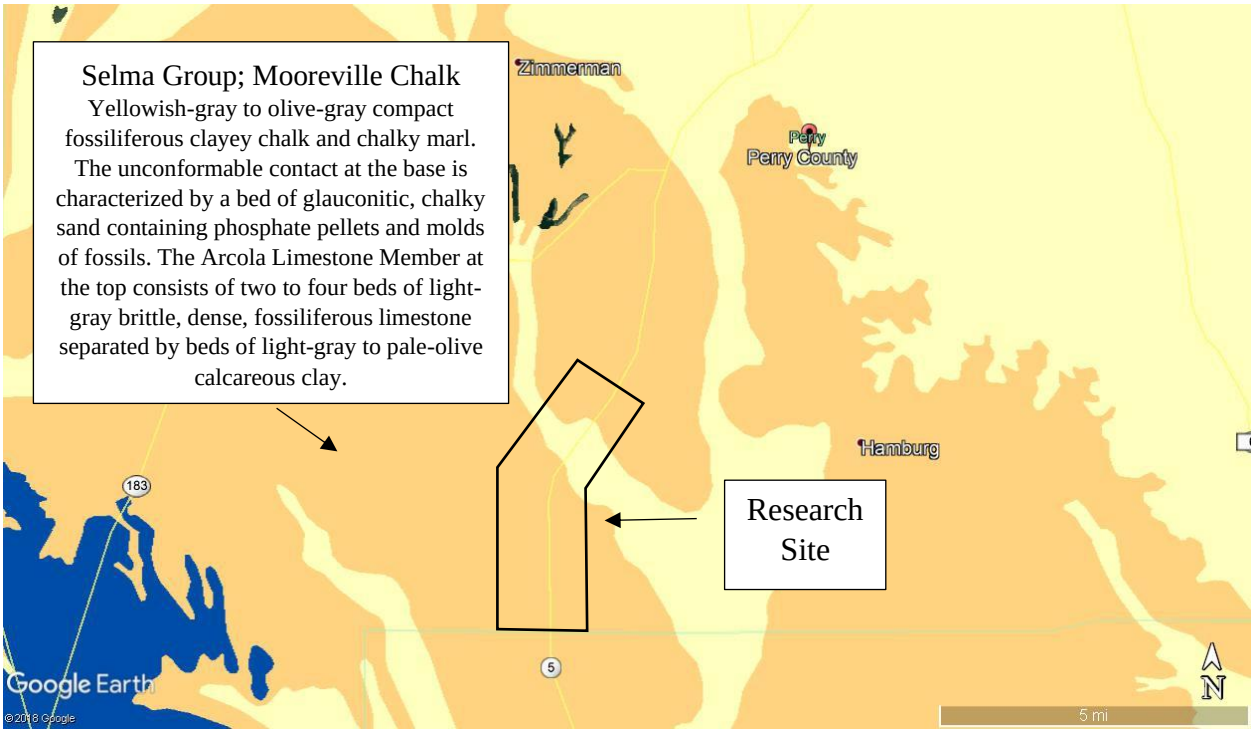

Figure 25: Geologic Map of Perry County, AL (Google 2019) Study Area Outlined overlaid with USGS Soil Survey Map (Szabo et al. 1988)

3.2.2 Site USDA Soil Survey

The United States Department of Agriculture (USDA) performed a soil survey on Perry County which included the research site in 1998. The soil map with the USDA survey is shown in Figure 26 with the research area outlined. As shown below, the research site consists of mostly Vaiden-Okolona-Sucarnoochee soils. These soils are brown to olive to gray clays and show poorly drained conditions. The parent material is most likely the underlying Mooreville Chalk formation, but some areas show evidence of clayey alluvium (Harris 1998).

A more detailed soil map from The United States Geological Survey (USGS) was studied to determine which specific soils are located on the project site. The map showed the main types of soil were Vaiden Clay and Okolona Silty Clay Loam with smaller soil sections consisting on Kipling Clay Loam and Sucarnoochee Clay. Soil properties for these soils can be seen in Table

5. The soil types are similar with most of them having high to very high swell potential. The highlighted material in Table 5 represents the material most likely found at AL-5.

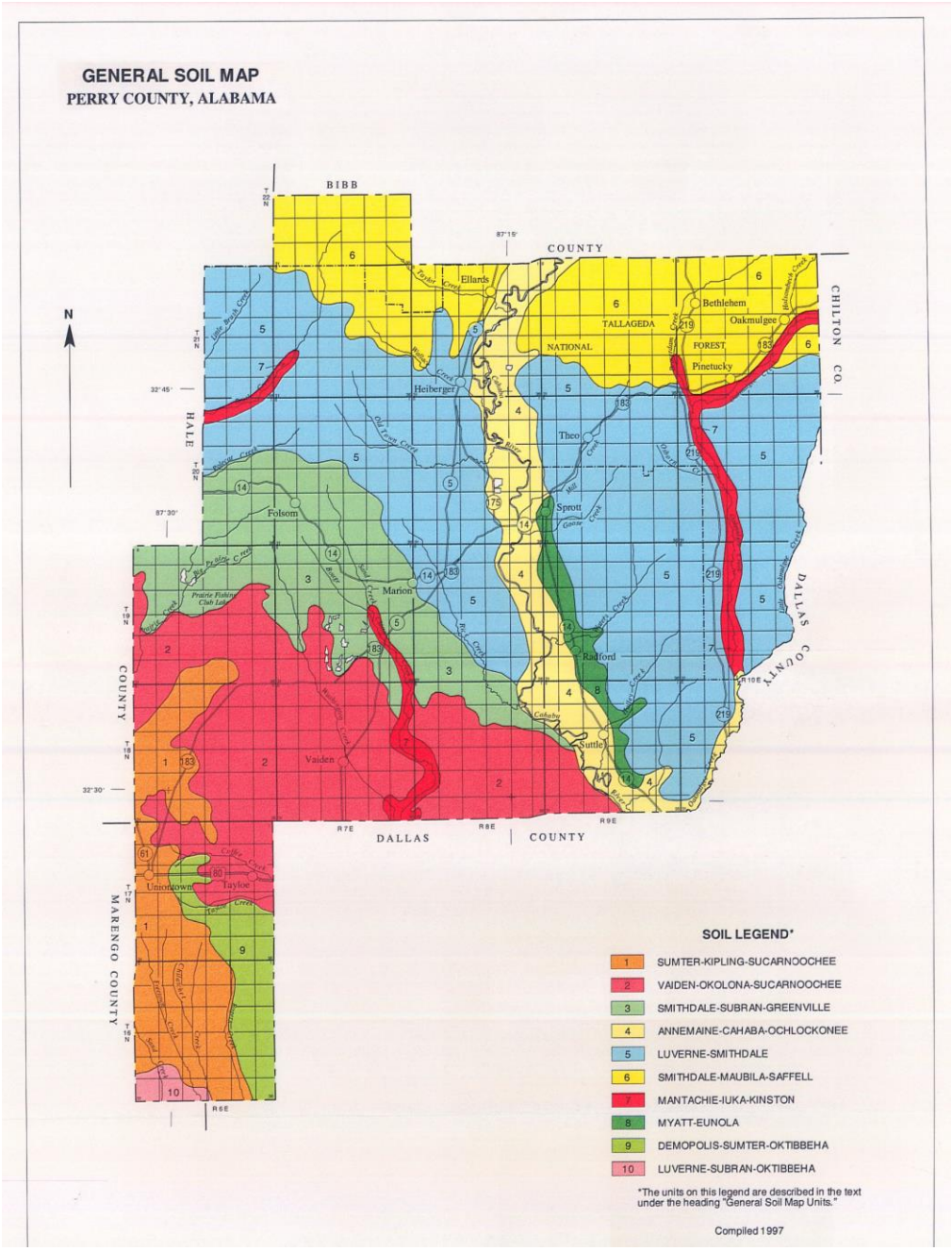

Figure 26: USDA Soil Survey General Soil Map (Harris 1998)

Table 5: Soil Properties from USDA Soil Survey (Harris 1998)

Type	Depth (in)	USCS Classification	% Passing 200	LL	PI	Permeability (in/hr)	Shrink-Swell potential
Okolona Silty Clay Loam	0-6	CL, CH	85-98	46-55	25-32	<0.06	High
	6-60	CH, MH	90-98	60-90	29-65	<0.06	Very High
Vaiden Clay	0-5	MH, CH	90-100	50-60	20-30	0.06-0.2	High
	5-21	CH, MH	85-100	50-90	30-50	<0.06	Very High
	21-60	CH	85-100	50-90	30-52	<0.06	Very High
Kipling Clay Loam	0-5	CL	85-95	30-45	15-25	0.06-0.2	Moderate
	5-65	CH, CL	85-95	38-70	22-45	0.06-0.2	High
	65-80	CH, CL	75-95	48-80	26-50	<0.06	Very High
Sucarnoochee Clay	0-16	CL, CH, MH	85-95	40-65	15-35	0.06-0.2	High
	16-54	MH, CH, CL	85-98	45-70	20-40	<0.06	High
	54-60	CH, MH	85-98	50-80	25-45	<0.06	High

3.3 Climate

The climate of the research site is generally influenced by moist tropical air moving north from the Gulf of Mexico. Summers in Perry County are long and hot; whereas, the winters are short and cool. The NOAA National Climatic Data Center has published 30-year climate normal for Selma, Alabama from 1981 to 2010. Table 6 includes the seasonal precipitation and the maximum, minimum, and average seasonal temperatures. As shown, winter and summer contribute more to the annual amount of rainfall for Selma, AL. It is possible that a natural weather event like a hurricane or tropical storm could cause heavy rain to the research site for several days (Harris 1998).

Table 6: Historical Seasonal Weather Data for Selma, Alabama, 1981-2010 (NOAA National Climatic Data Center 1981-2010)

Season	Total Precipitation	Mean Maximum Temperature	Mean Minimum Temperature	Mean Average Temperature
Annual	51.09	76.3	53.5	64.9
Winter	14.67	59.2	37.2	48.2
Summer	13.21	91.2	70.2	80.7
Spring	12.66	76.7	52.1	64.4

Season	Total Precipitation	Mean Maximum Temperature	Mean Minimum Temperature	Mean Average Temperature
Autumn	10.55	77.7	54.4	66.1

3.4 Traffic Data

Traffic data from 2018 was collected from ALDOT's traffic database. There is a traffic counting station located at mile point 51.30 which is between the boundaries of the research site. The station recorded an average annual daily traffic (AADT) of 1179 vehicles. Of these vehicles, 25 percent were composed of trucks of all types. Therefore, the average annual daily truck traffic was 294 trucks for 2018 (ALDOT 2018). Observations at the site support the theory that a large number of heavily loaded or overloaded trucks travel AL-5 each day.

3.5 Remediation Techniques

ALDOT and Auburn University selected remediation techniques for this project based on extensive literature review, current state of practice, and local experience with the expansive soils. The techniques are briefly described below. More details on the construction of the remediation techniques can be found in Jones (2017).

3.5.1 Sand Blanket

Test Section 1 consists of a sand blanket (SB) layer. This layer creates a drainage layer in the subgrade to maintain a more constant moisture content. The sand blanket layer also acts as a flexible barrier between the expansive soils and pavement; therefore, it helps to minimize the differential heave acting on the pavement. Construction of the sand blanket required the complete removal of the existing pavement which is different than all other Test Sections. Figure

27 is a cross-section of the sand blanket test section and Figure 28 shows the construction of the sand blanket.

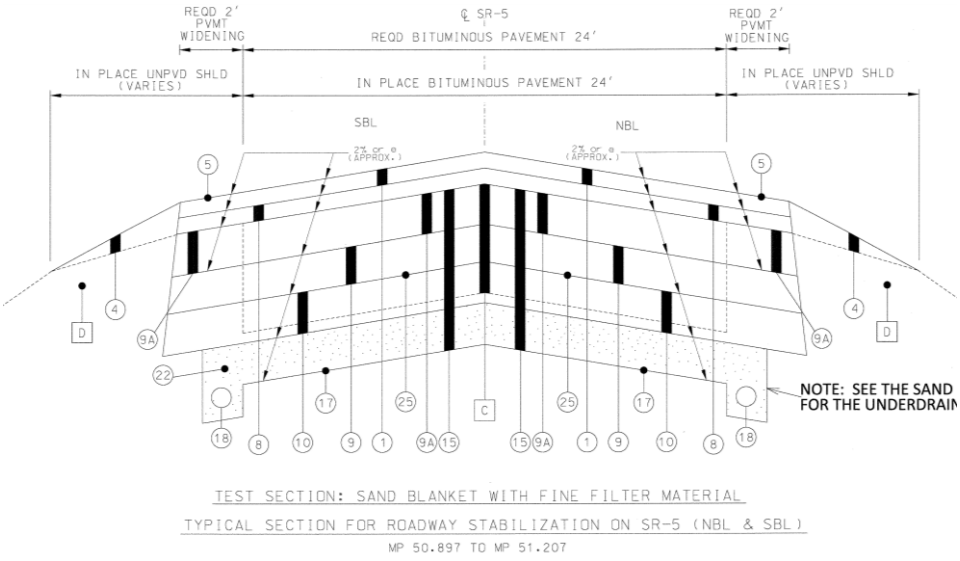

Figure 27: Sand Blanket Cross Section (ALDOT 2015)

Figure 28: Sand Blanket Construction

3.5.2 Vertical Barriers

Vertical moisture barriers (VB) are in trenches along the edge of the pavement and consist of sheets of impervious geomembrane. The purpose of the geomembrane is to limit the amount of lateral flow of water into and out of the subgrade. Nelson and Miller (1992) say that it is normally impractical to install vertical barriers the entire depth of the active zone, but rather a depth of one-half to two-thirds of the active zone will suffice. Figure 29 shows the typical cross-section for the vertical barriers test section. Ten-foot barriers were supposed to be constructed on the north side of the Test Section and six-foot barriers on the south side of the Test Section; however, the soils began to cave in when the ten-foot trench was constructed. Therefore, only six-foot trenches were placed along the entire Test Section. Figure 30 shows the final construction of the vertical barriers test section. After the base course of asphalt was placed on the vertical barriers, cracking, rutting, and spalling developed above the vertical barriers. In some places, the geosynthetic protruded through the asphalt. These issues were likely caused by poor construction practice and compaction efforts and can be seen in Figure 31 and Figure 32.

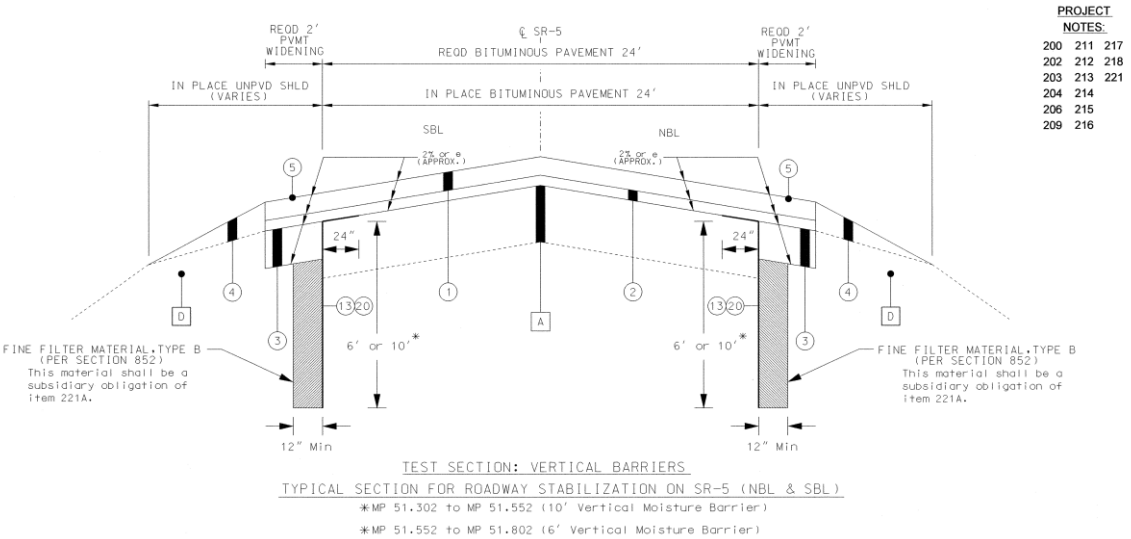

Figure 29: Vertical Barriers Cross Section (ALDOT 2015)

Figure 30: Construction of Vertical Barriers

Figure 31: Cracking and Rutting Observed above Vertical Barriers

Figure 32: Geosynthetic Protruding Through Base Course of Asphalt

3.5.3 Lime Columns

Lime columns (LC) were used to chemically stabilize the subgrade in Test Section 3. According to Nelson and Miller (1992), lime stabilization causes fine grained soils to show less plasticity and improved workability. There was no design method available for the columns. The method was based upon experience with the method as previously employed by ALDOT. Lime was packed into holes drilled in the pavement and shoulder of the roadway to a depth of one foot below the ditch line. The holes were drilled in an arbitrary pattern. Figure 33 and Figure 34 display the cross-section and the layout of the lime columns. Figure 35 and Figure 36 shows the small track hoe with the auger mount used to drill the lime columns.

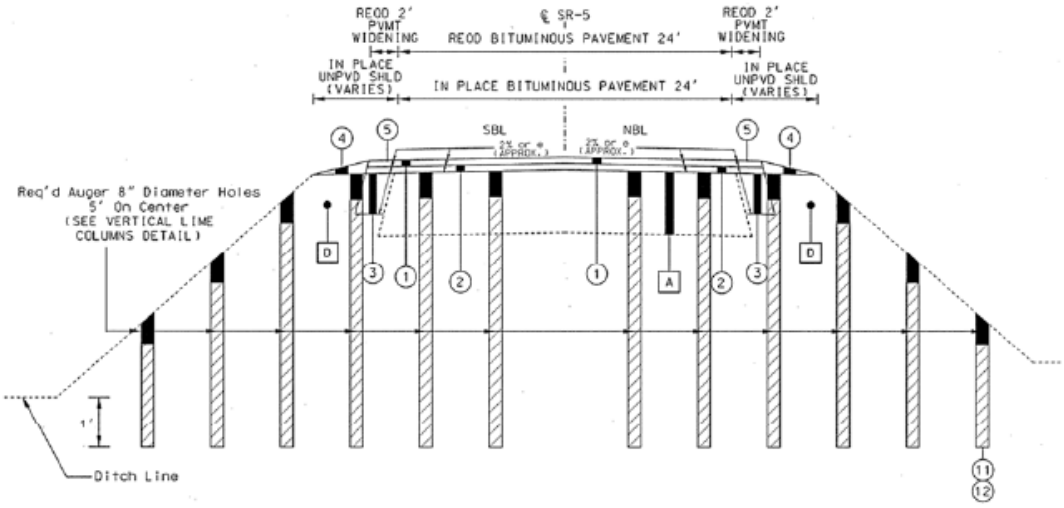

Figure 33: Lime Columns Cross Section (ALDOT 2015)

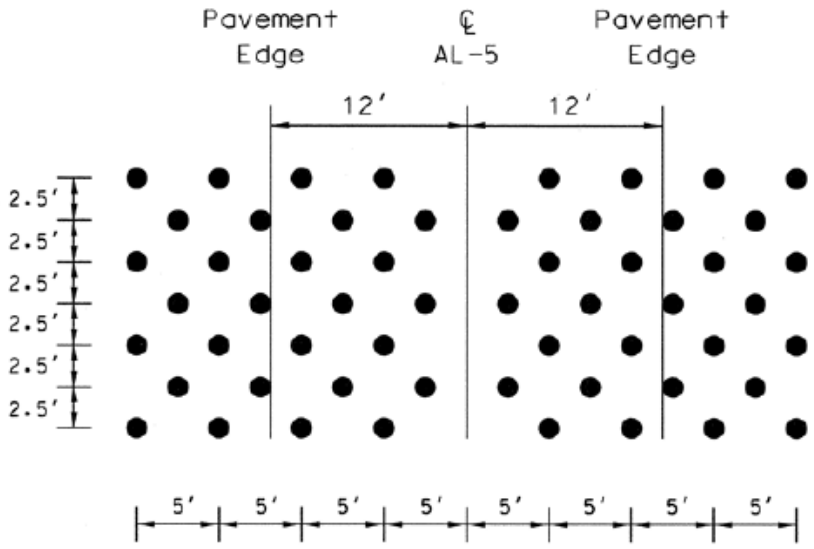

Figure 34: Lime Columns Layout (ALDOT 2015)

Figure 35: Drill Used for Lime Column Installation

Figure 36: Auger used for Lime Column Installation

After the construction of the lime columns and before the placement of the final wearing surface, the lime columns reflected through the base course and were holding water. This issue is shown in Figure 37 and is most likely due to insufficient compaction during construction of the lime columns.

Figure 37: Lime Columns Reflected Through Base Course and Holding Water

3.5.4 Paved Shoulders

After the initial site investigation, it was noted that longitudinal cracks were very common especially near the outside wheel path as shown in Figure 38. Six-foot paved shoulders (PS) were investigated as a means to relocate the longitudinal cracks from the travel lane. By increasing the width of the shoulder, the longitudinal cracks would develop in the shoulder instead of the outside wheel path. Figure 39 displays the cross-section of the paved shoulders test section. A photograph following the paving of the paved shoulders is shown in Figure 40.

Figure 38: Longitudinal Crack Along Edge of AL-5

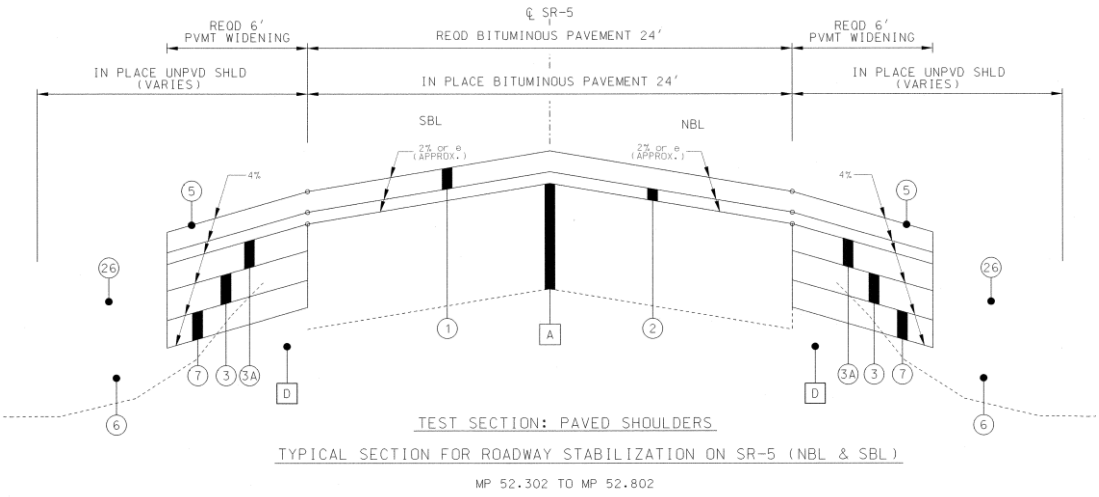

Figure 39: Paved Shoulder Cross Section (ALDOT 2015)

Figure 40: Paved Shoulders After Paving

3.5.5 Edge Drains

Edge drains (ED) were installed at the edge of the pavement in order to stabilize the moisture content of the subgrade. Heaving of the pavement would be reduced if the moisture content of the subgrade was more stable. Figure 41 illustrates the cross-section for the edge drain Test Section. A picture of the edge drains after being backfilled with #57 stone is shown in Figure 42.

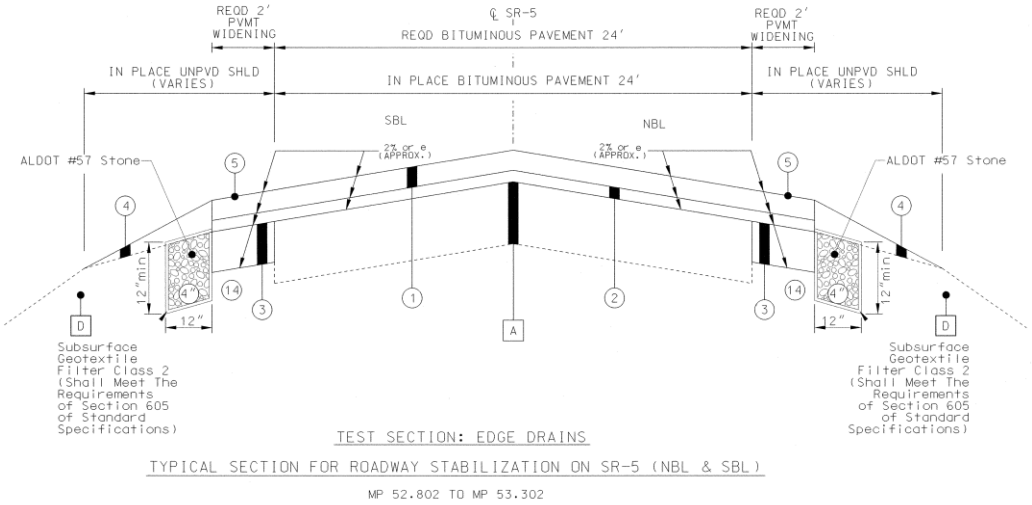

Figure 41: Edge Drain Cross Section (ALDOT 2015)

Figure 42: Edge Drains after Backfilling with Stone

3.5.6 Deep Mixing – Cancelled

It was recommended by ALDOT and Auburn University to use deep soil mixing in Test Section 7 at AL-5. This procedure included mixing Portland cement with the existing expansive soil with the hopes that the expansive soils will become stable. The cross-section and layout of the columns are shown in Figure 43 and Figure 44. This remediation technique was cancelled because of constructability issues and served as an additional control section.

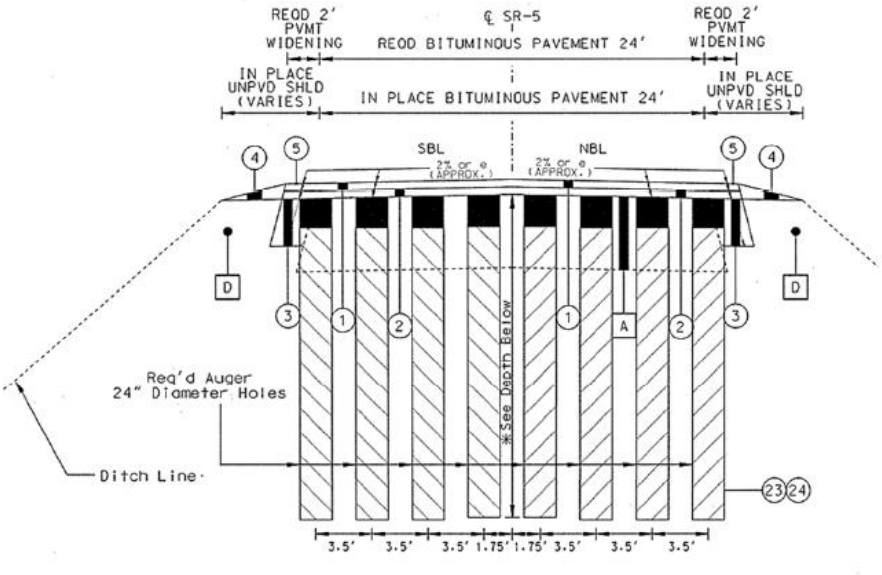

Figure 43: Deep Mixed Columns Cross Section (ALDOT 2015)

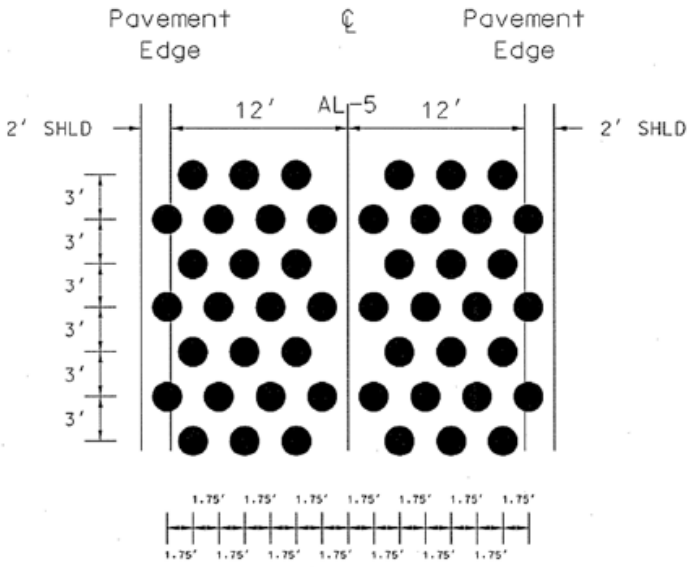

Figure 44: Deep Mixed Columns Layout (ALDOT 2015)

CHAPTER 4: PREVIOUS RESEARCH

4.1 Site Investigation and Laboratory Work

A rigorous site investigation and laboratory testing programs were previously performed on the subgrade and are explained in detail in prior documents (Herman 2015 and Stallings 2016). There was a total of 17 borings drilled for the research site located approximately a quarter of a mile apart. Figure 45 shows the locations of the boreholes. The soils obtained from the Shelby tubes agreed with the description of the Mooreville Chalk and the soil types described in the USDA soil survey (Herman 2015).

Figure 45: Boring Locations (After Google Earth)

Laboratory tests were completed on the soil samples and included grain size analysis, Atterberg limits, and specific gravity tests. One-dimensional swell tests were also performed;

along with, soil-water characteristic curves. According to the laboratory tests, it was determined that the underlying soil of Alabama Highway 5 are expansive and are predicted to be the cause of the pavement distress (Stallings 2016). A summary of the laboratory tests performed on the soil is shown in Table 7.

Table 7: Summary of AL-5 Laboratory Data (Stallings 2016)

Borehole	Depth (ft)	LL	PI	%<#200	Water Content (%)	Dry Density (pcf)	Specific Gravity	Swell Pressure (psf)
B-1A	1.5	70	46					
B-1A	3.5	88	58					
B-1A	5.5	110	83					
B-1A	7.5	79	50					
B-1A	9.5	103	74					
B-1.5A	1.5	97	68					
B-1.5A	3.5	66	42	98	37.0	84.0	2.75	736.0
B-1.5A	7.5	91	66					
B-1.5A	9.5	85	61	98	32.9	87.5	2.62	1301.0
B-2A	3.0	83	52					
B-2A	5.0	73	48					
B-2A	7.0	86	59					
B-2A	9.0	95	68					
B-2.5A	1.5	70	46					
B-2.5A	3.5	84	58	93	31.9	90.1	2.75	927.0
B-2.5A	5.5	79	47					
B-2.5A	7.5			98	29.2	92.4	2.72	1560.0
B-3A	1.5	93	67					
B-3A	3.5	65	41					
B-3A	7.5	74	49					
B-3.5A	1.3	68	40	99	38.6	82.5	2.70	1035.0
B-3.5A	3.3	87	59					
B-3.5A	5.3	84	57					
B-3.5A	7.3			97	41.5	77.7	2.74	1073.0
B-4A	1.8	72	47					
B-4A	5.8	93	70					
B-4.5A	1.2	68	40	97	38.8	81.5	2.72	1082.0
B-4.5A	5.2	97	69					
B-4.5A	7.2			96	33.3	84.4	2.73	
B-5A	1.5	50	26					
B-5A	7.5	91	68					
B-5.5A	1.0	86	60	96	39.6	81.0	2.75	871.0
B-5.5A	7.0	88	61	96	33.3	87.7	2.70	1393.0

Borehole	Depth (ft)	LL	PI	%<#200	Water Content (%)	Dry Density (pcf)	Specific Gravity	Swell Pressure (psf)
B-Tree C	3.0			94	39.6	79.3		622.0
B-Tree C	7.0			94	32.2	89.8		1374.0
B-6A	1.5	97	73					
B-6A	7.5	80	50					
B-6.5A	1.5						2.69	
B-6.5A	3.5	71	47	60	28.2	90.2		509.0
B-6.5A	5.5	57	39					
B-6.5A	7.5	50	35					
B-6.5A	8.8			45				
B-7A	3.5	57	40					
B-7A	5.5	58	38					
B-7A	7.5	63	42					
B-7.5A	5.0	67	49	81	29.2	93.9	2.72	608.0
B-7.5A	7.0	60	42	78	27.8	95.4	2.81	709.0
B-8A	5.0	64	48					
B-8A	7.0	50	34					
B-8.5A	1.0			90				
B-8.5A	3.0			78				

4.2 International Roughness Index

International roughness index (IRI) data was collected before the construction of the remediation techniques to determine the baseline condition of the roadway. An IRI survey measures the differences in the surface of the pavement by creating longitudinal profiles. The surveys were performed by a technician from the National Center for Asphalt Technology (NCAT). There is a failure threshold of 170 inches/mile defined by the Federal Highway Administration (FHWA). The IRI values collected were determined to be higher than the threshold; therefore, the roadway is experiencing unsafe conditions. The results of the initial IRI data is shown in Figure 46 through Figure 49.

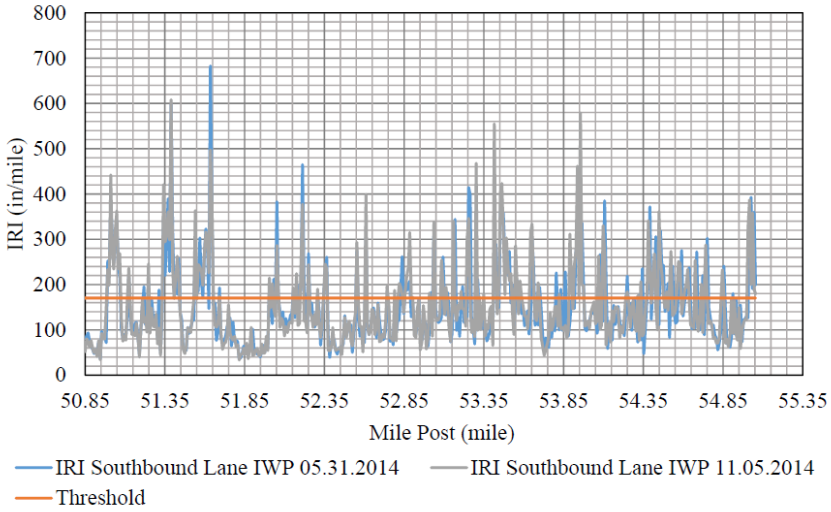

Figure 46: Southbound, Inside Wheel Path IRI Results for May and November 2014 (Stallings 2016)

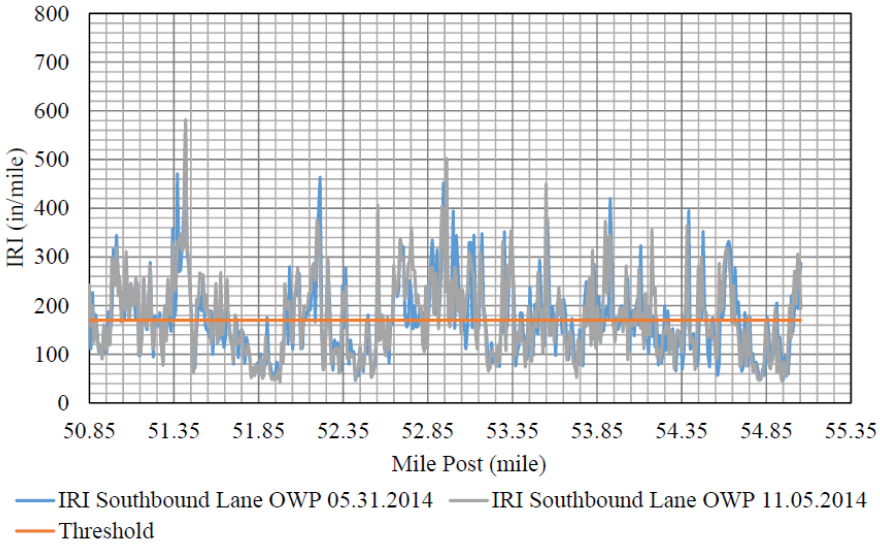

Figure 47: Southbound, Outside Wheel Path IRI Results for May and November 2014 (Stallings 2016)

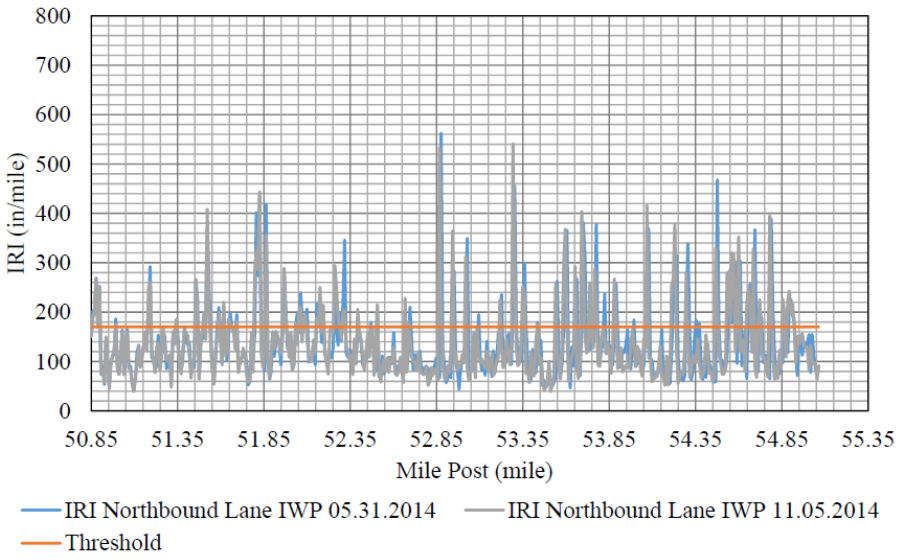

Figure 48: Northbound, Inside Wheel Path IRI Results for May and November 2014 (Stallings 2016)

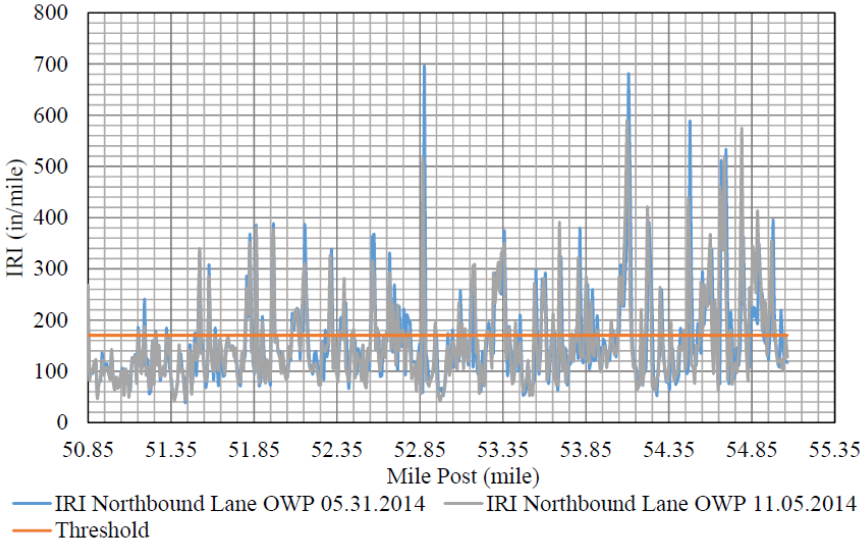

Figure 49: Northbound, Outside Wheel Path IRI Results for May and November 2014 (Stallings 2016)

IRI test have been performed on the roadway following the construction of the remediation techniques. These test results can be seen in Figure 50. There is a significant decrease in the IRI values after 2014 and after the construction of the remediation techniques.

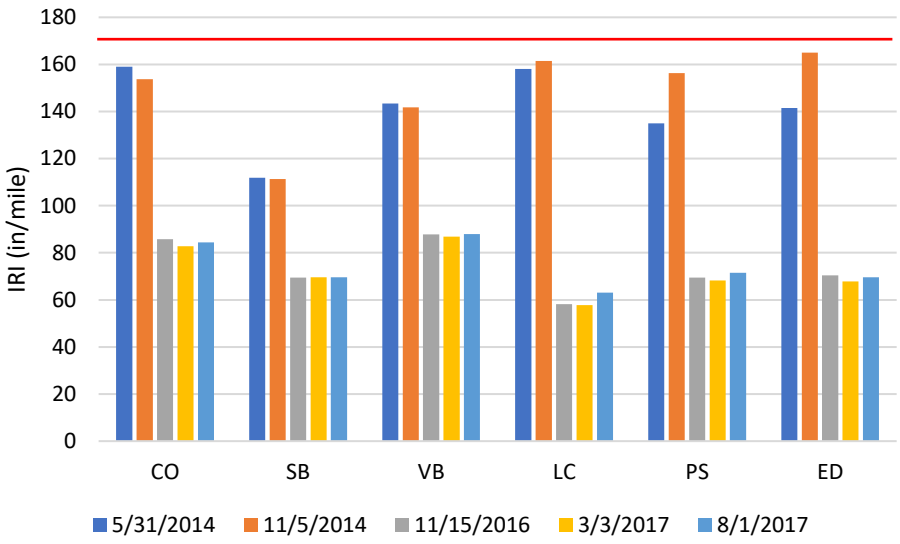

Figure 50: Average IRI by Test Section

4.3 Electrical Conductivity Survey

An electrical conductivity survey was performed on the research site to detect any sulfates in the soil and were conducted by Herman (2015). Sulfates combined with lime can result in the expansive material called ettringite (Little 1995). There is a threshold of 100 mS/m which indicates sulfates are present in the soil. The survey is shown in Figure 51. Many of the points were located beneath the threshold which indicates that sulfates are present.

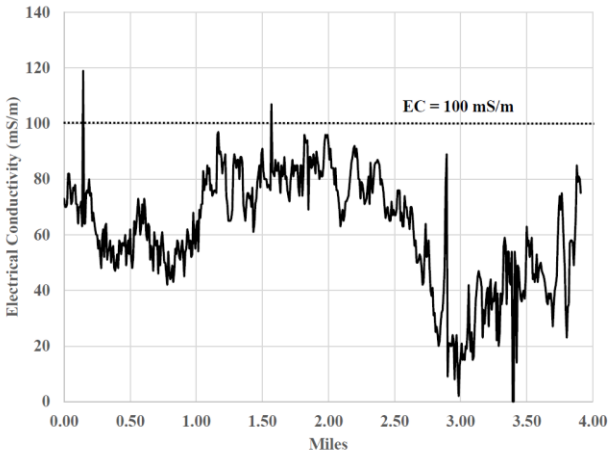

Figure 51: Longitudinal Electrical Conductivity Profile for AL-5 (Herman 2015)

4.4 Instrumentation

Each test section was instrumented with numerous sensors to better understand the behavior of the subgrade and pavement conditions at AL-5. Seven different stations were installed with one station in each remediation technique including one in the control section and one near a section of vegetation being monitored. The sensors measure the moisture content of the soil, matric suction, pore water pressure, and asphalt strain. The vegetation section being monitored measured the matric suction and moisture content. A weather station was installed near the lime column station to provide environmental conditions at AL-5 including temperature and amount of rainfall. Selection, installation, and calibration of the sensors are described in much greater detail in a previous publication (Jackson 2016).

4.4.1 Moisture Sensors

The volumetric moisture content (VMC) of the soil throughout the project was measured using the GS1 made by Decagon Devices. The VMC is measured by the dielectric permittivity of the soil and correlating it to VMC (Jackson 2016). The installed sensor is shown in Figure 52.

Figure 52: Decagon Devices GS1 Moisture Content Sensor (Jackson 2016)

Jackson (2016) performed a calibration test for the GS1 sensor. There is not much difference between different sensors; therefore, a single calibration was used for all GS1s. Soil samples with approximately the same dry density as the soil in the field was used with varying moisture contents to perform the test. Jackson (2016) developed a calibration curve and equation used for all GS1 sensors as shown in Figure 53.

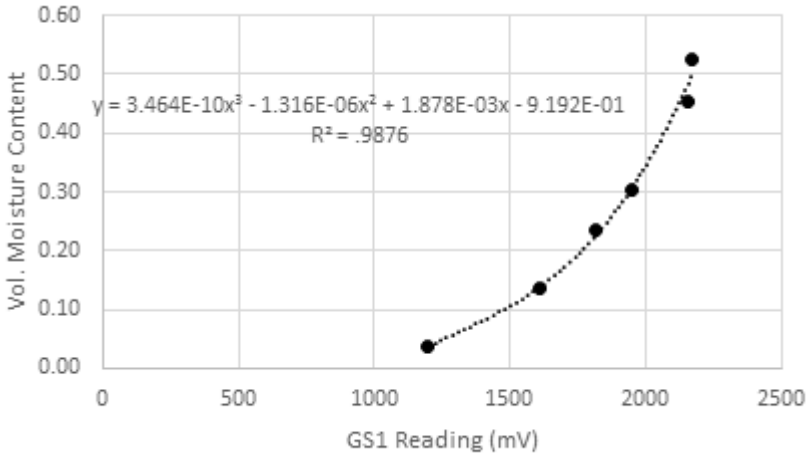

Figure 53: GS1 Calibration Curve and Equation (Jackson 2016)

4.4.2 Suction Sensors

A Decagon MPS6 sensor was installed to measure the matric suction and is shown in Figure 54. The sensor uses a ceramic disk that is hydraulically placed in contact with the soil. Similar to the Decagon DS1 sensors, the water content of the ceramic disk is measured using a dielectric technique. A moisture characteristic curve of the ceramic disk can then be used to determine the matric suction by a correlation with the ceramic disk water content. Manufacturer calibrations were used for this sensor throughout the project (Jackson 2016).

Figure 54: Decagon MPS6 (Jackson 2016)

4.4.3 Piezometers

Vibrating wire piezometers were installed to measure the positive pore pressure if the soil ever became fully saturated. Geokon 4500S sensors were used and each sensor has its own calibration provided by the manufacturer (Jackson 2016). An example of the 4500S sensor is shown in Figure 55.

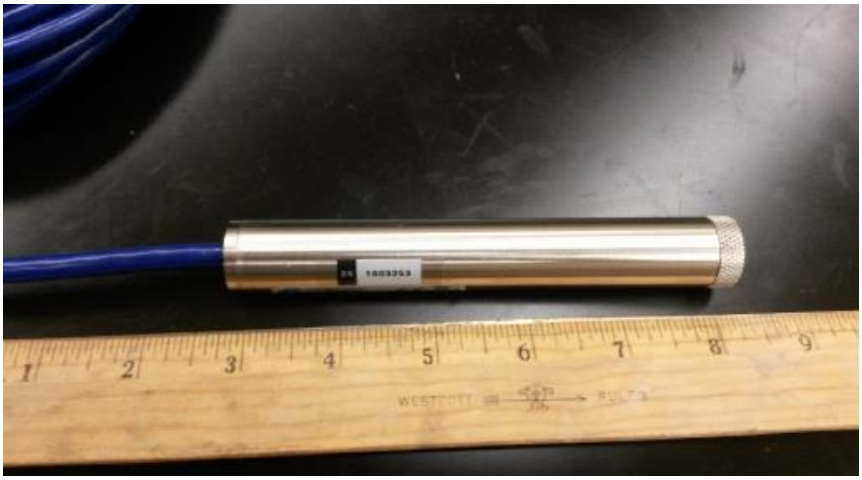

Figure 55: Geokon 4500S (Jackson 2016)

4.4.4 Asphalt Strain Gages

Asphalt strain gages (ASGs) were installed in the pavement to measure the amount of pavement distress AL-5 is experiencing. A total of twelve strain gages were installed in the sand blanket test section and eight gages in all the remaining test sections. The ASG-152 by CTL group was used in the sand blanket section; however, due to time and cost constraints, a less expensive ASG manufactured by Geocomp was used in the other test sections. Figure 56 and Figure 57 show the two different ASGs. The gages were calibrated by the manufacturer (Jackson 2016).

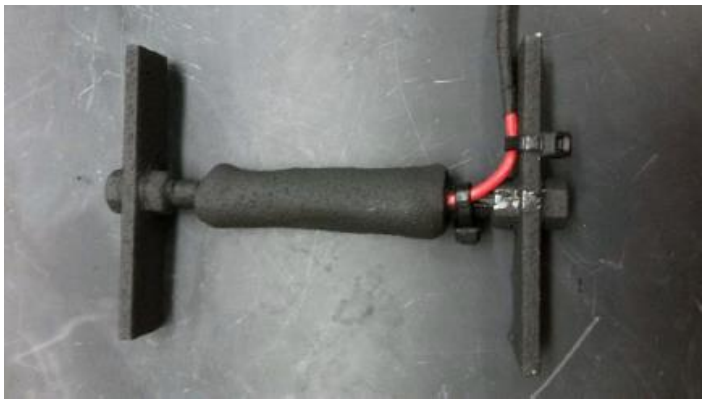

Figure 56: CTL ASG-152 Asphalt Strain Gage (Jackson 2016)

Figure 57: Geocomp Asphalt Strain Gage (Jackson 2016)

All the Test Sections had the same strain gage layout except for the sand blanket test section. Figure 58 shows the layout for the sand blanket section and Figure 59 shows the layout for the remaining test sections. The centerline of the layout of strain gages were approximately at the centerline of the travel lane.

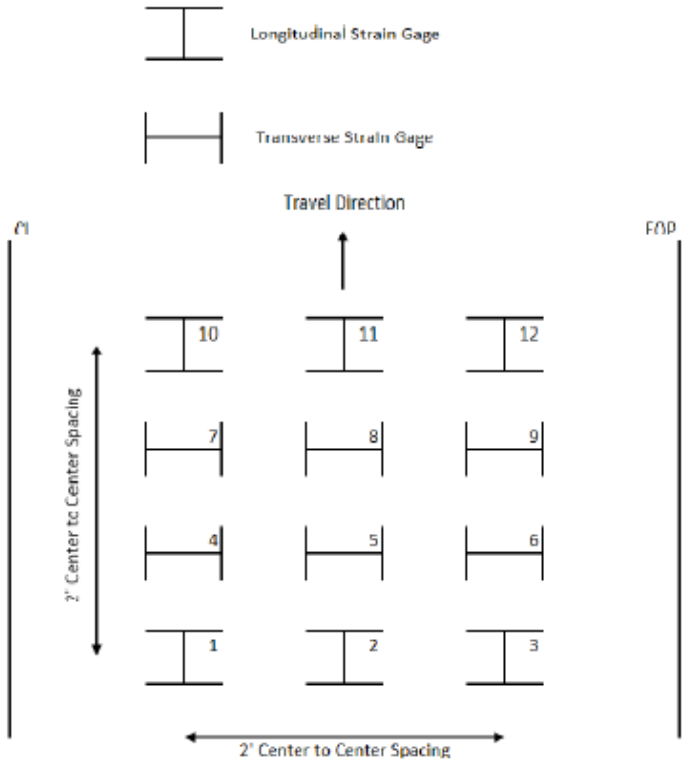

Figure 58: Sand Blanket Strain Gage Layout (Jackson 2016)

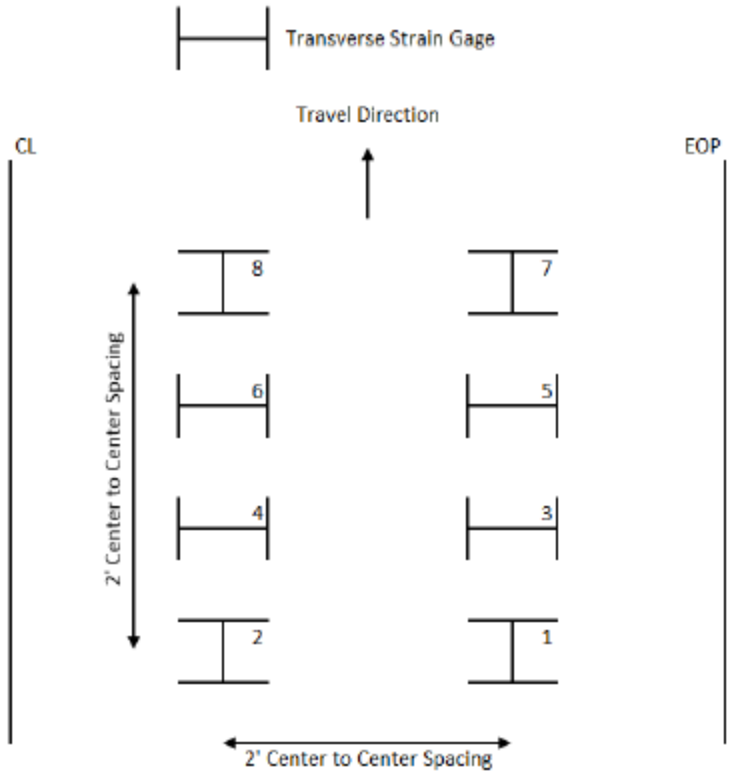

Figure 59: Strain Gage Layout for Remaining Test Sections (Jackson 2016)

4.4.5 Data Acquisition System and Weather Station

Campbell Scientific CR6 dataloggers were used to monitor the sensors in each test section. The datalogger is powered by a BP12/CH200 power supply and charging regulator manufactured by Campbell Scientific. A solar panel was installed with each station to recharge the batteries when needed. There were three AM16/32B multiplexers at each station to connect the moisture sensors, piezometers, and asphalt stain gauges together. Figure 60 shows an example of the data acquisition system used in each test section.

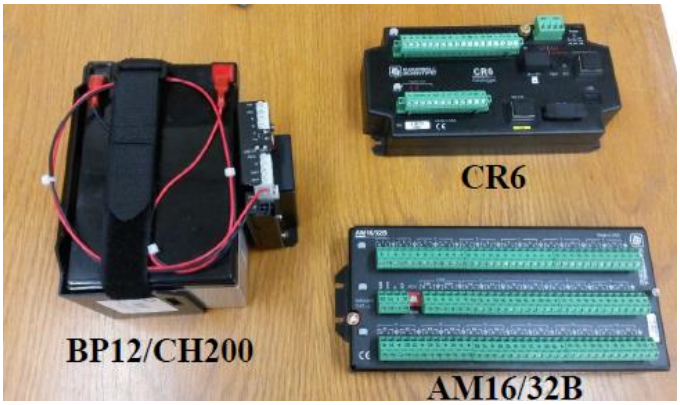

Figure 60: Data Acquisition System (Jackson 2016)

A WTX520 weather sensor manufactured by Campbell Scientific was also installed to measure the air temperature, barometric pression, wind speed, wind direction, relative humidity, and precipitation. The WTX250 is displayed in Figure 61.

Figure 61: Campbell Scientific WTX520 (Jackson 2016)

4.4.6 Installation Summary

The sensors were installed in a 6-inch borehole that was drilled to a depth of 12 feet. Sensors were placed in the subgrade beneath the pavement and in the adjacent shoulder. In each borehole, the sensors were installed from the bottom up with four moisture sensors, four suction sensors, and two piezometers. For the moisture and suction sensors, there was a target depth of 10 feet, 7.5 feet, 5 feet, and 2.5 feet. For the piezometers, the target depths were 12 feet and 7.5 feet. The boreholes were back filled with native material and compacted with an inclinometer tube.

As mentioned previously, 12 strain gages were installed in the sand blanket test section while the remaining test sections only have 8 strain gages. The ASGs in the sand blanket test section were installed on the subgrade due to the method of construction. For the remaining test sections, the ASGs were placed in the pavement. A 3-inch milled section of roadway was prepared for the installation of the strain gages as shown in Figure 62. A more detailed explanation of the installation process can be found in previous publications (Jackson 2016). The survivability of the sensors after installation was very good at the research site and a summary of the survivability is shown in Table 8.

Figure 62: Gage Array on Milled Surface Covered with Screened Asphalt (Jackson 2016)

Table 8: Sensor Survival Summary (Jackson 2016)

	Moisture			Suction		
Test Section	**Surviving**	**Total**	**Percent Surviving**	**Surviving**	**Total**	**Percent Surviving**
Control	8	8	100%	8	8	100%
Sand Blanket	8	8	100%	8	8	100%
Vertical Barriers	8	8	100%	6	8	75%
Lime Columns	8	8	100%	7	8	88%
Paved Shoulders	8	8	100%	6	8	75%
Edge Drains	8	8	100%	6	8	75%
Trees	4	4	100%	3	4	75%
Total	52	52	100%	44	52	85%
	Piezometer			**ASG**		
Test Section	**Surviving**	**Total**	**Percent Surviving**	**Surviving**	**Total**	**Percent Surviving**
Control	4	4	100%	7	8	88%
Sand Blanket	4	4	100%	11	12	92%
Vertical Barriers	4	4	100%	8	8	100%
Lime Columns	4	4	100%	6	8	75%
Paved Shoulders	4	4	100%	8	8	100%
Edge Drains	4	4	100%	7	8	88%
Trees	NA	NA	NA	NA	NA	NA
Total	24	24	100%	47	52	90%

CHAPTER 5: CONTINUOUS MONITORING OF AL-5

Test sections at AL-5 have been continuously monitored since the installation of the sensors and gages. Quarterly reports have been written for ALDOT to show the progress and results of the roadway conditions with the remediation techniques. All data is current as of the publication of this thesis. It is important to note that some sensors and gages no longer function likely due to sensor degradation over time.

6.1 Weather Data

The total rainfall and temperature have been monitored since November 2016. The amount of rainfall fluctuates with the seasonal changes. Figure 63 shows the monthly measured rainfall and average temperature at the project site. Recently, the weather station stopped measuring rainfall and temperatures in June 2019; therefore, no data was collected from the weather station. However, there is a nearby weather station in union Town to the west that is recording rainfall and temperature. Historic Union Town weather data was compared to the AL-5 weather station and it was concluded the Union Town station aligned with the AL-5 data. Thus, the Union Town weather data was used to plot the rainfall totals for June 2019 through October 2019.Generally, during the months when the average temperature was higher, the total rainfall decreased.

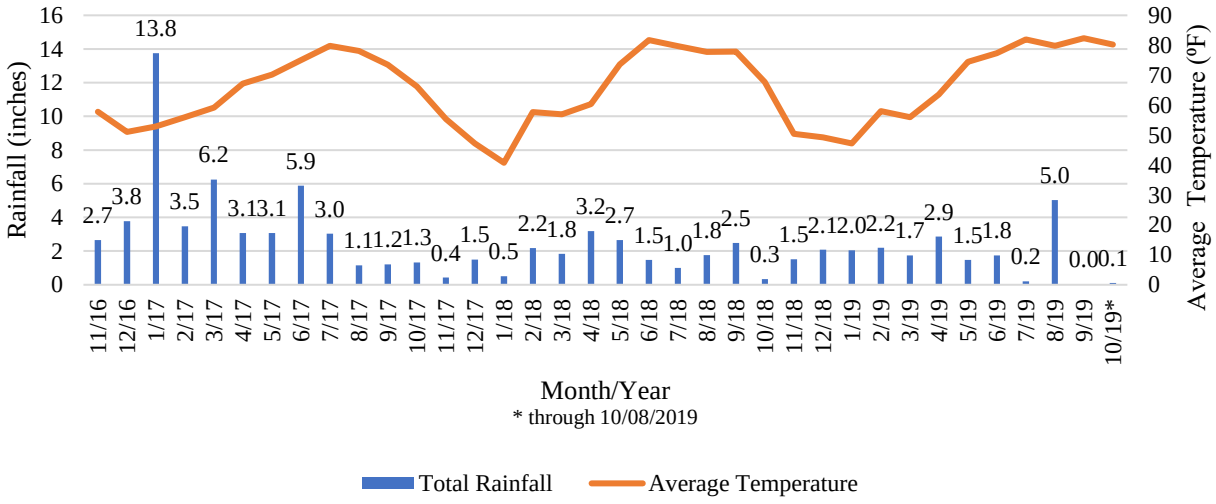

Figure 63: Rainfall Data

6.2 IRI Data

Four additional IRI tests were completed on AL-5 during the research for this thesis. Two tests were completed in 2018 and two were completed in 2019. Figure 64 through Figure 71 show the northbound and southbound lane IRI results from each survey completed. It is important to note that there are many points on the roadway that exceed the 170 in/mile IRI threshold.

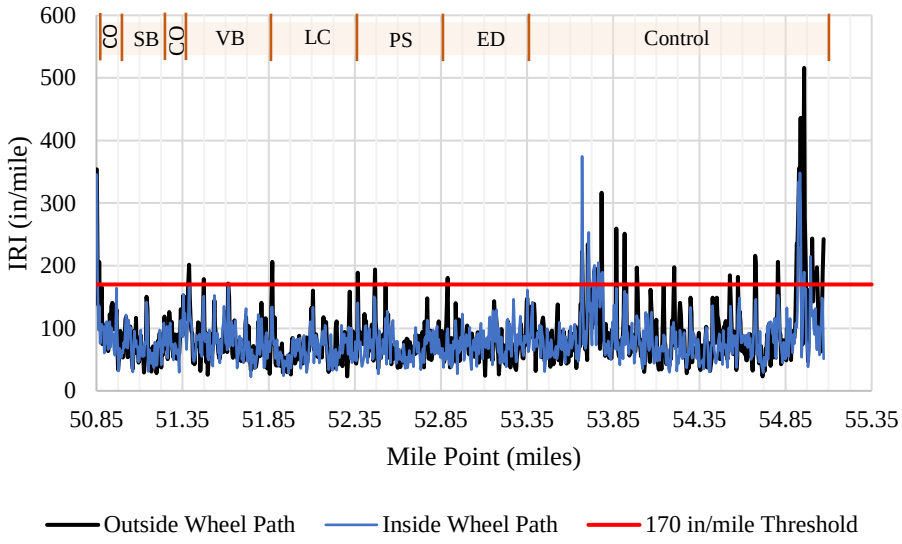

Figure 64: Northbound IRI Results for February 2018

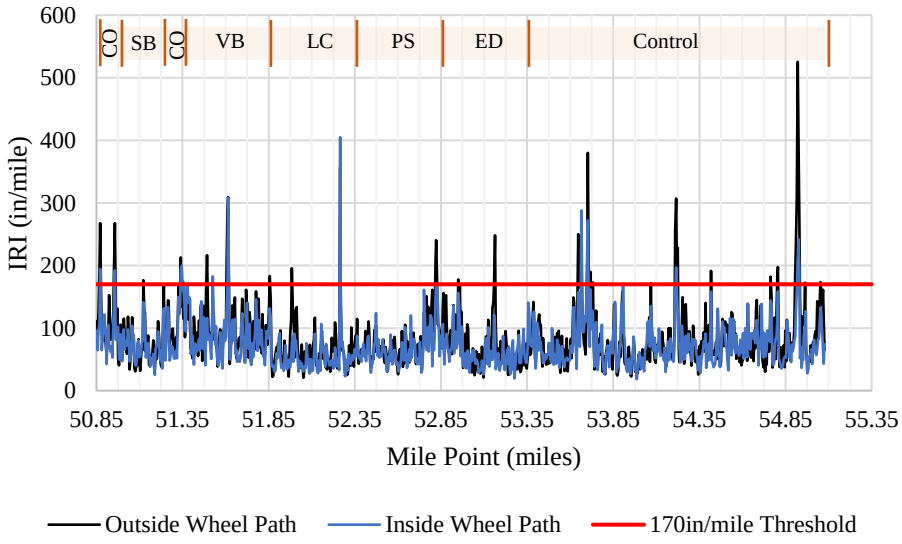

Figure 65: Southbound IRI Results for February 2018

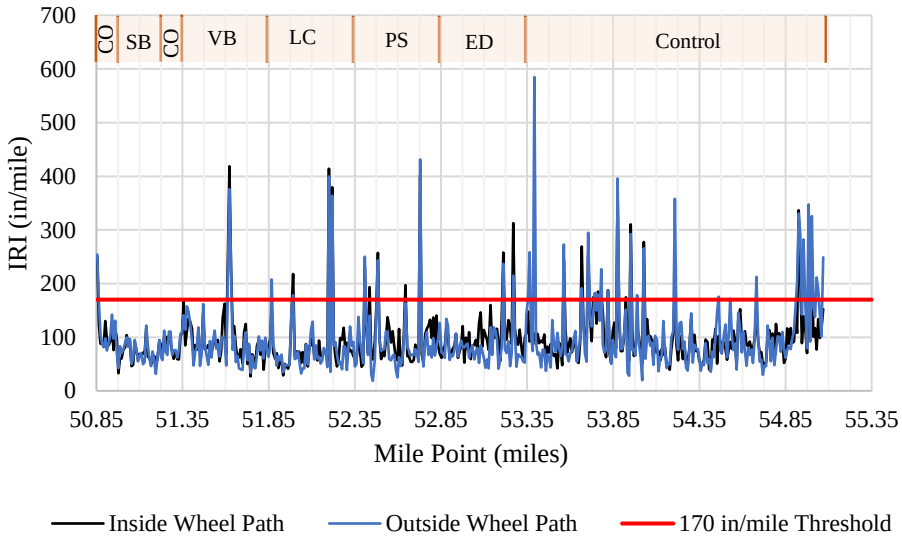

Figure 66: Northbound IRI Results for December 2018

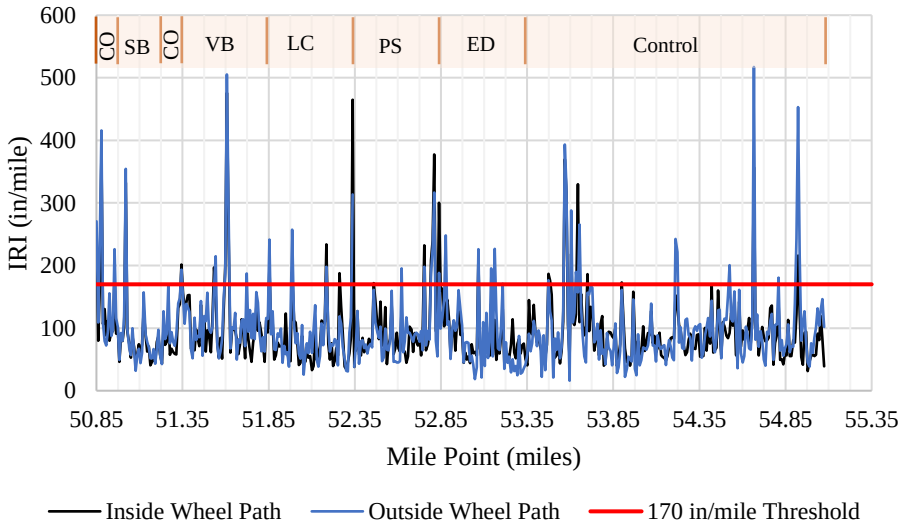

Figure 67: Southbound IRI Results from December 2018

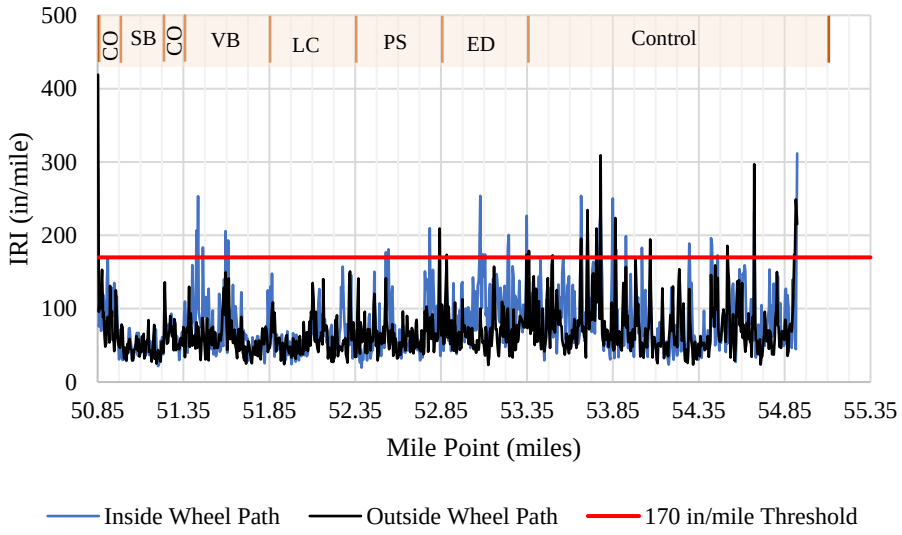

Figure 68: Northbound IRI Results from May 2019

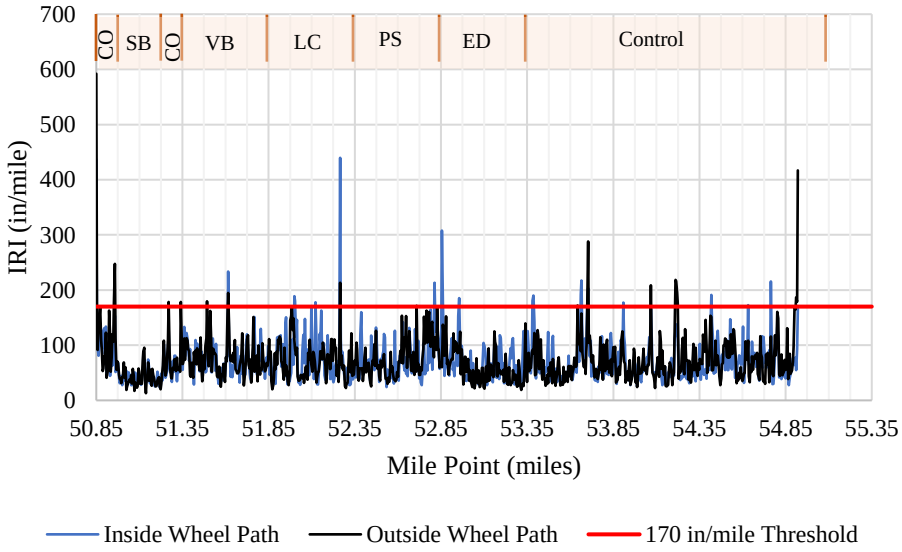

Figure 69: Southbound IRI Results from May 2019

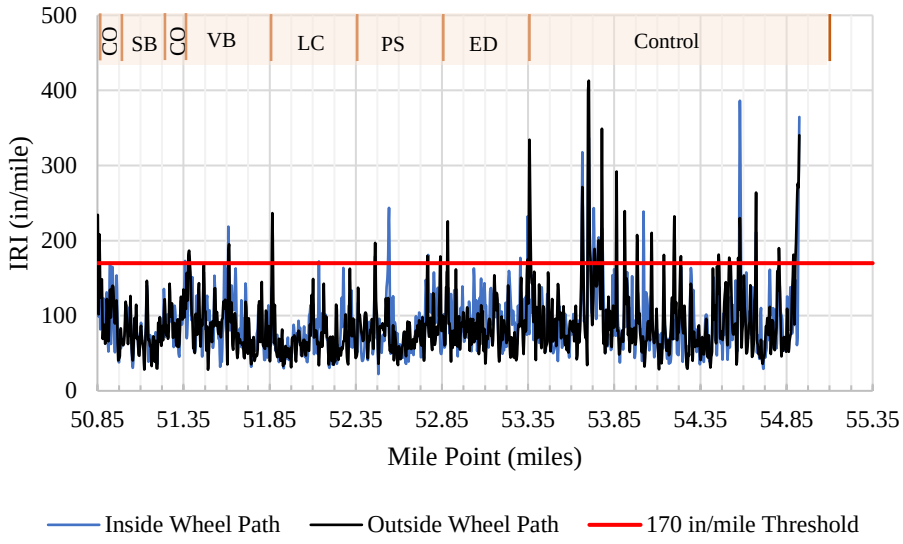

Figure 70: Northbound IRI Results from October 2019

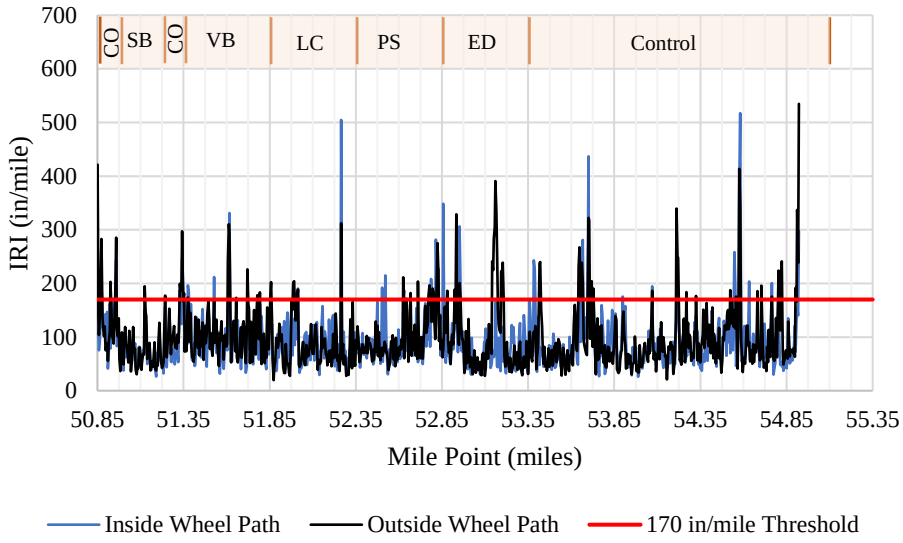

Figure 71: Southbound IRI Results from October 2019

Figure 72 shows the combined average IRI data for all test sections. The average IRI data from each test section plotted beneath the 170 in/mile threshold. There was a significant decrease in the IRI after the data collection from November 5th, 2014. The IRI remained fairly constant for the next four IRI surveys, but there was in increase in IRI during the December 4th,

2018 survey. The survey on May 23rd, 2019 resulted in low IRI values which could be from a flaw in the testing because the survey completed in October 2019 showed larger IRI values than the previous survey. It is important to note that the survey completed in October 2019 resulted in lower IRI values than the survey in December 2018. Generally, IRI values would not improve unless a moderation was made to enhance the roadway; therefore, it was assumed that the surveys in December 2018 and May 2019 resulted in poor data likely due to the equipment.

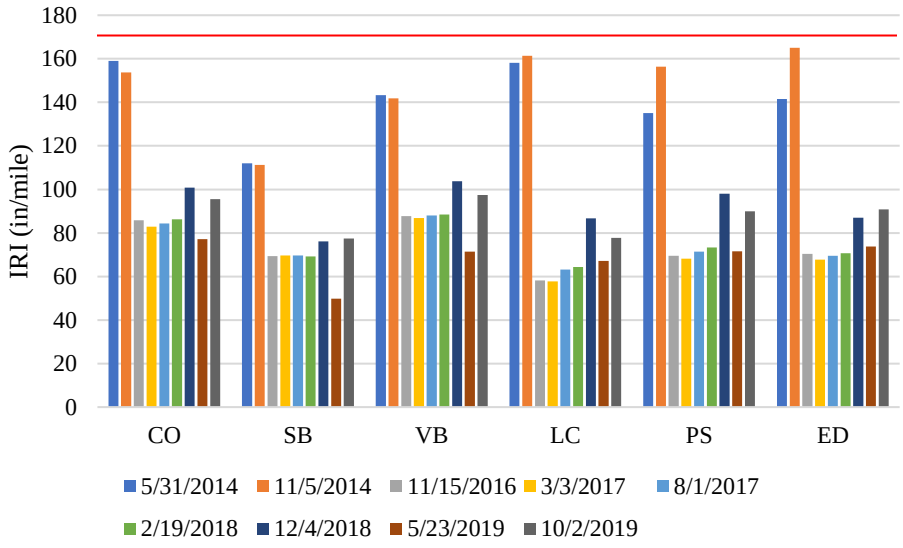

Figure 72: Combined IRI Data for AL-5

Overall, the lime columns test section was the most improved test section according to the IRI data. There was a significant decrease in IRI after the construction of the remediation techniques. The lime columns test section had the lowest values for IRI compared to the other test sections with a decrease in IRI by 103 in/mile. The edge drains test section also performed well with slightly higher IRI values than the lime columns test section with a decrease in IRI by 95 in/mile. It is important to note that the control, sand blanket, and vertical barriers test sections were resurfaced in 2014 prior to the first IRI survey; therefore, there is no baseline for these test section on the level of pavement distress before the resurfacing. The IRI values in 2014 for the

sand blanket and vertical barriers test sections were lower than the other starting IRI values likely due to the resurfacing. The sand blanket and vertical barriers test sections were the least improved test sections with IRI values decreasing roughly by 40 in/mile and 55 in/mile, respectively.

6.3 Sand Blanket (B1.5)

Strain data for the sand blanket test section is shown in Figure 73. The strain followed a compressive trend at the beginning of the project and has fluctuated from compression to tension throughout the entire project. There have been a few gages that have stopped sending data to the dataloggers. These gages include strain gage 3, 4, 5, and 8. Figure 74 shows the volumetric moisture content for the sand blanket test section. There have been increasing and decreasing trends depending on the season. There is normally an increase in VMC during the summer months and a decrease in VMC during the winter months. The sensor in the shoulder at a depth of 10 feet does not send data to the datalogger. Figure 75 shows the pore pressure data from the sand blanket section. The observed pore pressures have been relatively constant with minor fluctuations throughout the entire project.

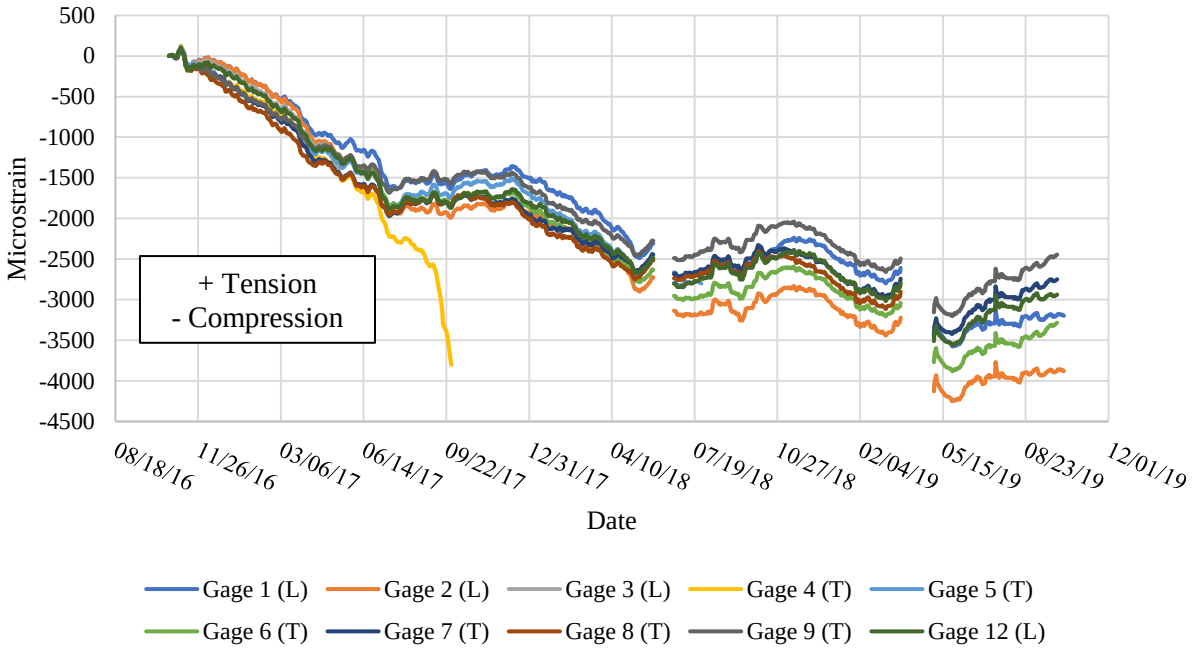

Figure 73: Strain with Time – Sand Blanket

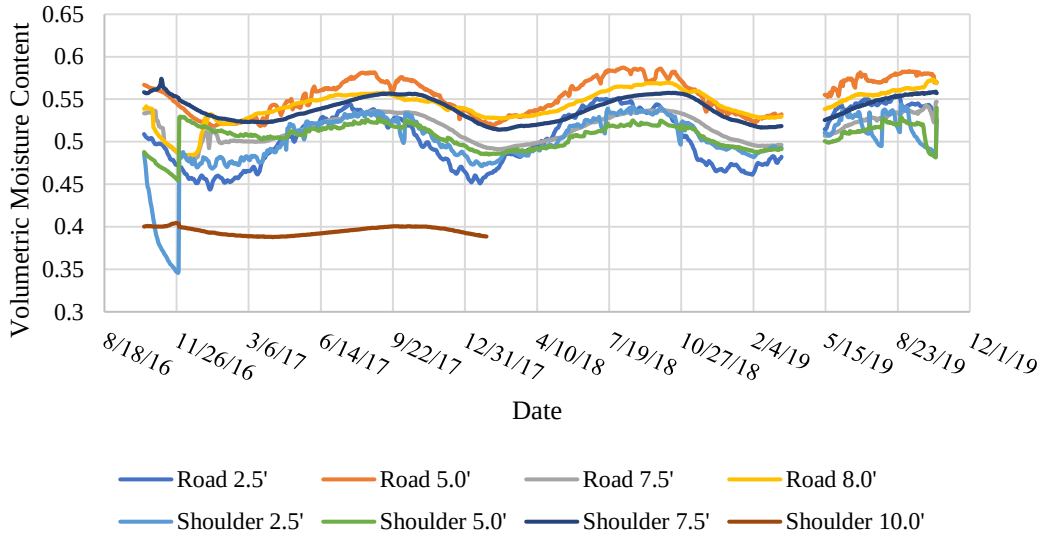

Figure 74: Volumetric Moisture Content with Time – Sand Blanket

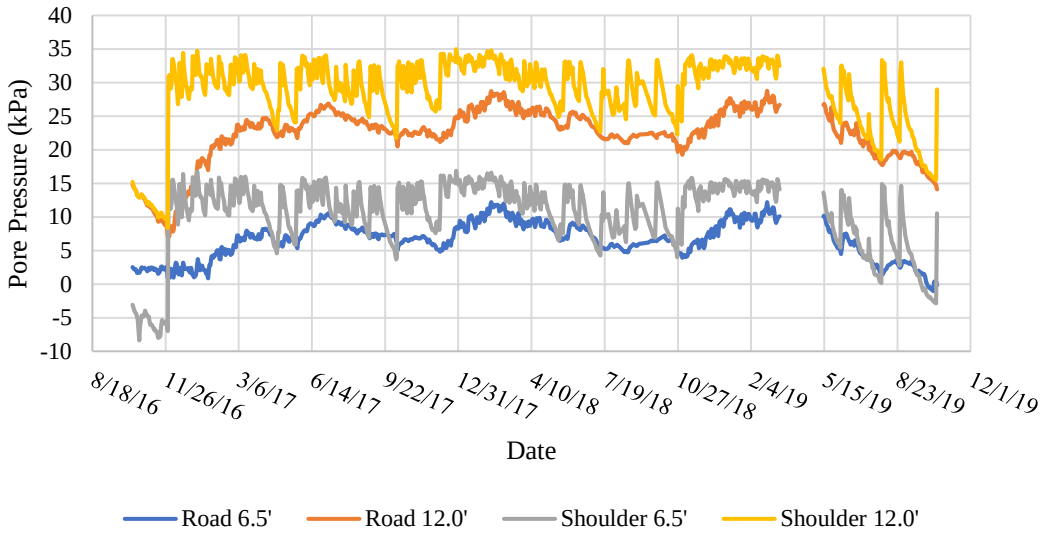

Figure 75: Pore Pressure with Time – Sand Blanket

6.4 Vertical Barriers (B2.5)

The strain data for the vertical barriers is shown in Figure 76. The strain has shown a slight compressive trend the entire project duration. There has been some increase in strain during the months of August 2017, May 2018, and June 2019. Gages 2 and 8 no longer send data to the datalogger. The moisture and pore pressure data are shown in Figure 77 and Figure 78. The VMC has remained relatively constant throughout the entire project except for the sensors at a depth of 2.5 feet in the road and shoulder. These two sensors decreased dramatically during the summer months of 2018. It is important to note that the sensors that are placed deeper into the soil have less variations in VMC than sensors closer to the asphalt concrete. The pore pressures had minor fluctuations with a larger decreasing magnitude in pore pressure in September 2019. Figure 79 shows the suction for the vertical barriers. There has been significant suction during August and September of 2019. This is thought to be caused by severe drought conditions experienced during these two months.

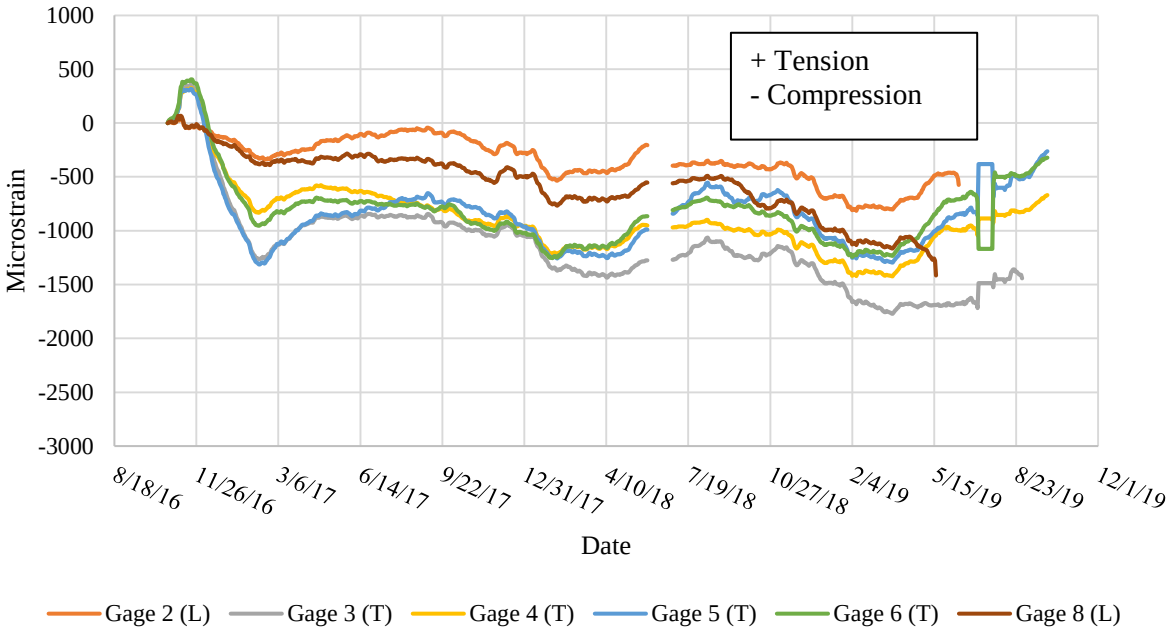

Figure 76: Strain with Time – Vertical Barriers

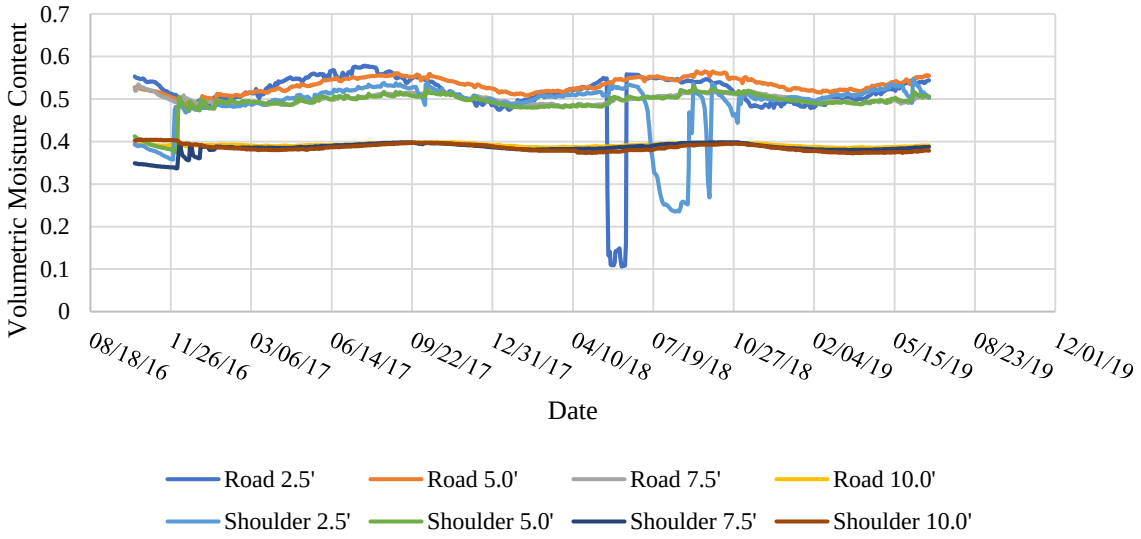

Figure 77: Volumetric Moisture Content with Time – Vertical Barriers

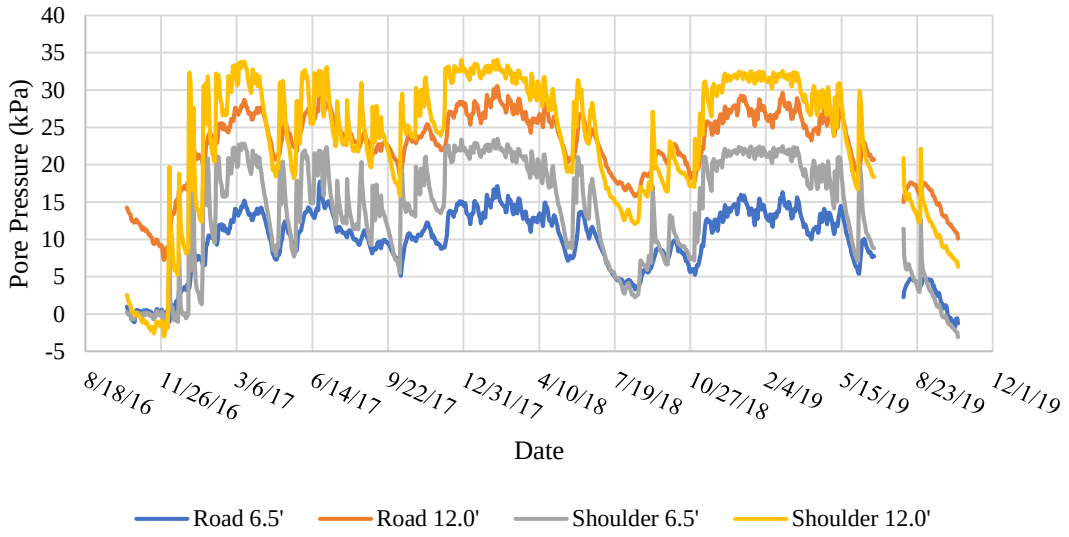

Figure 78: Pore Pressure with Time – Vertical Barriers

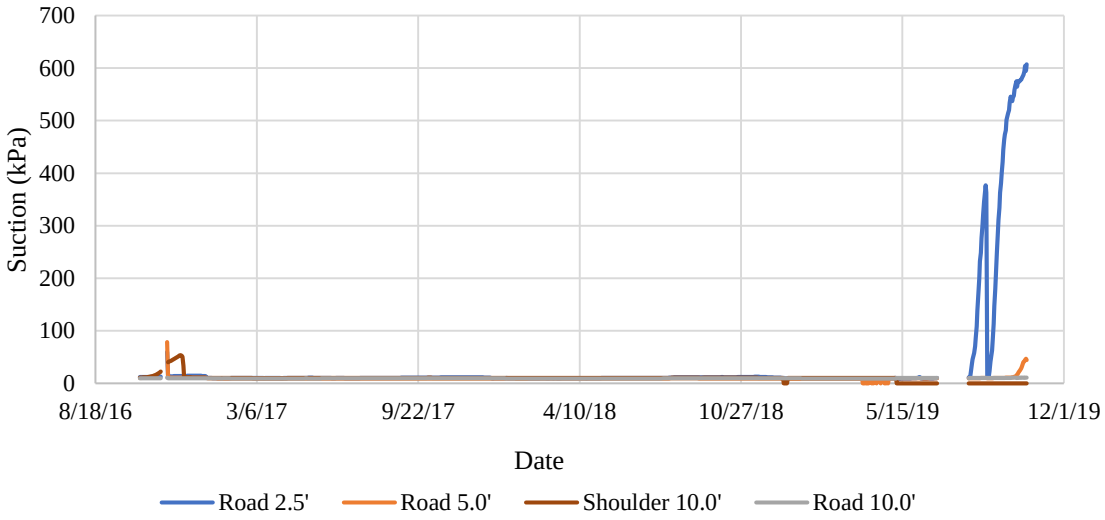

Figure 79: Suction with Time – Vertical Barriers

6.5 Lime Columns (B3.5)

Strain data for the lime columns section is shown in Figure 80. There have been fluctuating tension and compression trends during the duration of the project for the strain in the lime columns section. There are currently no strain gages sending data to the datalogger anymore. The last gage which was sending data was gage 5 and this gage stopped recording data

in the middle of July 2019. Figure 81 shows the volumetric moisture content values. As previously stated, the VMC increases and decreasing depending on the season. The sensors at a depth of 10 feet in the shoulder and the road does not vary as much as the remaining sensors. The pore pressures are shown in Figure 82. The piezometers show minor fluctuations with a large decrease in pore pressure during the month of June 2019.

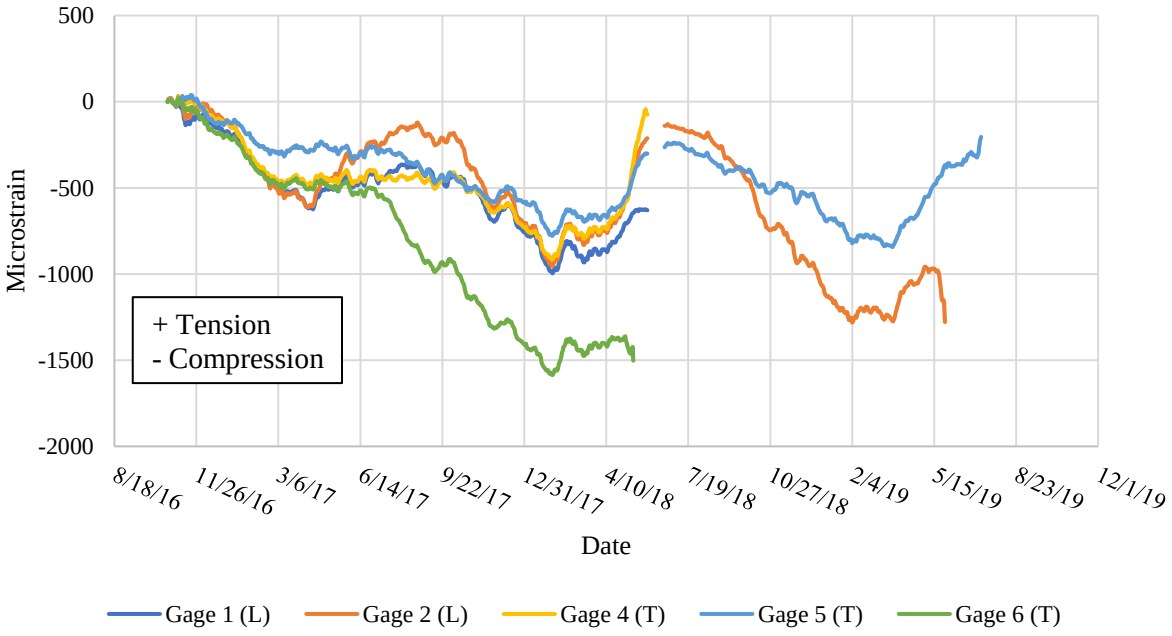

Figure 80: Strain with Time – Lime Columns

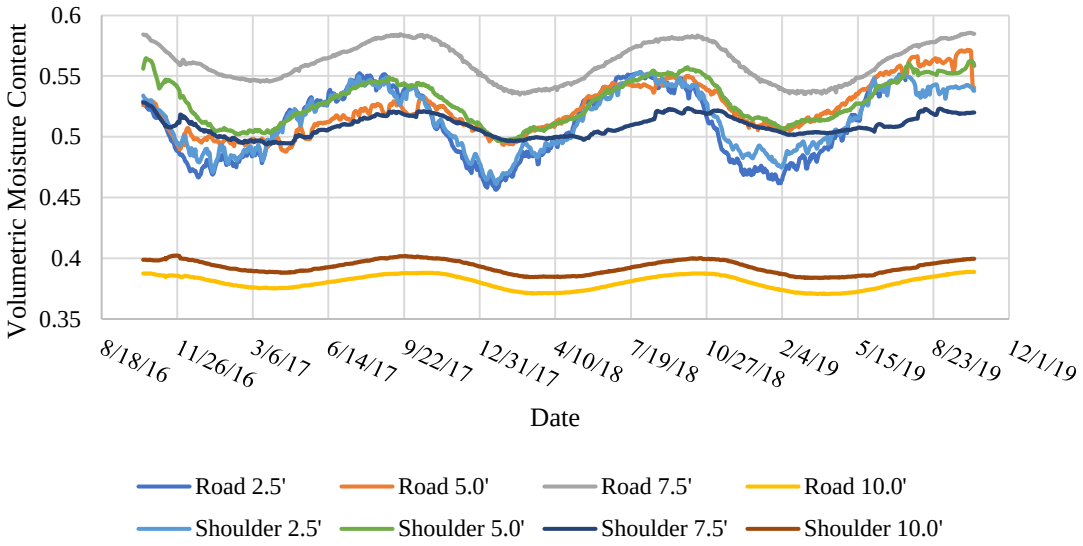

Figure 81: Volumetric Moisture Content with Time – Lime Columns

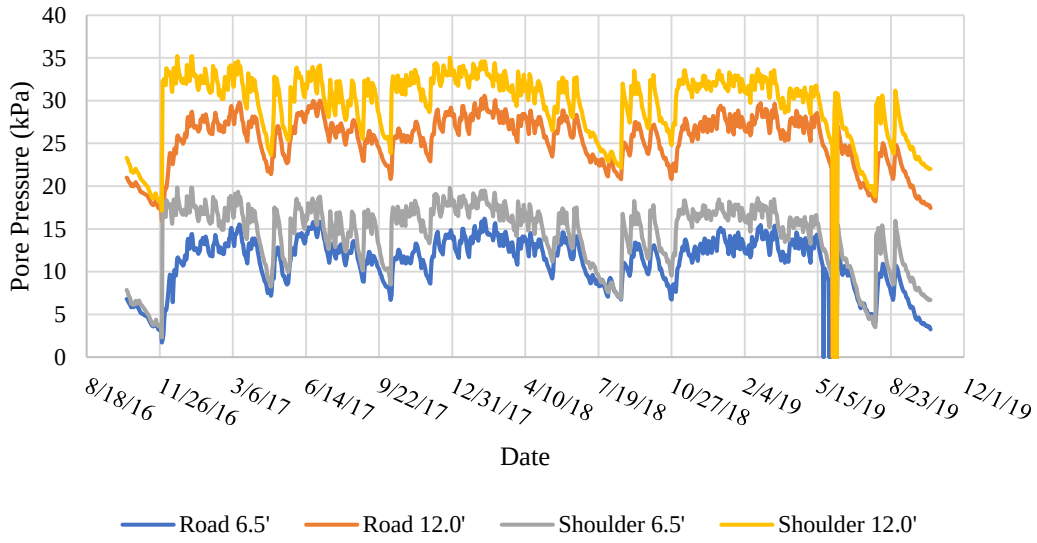

Figure 82: Pore Pressure with Time – Lime Columns

6.6 Paved Shoulders (B4.5)

The strain data is shown in Figure 83 for the paved shoulder test section. There have been increasing and decreasing trends throughout the project duration. Currently, there is only one gage still sending data to the datalogger. Gage 7 is still recording data for the paved shoulder

section. The strain tends to show a compressive trend during the winter months and a tensive trend during the summer months. The volumetric moisture content and pore pressure data are shown in Figure 84 and Figure 85. The sensors in the shoulder at a depth of 7.5 feet has recorded inaccurate data for this test section during the months of April 2019 through July 2019. There have been larger fluctuations in the VMC in the sensors closer to the surface. The pore pressures have shown minor variations; however, starting in May 2019, the magnitude of the pore pressures started to increase with some values becoming negative. Figure 86 shows the suction with time for the paved shoulder test section. There has been significant suction in this test section throughout the duration of the project. The sensor in the shoulder at a depth of 2.5 feet has shown the most amount of suction with values up to 1100 kPa.

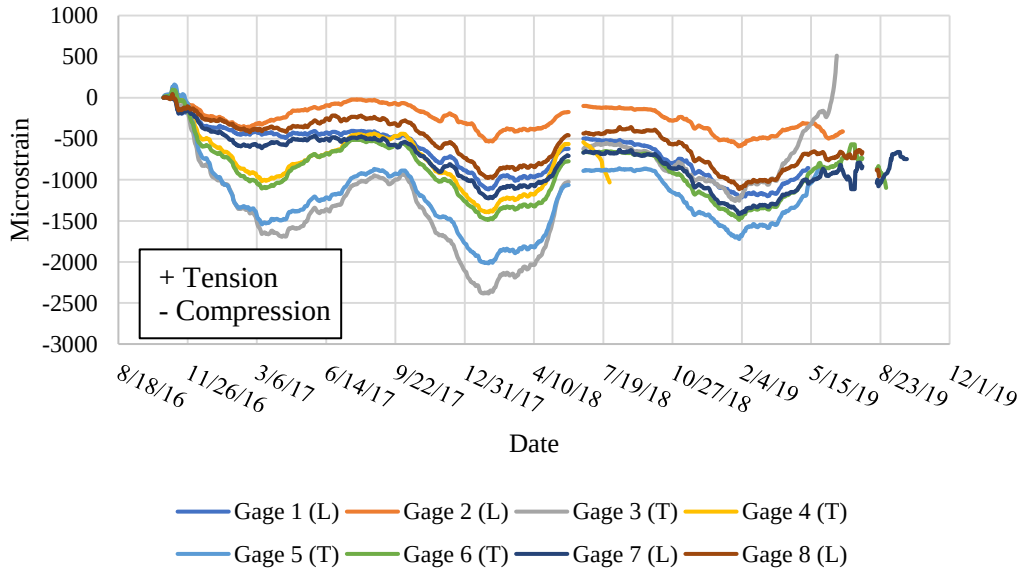

Figure 83: Strain with Time – Paved Shoulders

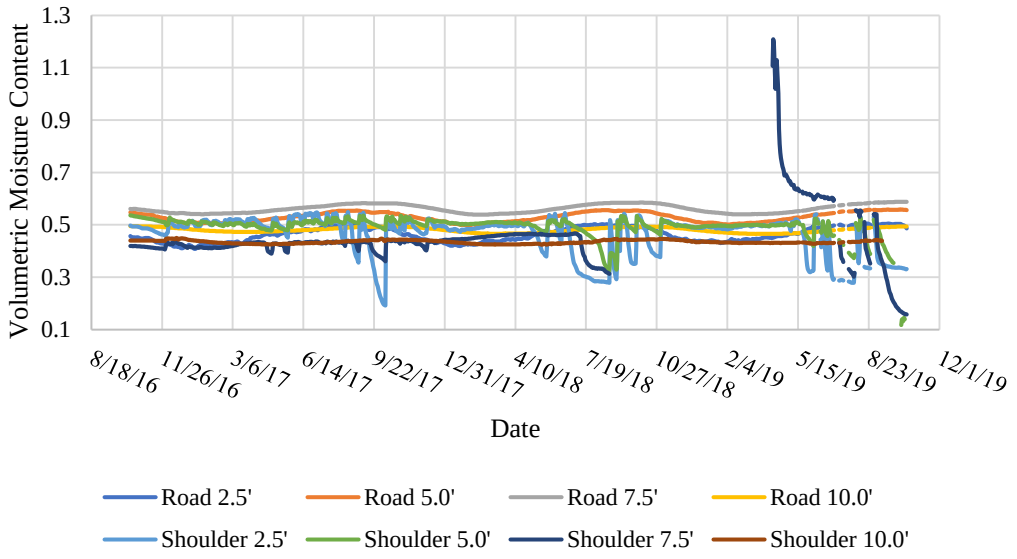

Figure 84: Volumetric Moisture Content with Time – Paved Shoulders

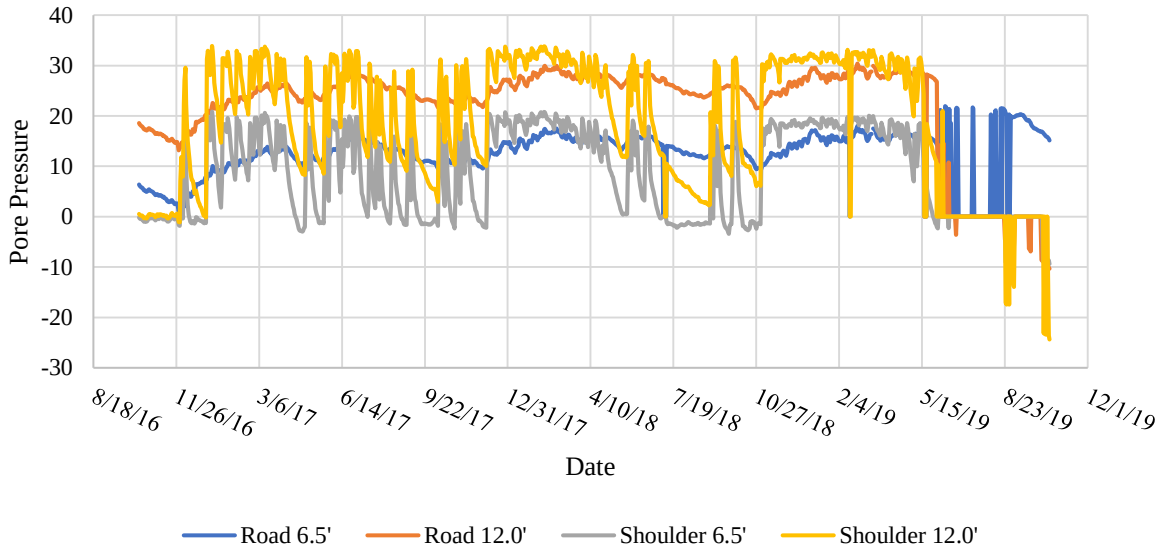

Figure 85: Pore Pressure with Time – Paved Shoulders

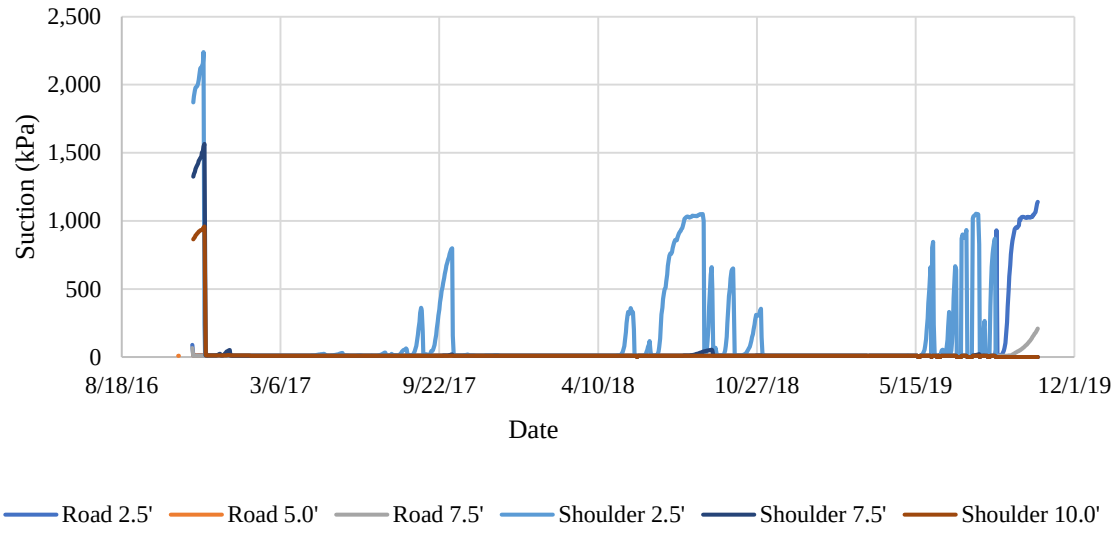

Figure 86: Suction with Time – Paved Shoulders

6.7 Edge Drains (B5.5)

The edge drain test section has provided sporadic data since October 2018; therefore, the data for the edge drains was truncated after October 2018. The inaccurate data is likely caused from a multiplexer issue in the test section because all the data from the moisture sensors, piezometers, and stain gages have been considered bad data. Strain data for the edge drains is shown in Figure 87. The strain had small variations at the beginning of the project; however, the variations of the strain data between the gages has gotten larger during the year of 2019. There has been a tensive trend the entire year of 2019. The volumetric moisture content is shown in Figure 88. The VMC increases during the summer months and decreases during the winter months. The sensors recording the VMC have not been recording properly since December 2018. There has been no new data since February 2019. The pore pressures are shown in Figure 89. There have been minor fluctuations throughout the entire project duration. There has also been significant suction in the edge drains test section as seen in Figure 90. The suction is primarily in

the sensors in the shoulder, but the road sensor at a depth of 5 feet is also showing suction with values up to 1150 kPa.

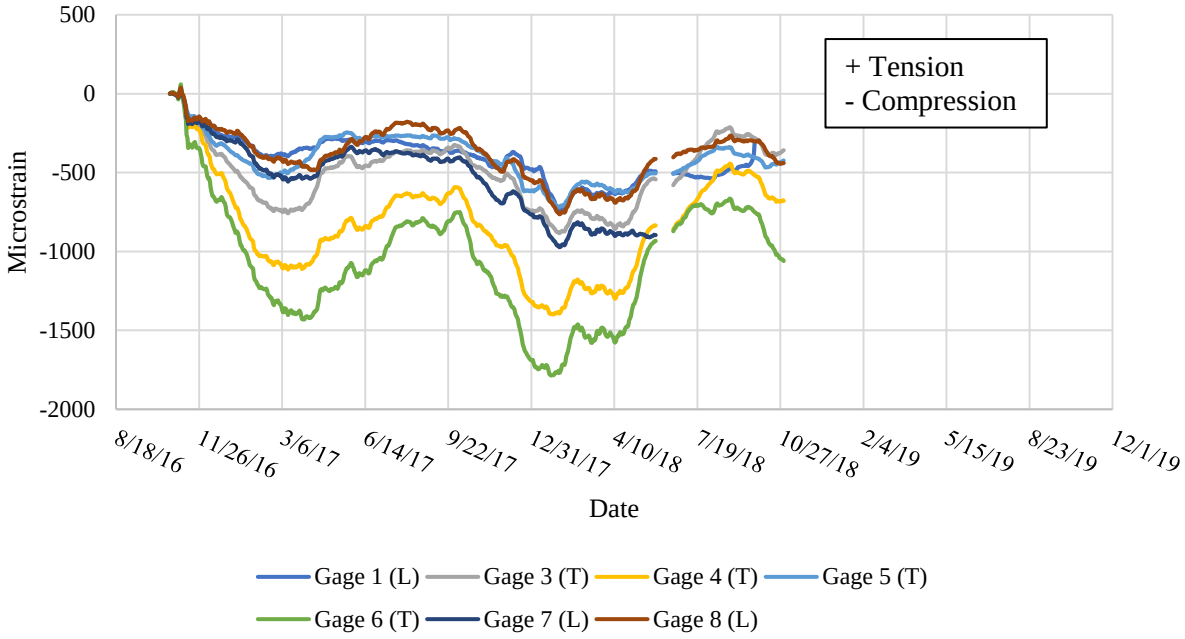

Figure 87: Strain with Time – Edge Drains

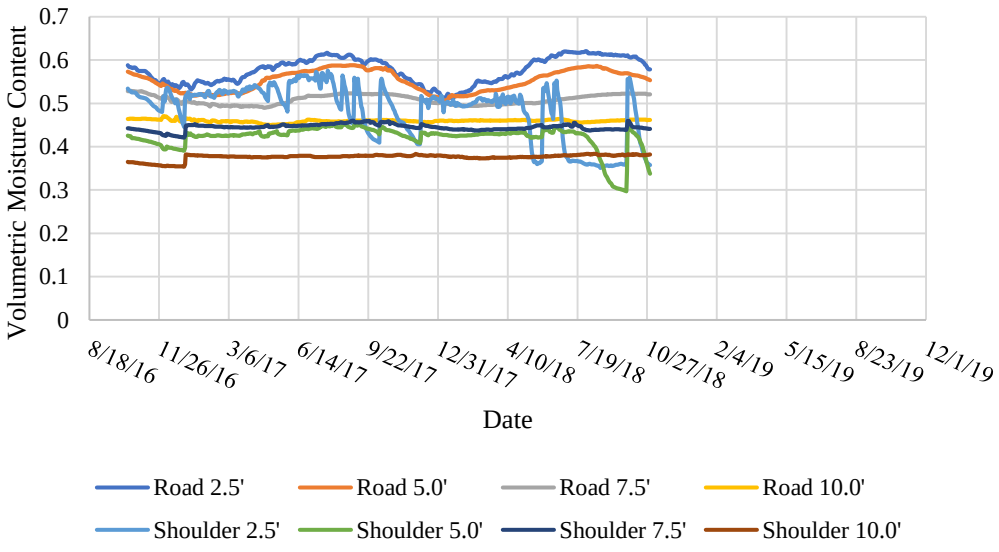

Figure 88: Volumetric Moisture Content with Time – Edge Drains

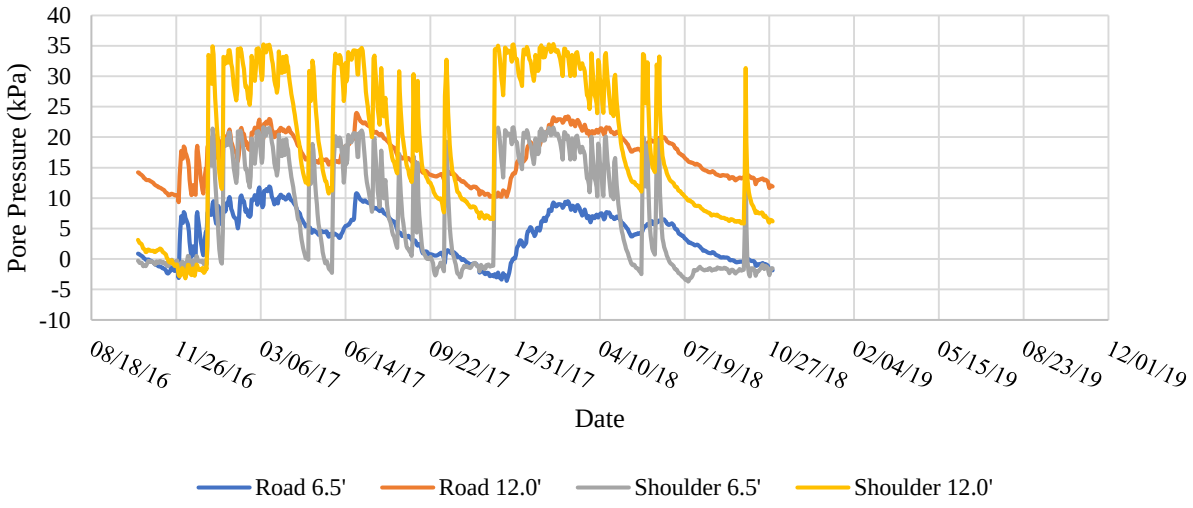

Figure 89: Pore Pressure with Time – Edge Drains

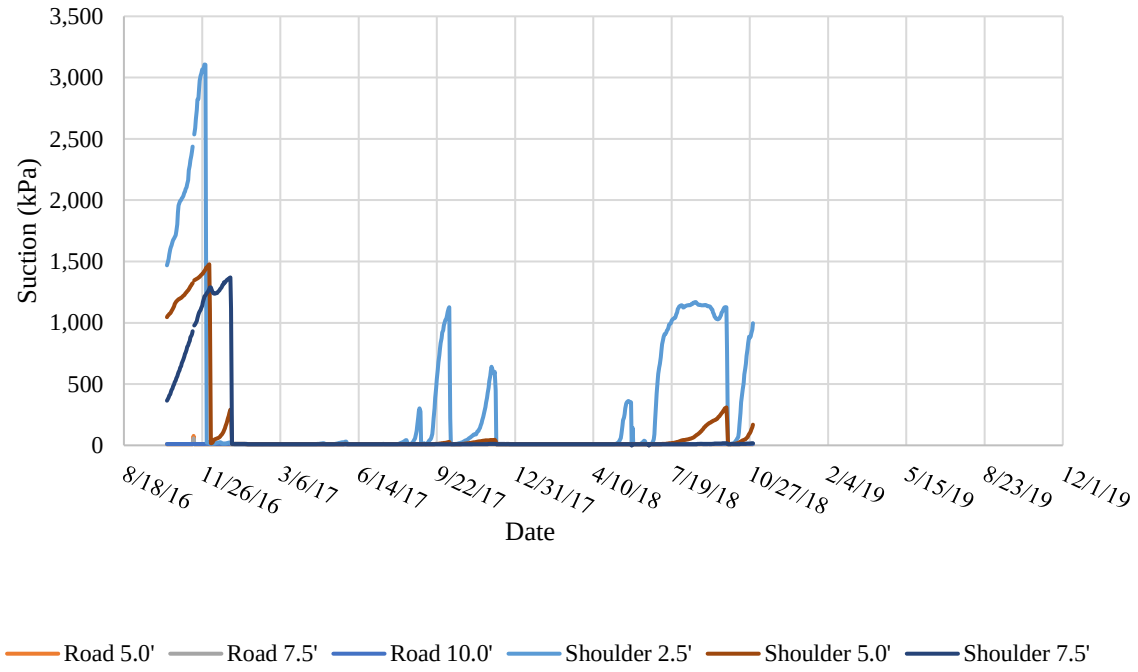

Figure 90: Suction with Time – Edge Drains

6.8 Control

Strain gage data for the control section in shown in Figure 91. The strain shows decreasing trends during the winter months and increasing trends in the summer months. There is

only one gage left recording data which is gage 7. The variation of the strain at the beginning of the project was very small, but the variation of the gages increases as the project continues. The moisture and pore pressure data are shown in Figure 92 and Figure 93. The VMC has fluctuated depending on the season. The sensors at the shallower depths have larger variations than the sensors that are deeper into the subgrade. The pore pressures have had minor fluctuations throughout the entire project.

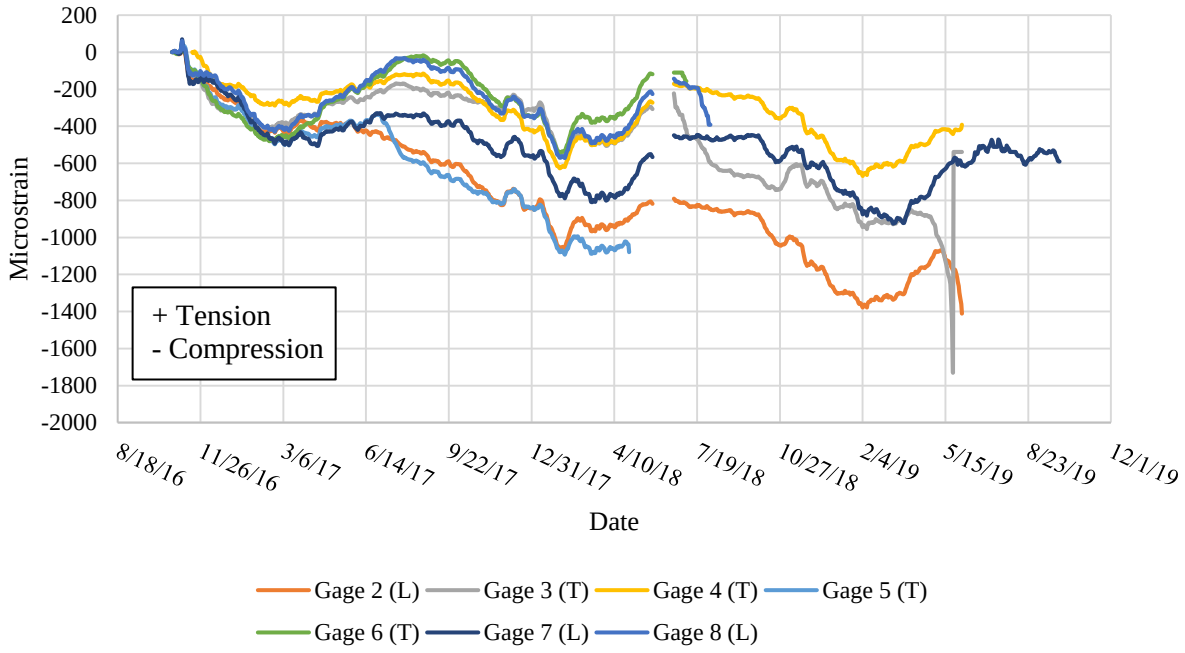

Figure 91: Strain with Time – Control

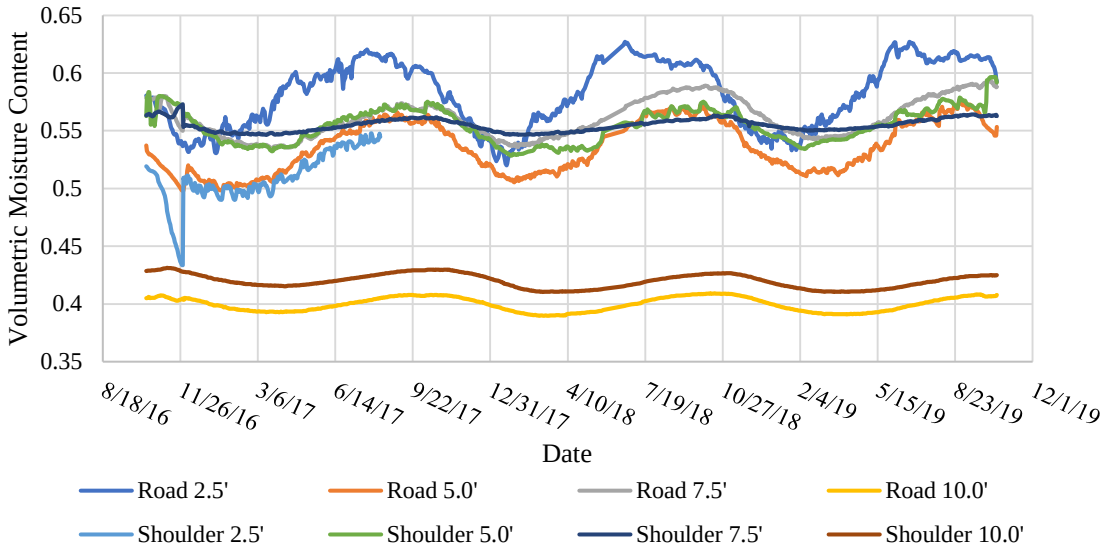

Figure 92: Volumetric Moisture Content with Time – Control

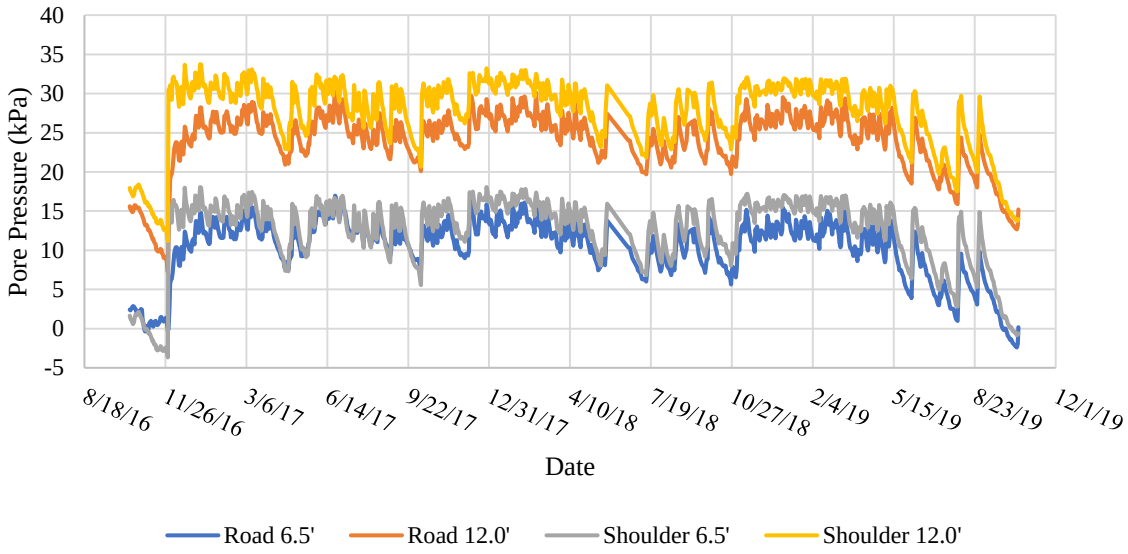

Figure 93: Pore Pressure with Time – Control

6.9 Trees

Additional moisture and suctions sensors were installed at mile point 53.287 to evaluate the subgrade. The location of these sensors are near a large tree. These sensors were placed near the tree to determine if the trees or vegetation have any affect on the performance of the

subgrade. The volumetric water content is shown in Figure 94. There have been large decreases and increases in the VMC for the tree sensors specifically from June 2018 to November 2018 and May 2019 to present. It is important to note that these large variations occur during the summer when drought conditions are possible. Significant suction has been seen in this test section also. Figure 95 shows the suctions with time for the tree sensors. Suction can be seen close to the roadway at depth of 2.5 feet and close to the tree at a depth of 5 feet. Suction values have been as high as 1500 kPa in this test section.

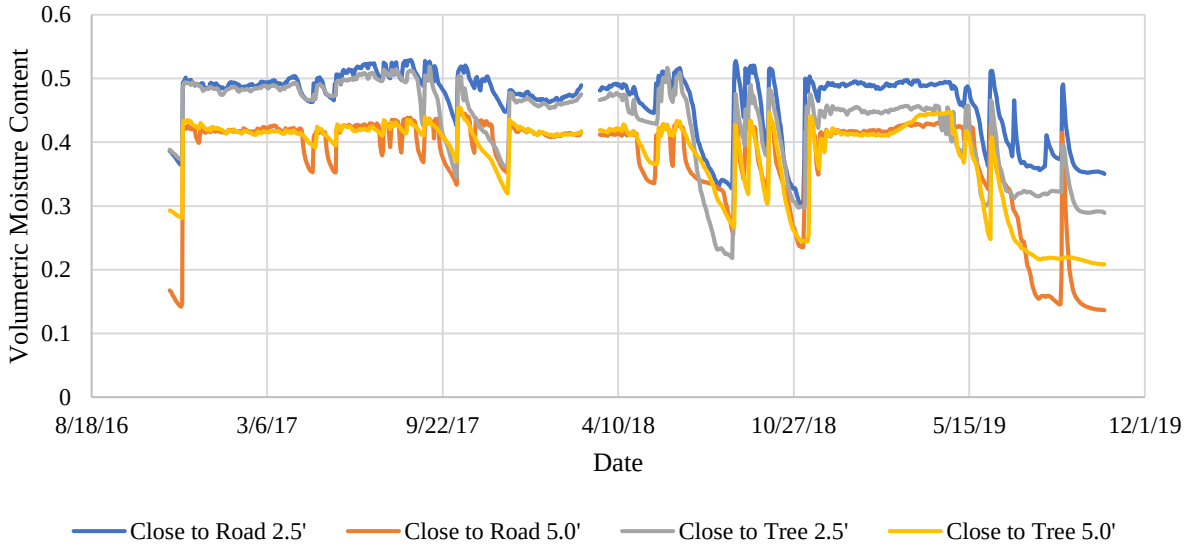

Figure 94: Volumetric Moisture Content with Time – Trees

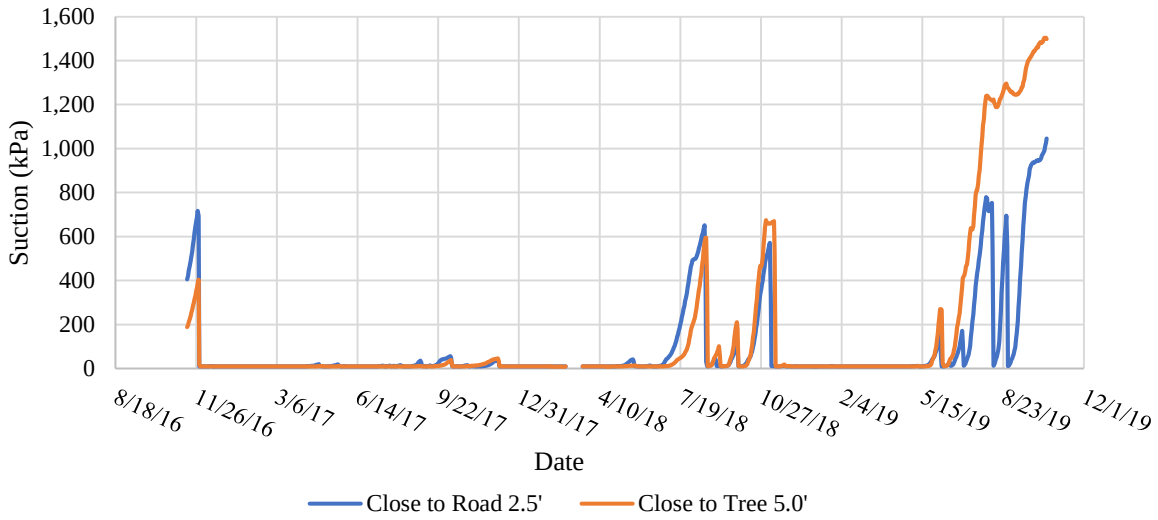

Figure 95: Suction with Time – Trees

6.10 Combined Data

The remediation techniques were placed throughout the subgrade of AL-5 to stabilize the moisture contents of the soil. The fluctuating moisture contents caused the expansive clays to shrink and swell based on seasonal variations. The moistures sensors were compared from each location and depth to determine if one remediation technique stabilized the moisture contents better than others. The average VMC was subtracted from the daily VMC for each sensor at each depth to obtain a normalized VMC. The normalized VMC allows the tests sections to be compared to each other without the effect of different initial conditions. The VMC for sensors installed in the roadway at depths of 2.5 ft, 5.0 ft, 7.5 ft, and 10 ft are shown in Figure 96 through Figure 99.

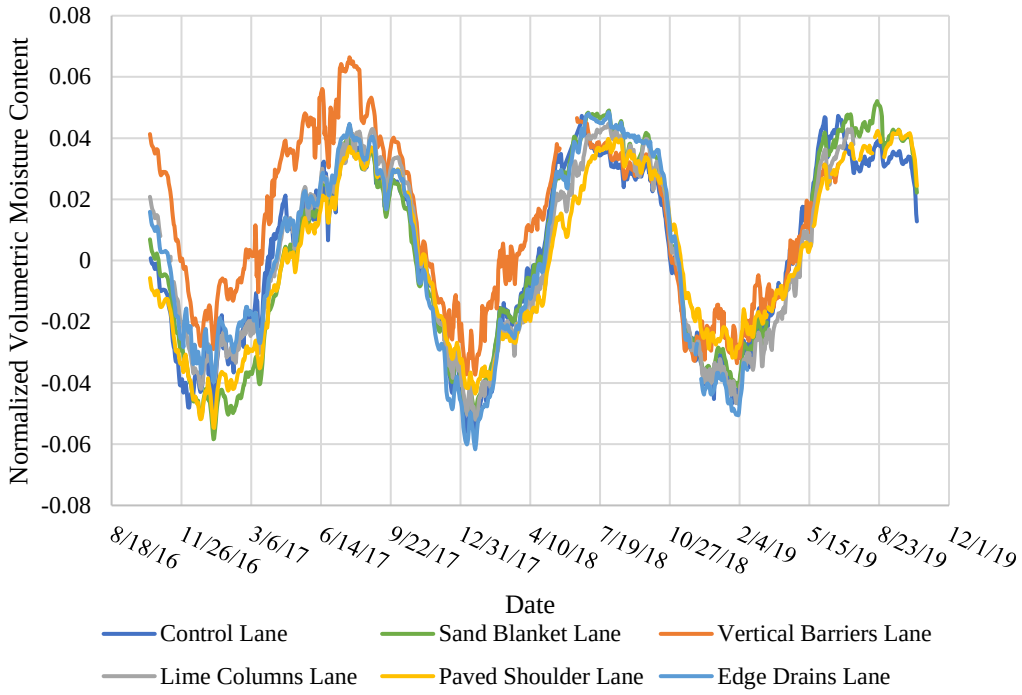

Figure 96: Normalized VMC of Roadway at a Depth of 2.5'

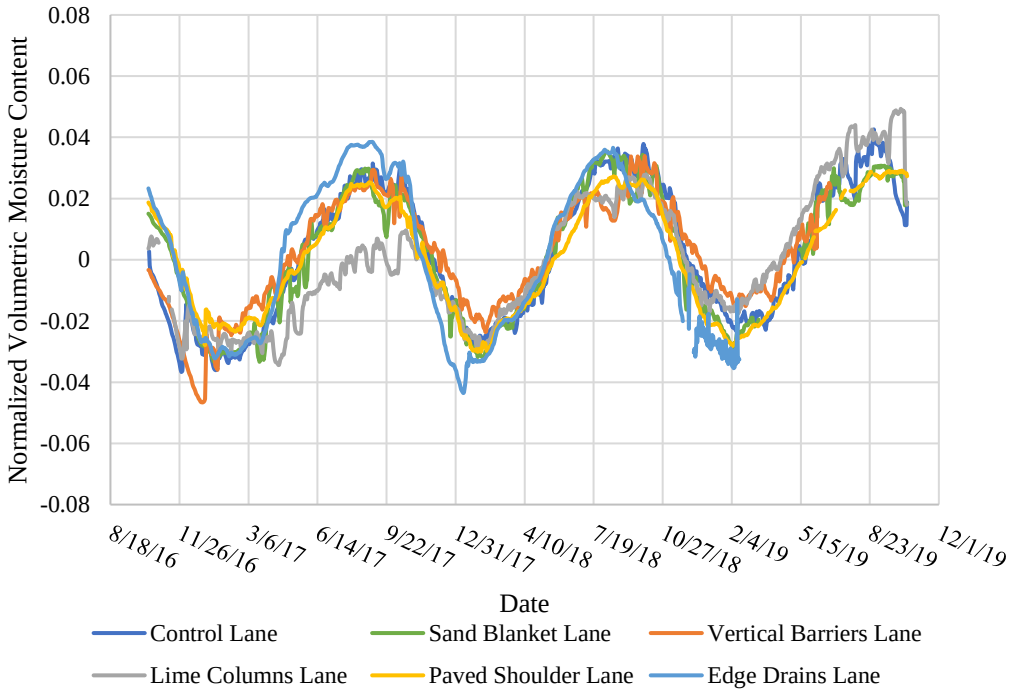

Figure 97: Normalized VMC of Roadway at a Depth of 5.0'

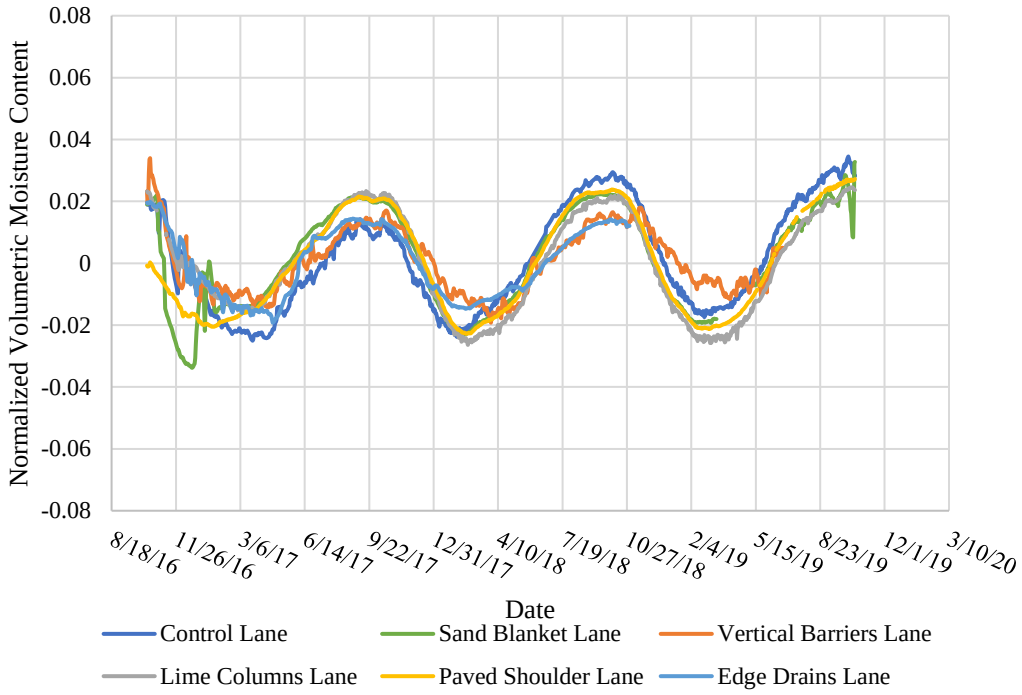

Figure 98: Normalized VMC of Roadway at a Depth of 7.5'

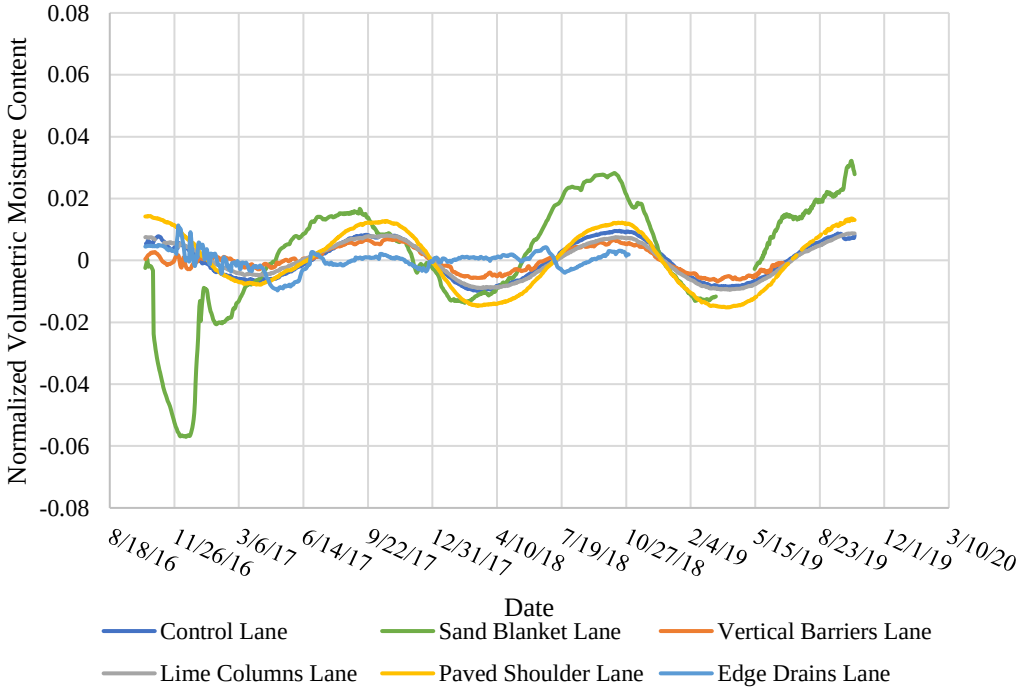

Figure 99: Normalized VMC of Roadway at a Depth of 10.0'

In Figure 96, the VMC varied with seasonal changes. During the summer months, the VMC increased and during the winter months, the VMC decreases. On average, the fluctuations of the moisture content had a magnitude of 0.06 or 6% from average. All the test sections performed similar with the fluctuations varying with the season. In Figure 97, the fluctuations of the VMC had a magnitude of 0.04 to 0.05 or 4% to 5%. The lime column test section had the lowest recorded normalized VMC for the sensors installed at 5 ft. In Figure 98, the variations in VMC for each section had a magnitude of 0.02 to 0.03 or 2% to 3%. The vertical barriers and edge drains test sections stabilized the subgrade the best according to the normalized VMC. The edge drains test section started recording sporadic data during Fall 2018; therefore, the data was truncated in October 2018. In Figure 99, the variations in the seasonal VMC had a magnitude of 0.01 to 0.02 or 1% to 2% for the majority of the test sections. The sand blanket VMC had larger fluctuations for the normalized VMC with a magnitude of 0.02 to 0.06 or 2% to 6%. The lime columns and edge drain test sections had the lowest VMC compared to the other test sections. As shown in the figures above, as the sensor depth increases, the magnitude of the fluctuations decreases and the normalized VMC becomes more of a straight line. Based on the VMC from the roadway sensors, the lime columns and edge drain test sections performed the best in stabilizing the water content with low VMC values and small fluctuation magnitudes.

The VMC sensors in the shoulder were located at depths of 2.5 ft, 5.0 ft, 7.5 ft, and 10 ft. There were seasonal variations in VMC as shown in Figure 100 through Figure 103. The VMC for each sensor was normalized with the average VMC as explained previously.

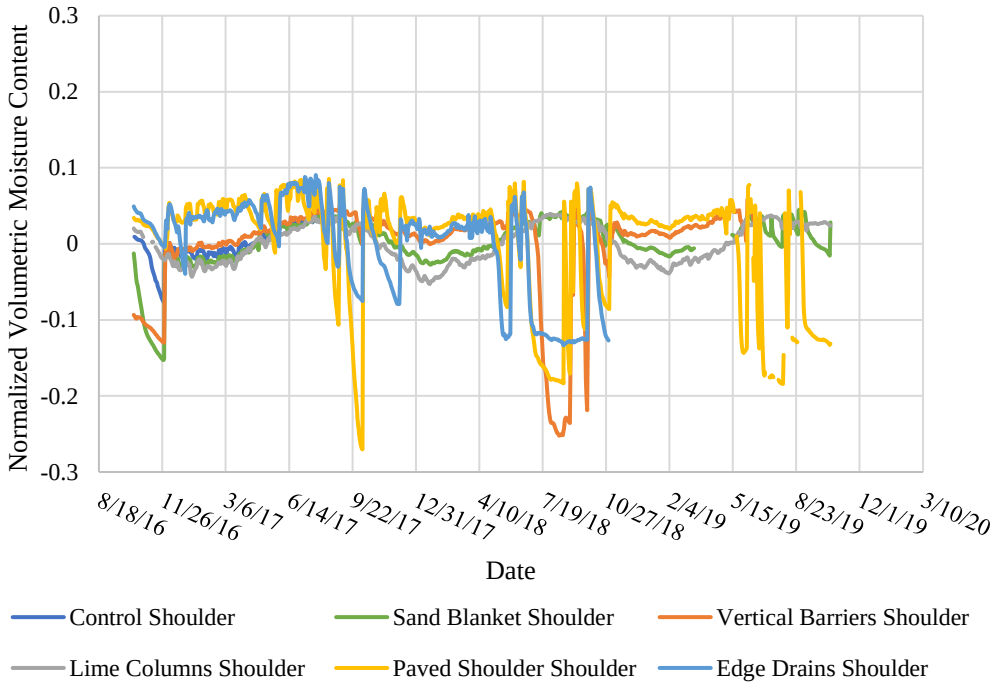

Figure 100: Normalized VMC for Shoulder at a Depth of 2.5'

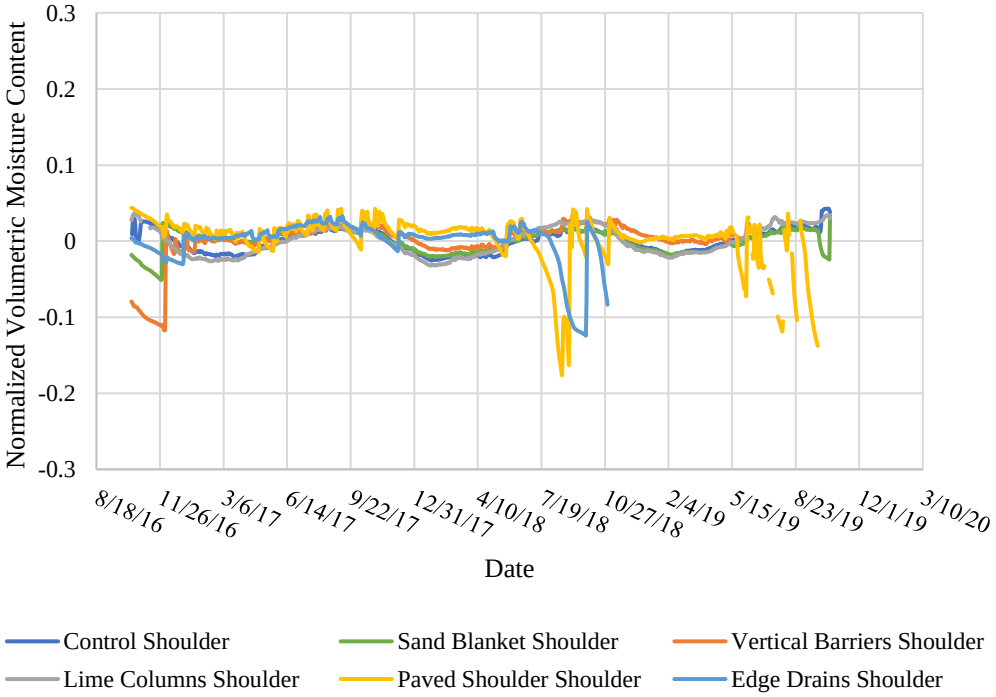

Figure 101: Normalized VMC for Shoulder at a Depth of 5.0'

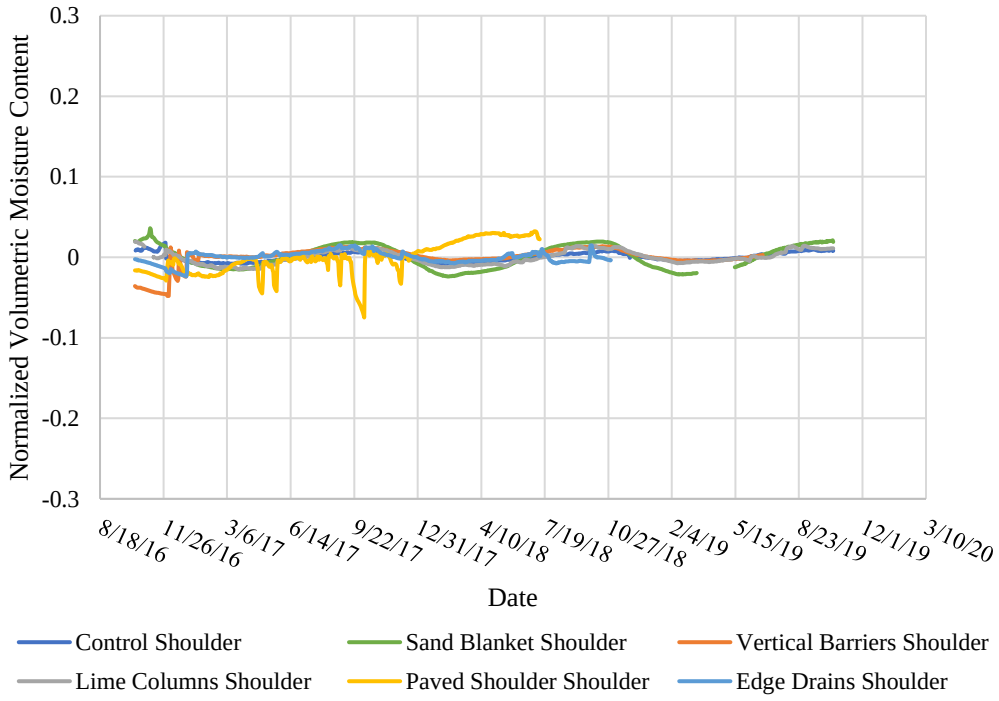

Figure 102: Normalized VMC for Shoulder at a Depth of 7.5'

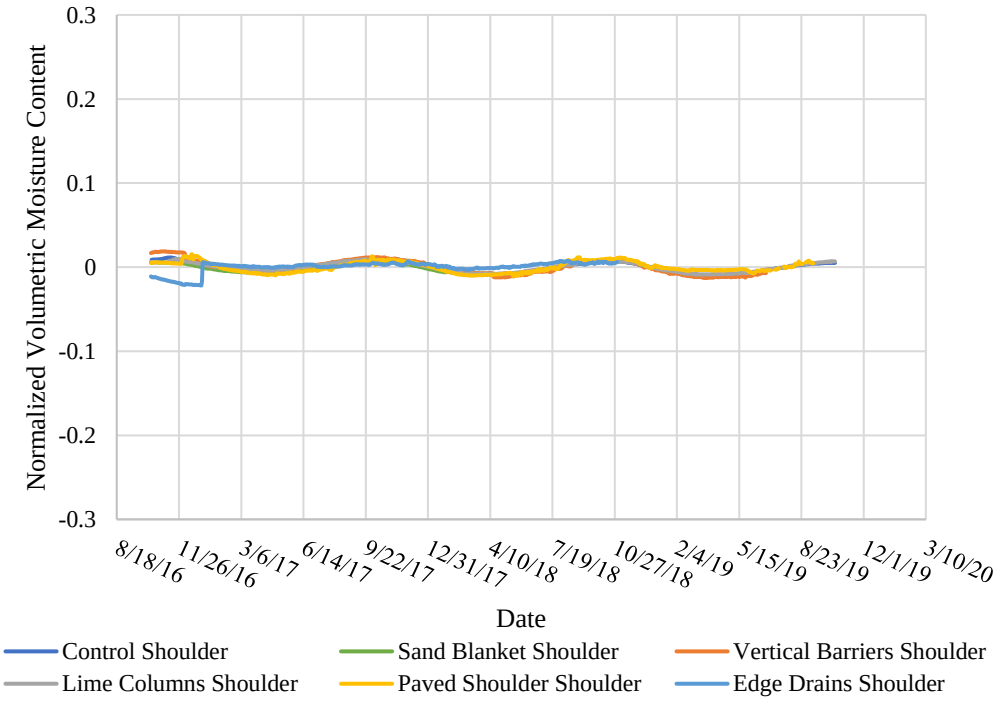

Figure 103: Normalized VMC for Shoulder at a Depth of 10.0'

In Figure 100, there were large fluctuations in the VMC sensor at a depth of 2.5 ft for the paved shoulders, edge drains, and vertical barriers test sections. The fluctuations had a magnitude ranging from 0.12 to 0.25 or 12% to 25%. The remaining test sections had smaller variations with a magnitude of 0.04 to 0.05 or 4% to 5%. As mentioned previously, the edge drains VMC data was truncated at the end of October 2018 due to a faulty sensor. In Figure 101, the edge drains and paved shoulder test sections had larger variations in VMC than the remaining test sections. These test sections had fluctuation magnitudes of 0.12 to 0.17 or 12% to 17%. The remaining test sections had variation magnitudes of 0.02 to 0.03 or 2% to 3%. The lime columns, vertical barriers, and sand blanket test sections resulted in the lowest VMC for the sensors installed at a depth of 5.0 ft. In Figure 102, The paved shoulder test section had the largest variation in VMC with magnitudes up to 0.07 or 7%. All other test sections had fluctuation magnitudes of 0.01 to 0.02 or 1% to 2%. The vertical barriers and lime columns test sections resulted in the lowest VMC for sensors installed at a depth of 7.5 ft. However, the control test section had the smallest variation in VMC throughout the years. In Figure 103, the test sections had fluctuation magnitudes of 0.01 to 0.02 or 1% to 2%. The edge drains resulted in the smallest variation in VMC and the lowest VMC values. As the sensor depth increases, the fluctuations in VMC decreases. Based on the VMC sensors in the shoulder of each test section, the sand blanket and lime column test sections consistently stabilized the VMC more than the remaining test sections.

6.11 Photographs

After construction of the remediation techniques and installation of the sensors and gages, photographs were taken during each site visit. The vertical barriers test section was the

first section to experience cracking. These cracks were observed on a site visit on December 15th, 2016 and can be seen in Figure 104.

Figure 104: Longitudinal Crack in Vertical Barrier Section December 2016

The research site was visited in September 2017. The roadway was still smooth with no signs of heaving due to the subgrade. A small patch of asphalt had been placed over a culvert in the lime columns test section resulting in an increase in the IRI at that mile point. The patched roadway is shown in Figure 105.

Figure 105: Location of IRI Spike (Culvert Patch) in Southbound Lime Columns Section September 2017

During a site visit in December 2017, continuous cracking of the vertical barriers test section was observed as shown in Figure 106. These cracks have been stable for nearly a year and have not developed into larger cracks. All other test sections have not shown signs of cracking.

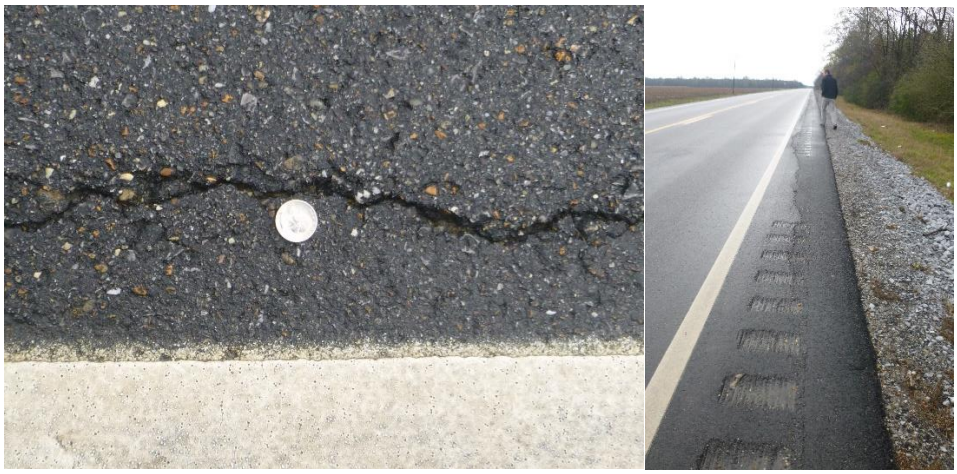

Figure 106: Cracking along Vertical Barriers December 2017

Additional photographs were taken of AL-5 between US 80 and the Dallas County line during the site visit in December 2017. The roadway was experiencing major pavement distress

specifically where non-pine species trees encroach the roadway. Figure 107 shows the distress on AL-5 that continues into the town of Safford. There is a section of roadway near Safford where the shoulder was constructed 8 feet wide. As shown in Figure 108, the pavement distress throughout this section of roadway was contained in the paved shoulder area.

Figure 107: Tree Related Distress on AL-5 in Dallas County December 2017

Figure 108: Paved Shoulder Section of AL-5 in Dallas County December 2017

A site visit was completed in November 2018. New cracks had formed in the paved shoulder test section and can be seen in Figure 109. It is important to note that the cracks formed in the shoulder and not in the travel lane. Figure 110 shows pavement distress in the traffic lane of the paved shoulders test section. The type of distress is known as shoving and was thought to

have occurred from poor construction or asphalt mixing techniques. Continuous cracking in the vertical barriers test section was also observed.

Figure 109: Cracks in Paved Shoulder Test Section November 2018

Figure 110: Paved Shoulder Test Section Travel Lane November 2018

During a site visit in December 2018, additional cracks were observed in the paved shoulder test section only one month after the previous site visit. Figure 111 shows the pavement

distress and cracks in the paved shoulder test section. The pavement distress was thought to have occurred because of poor asphalt concrete construction.

Figure 111: Pavement Distress and Cracks in Paved Shoulder Test Section December 2018

In June 2019, a site visit confirmed more damage to the paved shoulder test section with the cracks becoming deeper and wider. These cracks can be seen in Figure 112. The vertical barriers test section continued to develop minor cracks.

Figure 112: Paved Shoulder Cracks June 2019

The most recent site visit occurred on October 16th, 2019. The cracks in the vertical barriers test section had significantly worsened. During the site visit, large tractor tires were visible on the shoulder of the roadway; therefore, it is thought that the wide track farming

equipment caused the existing crack to widen and settle as shown in Figure 113. Cracks developed in the shoulder and lane in the edge drain test section. These cracks can be seen in Figure 114.

Figure 113: Vertical Barriers Crack October 2019

Figure 114: Shoulder and Lane Cracking in the Edge Drain Test Section October 2019

CHAPTER 6: LABORATORY RESEARCH METHODS

6.1 Torsional Ring Shear Apparatus

Drained torsional ring shear tests were conducted on material from AL-5 using a Controls Group (Wykeham Farrance) Bromhead Ring Shear Apparatus. Figure 115 shows the ring shear testing device used for research labeled with parts.

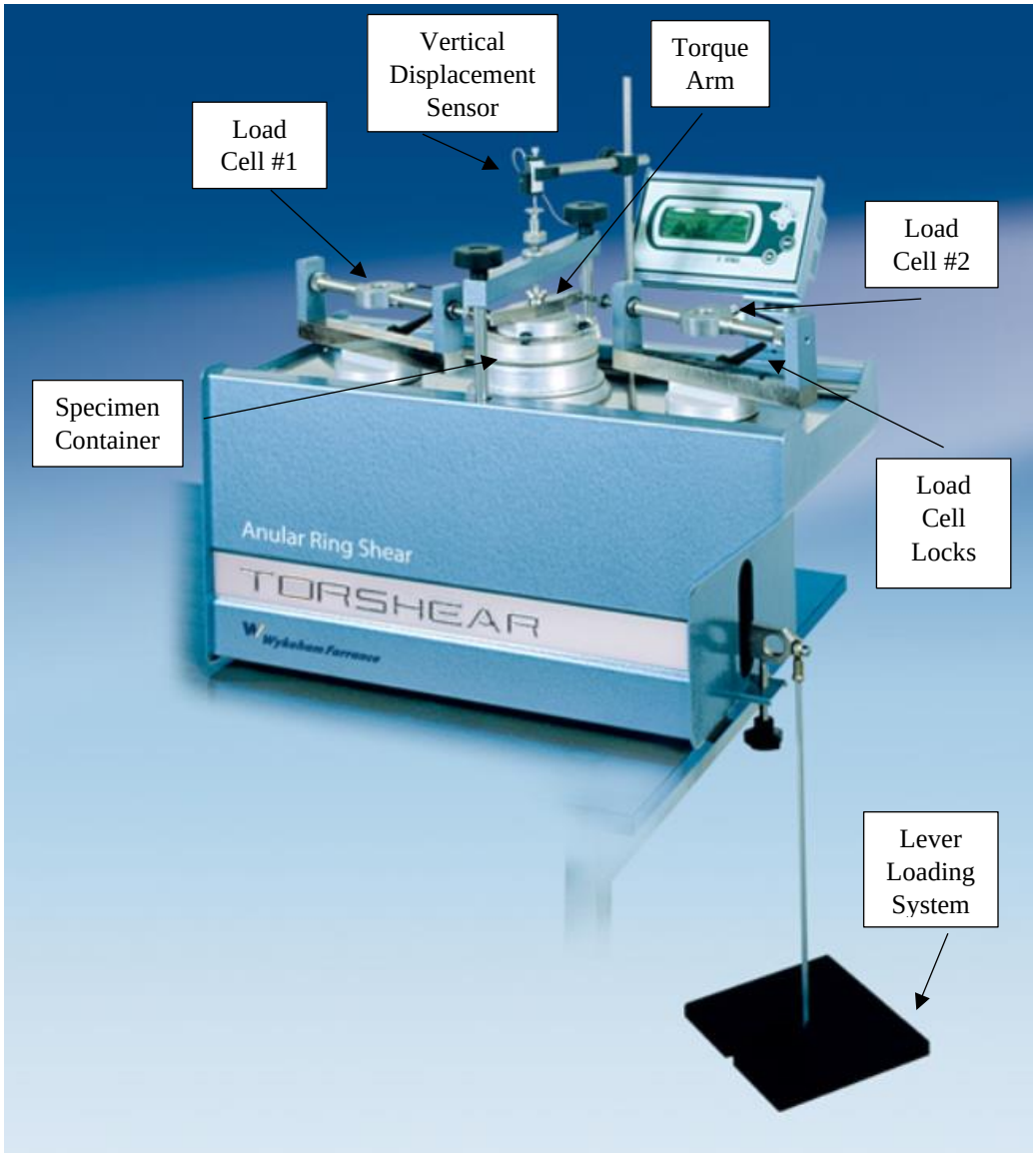

Figure 115: Controls Group Bromhead Ring Shear Apparatus (Controls Group 2019)

Normal stress is applied using a counter balanced lever loading system with a 10:1 mechanical advantage. The GEODATALOG 8, shown in Figure 116, is a multichannel data logger used to collect measurements from the ring shear apparatus and transfer the information to a computer in real time. DATACOMM 2 is the computer software used to collect data from the data logger. Data collection rates can be changed using the software along with programing a start and/or end time automatically when certain criteria conditions are met.

Manufacturer zero offset factors for the sensors were used for the ring shear device. No zero offset for Load Cell #1 was needed as the load cells only reach a value of around 100 N. Load Cell #2 has a zero offset of -0.1 N at a force of 100 N. The displacement transducer has a zero offset of +0.003 mm when the instrument reaches 1.000 mm.

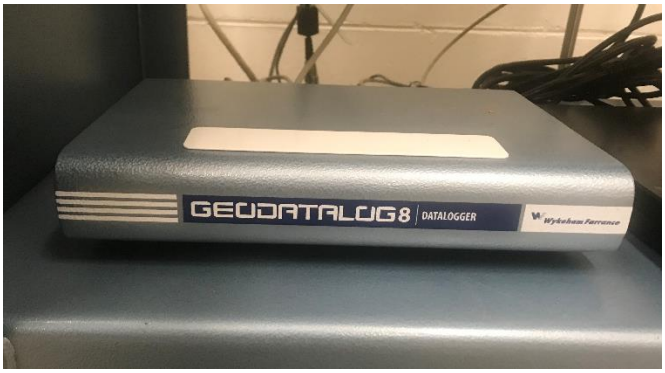

Figure 116: GEODATALOG 8 Data Logger

6.2 Porous Stone

A new porous stone design used in the modified Bromhead ring shear apparatus was constructed (Stark and Hisham 1993) and the procedure described in ASTM D6467 were used to measure the drained residual shear strength of the material (ASTM 2013). The procedure described in ASTM D7608 was used to measure the fully softened strength or peak strength of

the material (ASTM 2018). The specimen container has an outside diameter of 100 millimeters, an inside diameter of 70 millimeters, and an initial height of 8 millimeters. Multiple thinner 3-millimeter bronze porous stones were machined using a Haas CNC milling machine in order to reduce the amount of wall friction the porous stone contributes to the container. As the top porous stone settles into the soil specimen, the wall friction increases resulting in an increase in measured residual strength. The porous stone should also be "flush" with the top of the container in order to reduce the amount of settlement of the soil specimen; therefore, decreasing the amount of wall friction. A more aggressive serration pattern was also cut into the porous stone to provide better interlocking between the soil specimen and the porous stone (Stark 2016). Figure 117 shows an example of one of the porous stone used for AL-5 torsional ring shear testing and Figure 118 displays the final apparatus used for testing. When the porous stones are not being used, they are in a vacuum water bath to clean the stones and keep them moist.

Figure 117: Machined Porous Stone with Serration Pattern

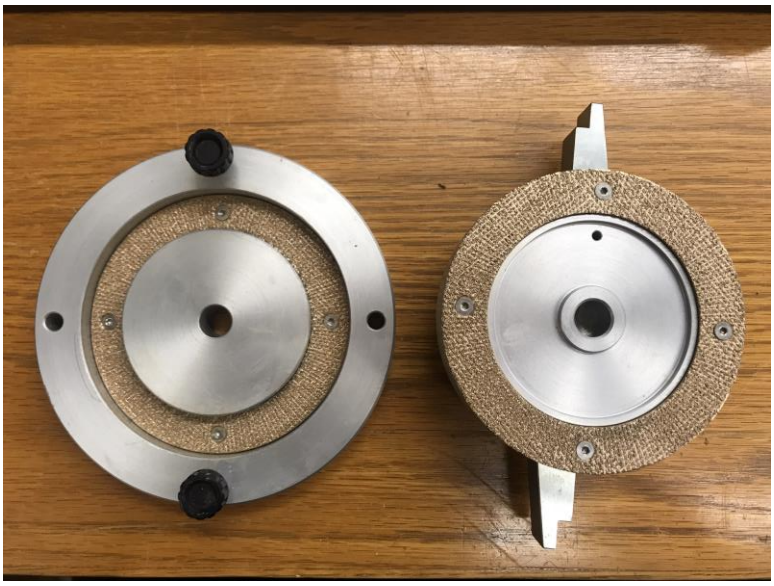

Figure 118: Ring Shear Apparatus with Porous Stones

6.3 Specimen Preparation

An initial subsurface investigation was performed in November 2013. Seventeen boreholes were drilled using a CME 55 truck mounted drill rig with solid stem augers and an automatic hammer. Additional boreholes were drilled in April 2015 and May 2016. The soil was collected using thin-walled tubes and two-inch outer diameter split barrel samplers. Boring logs reported layer 1 was located from the subsurface to a depth of 7 to 17 feet depending on the location and generally consisted of clay. Layer 2 was beneath layer 1 to a depth in which the sampling was terminated. Layer 1 consisted of fat clay and layer 2 was chalk material. The boring logs can be found in Appendix A: Boring logs.

The material from the previous subsurface investigation was oven dried and sieved. The material passing through U.S. Standard Sieve No. 40 or having a grain size less than 0.42 millimeters, was collected and separated for each borehole location and layer. Distilled water was added to the material until a target average field volumetric moisture content was achieved.

The soil specimens were supposed to be prepared to a water content near the liquid limit; however, when this material was prepared to the liquid limit, the soil had too high of a water content to test. Figure 119 shows material from the sand blanket test section prepared to the liquid limit. Therefore; in order to achieve the target VMC, an equation relating gravimetric water content and volumetric moisture content must be used as shown in Equation 13. Table 9 shows the target volumetric moisture contents and Table 10 shows the target gravimetric moisture contents computed using Equation 13.

Figure 119: Sand Blanket Material Prepared to Liquid Limit

$$VMC = \frac{GWC}{100} * \frac{\rho_d}{\rho_w} \qquad \text{Equation 13}$$

Where VMC = volumetric moisture content expressed as a decimal

GWC= gravimetric water content

ρ_d = dry density of soil

ρ_w= density of water

Table 9: Target Volumetric Moisture Contents

	Road 2.5' VMC	Road 5.0' VMC	Road 7.5' VMC	Road 10.0' VMC	Average VMC
Control	0.576	0.531	0.557	0.399	0.515
Sand Blanket	0.497	0.549	0.512	0.539	0.524
Vertical Barriers	0.512	0.531	0.500	0.392	0.484
Lime Columns	0.508	0.519	0.559	0.380	0.491
Paved Shoulders	0.458	0.527	0.559	0.480	0.506
Edge Drains	0.569	0.547	0.506	0.458	0.520

Table 10: Target Gravimetric Moisture Contents

	Average Dry Density (pcf)	Target GWC (%)
Control	81.34	39.54
Sand Blanket	85.75	38.14
Vertical Barriers	91.25	33.07
Lime Columns	80.10	38.29
Paved Shoulders	82.95	38.07
Edge Drains	84.35	38.47

Once the soil was prepared with the correct water content, the material was allowed to rehydrate for at least 24 hours in a humidity-controlled environment. The specimen container and one bronze porous stone were weighed, and the value was recorded. The top platen with a moist porous stone was also weighed and this value was recorded. After 24 hours, the soil was placed into the specimen container using a spatula and a razor blade was used to cut the soil flush with the top of the specimen container. The mass of the specimen and container was weighed to determine the amount of soil in the container.

6.4 Procedure

6.4.1 Preconsolidation

The specimen container and specimen were placed in the ring shear water bath and secured to the apparatus. The top platen with a moist porous stone was placed on top of the specimen. A small seating load of 0.1 kilograms was placed on the lever along with the weight of the top platen to achieve a normal stress of approximately 4.6 kPa. The vertical displacement sensor was moved to obtain an initial vertical displacement reading. Next, the water bath was filled with distilled water and water was added as needed to keep the soil saturated for the remaining tests.

5.4.2 Consolidation

Consolidate the specimen to the highest desired normal stress. For AL-5, the specimens were consolidated using a weight of 10.1 kilograms on the weight lever. The weight produced 247 kPa of normal stress on the soil specimen. The specimen was allowed to consolidate for 24 hours or until the consolidation process was complete. The specimen must not settle more than 15% of the initial specimen height as mentioned previously. The soil specimens could settle 1.2 millimeters; however, the specification for 0.75 millimeters of settlement was used for AL-5 during consolidation. If the soil specimens settled more than 0.75 millimeters, additional soil was added to the specimen container until the material was flush with the top of the specimen container. This material was then reconsolidated.

When consolidation was complete, the normal deformation versus log time was plotted to determine if the curve was well defined. If the plot was well defined, the time to failure could be computed using the following equation from Test Method D2435 (ASTM 2011).

$$t_f = 50t_{50}$$ Equation 14

Where t_f = total estimated elaspsed time to failure (min.)

t_{50} = time required for the specimen to achieve 50% consolidation under the maximum normal stress increment (min.)

However, if the curve was not well defined for the relationship between the normal deformation versus log time, the relationship between the normal deformation versus square root time could be used. This method followed Test Method D2435 (ASTM 2011) and the time to failure should be computed using Equation 15.

$$t_f = 11.6t_{90}$$ Equation 15

Where t_{90} = time required for the specimen to achieve 90% consolidation under the maximum normal stress increment (min.)

6.4.3 Shearing

The shearing displacement rate was first computed for the soil specimen. The displacement rate should allow any shear-induced pore water pressure to dissipate. A common guide to estimate a displacement rate is shown in Equation 16 (ASTM 2013).

$$d_r = \frac{d_f}{t_f}$$ Equation 16

Where d_r = displacement rate (mm/min)

d_f = estimated shear displacement at failure (mm)

Test Method D6467 recommended as a guide to shear the specimen at a rotation rate of 0.03 degrees/min for a clay with high plasticity. The rotation rate could be converted to displacement rate by considering the rotation along the mean diameter of the soil specimen. Test Method D6467 also recommended as a guide that the estimated shear displacement at failure would be 5 millimeters for a clay of high plasticity (ASTM 2013). These values were all a guide for shearing since the rotation rate and shear displacement at failure would change for each soil specimen. For AL-5, a shearing rotation rate of 0.019 degrees/minute was used for much of the testing to get an average shear displacement at failure of roughly 20 millimeters.

The soil specimen was unloaded to the desired normal stress level for the particular test being performed. The specimen was allowed to come to equilibrium after consolidation if the material was unloaded to a smaller desired normal stress for the shearing test. Therefore, for the normal stress values used for the shearing test, two specimens were over consolidated and one specimen was normally consolidated. If the material was over consolidated, the specimen would have an over consolidated ratio (OCR) value of greater than one. An OCR value of greater than one indicated the material has experienced larger stress in the past than the present stress on the material. However, for a normally consolidated specimen, the OCR would be equal to one. The two proving rings or load cells were swung towards the specimen container to create a right angle with the bearing stops on the torque arm and the load cell rods. The rods should be

adjusted so they were just touching the torque arm. The load cell rods were then locked into place. Figure 120 shows the ring shear apparatus set up to shear the specimen with the load cell rods touching the torque arm. The initial time of the test was recorded along with the initial vertical and shear displacement readings. There was a datum set up on the container to record the initial location of the soil specimen before rotation starts. The initial degree location was determined and recorded. Figure 121 shows the location of the datum on the ring shear container.

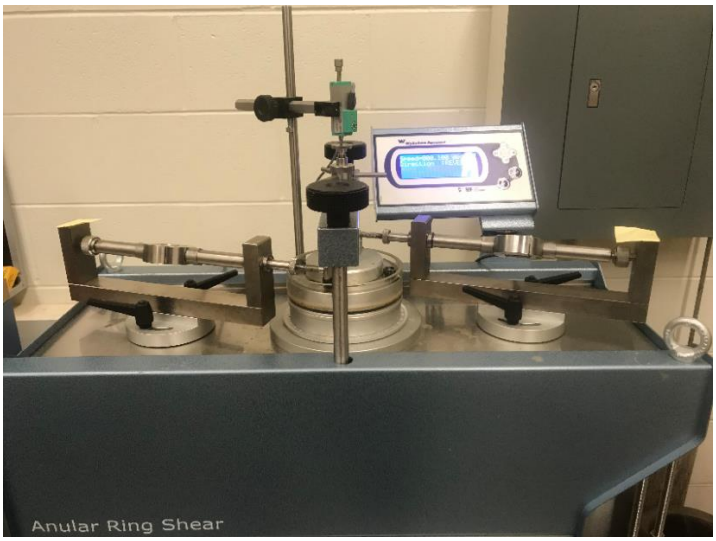

Figure 120: Ring Shear Apparatus Set-up for Shearing Test

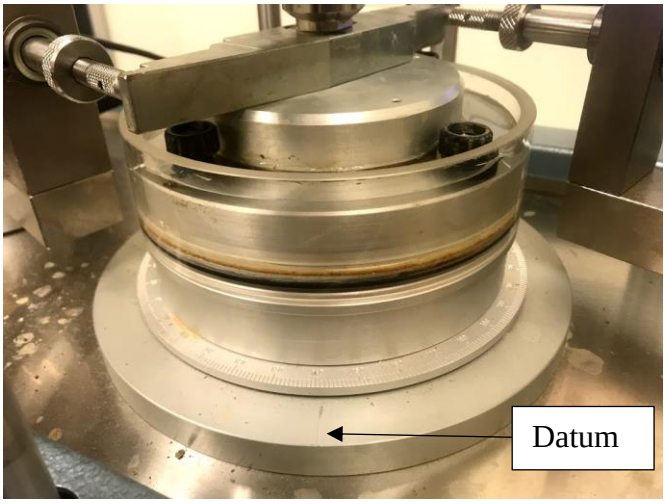

Figure 121: Soil Specimen Container with Datum Location Labeled

The test may be started, and data recorded using the data logger and computer software. Data was recorded for 24 hours or until a well-defined residual strength state was obtained. The load cells could be detached from the torque arm using the adjustable rods. The final degree location must be recorded after shearing was completed to determine the total amount of rotation the specimen endured. Carefully separate the top platen from the specimen with a sliding motion in the same direction as the failure plane to ensure damage to the specimen is minimal. Photos of the failure surface were very helpful to describe the failure surface; therefore, take photos or describe the failure surface in writing for future discussions.

6.4.4 Final Conditions and Clean Up

A sample of the soil specimen was collected to determine the final water content of the soil. The specimen container and porous stone were thoroughly cleaned for the next test performed. The porous stones were placed in a vacuum bath to ensure the pores were unclogged before the stones were used again. Figure 122 shows the vacuum bath the porous stones soaked in until the next test to prevent the pores from clogging.

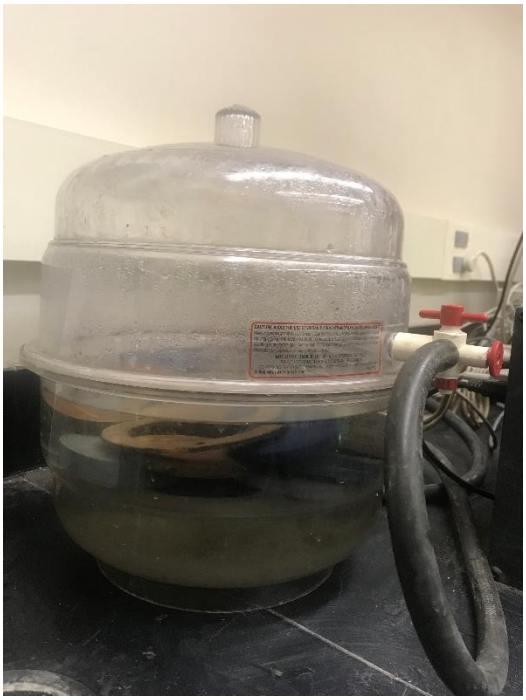

Figure 122: Vacuum Bath for Porous Stones

6.5 Calculations and Graphs

The average shear stress was computed for each test. The shear stress resisted the two surfaces of the failure plane slipping between each other. Equation 17 shows how to calculate the average shear stress. The normal stress acting on the failure plane was calculated using Equation 18. The actual displacement rate can be calculated using Equation 19 and Equation 20.

$$\tau = \frac{3(F_1 + F_2)L}{4\pi(R_2^3 - R_1^3)} \qquad \text{Equation 17}$$

Where τ= shear stress (MPa)

F_1, F_2 = load on the load cells (N)

R_1, R_2 = inner and outer specimen radii (mm)

L = torque arm length (mm)

$$\sigma_n' = \frac{P}{\pi(R_2^2 - R_1^2)} \quad \text{Equation 18}$$

Where $\sigma' n$ = normal stress (MPa)

P = normal vertical force acting on the specimen (N)

$$d_r = \frac{d_h}{t_e} \quad \text{Equation 19}$$

where d_r = shear displacement rate (mm/min)

d_h = shear displacement rate (mm)

t_e = elapsed time of test (min)

$$d_h = degrees\ traveled * (\frac{\pi}{180°})(\frac{R_1 + R_2}{2}) \quad \text{Equation 20}$$

Graphs were plotted for each normal stress level plotting the shear stress versus the shear displacement. A value for the residual shear strength can be determined from the plot. The residual shear strength was the minimum shear stress value or the value which became horizontal on the plot of the shear stress versus shear displacement. For the peak shear strength failure envelope, the material must be normally consolidated; therefore, only stress level 3 values of the

normal stress and peak shear stress were used to plot the failure envelope. Using the residual shear strength, a graph was created for each normal stress versus residual shear strength to determine the residual shear strength envelope. The envelope or trendline of the values should pass through the origin and may be nonlinear. The inverse tangent of the slopes of the envelopes were computed and the angle of peak and residual shear resistance was determined.

CHAPTER 7: RESULTS AND DISSCUSSION

7.1 Ring Shear

7.1.1 Sand Blanket (B1.5)

Three tests were performed on the soil samples from the sand blanket test section with a specific gravity of 2.685. Initial conditions for each stress level can be seen in Table 11. As mentioned previously, the sand blanket test section has a target VMC of 52.01% or a GMC of 38.47%. The specimen for stress level 2 was drier than the other two specimens at the start of the consolidation phase. However, the soil became fully saturated when the soil specimens were placed in the water bath. Consolidation for each stress level was completed with a desired normal stress of 249.55 kPa. Since 249.55 kPa was the highest desired normal stress for the shear phase of testing, this normal stress was used for all of the consolidation testing. All the specimens had to be consolidated twice to ensure the soil did not settle more than 0.75 millimeters. After the first consolidation tests for each specimen, additional material was added to the specimen container and was reconsolidated. Figure 123 shows the consolidation plots for all stress levels. Taylor's method was used to determine the average t_{90} value of 1.13 minutes.

Table 11: Initial Conditions for Sand Blanket (B1.5)

Initial Conditions	Stress Level 1	Stress Level 2	Stress Level 3
Specimen Thickness (mm)	8	8	8
Outer Specimen Radius (mm)	50	50	50
Inner Specimen Radius (mm)	35	35	35
Gravimetric Water Content (%)	37.66	35.95	38.01
Volumetric Water Content (%)	51.75	49.40	52.24
Percent Saturation (%)	97	93	99

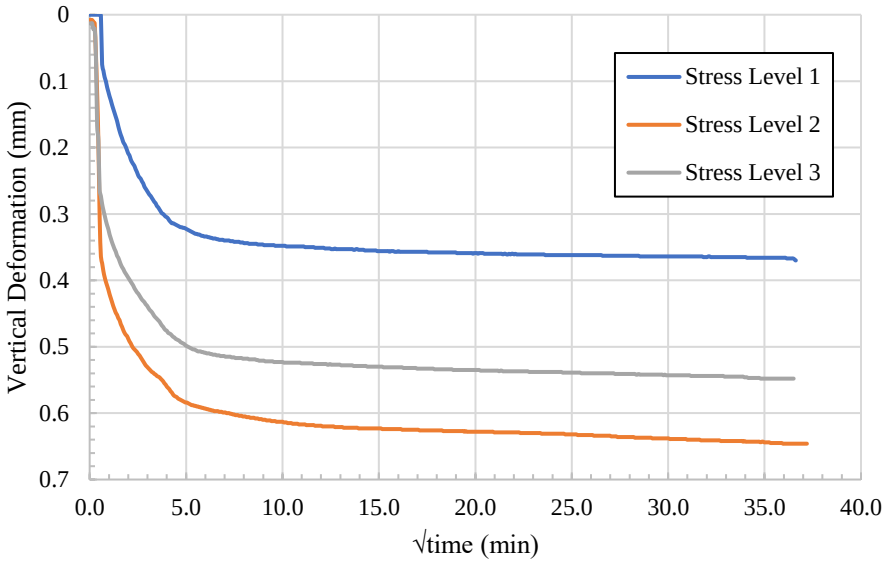

Figure 123: Consolidation Plots for Sand Blanket (B1.5) All Stress Levels

The specimen for stress level 2 had the largest amount of vertical deformation, but was still less than 0.75 mm. However, consolidation was achieved because the plots tailed off at the end of the consolidation tests.

The three normal stress levels used for stress level 1, 2, and 3 were 127.09, 176.08, and 249.55 kPa, respectively. The initial consolidation stress was constant to ensure the specimen was fully consolidated, but the loading stress varied in order to create a failure envelope for the strength. The specimens were sheared at a rotation rate of 0.019 degrees/minute. All the specimens had an average shear displacement of approximately 20 mm. Table 12 shows the initial and final conditions for the specimens before and after the shearing test. Figure 124 shows the shear stress versus the average shear displacement for each stress level. From this figure, the peak and residual shear strength value can be determined and are shown in Table 12. Figure 125 shows the change in specimen thickness during the shearing test. Raw data for the consolidation

and ring shear testing can be found in Appendix B: Raw Data. Photographs of the specimens before and after testing can be seen in Appendix C: Laboratory Photos.

Table 12: Initial and Final Conditions of Specimens for the Shear Test for Sand Blanket (B1.5)

Conditions at Start of Shear			
Specimen thickness(mm)	7.63	7.354	7.452
Dry unit weight (kN/m^3)	12.91	12.95	12.95
Normal Stress (kPa)	127.09	176.08	249.55
Rate of Shear Displacement (º/min)	0.019	0.019	0.019
OCR	1.96	1.42	1.00
Conditions at End of Shear			
Peak Shear Strength (kPa)	72.69	76.53	92.27
Residual Shear Strength (kPa)	32	37	47
Average Shear Displacement (mm)	20.03	20.08	20.55
Change in Specimen Thickness (mm)	-0.060	-0.164	-0.347
Gravimetric Water Content (%)	37.75	35.11	34.60
Volumetric Water Content (%)	51.87	48.25	47.54

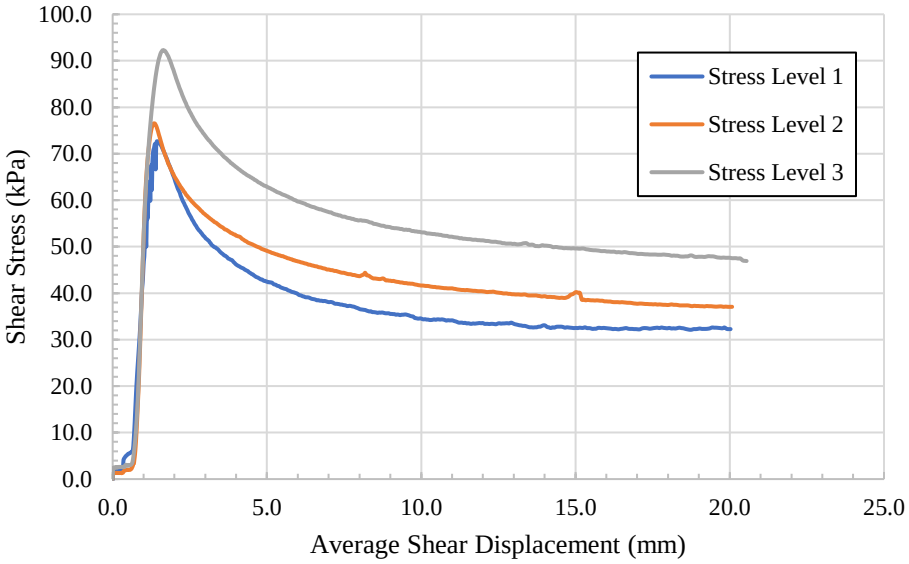

Figure 124: Shear Stress versus Average Shear Displacement for Sand Blanket (B1.5)

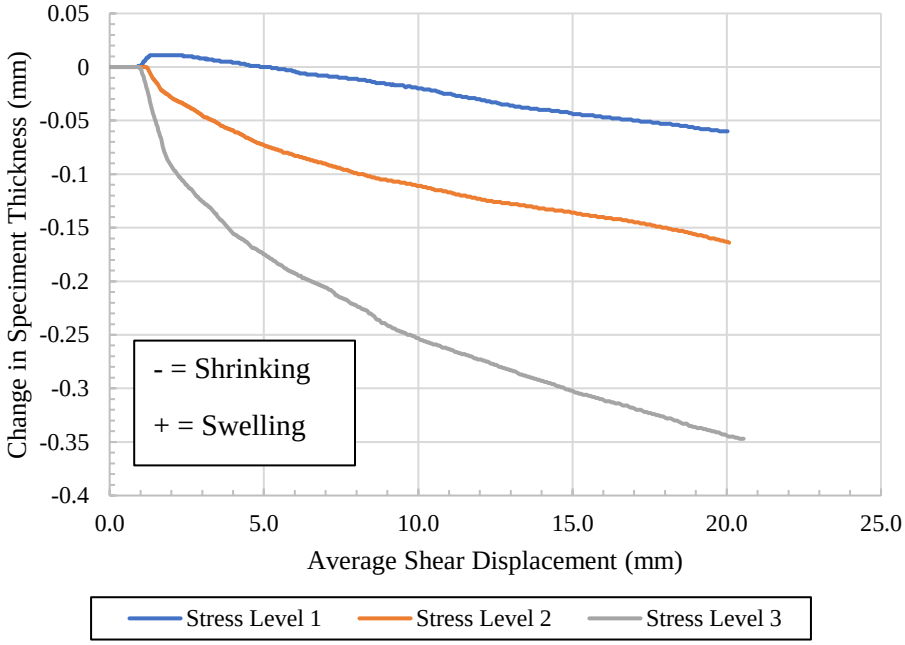

Figure 125: Change in Specimen Thickness During Shearing for Sand Blanket (B1.5)

During the shearing phase, the peak shear strength and residual shear strength increased with each step-in stress level. A slow rotation was applied to the specimen in order to dissipate any pore pressure that has built up in the specimen. The specimen for stress level 1 experienced some swelling until an average shear displacement of roughly 5 mm. This swelling was likely due to the specimen experiencing an unloading and decrease in stress. The specimen then started to decrease in specimen thickness after reaching the shear displacement of 5 mm. The specimens for stress level 2 and 3 only experienced shrinkage and decreased in specimen thickness throughout the duration of the tests.

The peak and residual strength were plotted with the normal stress for each stress level. An assumed cohesion of 0 kPa was used for the trendlines. From these plots, an angle of peak and residual shear resistance was calculated by using the equations located on the plots. Figure

126 and Figure 127 show the peak and residual shear strength envelopes. Table 16 shows the calculated angles of peak and shear resistance for the sand blanket test section.

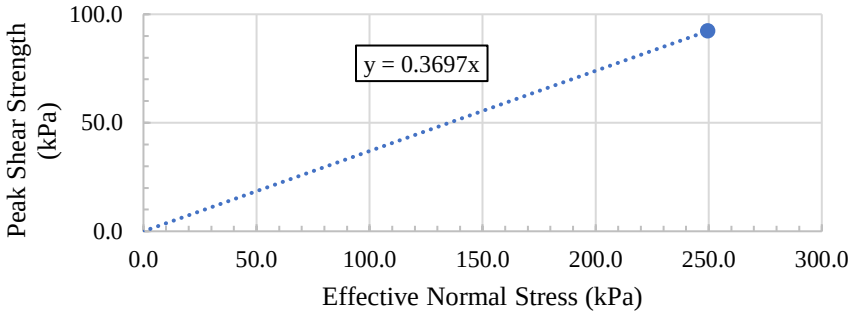

Figure 126: Peak Shear Strength versus Effective Normal Stress for Sand Blanket (B1.5) All Stress Levels

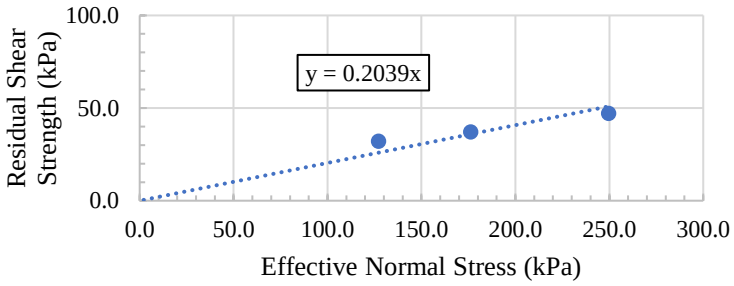

Figure 127: Residual Shear Strength versus Effective Normal Stress for Sand Blanket (B1.5) All Stress Levels

Table 13: Angle of Peak and Residual Shear Resistance for Sand Blanket (B1.5)

Peak Shear Strength	
Effective Cohesion (kPa)	0
Angle of Peak Shear Resistance (º)	20.3
Residual Shear Strength	
Effective Cohesion (kPa)	0
Angle of Residual Shear Resistance (º)	11.5

From these plots, the angle of peak shear resistance was determined to be 20.3 degrees and the angle of residual shear resistance was 11.5 degrees when the envelope was forced through the origin. The envelope should pass through the origin for the drained shear strength of

the material. Referencing Table 1, these are very low angles of shear resistance meaning the material is very weak.

7.1.2 Vertical Barriers (B2.5)

Three tests were performed on three different soil samples from the vertical barriers test section with a specific gravity of 2.735. Initial conditions for each stress level can be seen in Table 14. Recall that the soil has a target VMC of 48.36% or target GWC of 33.07%. The soil was determined to be a little dry of the target volumetric moisture content at the start of the consolidation phase. However, the soil became fully saturated when the soil specimens were placed in the water bath; therefore, the volumetric water content at the end of the shearing test is higher than the target volumetric water content value.

Table 14: Initial Conditions for Vertical Barriers (B2.5)

	Stress Level 1	Stress Level 2	Stress Level 3
Specimen Thickness (mm)	8	8	8
Outer Specimen Radius (mm)	50	50	50
Inner Specimen Radius (mm)	35	35	35
Gravimetric Water Content (%)	32.15	30.91	32.26
Volumetric Water Content (%)	47.01	45.20	47.17
Percent Saturation (%)	85	87	88

Consolidation for each specimen was completed first with a desired normal stress of 249.55 kPa. The specimen for stress level #2 had to be consolidated twice to ensure the specimen did not settle more than 0.75 millimeters. Soil was added to the specimen after the first consolidation test and reconsolidated. Figure 128 shows the consolidation plots for all stress levels tested. Taylor's method was used to determine the average t_{90} value from each stress level was 0.44 minutes.

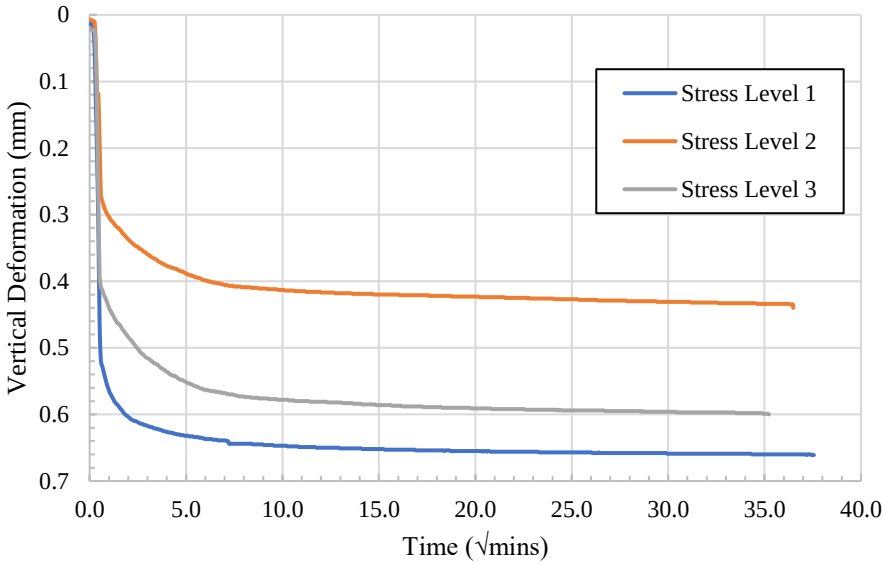

Figure 128: Consolidation Plots for Vertical Barriers (B2.5) All Stress Levels

Since the specimens of stress level 1 and 3 did not have to be reconsolidated twice, the vertical deformation of these specimens are larger than the vertical deformation of the specimen for stress level 2. However, consolidation was achieved since the plots tailed off at the end of the test.

The three normal stress levels used for stress level 1, 2, and 3 were 127.1, 176.07, and 249.55 kPa, respectively. The first specimen was sheared at a rate of 0.055 degrees/minute while the remaining two test specimens were sheared at a rotation rate of 0.019 degrees/minute. Test specimen 1 had an average shear displacement of 58 millimeters. Test specimen 2 and 3 had an average shear displacement of approximately 20 millimeters. Table 15 shows the initial and final conditions of the specimens during the shearing test. Figure 129 plots the shear stress versus the average shear displacement for each stress level. From this plot a peak and residual shear strength value could be determined and seen in Table 15. Figure 130 shows the change in specimen thickness during the shear test. Raw data for the consolidation and ring shear testing

can be found in Appendix B: Raw Data. Photographs of the specimens before consolidation and after shearing can be found in Appendix C: Laboratory Photos.

Table 15: Initial and Final Conditions of Specimens for the Shear Test for Vertical Barriers (B2.5)

Conditions at Start of Shear			
	Stress Level 1	Stress Level 2	Stress Level 3
Specimen thickness(mm)	7.339	7.56	7.4
Dry unit weight (kN/m^3)	13.19	13.58	13.38
Normal Stress	127.10	176.07	249.55
Rate of Shear Displacement (deg/min)	0.055	0.019	0.019
OCR	1.96	1.42	1.00
Conditions at End of Shear			
Peak Shear Strength (kPa)	73.04	79.80	96.58
Residual Shear Strength (kPa)	24	35	43
Average Shear Displacement (mm)	58.75	20.77	20.62
Change in Specimen Thickness (mm)	-0.191	-0.21	-0.308
Gravimetric Water Content (%)	37.88	37.47	36.77
Volumetric Water Content (%)	55.39	54.80	53.77

.

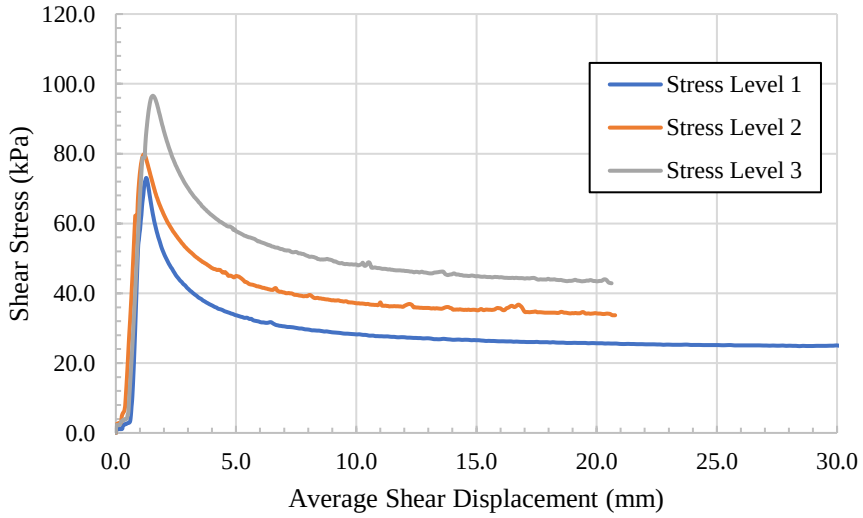

Figure 129: Shear Stress versus Average Shear Displacement for Vertical Barriers (B2.5)

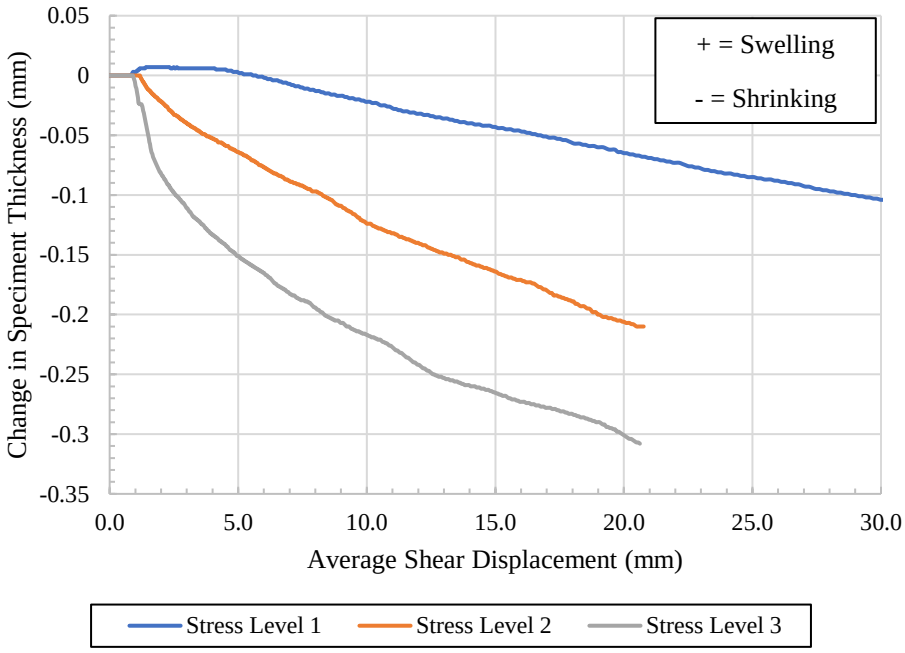

Figure 130: Change in Specimen Thickness During Shearing for Vertical Barriers (B2.5)

Figure 129 and Figure 130 were truncated at an average shear displacement of 30 mm. As mentioned previously, stress level 1 had an average shear displacement of 58 mm. The residual shear strength value remained constant from 30 mm to 58 mm; therefore, the plot was truncated. The specimen did continue to decrease in thickness; however, since the residual strength was constant, the decrease in thickness was not concerning.

During the shearing phase, a slow rotation rate was applied to the specimen in order to dissipate any pore pressure that has built up in the specimen. With each increase in desired normal stress, the peak shear strength and residual shear strength values increased. The change in the specimen thickness was also monitored during the shearing phase as shown in Figure 130. Stress level 1 experienced some swelling until an average shear displacement of roughly 5 mm. The specimen then started to shrink and the change in specimen thickness became negative. The

specimens for stress level 2 and 3 remained a constant thickness until approximately 2 mm of average shear displacement when the specimen then began to decrease in thickness.

The peak and residual strength were plotted with the normal stress for each stress level. From these plots an angle of peak and residual shear resistance was calculated by using the equations located on the plots. Figure 131 and Figure 132 show the peak and residual shear strength envelopes represented by the linear trendlines. Table 16 shows the angles of peak and residual shear resistance for the vertical barriers test section.

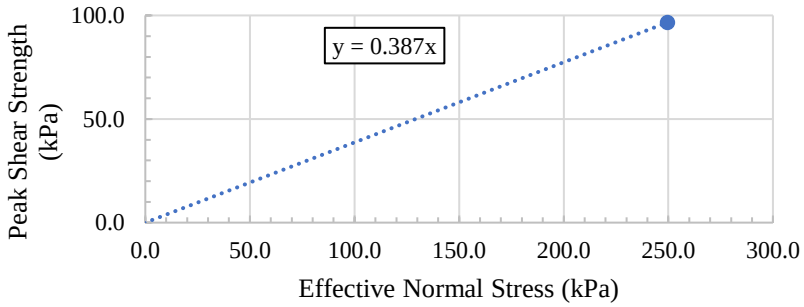

Figure 131: Peak Shear Strength versus Effective Normal Stress for Vertical Barriers (B2.5) All Stress Levels

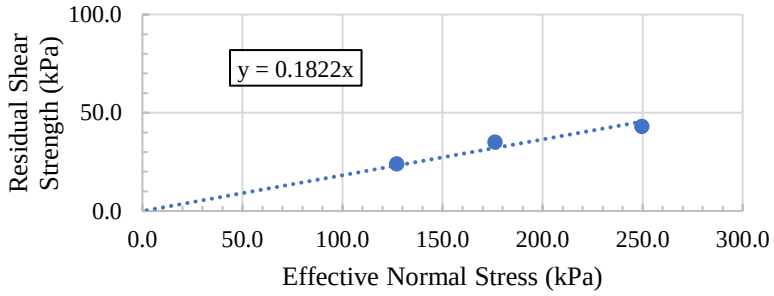

Figure 132: Residual Shear Strength versus Effective Normal Stress for Vertical Barriers (B2.5) All Stress Levels

Table 16: Angle of Peak and Residual Shear Resistance for Vertical Barriers (B2.5)

Peak Shear Strength	
Effective Cohesion (kPa)	0
Angle of Peak Shear Resistance (º)	21.2
Residual Shear Strength	
Effective Cohesion (kPa)	0
Angle of Residual Shear Resistance (º)	10.3

From these trendlines, the angle of the slope was calculated and represented the angle of shear resistance or the internal angle of friction. The angle of peak shear resistance was calculated to be 21.2 degrees and the angle of residual shear resistance was determined to 10.3 degrees when the cohesion was 0 kPa. The angle of shear resistance was very low for this material; therefore, the soil could be considered to be weak material.

7.1.3 Lime Columns (B3.5)

Three ring shear tests were completed on three prepared specimens from the lime columns test section with a specific gravity of 2.72. Initial conditions before consolidation can be seen in Table 17. The soil was prepared to achieve a target VMC of 49.15% or a target GWC of 38.29%. Specimens for stress level 1 and 2 were slightly dry of the target VMC, but the specimen for stress level 3 was slightly wet of the target VMC. Consolidation for each stress level was completed using a desired normal stress of 249.5 kPa. All the test specimens had to be consolidated twice. The specimens settled more than 0.75 mm for the first consolidation test; therefore, soil was added to the specimen container and reconsolidated. Figure 133 shows the consolidation plots for all the stress levels for the lime columns test section. An average t_{90} value of 0.42 minutes was determined.

Table 17: Initial Conditions for Lime Columns (B3.5)

Initial Conditions	Stress Level 1	Stress Level 2	Stress Level 3
Specimen Thickness (mm)	8	8	8
Outer Specimen Radius (mm)	50	50	50
Inner Specimen Radius (mm)	35	35	35
Gravimetric Water Content (%)	36.29	36.47	38.96
Volumetric Water Content (%)	46.58	46.81	50.01
Percent Saturation (%)	95	96	99

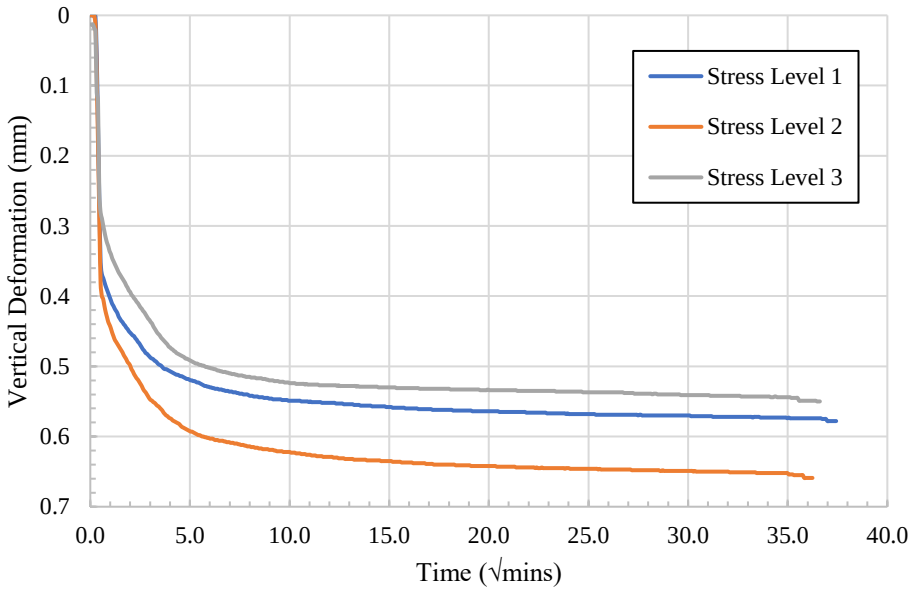

Figure 133: Consolidation Plots for Lime Columns (B3.5) All Stress Levels

The three normal stress levels used for stress level 1, 2, and 3 were 127.1, 176.08, and 249.55 kPa, respectively. All the specimens were sheared at a rotation rate of 0.019 degrees/minute. The specimens had an average shear displacement of approximately 20 millimeters. Table 18 shows the initial and final conditions of the specimens during the shearing test. Figure 134 plots the shear stress versus the average shear displacement for each stress level. From this plot a peak and residual shear strength value can be determined and seen in Table 18. Figure 135 shows the change in specimen thickness during the shear test. Raw data for the

consolidation and ring shear testing can be found in Appendix B: Raw Data. Photographs of the specimens before consolidation and after shearing can be found in Appendix C: Laboratory Photos.

Table 18: Initial and Final Conditions of Specimens for the Shear Test for Lime Columns (B3.5)

Conditions at Start of Shear			
Specimen thickness(mm)	7.422	7.341	7.45
Dry unit weight (kN/m^3)	13.11	13.14	12.90
Normal Stress (kPa)	127.10	176.08	249.55
Rate of Shear Displacement (deg/min)	0.019	0.019	0.019
OCR	1.96	1.42	1.00
Conditions at End of Shear			
Peak Shear Strength (kPa)	62.83	74.39	97.72
Residual Shear Strength (kPa)	24	32	52
Average Shear Displacement (mm)	20.62	19.29	20.62
Change in Specimen Thickness (mm)	-0.176	-0.276	-0.279
Gravimetric Water Content (%)	38.37	36.74	36.03
Volumetric Water Content (%)	49.25	47.17	46.25

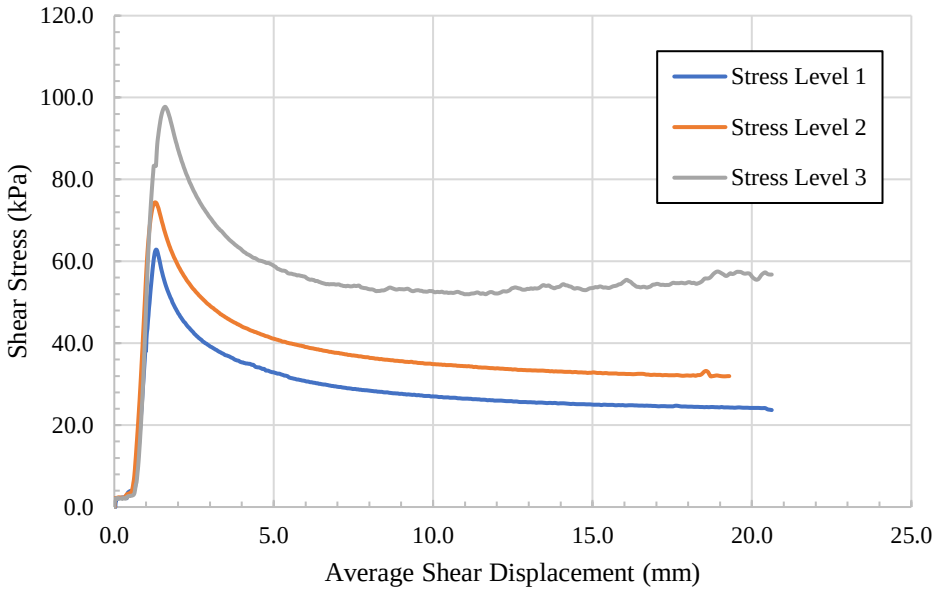

Figure 134: Shear Stress versus Average Shear Displacement for Lime Columns (B3.5)

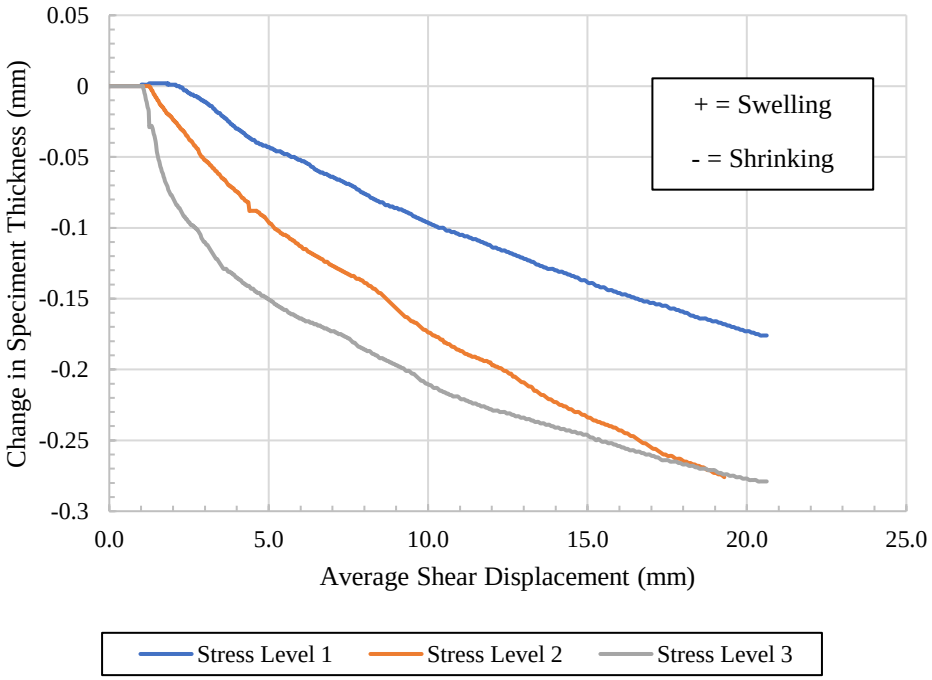

Figure 135: Change in Specimen Thickness During Shearing for Lime Columns (B3.5)

As the stress levels increased, the peak shear strength and residual shear strength values increased. The specimens for stress level 1 and 2 reached failure at approximately 1.5 mm of shear displacement. The specimen for stress level 3 reached failure at an average shear displacement at roughly 2 mm. The residual shear stress increased slightly at the end of the testing; however, the minimum shear stress value was used as the residual shear strength. There was a slightly increase in specimen thickness for the specimen used for stress level 1. However, once an average shear displacement of 2 mm was achieved, the specimen quickly started to decrease in thickness. The specimens for stress level 1 and 2 remained constant until an average shear displacement of 1.5 mm and then started to shrink in thickness.

The peak and residual strength were plotted with the normal stress for each stress level. From these plots an angle of peak and residual shear resistance was calculated by using the equations located on the plots. Figure 136 and Figure 137 show the peak and residual shear

strength envelopes. Table 19 shows the angles of peak and residual shear resistance for the vertical barriers test section.

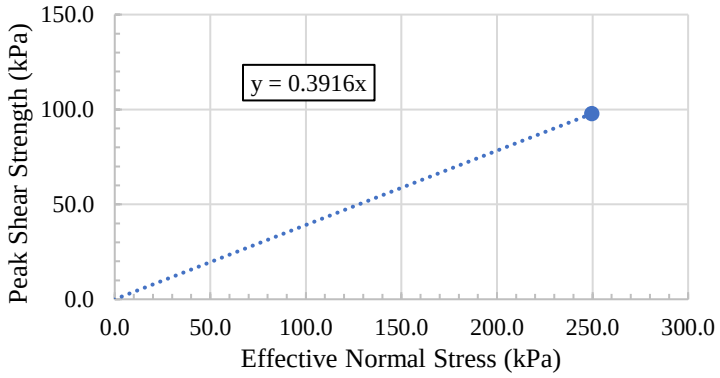

Figure 136: Peak Shear Strength versus Effective Normal Stress for Lime Columns (B3.5) All Stress Levels

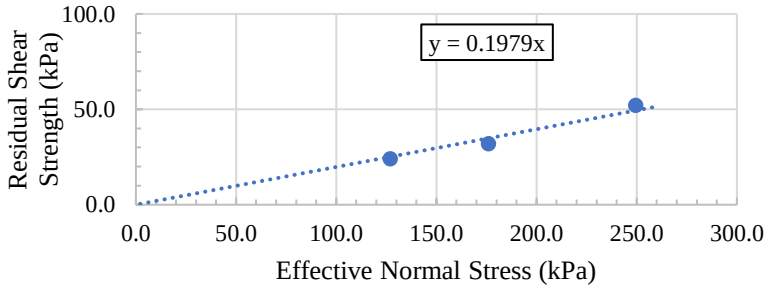

Figure 137: Residual Shear Strength versus Effective Normal Stress for Lime Columns (B3.5) All Stress Levels

Table 19: Angle of Peak and Residual Shear Resistance for Lime Columns (B3.5)

Peak Shear Strength	
Cohesion (kPa)	0
Angle of Peak Shear Resistance (º)	21.4
Residual Shear Strength	
Cohesion (kPa)	0
Angle of Residual Shear Resistance (º)	11.2

These plots resulted in an angle of peak shear resistance of 21.4 degrees and an angle of residual shear resistance of 11.2 degrees when the cohesion was 0 kPa. There was a large

decrease in the angle of shear resistance between the peak shear strength and the residual shear strength. These low angles of resistance generally describe weak materials.

7.1.4 Paved Shoulders (B4.5)

Three tests were performed on three different soil specimens from the paved shoulders test section with a specific gravity of 2.725. Initial conditions for each stress level can be seen in Table 20. The target VMC and GWC was 50.61% and 38.07%, respectively. All the specimens are slightly dry of the target VMC. Consolidation was completed with a normal stress of 249.5 kPa for each specimen. Specimens for stress level 1 and 3 had to be consolidated twice to ensure the specimen did not settle more than 0.75 millimeters. Figure 138 shows the consolidation plots for all stress levels tested. Taylor's Method was used to determine the average t_{90} value for all stress levels and the value was determined to be 0.85 minutes.

Table 20: Initial Conditions for Paved Shoulders (B4.5)

Initial Conditions	Stress Level 1	Stress Level 2	Stress Level 3
Specimen Thickness (mm)	8	8	8
Outer Specimen Radius (mm)	50	50	50
Inner Specimen Radius (mm)	35	35	35
Gravimetric Water Content (%)	34.56	36.67	37.57
Volumetric Water Content (%)	45.94	48.74	49.94
Percent Saturation (%)	93	91	96

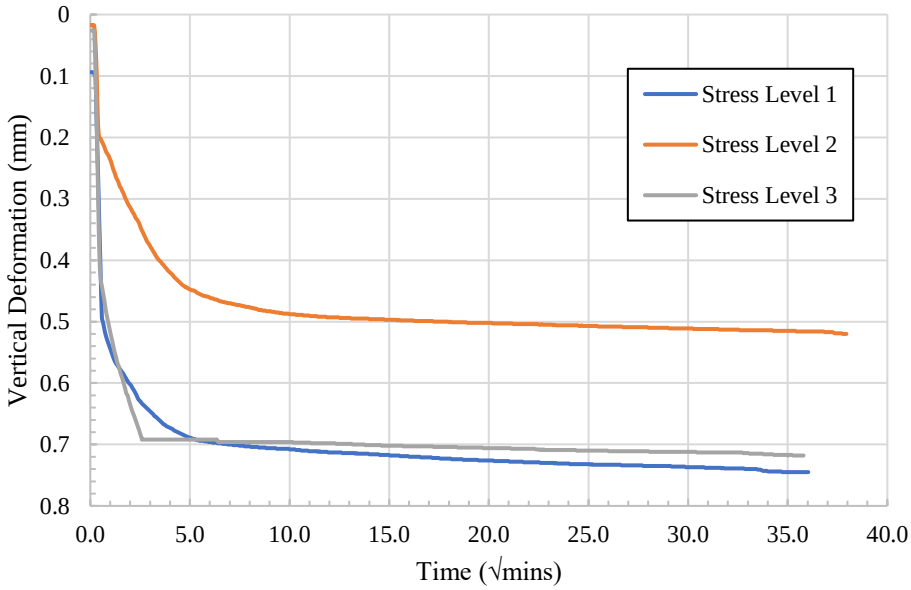

Figure 138: Consolidation Plots for Paved Shoulders (B4.5) All Stress Levels

The consolidation plot for stress level 3 looks different than the other plots. The ring shear software stopped the consolidation testing for roughly 5 minutes and then continued to collect data after that time period. Therefore, two separate curves were extracted from the software. These curves were attached together explaining why there is a sharp angle in the consolidation plot.

The normal stress levels for stress level 1, 2, and 3 were 127.09, 176.08, and 249.55 kPa, respectively. All the specimens were sheared at a rotation rate of 0.019 degrees/minute with an average shear displacement of roughly 20 millimeters. Table 21 shows the initial and final conditions of the specimens during the shearing test. Figure 139 plots the shear stress versus the average shear displacement for each stress level. From this plot a peak and residual shear strength value can be determine and this value is recorded in Table 21. Figure 140 shows the change in specimen thickness during shearing for each stress level. Raw data for the

consolidation test and ring shear test can be found in Appendix B: Raw Data. Photographs of the specimens before and after testing can be seen in Appendix C: Laboratory Photos.

Table 21: Initial and Final Conditions of Specimens for the Shear Test for Paved Shoulders (B4.5)

Conditions at Start of Shear			
Specimen thickness(mm)	7.255	7.48	7.282
Dry unit weight (kN/m^3)	13.28	12.77	12.90
Normal Stress	127.09	176.08	249.55
Rate of Shear Displacement (deg/min)	0.019	0.019	0.019
OCR	1.96	1.42	1.00
Conditions at End of Shear			
Peak Shear Strength (kPa)	63.01	87.25	95.80
Residual Shear Strength (kPa)	24	35	51
Average Shear Displacement (mm)	20.25	19.72	20.40
Change in Specimen Thickness (mm)	-0.161	-0.114	-0.284
Gravimetric Water Content (%)	35.79	35.16	35.82
Volumetric Water Content (%)	47.58	46.74	47.62

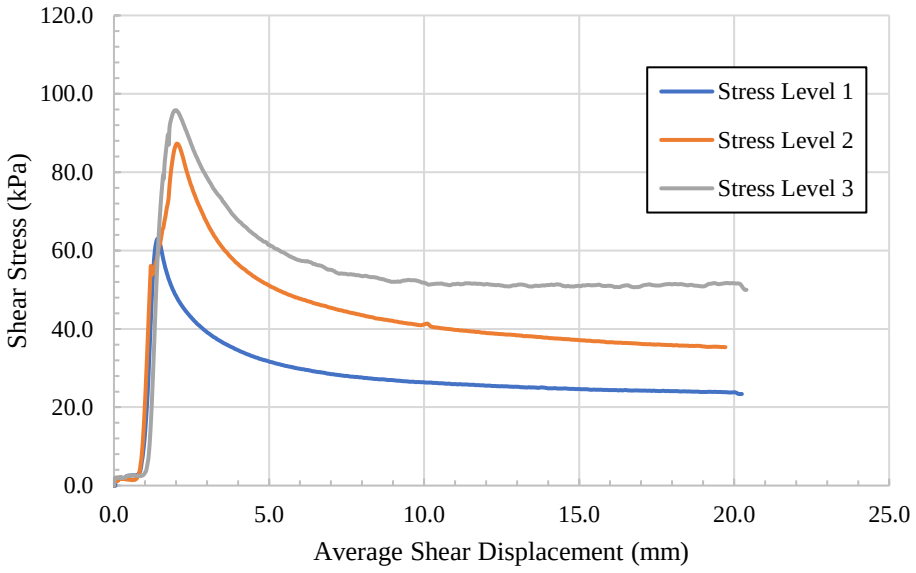

Figure 139: Shear Stress versus Average Shear Displacement for Paved Shoulders (B4.5)

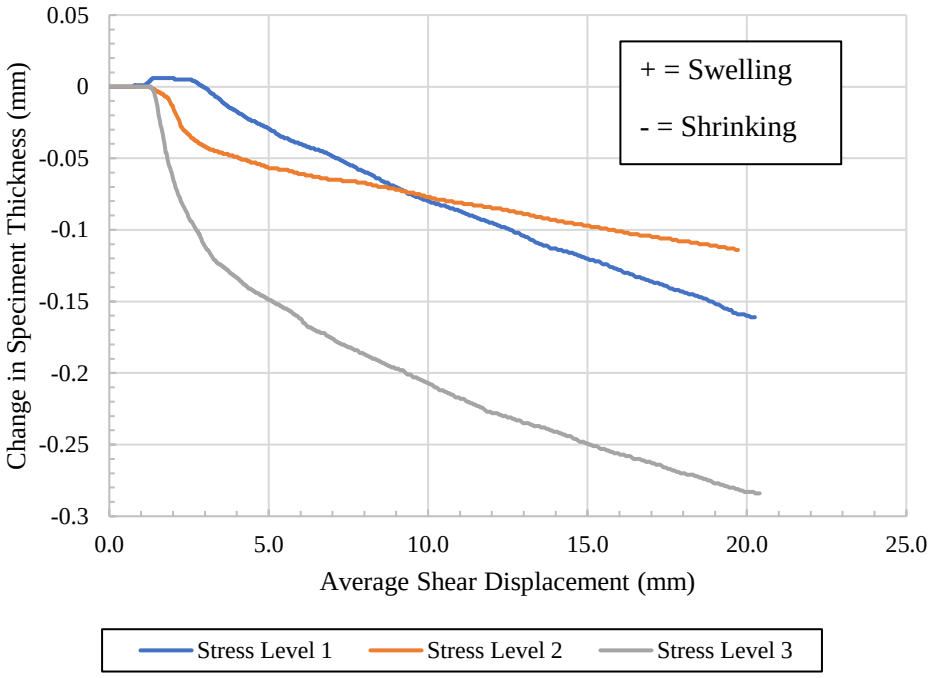

Figure 140: Change in Specimen Thickness During Shearing for Paved Shoulders (B4.5)

The peak and residual shear stress increased with each step-in stress level. The specimen for stress level 1 failed when the average shear displacement was approximately 1.5 mm. The specimens for stress levels 2 and 3 failed at an average shear displacement of roughly 2.5 mm. The specimen for stress level 1 experienced some swelling at the beginning of the shear testing. However, when the shear displacement was approximately 2 mm all the specimens started to decrease in thickness.

The peak and residual strength were plotted with the normal stress for each stress level. A value of 0 was assumed for the cohesion in order for the trendline to pass through the origin, but an additional trendline was added that allowed an intercept. From these plots, an angle of peak and residual shear resistance was calculated by using the equations located on the plots. Figure 141 and Figure 142 show the peak and residual shear strength envelopes. Table 22 shows the angles of peak and residual shear resistance for the paved shoulders test section.

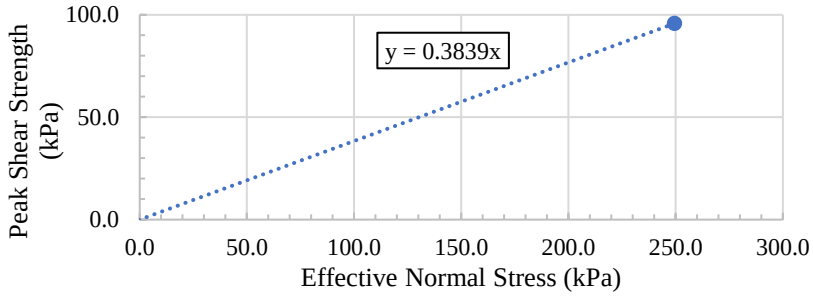

Figure 141: Peak Shear Strength versus Effective Normal Stress for Paved Shoulders (B4.5) All Stress Levels

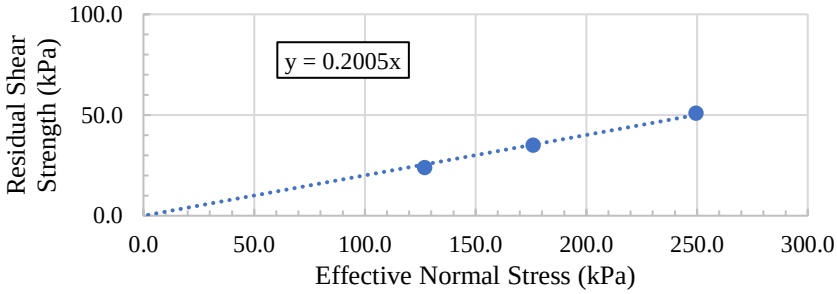

Figure 142: Residual Shear Strength versus Effective Normal Stress for Paved Shoulders (B4.5) All Stress Levels

Table 22: Angle of Peak and Residual Shear Resistance for Paved Shoulders (B4.5)

Peak Shear Strength	
Cohesion (kPa)	0
Angle of Peak Shear Resistance (º)	21.0
Residual Shear Strength	
Cohesion (kPa)	0
Angle of Residual Shear Resistance (º)	11.3

From these plots, the angle of peak shear resistance was determined to be 21.0 degrees and the angle of residual shear resistance was determined to be 11.3 degrees when the cohesion was 0 kPa. The soil continued to decrease in strength after failure and was considered to be weak material.

7.1.5 Edge Drains (B5.5)

Three tests were completed on soil specimens from the edge drains test section with a specific gravity of 2.725. Initial conditions for the specimens can be seen in Table 23. The target volumetric and gravimetric water content was 52.0% and 38.47%, respectively. The VMC was slightly low for specimens 1 and 2, but it was too high for specimen 3. A normal stress of 249.55 kPa was applied to the specimens to complete the consolidation phase of the testing. All the specimens had to be consolidated twice to achieve an acceptable settlement of the soil. Consolidation plots for each stress level is shown in Figure 143. An average t_{90} value of 4.41 minutes was determined from the consolidation plots for each test specimen.

Table 23: Initial Conditions for Edge Drains (B5.5)

Initial Conditions	Stress Level 1	Stress Level 2	Stress Level 3
Specimen Thickness (mm)	8	8	8
Outer Specimen Radius (mm)	50	50	50
Inner Specimen Radius (mm)	35	35	35
Gravimetric Water Content (%)	36.39	38.39	41.73
Volumetric Water Content (%)	49.19	51.89	56.40
Percent Saturation (%)	97	98	101

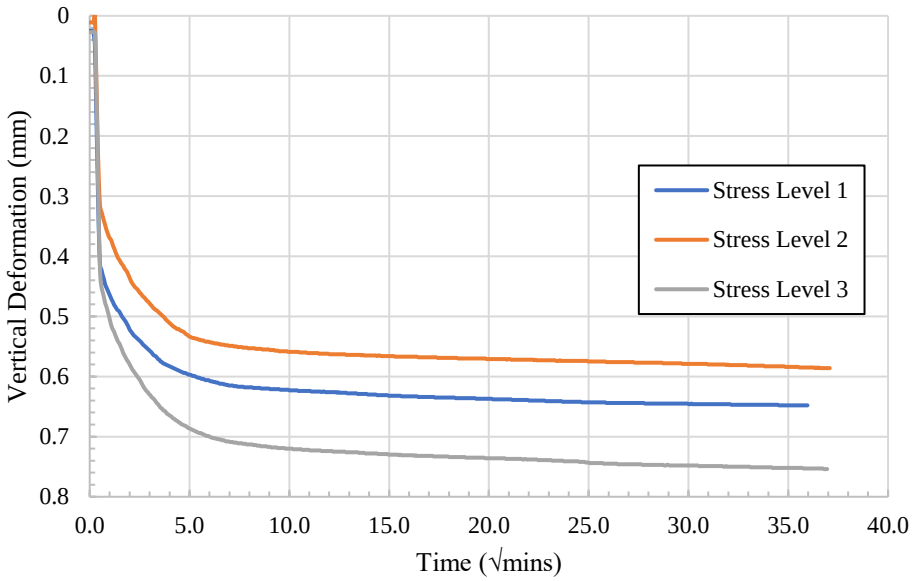

Figure 143: Consolidation Plots for Edge Drains (B5.5)

The normal stress for stress level 1, 2, and 3 were 127.10, 176.07, and 249.55 kPa, respectively. All the specimens were sheared at a rotation rate of 0.019 degrees per minute. The average shear displacement for each specimen was slightly larger than 20 millimeters. Table 24 shows the initial and final conditions of the specimens before and after the shearing test. Figure 144 shows the shear stress versus the average shear displacement for each stress level. From this plot, a peak and residual shear strength value can be determined and this value is recorded in Table 24. Figure 145 shows the change in thickness for each specimen during the shear test. Raw data for the consolidation and ring shear testing can be found in Appendix B: Raw Data and photographs of the specimens before and after testing can be found in Appendix C: Laboratory Photos.

Table 24: Initial and Final Conditions of Specimens for the Shear Test for Edge Drains (B5.5)

Conditions at Start of Shear			
Specimen thickness(mm)	7.353	7.414	7.246
Dry unit weight (kN/m^3)	13.19	12.94	12.57
Normal Stress	127.10	176.07	249.55
Rate of Shear Displacement (deg/min)	0.019	0.019	0.019
OCR	1.96	1.42	1.00
Conditions at End of Shear			
Peak Shear Strength (kPa)	61.61258482	69.11248899	87.07737571
Residual Shear Strength (kPa)	24	31	43
Average Shear Displacement (mm)	20.77	19.72	20.77
Change in Specimen Thickness (mm)	-0.215	-0.267	-0.364
Gravimetric Water Content (%)	36.76	37.62	36.64
Volumetric Water Content (%)	49.69	50.86	49.52

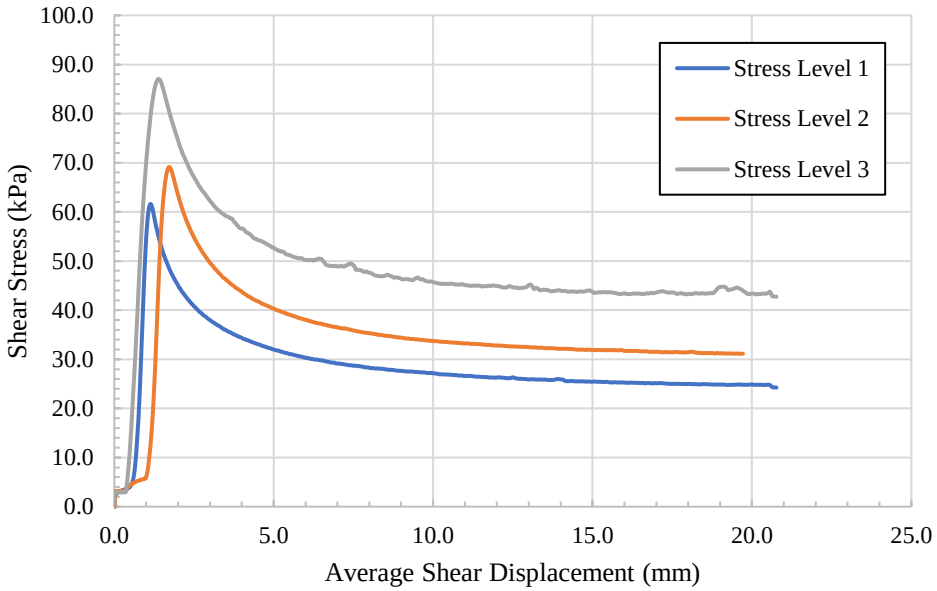

Figure 144: Shear Stress versus Average Shear Displacement for Edge Drains (B5.5)

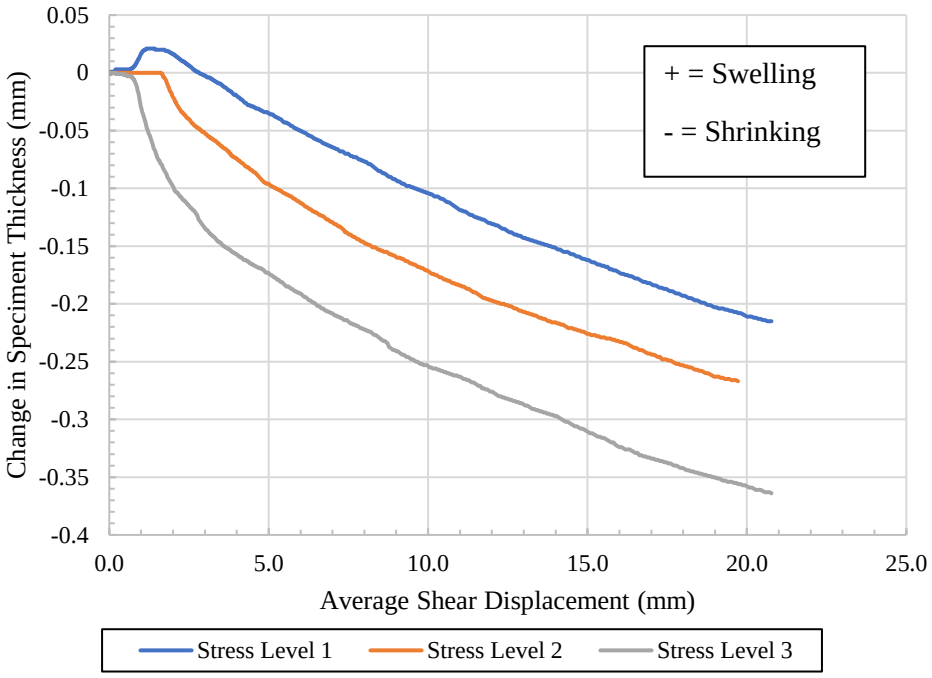

Figure 145: Change in Specimen Thickness During Shearing for Edge Drains (B5.5)

The peak and residual shear stress increased with each stress level. As shown in Figure 144, failure occurred for each stress level at different values of shear displacement. For stress level 1, 2, and 3, the average shear displacement at failure was 1, 2, and 1.5 mm, respectively. The specimen used for stress level 1 testing experienced some swelling at the beginning of the shearing test. Swelling occurred until an average shear displacement of 3 mm. After 3 mm, the specimen decreased in thickness. The specimens for stress level 2 and 3 remained constant at the beginning of the test, but quickly decreased in thickness around an average shear displacement of roughly 2 mm.

The peak and residual strength values were plotted with the normal stress for each stress level. The cohesion was assumed to be 0 kPa. Figure 146 and Figure 147 show the peak and residual shear strength envelopes. Table 25 shows the angles of peak and residual shear resistance for the edge drains test section.

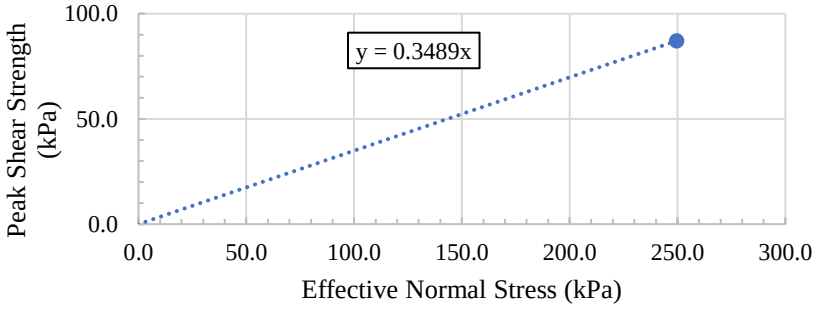

Figure 146: Peak Strength versus Effective Normal Stress for Edge Drains (B5.5) All Stress Levels

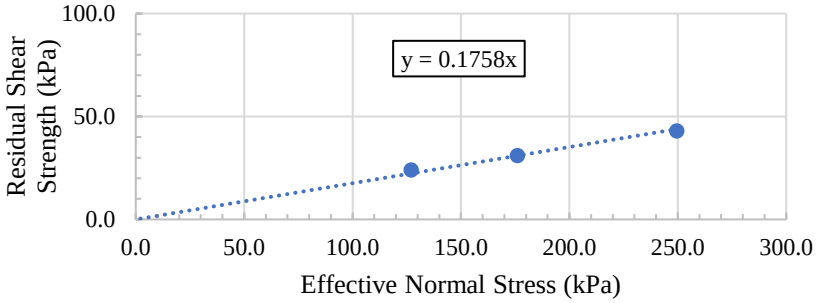

Figure 147: Residual Shear Strength Effective versus Normal Stress for Edge Drains (B5.5) All Stress Levels

Table 25: Angle of Peak and Residual Shear Resistance for Edge Drains (B5.5)

Peak Shear Strength	
Cohesion (kPa)	0
Angle of Peak Shear Resistance (º)	19.2
Residual Shear Strength	
Cohesion (kPa)	0
Angle of Residual Shear Resistance (º)	10.0

The angle of peak shear resistance was determined to be 19.2 degrees and the angle of residual shear resistance was calculated to be 10.0 degrees when the cohesion was 0 kPa. The results from the ring shear tests concluded the material being tested was very weak.

7.1.6 Control

Three soils samples from the control test section were extruded from a Shelby tube. The material was oven dried and ball milled until there was enough material to produce three specimens for testing. A specific gravity of 2.65 is assumed for this soil. Initial conditions for each stress level can be seen in Table 26. Recall that the control section has a target VMC of 51.55% and a GWC of 39.54%. Test specimen 1 had a VMC and GWC that was higher than the target values. Consolidation for each specimen was completed using a normal stress of 249.55 kPa. Test specimen 1 had to be consolidated three times to ensure a porous stone settlement of less than 0.75 mm. This was probably caused by the high-water content. Figure 148 shows the consolidation plots for all stress levels. Taylor's method was used to determine the average t90 value of 5.06 minutes.

Table 26: Initial Conditions for Control

Initial Conditions	Stress Level 1	Stress Level 2	Stress Level 3
Specimen Thickness (mm)	8	8	8
Outer Specimen Radius (mm)	50	50	50
Inner Specimen Radius (mm)	35	35	35
Gravimetric Water Content (%)	48.99	40.79	39.50
Volumetric Water Content (%)	63.86	53.17	51.49
Percent Saturation (%)	108	95	100

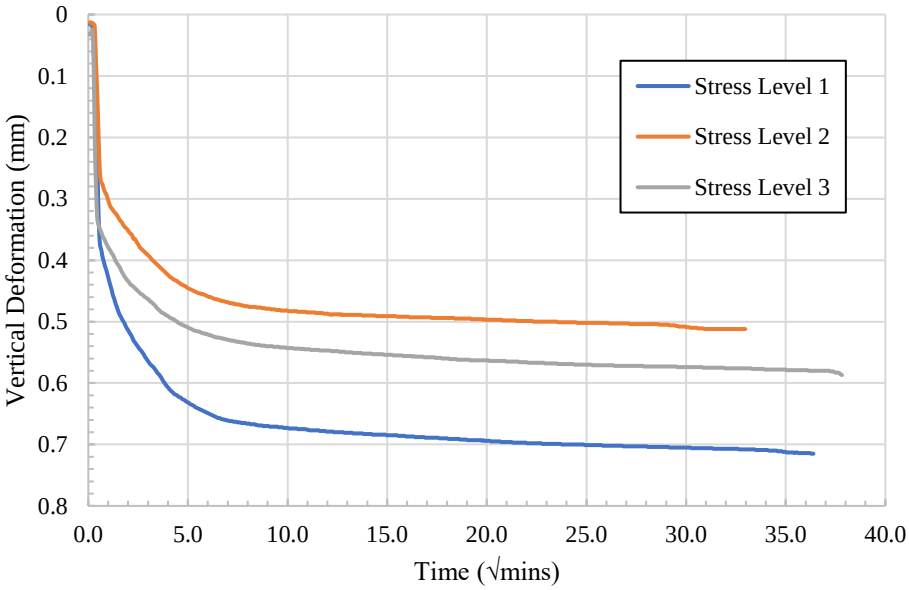

Figure 148: Consolidation Plots for Control

The three normal stress levels used for testing were 127.1, 176.07, and 249.55 kPa. All the tests were sheared at a rotation rate of 0.019 degrees/minute and had an average shear displacement of just over 20 mm. Table 27 shows the initial and final conditions of the specimens at the start and ending of the shearing test. Figure 149 shows the shear stress versus the average shear displacement for each stress level. From this plot, a peak and residual shear strength value can be determined and are shown in Table 27. Figure 150 shows the change in specimen thickness throughout the shear testing for each stress level. Raw data for the consolidation and ring shear testing can be found in Appendix B: Raw Data and photographs of the specimens before and after testing can be found in Appendix C: Laboratory Photos.

Table 27: Initial and Final Conditions of Specimens for the Shear Test for Control

Conditions at Start of Shear			
Specimen thickness(mm)	7.285	7.488	7.413
Dry unit weight (kN/m^3)	11.81	12.14	12.72
Normal Stress	127.10	176.07	249.55
Rate of Shear Displacement (deg/min)	0.019	0.020	0.019
OCR	1.96	1.42	1.00
Conditions at End of Shear			
Peak Shear Strength (kPa)	53.02	71.12	88.95
Residual Shear Strength (kPa)	20	28	41
Average Shear Displacement (mm)	20.77	20.44	20.40
Change in Specimen Thickness (mm)	-0.107	-0.162	-0.489
Gravimetric Water Content (%)	43.07	42.63	39.35
Volumetric Water Content (%)	56.15	55.58	51.30

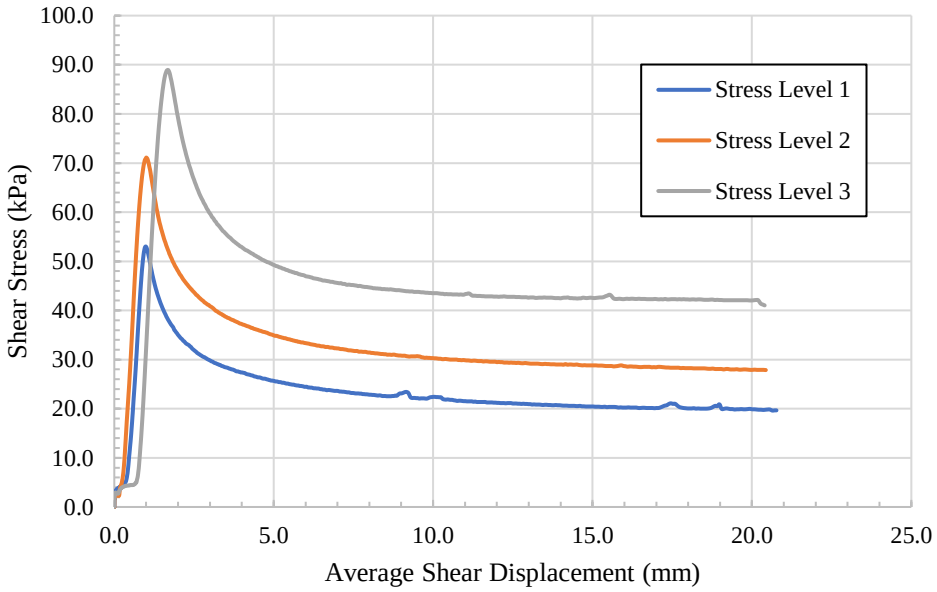

Figure 149: Shear Stress versus Average Shear Displacement for Control

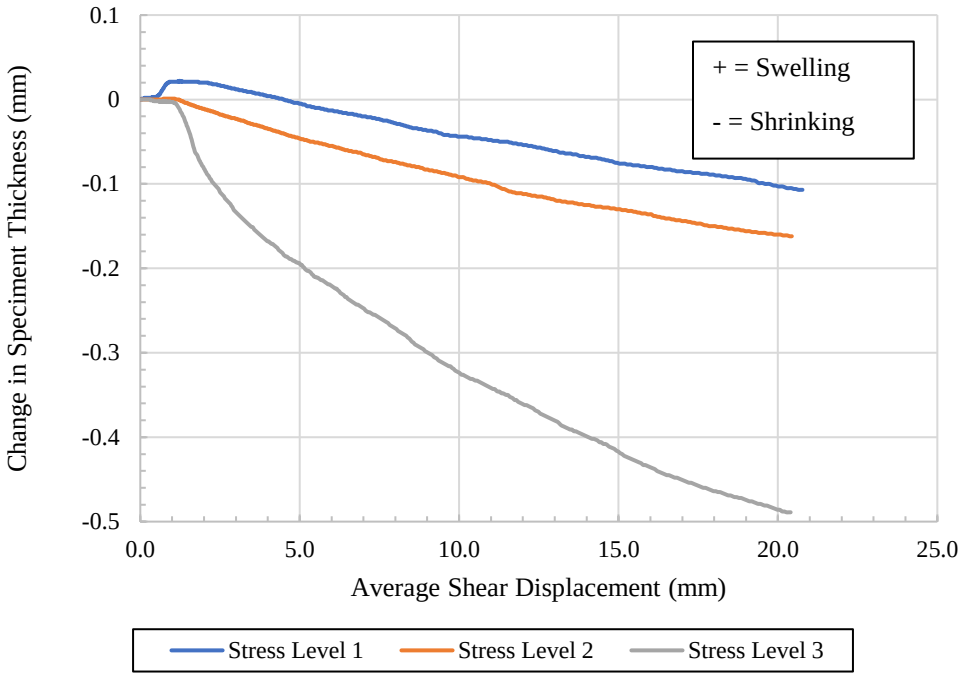

Figure 150: Change in Specimen Thickness During Shearing for Control

The specimens for stress level 1 and 2 failed when the average shear displacement reached approximately 1 mm; whereas, the specimen for stress level 3 failed at a shear displacement of roughly 2 mm. The peak and residual shear stress increased with each stress level. The specimen used in stress level 1 testing swelled at the beginning of the shear testing and started to decrease in thickness around an average shear displacement of 4 mm. The specimens for stress level 2 and 3 remained constant at the beginning of the test, but quickly started to decrease in thickness.

The peak and residual shear strengths were plotted with the normal stress for each specimen. As previously stated, the cohesion was assumed to be 0 kPa. From these plots, a peak and residual shear resistance can be determined. Figure 151 and Figure 152 show the peak and residual shear strength envelopes. Table 28 shows the angles computed for the peak and residual shear resistance for the control test section.

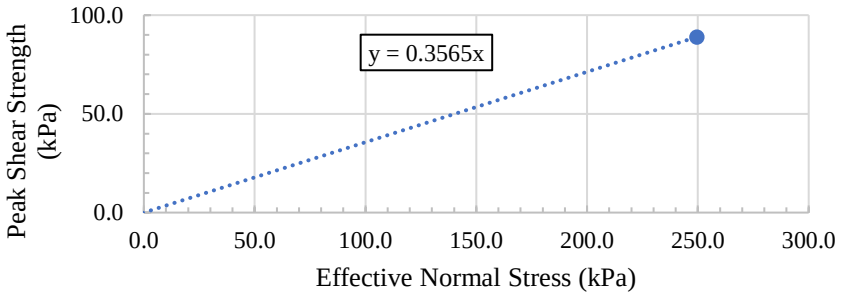

Figure 151: Peak Strength versus Effective Normal Stress for Control All Stress Level

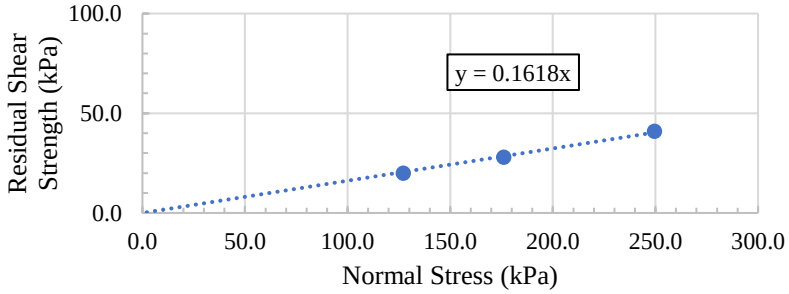

Figure 152: Residual Shear Strength versus Effective Normal Stress for Control All Stress Levels

Table 28: Angle of Peak and Residual Shear Resistance for Control

Peak Shear Strength	
Cohesion (kPa)	0
Angle of Peak Shear Resistance (º)	19.6
Residual Shear Strength	
Cohesion (kPa)	0
Angle of Residual Shear Resistance (º)	9.2

The angle of peak shear resistance was determined to be 19.6 degrees and the angle of residual shear resistance was calculated to be 9.2 degrees when the trendline was forced through the origin. The failure envelopes are very low angles; therefore, the material was considered to be very weak.

7.1.7 Combined Ring Shear Data

Table 29 summarizes all the data determined using the Bromhead ring shear testing device for each test section. The data is similar for each stress level in the different test section. The peak shear stress values have more variability than the residual stress values between the different test sections.

Table 29: Summary of Ring Shear Results

	Stress Level	Normal Stress (kPa)	Peak Shear Stress (kPa)	Residual Shear Stress (kPa)	Angle of Peak Shear Resistance, φ_p (º)	Angle of Residual Shear Resistance, φ_r (º)	Plasticity Index (%)
Sand Blanket (B1.5)	1	127.09	72.7	32	-	14.13	59
	2	176.08	76.53	37	-	11.87	
	3	249.55	92.27	47	20.3	10.66	
Vertical Barriers (B2.5)	1	127.1	73.04	24	-	10.69	50
	2	176.07	79.8	35	-	11.24	
	3	249.55	96.58	43	21.2	9.78	
Lime Columns (B3.5)	1	127.1	62.83	24	-	10.69	52
	2	176.08	74.39	32	-	10.30	
	3	249.55	97.72	52	21.4	11.77	
Paved Shoulders (B4.5)	1	127.09	63	24	-	10.69	55
	2	176.08	87.25	35	-	11.24	
	3	249.55	95.8	51	21	11.55	
Edge Drains (B5.5)	1	127.1	61.61	24	-	10.69	61
	2	176.07	69.11	31	-	9.99	
	3	249.55	87.1	43	19.2	9.78	
Control	1	127.1	53.02	20	-	8.94	48
	2	176.07	71.19	28	-	9.03	
	3	249.55	88.95	41	19.6	9.33	

Using the relationship between the plasticity index and sin φ in Lambe and Whitman (1969), Figure 153 was generated. The peak angles of shear resistance were used in this plot to compare the AL-5 ring shear data to the previous correlations determined by Kenney (1959). The peak shear strength results from the ring shear device are relatively close to the empirical

trendline. The peak shear strength data produced from the ring shear testing fits well with previous research on highly plastic clays.

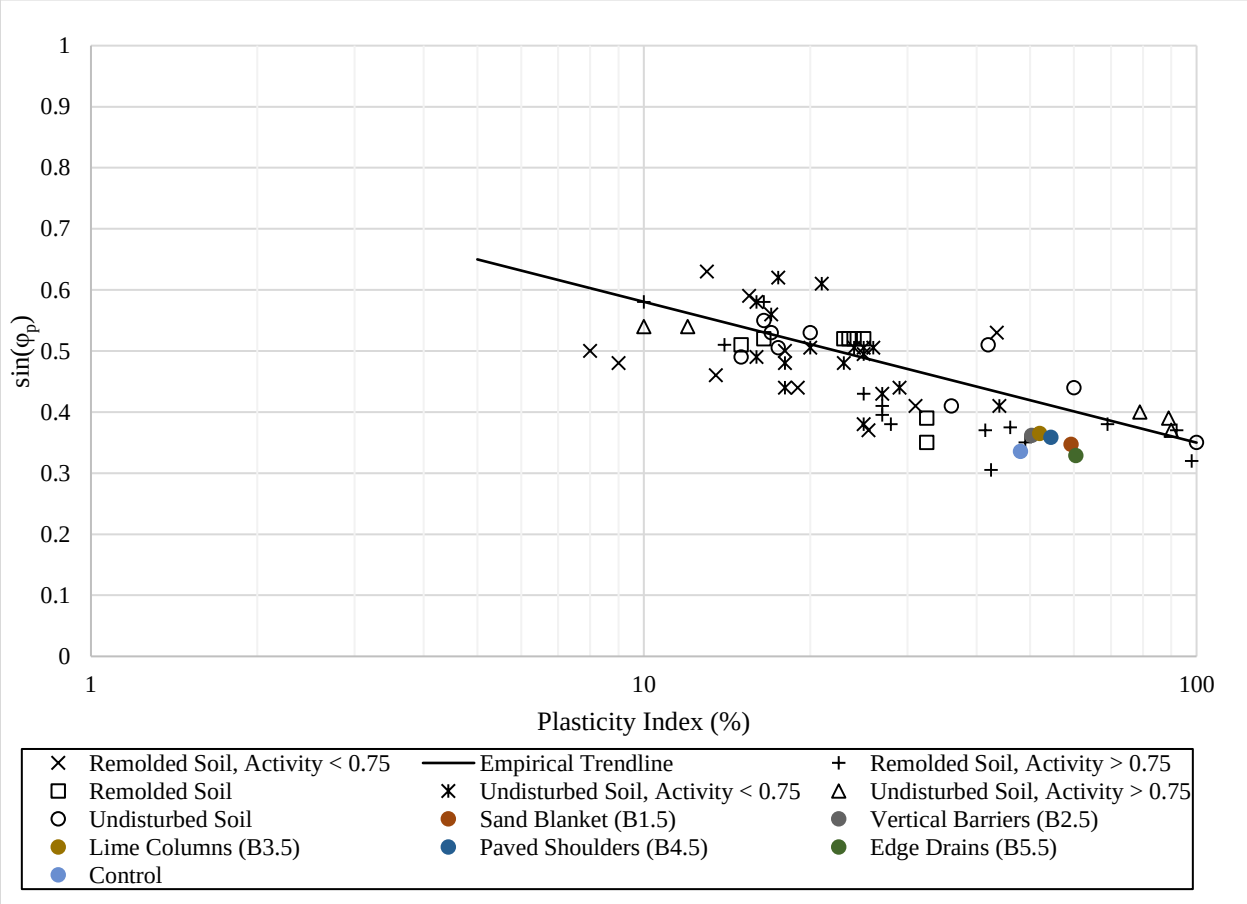

Figure 153: Plasticity Index versus Sin φ_p Using Data from Kenney (1959) (After Lambe and Whitman 1969)

Figure 153 shows different data used from Kenney (1959). There were two different types of soil tested including remolded specimens and undisturbed specimens. The activity of these specimens was then determined. If the activity of the specimen was greater than 0.75 then the specimen had a larger water holding capacity; therefore, was attracted to water more.

Referencing the typical values of residual friction angles as a function of effective normal stress by Mitchel and Soga (2005), the residual friction angles for each stress level was computed

and plotted for the material from AL-5. Figure 154 shows the residual friction angle versus the normal effective stress raised to the minus one third power. The material from AL-5 lines up very well with the residual friction angles for the material containing weald clay and montmorillonite.

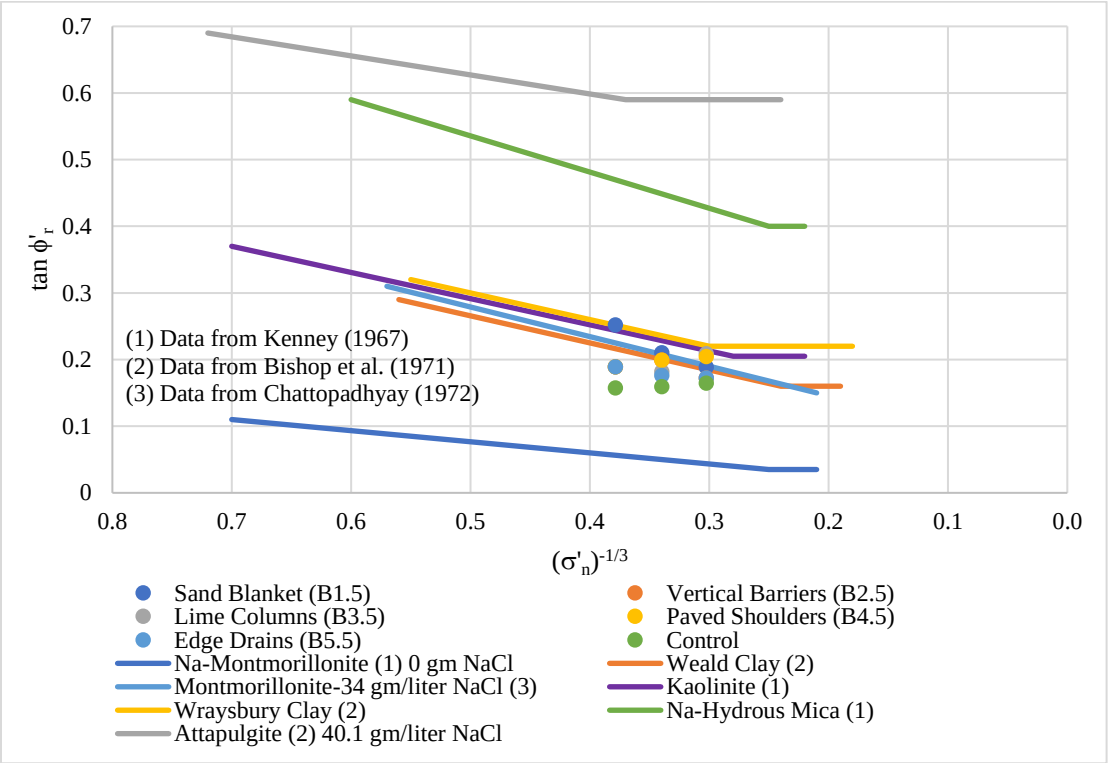

Figure 154: Comparing Residual Friction Angles versus Effective Normal Stress Raised to the One Third Power from AL-5 (After Mitchel and Soga 2005)

7.2 Slope Stability

Slope stability analyses were performed on all test sections with remediation techniques applied to them. Bishop's Method was used to analyze the road embankments using SLIDE. SLIDE is a slope stability software by RocScience. The soil profiles were determined by using boring logs provided in Appendix A. The water table was placed at the bottom of the embankment because observations during site visits concluded there had been pooling water at

the toe of the embankments. Suction was not accounted for above the water table for these analyses. The geometry of the embankments was determined by using the plans provided by ALDOT for each test section. An average slope of 3:1 was used for all the scenarios. Figure 155 shows a typical slope of the roadway embankment at AL-5.

Figure 155: Typical Slope for AL-5 Roadway Embankments

Figure 156 shows an example of the soil profile for the sand blanket test section using the residual strength values for the analysis. As stated in the literature review and using Table 2, the worst case cohesion and internal angle of friction value for the asphalt concrete was used. Therefore, a cohesion value of 7700 psf and internal angle of friction value of 34.1 degrees were inputted into the software for the material properties of the asphalt concrete. Table 30 shows the

correlated undrained shear strength values for layer 2 and 3 of the boring logs. These values were correlated using the plasticity index as stated in the literature review.

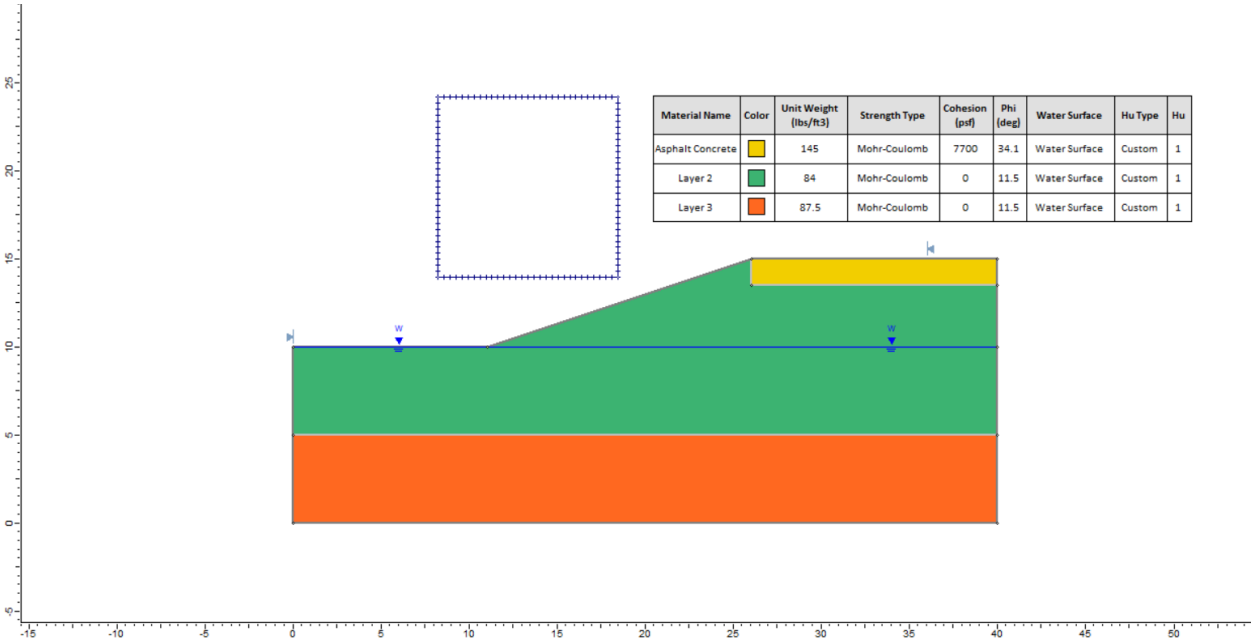

Figure 156: Example of Soil Profile for B1.5 using Residual Strength Values

Table 30: Correlated Undrained Shear Strength from Plasticity Index

Boring #	Layer	Undrained Shear Strength (psf)
1.5	AC	-
	2	164.42
	3	250.10
2.5	AC	-
	2	175.21
	3	193.70
3.5	AC	-
	2	146.17
	3	205.37
4.5	AC	-
	2	134.48
	3	209.70
5.5	AC	-
	2	167.44
	3	230.46

Three different scenarios were computed for each test section. The factor of safety was determined for the end of construction of the roadway; therefore, the undrained shear strength was inputted into the software. The factor of safety was determined under drained conditions; therefore, the peak shear strength envelope value from the ring shear testing was used and lastly, the factor of safety after localization or failure was computed. The factor of safety after failure used the residual shear strength envelope in the software determined by the ring shear testing. Figure 157 shows the output of the analysis when the software is run. The minimum factor of safety for the residual strength values for the sand blanket test section is 0.571; therefore, the embankment is very unstable and would be expected to have slope stability problems. The software was used for each scenario for each test section and the results from the slope stability analyses are shown in Table 31.

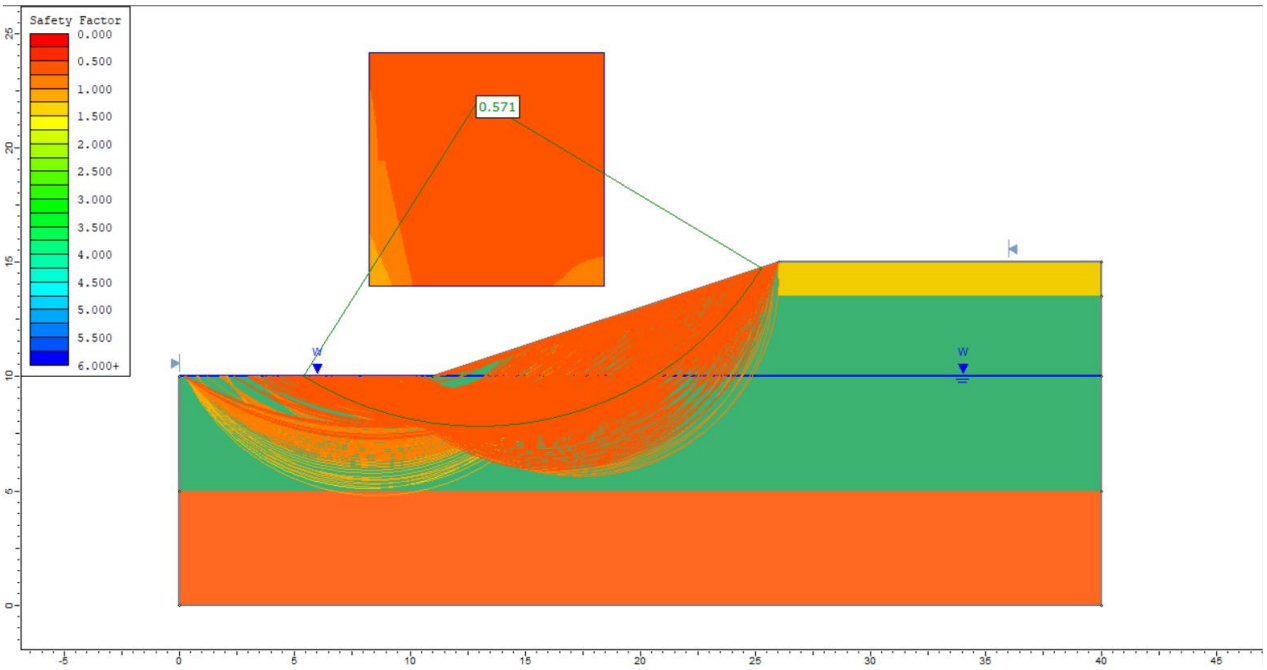

Figure 157: Minimum Failure Surfaces for B1.5 using Residual Strength Values

Table 31: Factor of Safety for Slope Stability

	Factor of Safety		
Test Section	Undrained Shear Strength, End of Construction (Correlated)	Peak Shear Strength, Drained	Residual Shear Strength, After Failure
Sand Blanket (B1.5)	3.115	1.038	0.571
Vertical Barriers (B2.5)	3.343	1.274	0.535
Lime Columns (B3.5)	2.93	1.154	0.549
Paved Shoulders (B4.5)	2.953	1.19	0.55
Edge Drains (B5.5)	3.332	1.045	0.483

As shown in Table 31, all of the slopes were stable after construction was completed with factor of safety values as high was 3.34. However, as time has passed, the factor of safety has decreased until failure of the slope or embankment was met. At the time of failure, the factor of safeties are very close to 1. After failure, the strength value of the material was decreasing and caused the factor of safety to decrease. Using the residual strength values results in factor of safeties around 0.5; therefore, all the slopes would likely experience stability issues if the residual strength of the material was reached. These slope failures could be an explanation of the cracks seen in the pavement and the pavement distress in the travel lanes. The analyses have shown relatively deep circular failures which has been observed on the embankments along AL-5.

The preliminary slope stability analysis was completed for AL-5. Limitations and assumption were incorporated with each analysis. The water table was assumed to be located at the toe of the embankment. The geometry of the soil profiles was very simple and was determined from the cross sections of each test section and the boring logs. Suction was not accounted for above the water table. Each layer thickness was assumed to have reached the residual strength throughout the entire layer. Another limitation was the correlated undrained

shear strength values inputted into the software since undrained shear strength test were not performed in the laboratory. These assumptions and limitations should be minimized in order to produce less conservative factors of safety.

CHAPTER 8: SUMMARY & CONCLUSIONS

8.1 Summary

AL-5 is an important farm-to-market roadway that has been built on expansive clays. The expansive clays are causing pavement distress to occur in the travel lanes of AL-5. Six remediation techniques were applied to eight half mile sections of the roadway. Sensors and gages were installed to continuously monitor the subgrade and the asphalt concrete. The primary objective of this investigation was to determine the drained residual shear strength of the subgrade causing pavement distress. Other objectives include observing the shrink and swell behavior of specimens during shearing, determining the drained peak shear strength of the subgrade, and determining if slope stability issues are present on the roadway embankments.

8.2 Conclusions

In conclusion, the objectives of this investigation were completed as follows:

- Continuous monitoring of the pavement and subgrade instrumentation has shown improvements in the pavement distress over the past few years. The lime column test section is the most improved section of roadway with low IRI values and stabilized volumetric moisture contents.
- The drained peak and residual shear strength of all test sections was completed using a Bromhead ring shear testing device. The results of the tests can be found in Chapter 7. The tests concluded very low angles of residual resistance for the subgrade; therefore, the material is very weak and could likely be the cause of the pavement distress.
- Observed slope stability issues were present on the roadway embankments at Al-5. The SLIDE analyses showed the potential for instability if the residual shear strength was

reached. The roadway was determined to be stable after the end of construction; however, the factor of safety quickly started to decrease as the peak shear strength of the subgrade was reached and continued to decrease after failure.

Based on these test results, it can be concluded that the subgrade is one of the major factors causing pavement distress in the roadway at AL-5.

8.3 Recommendations

It is recommended that additional ring shear tests at different effective normal stresses be performed. This will grow the sample size of the data points; therefore, statistical analysis can be completed for the shear strength of AL-5. Unconfined compressive tests can be performed in order to determine the undrained shear strength of the material. Triaxial tests could be performed to determine the undrained shear strength, but in the interest of time, an unconfined compression test would take less time to perform. The undrained shear strength values can then be used in a SLIDE analysis to determine a non-correlated end of construction factor of safety.

REFERENCES

Aitchison, G. D. (1961). *Relationship of Moisture and Effective Stress Functions in Unsaturated Soils.* British Nat. Soc. of Int. Soc. Mech. Found Eng. London, England: Pore Pressure and Suction in Soils Conf.

Alabama Department of Transportation. (2015). Research Project for Soil Stabilization of SR-5 from the Dallas County Line to 0.15 Miles North of E. Goley Road (MP 54.850). *Plans of Proposed Project Number 990305-535-005-401*.

Alabama Department of Transportation. (2018). *Alabama Traffic Data*. Retrieved August 20, 2019, from https://aldotgis.dot.state.al.us/atd/default.aspx#

Al-Mhaidib, A. I., & Al-Shamrani, M. A. (2006). Influence of Swell on Shear Strength of Expansive Soils. *Advances in Unsaturated Soil, Seepage, and Environmental Geotechnics*, GSP 148.

ASTM. (2011). *Standard Test Method for One-Dimensional Consolidation Properties of Soils Using Incremental Loading.* West Conshohocken: ASTM International.

ASTM. (2013). *Standard Test Method for Torsional Ring Shear Test to Determine Drained Residual Shear Strength of Cohesive Soils.* West Conshohocken: ASTM International.

ASTM. (2018). *Standard Test Method for Torsional Ring Shear Test to Measure Drained Fully Softened Shear Strength and Stress Dependent Strength Envelope of Fine-Grained Soils.* West Conshohocken: ASTM International.

Bishop, A. W. (1955). The use of the Slip Circle in the Stability Analysis of Slopes. In *Geotechnique* (pp. 7-17).

Bishop, A. W. (1959). *The Principle of Effective Stress.* Teknisk Ukeblad.

Bromhead, E. N. (1979). A Simple Ring Shear Apparatus. In *Ground Engineering* (Vol. 12, pp. 40-44).

Burrage, R. J. (2016). *Full Scale Testing of Two Excavations in an Unsaturated Piedmont Residual Soil.* Auburn University.

Castellanos, B. A. (2014). *Use and Measurement of Fully Softened Shear Strength.* Ph.D. Dissertation, Virginia Tech, Blacksburg.

Castellanos, B. A. (2014). *Use and Measurement of Fully Softened Shear Strength.* Ph.D. Dissertation, Virginia Tech, Blacksburg, VA.

Castellanos, B. A., Brandon, T. L., & VandenBerge, D. R. (2016). Correlations for Fully Softened Shear Strength Parameters. *Geotechnical Testing Journal, 39*(4).

Chattopadhyay, P. K. (1972). *Residual Shear Strength of Some Pure Clay Minerals.* Ph.D. Thesis, University of Alberta, Edmonton, Canada.

Christensen, D. W., Bonaquist, R., & Jack, D. P. (2000). *Evalutation of Triaxial Strength as a Simple Test for Asphalt Concrete Rut Resistance.* Pennsylvania State University. University Park: The Pennsylvania Transportation Institute.

Controls Group. (2019). Bromhead ring shear apparatus. Retrieved from https://www.controls-group.com/eng/soil-mechanics-testing-equipment/bromhead-ring-shear-apparatus.php

Croney, D., Coleman, J. D., & Black, W. P. (1958). *Movement and Distribution of Water in Soil in Relation to Highway Design and Performance.* Highway Res. Board Special Report no. 40, Washington, DC.

Fellenius, W. (1927). *Erdstatische Berechnungenmit Reibung und Kohasion.* Ernst, Berlin.

FHWA. (2001a). *Soil Slope and Embankment Design Reference Manual.* Federal Highway Administration, U.S. Department of Transportation. National.

Fredlund, D. G. (1973). *Volume Change Behavior of Unsaturated Soils.* Ph.D. Dissertation, University of Alberta, Edmonton, Alta., Canada.

Fredlund, D. G., & Morgenstern, N. R. (1977). Stress State Variables for Unsaturated Soils. *ASCE Journal of Geotechnical Engineering Division GT5*(103), 447-466.

Fredlund, D. G., & Rahardjo, H. (1993). *Soil Mechanics for Unsaturated Soils.* New York: John Wiley & Sons, Inc.

Fredlund, D. G., Rahardjo, H., & Fredlund, M. D. (2012). *Unsaturated Soil Mechanics in Engineering Practice.* Hoboken, NJ: John Wiley & Sons, Inc.

Google. (2019, August 20). *Google Earth Pro*.

Harris, M. C. (1998). *Soil Survey of Perry County, Alabama.* United States Department of Agriculture (USDA), Washington, D.C.

Herman, J. (2015). *Damage to Pavements from Expansive Clays: A Review of Behavior and Remediation Techniques.* Auburn Unversity: MCE Research Paper.

Herman, J. M. (2015). *Damage to Pavements from Expansive Clays: A Review of Behavior and Remediation Techniques.* MCE Research Paper, Auburn University.

Holtz, R. D., Kovacs, W. D., & Sheahan, T. C. (2011). *An Introduction to Geotechnical Engineering.* Upper Saddle River: Pearson Education.

Jackson, D. T. (2016). *Insitu Measurement of Pavement Distress and Causal Mechanisms in Expansive Soil along Alabama Highway 5.* MS Thesis Dissertation, Auburn University.

Jennings, J. E. (1961). *A Revised Effetive Stress Law for Use in the Prediction of the Behavior of Unsaturated Soils.* British Nat. Soc. of Int. Soc. Soil Mech. Found Eng. London, England: Pore Pressure and Suction in Soils Conf.

Jones, D. T. (2017). *Moisture Content Monitoring using a Nuclear Moisture Gauge and Preliminary FIndings at Alabama Highway 5.* MS Thesis Dissertation, Auburn University.

Kenney, T. C. (1959). Discussion. *Journal of the Soil Mechanics and Foundations Division, 85*, 67-79.

Kulhawy, F. H., & Mayne, P. W. (1990). Manual on Estimating Soil Properties for Foundation Design. *Electric Power Research Institute*, 308.

Lambe, T. W., & Whitman, R. V. (1969). *Soil Mechanics.* New York: John Wiley & Sons, Inc.

Little, D. N. (1995). *Handbook for Stabilization of Pavement Subgrades and Base Courses with Lime.*

Lu, N., & Likos, W. J. (2004). *Unsaturated Soil Mechanics.* Hoboken, NJ: John Wiley & Sons, Inc.

McCarthy, D. F. (2007). *Essentials of Soil Mechanics and Foundations: Basic Geotechnics* (7th ed.). Pearson.

Mesri, G., & Cepeda-Diaz, A. F. (1986). Residual Shear Strength of Clays and Shales. In *Geotechnique* (Vol. 36, pp. 269-274).

Mitchel, J. K., & Soga, K. (2005). *Fundamentals of Soil Behavior.* Wiley.

Nelson, J. D., & Miller, D. J. (1992). *Expansive Soils: Problems and Practice in Foundation and Pavement Engineering.* New York: John Wiley & Sons, Inc.

NOAA National Climatic Data Center. (1981-2010). *Selma Alabama 1981-2010 Climate Normals*. Retrieved from NOAA Satellite and Information Service.

Osborne, W. E., Copeland, C. W., & Wheat, D. H. (1989). Geologic Map of Alabama. *Special Map No. 221*. Geological Survey of Alabama, Tuscaloosa, Alabama.

Raymond, D. E., Osborne, W. E., Copeland, C. W., & Neathery, T. L. (1988). Alabama Stratigraphy. *Circular No. 140.* Geologic Survey of Alabama, Tuscaloosa, Alabama.

Stallings, E. G. (2016). *Investigation of Pavement and Subgrade Distress at Alabama Highway 5.* MS Thesis, Auburn University.

Stark, T. D. (2016). Discussion of "Correlations for Fully Softened Shear Strength Parameters" by B. A. Castellanos, T. L., Brandon, and D. R. VandenBerge, This Article Was Published in Geotechnical Testing Journal, Vol. 39, No. 4, 2016. [DOI:10.1520/GTJ20150184]. *Geotechnical Testing Journal*, *40*(3), 517-525.

Stark, T. D., & Eid, H. T. (1992). Comparison of Field and Laboratory Residual Strengths. *Proceedings of Specialty Conference Stability and Performance of Slopes and Embankments-II. I*, pp. 876-889. Berkeley, CA: ASCE.

Stark, T. D., & Hisham, E. (1993). Modified Bromhead Ring Shear Apparatus. *Geotechnical Testing Journal*, 100-107.

Stark, T. D., & Vettel, J. J. (1992). *Bromhead Ring Shear Test Procedure.* Philadelphia: American Society for Testing and Materials.

Steinberg, M. L. (1985). *Controlling Expansive Soil Destructiveness by Deep Vertical Geomembranes on Four Highways.* Transportation Research Board.

Szabo, M. W., Osborne, E. W., Copeland, C. W., & Neathery, T. L. (1988). Geologic Map of Alabama. *Special Map 220.* Geological Survey of Alabama.

APPENDIX A: BORING LOGS

AUBURN UNIVERSITY

BORING NUMBER B-1.5A
PAGE 1 OF 1

CLIENT Auburn Universtiy
PROJECT NAME AL-5 Research Project
PROJECT NUMBER 99-305-635-005-401
PROJECT LOCATION AL 5, Perry County
DATE STARTED 11/20/13 **COMPLETED** 11/20/13
GROUND ELEVATION 180 ft **HOLE SIZE** 4"
DRILLING CONTRACTOR ALDOT
GROUND WATER LEVELS:
DRILLING METHOD CME 55, Auto-Hammer, SFA w/ SPT
AT TIME OF DRILLING None Encountered
LOGGED BY **CHECKED BY**
AT END OF DRILLING None Encountered
NOTES
AFTER DRILLING None Encountered

ELEVATION (ft)	DEPTH (ft)	GRAPHIC LOG	MATERIAL DESCRIPTION	SAMPLE TYPE NUMBER	RECOVERY % SHELBY TUBE	BLOW COUNTS (N VALUE)	DRY UNIT WT. (pcf)	MOISTURE CONTENT (%)	ATTERBERG LIMITS: LIQUID LIMIT	ATTERBERG LIMITS: PLASTIC LIMIT	ATTERBERG LIMITS: PLASTICITY INDEX	FINES CONTENT (%)
180	0		Asphalt									
			FAT CLAY (CH) (A-7-6), gray, brown, medium, moist, Layer 1	ST	100				97	29	68	
175	5			ST	100		84.0	37.0	66	24	42	98
				ST	50							
				ST	100				91	25	66	
170	10			ST	75		87.5	32.9	85	24	61	98
			FAT CLAY (CH), yellow-brown, stiff, moist, Layer 1	ST	0							
				ST	100							
165	15		FAT CLAY (CH), light gray, hard (CHALK), Layer 2	SS	100	9-13-23 (36)						
			Boring was terminated at 16.7 feet.									
160	20											
155	25											
150	30											
145	35											

Figure 158: Boring Log for Sand Blanket (B1.5)

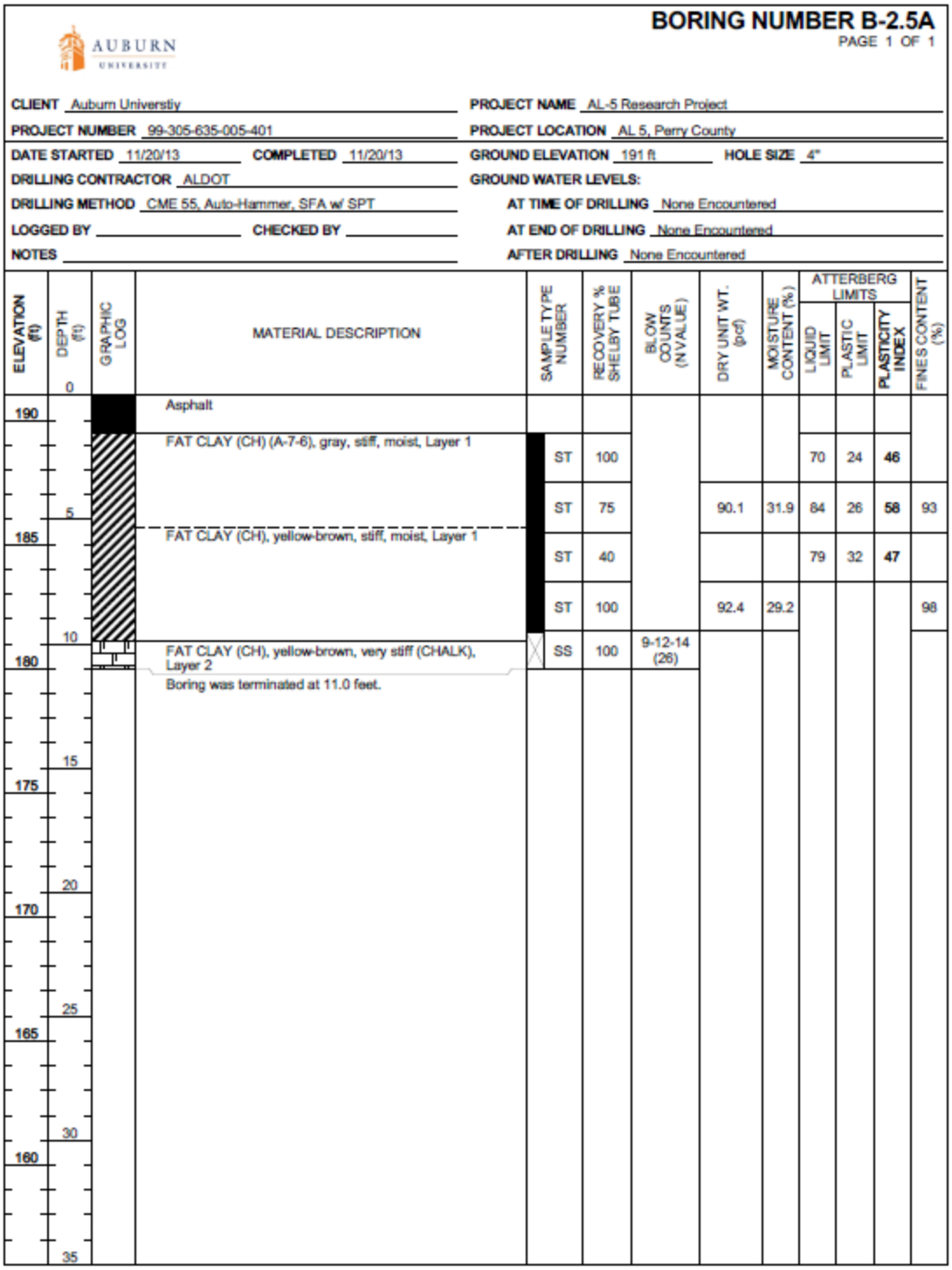

BORING NUMBER B-2.5A
PAGE 1 OF 1

AUBURN UNIVERSITY

CLIENT Auburn Universtiy
PROJECT NAME AL-5 Research Project
PROJECT NUMBER 99-305-635-005-401
PROJECT LOCATION AL 5, Perry County
DATE STARTED 11/20/13 COMPLETED 11/20/13
GROUND ELEVATION 191 ft HOLE SIZE 4"
DRILLING CONTRACTOR ALDOT
GROUND WATER LEVELS:
DRILLING METHOD CME 55, Auto-Hammer, SFA w/ SPT
AT TIME OF DRILLING None Encountered
LOGGED BY CHECKED BY
AT END OF DRILLING None Encountered
NOTES
AFTER DRILLING None Encountered

ELEVATION (ft)	DEPTH (ft)	GRAPHIC LOG	MATERIAL DESCRIPTION	SAMPLE TYPE NUMBER	RECOVERY % SHELBY TUBE	BLOW COUNTS (N VALUE)	DRY UNIT WT. (pcf)	MOISTURE CONTENT (%)	ATTERBERG LIMITS: LIQUID LIMIT	ATTERBERG LIMITS: PLASTIC LIMIT	ATTERBERG LIMITS: PLASTICITY INDEX	FINES CONTENT (%)
	0		Asphalt									
190			FAT CLAY (CH) (A-7-6), gray, stiff, moist, Layer 1	ST	100				70	24	46	
	5			ST	75		90.1	31.9	84	26	58	93
185			FAT CLAY (CH), yellow-brown, stiff, moist, Layer 1	ST	40				79	32	47	
				ST	100		92.4	29.2				98
	10											
180			FAT CLAY (CH), yellow-brown, very stiff (CHALK), Layer 2	SS	100	9-12-14 (26)						
			Boring was terminated at 11.0 feet.									
	15											
175												
	20											
170												
	25											
165												
	30											
160												
	35											

Figure 159: Boring Log for Vertical Barriers (B2.5)

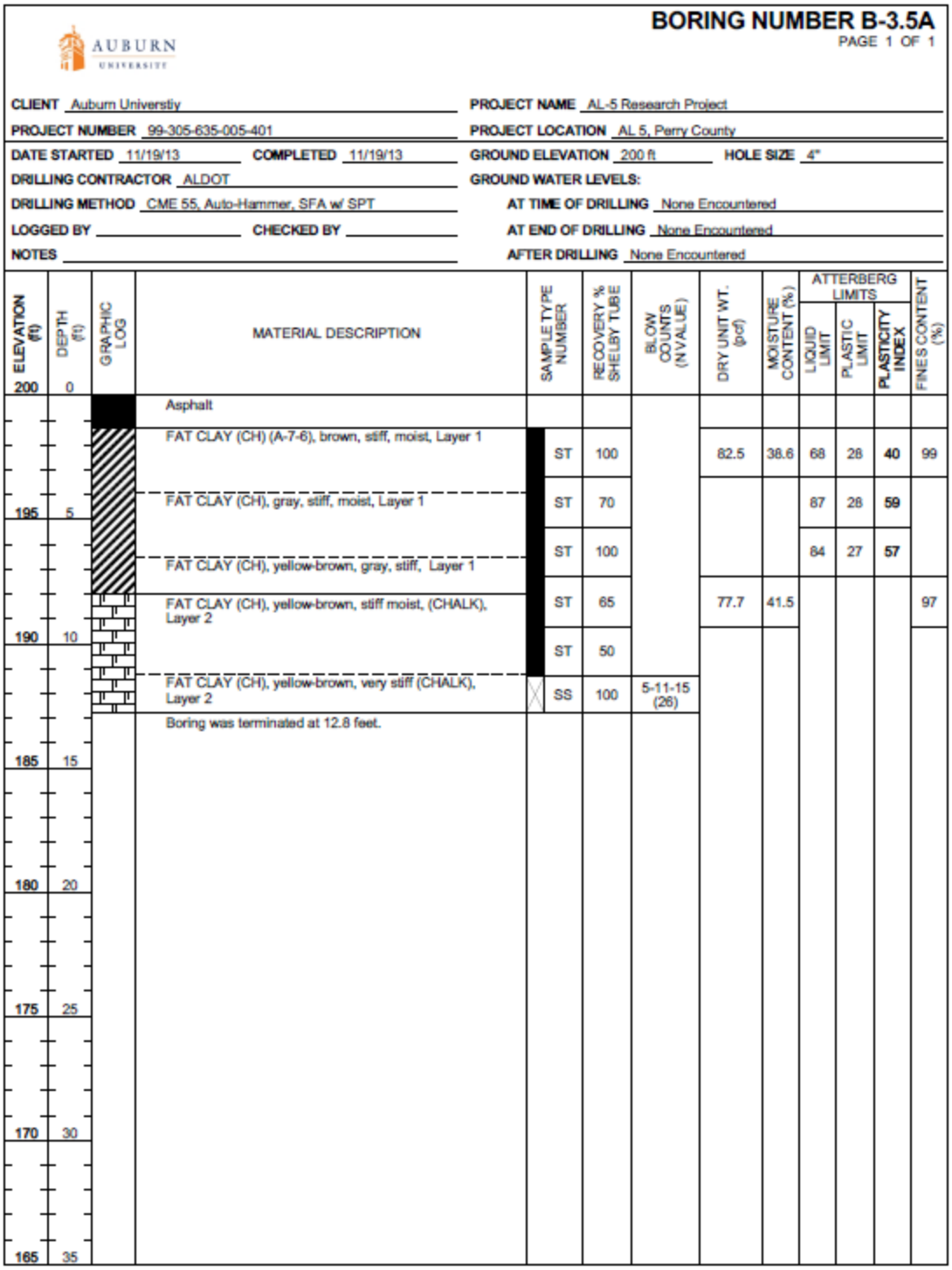

BORING NUMBER B-3.5A
PAGE 1 OF 1

AUBURN UNIVERSITY

CLIENT Auburn Universtiy
PROJECT NAME AL-5 Research Project
PROJECT NUMBER 99-305-635-005-401
PROJECT LOCATION AL 5, Perry County
DATE STARTED 11/19/13 COMPLETED 11/19/13
GROUND ELEVATION 200 ft HOLE SIZE 4"
DRILLING CONTRACTOR ALDOT
GROUND WATER LEVELS:
DRILLING METHOD CME 55, Auto-Hammer, SFA w/ SPT
AT TIME OF DRILLING None Encountered
LOGGED BY CHECKED BY
AT END OF DRILLING None Encountered
NOTES
AFTER DRILLING None Encountered

ELEVATION (ft)	DEPTH (ft)	GRAPHIC LOG	MATERIAL DESCRIPTION	SAMPLE TYPE NUMBER	RECOVERY % SHELBY TUBE	BLOW COUNTS (N VALUE)	DRY UNIT WT. (pcf)	MOISTURE CONTENT (%)	ATTERBERG LIMITS: LIQUID LIMIT	ATTERBERG LIMITS: PLASTIC LIMIT	ATTERBERG LIMITS: PLASTICITY INDEX	FINES CONTENT (%)
200	0		Asphalt									
			FAT CLAY (CH) (A-7-6), brown, stiff, moist, Layer 1	ST	100		82.5	38.6	68	28	**40**	99
195	5		FAT CLAY (CH), gray, stiff, moist, Layer 1	ST	70				87	28	**59**	
				ST	100				84	27	**57**	
			FAT CLAY (CH), yellow-brown, gray, stiff, Layer 1									
			FAT CLAY (CH), yellow-brown, stiff moist, (CHALK), Layer 2	ST	65		77.7	41.5				97
190	10			ST	50							
			FAT CLAY (CH), yellow-brown, very stiff (CHALK), Layer 2	SS	100	5-11-15 (26)						
			Boring was terminated at 12.8 feet.									
185	15											
180	20											
175	25											
170	30											
165	35											

Figure 160: Boring Log for Lime Columns (B3.5)

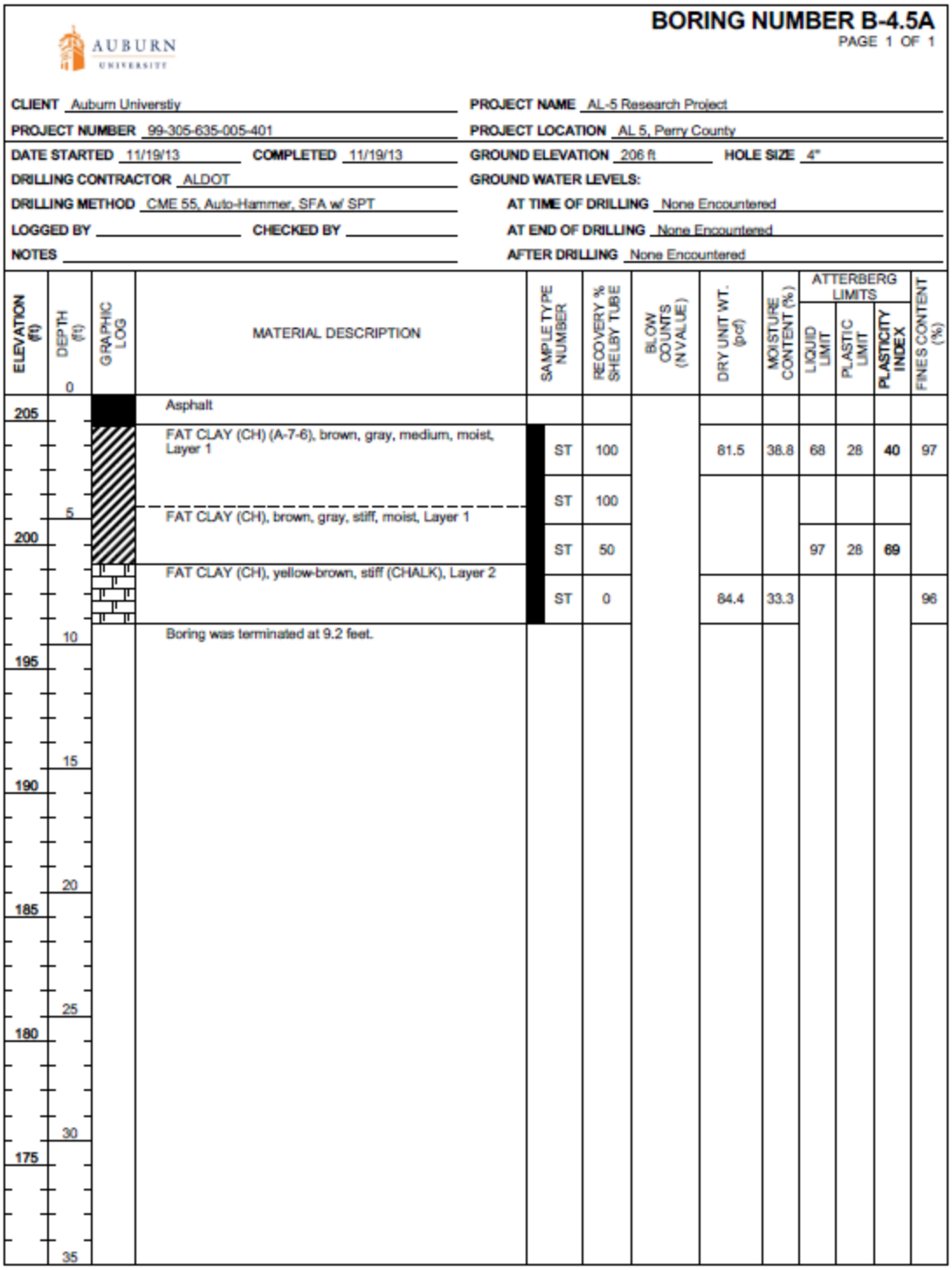

BORING NUMBER B-4.5A
PAGE 1 OF 1

AUBURN UNIVERSITY

CLIENT Auburn Universtiy
PROJECT NAME AL-5 Research Project
PROJECT NUMBER 99-305-635-005-401
PROJECT LOCATION AL 5, Perry County
DATE STARTED 11/19/13 COMPLETED 11/19/13
GROUND ELEVATION 206 ft HOLE SIZE 4"
DRILLING CONTRACTOR ALDOT
GROUND WATER LEVELS:
DRILLING METHOD CME 55, Auto-Hammer, SFA w/ SPT
AT TIME OF DRILLING None Encountered
LOGGED BY CHECKED BY
AT END OF DRILLING None Encountered
NOTES
AFTER DRILLING None Encountered

ELEVATION (ft)	DEPTH (ft)	GRAPHIC LOG	MATERIAL DESCRIPTION	SAMPLE TYPE NUMBER	RECOVERY % SHELBY TUBE	BLOW COUNTS (N VALUE)	DRY UNIT WT. (pcf)	MOISTURE CONTENT (%)	ATTERBERG LIMITS: LIQUID LIMIT	ATTERBERG LIMITS: PLASTIC LIMIT	ATTERBERG LIMITS: PLASTICITY INDEX	FINES CONTENT (%)
205	0		Asphalt									
			FAT CLAY (CH) (A-7-6), brown, gray, medium, moist, Layer 1	ST	100		81.5	38.8	68	28	**40**	97
	5			ST	100							
200			FAT CLAY (CH), brown, gray, stiff, moist, Layer 1	ST	50				97	28	**69**	
			FAT CLAY (CH), yellow-brown, stiff (CHALK), Layer 2	ST	0		84.4	33.3				96
	10		Boring was terminated at 9.2 feet.									
195												
	15											
190												
	20											
185												
	25											
180												
	30											
175												
	35											

Figure 161: Boring Logs for Paved Shoulders (B4.5)

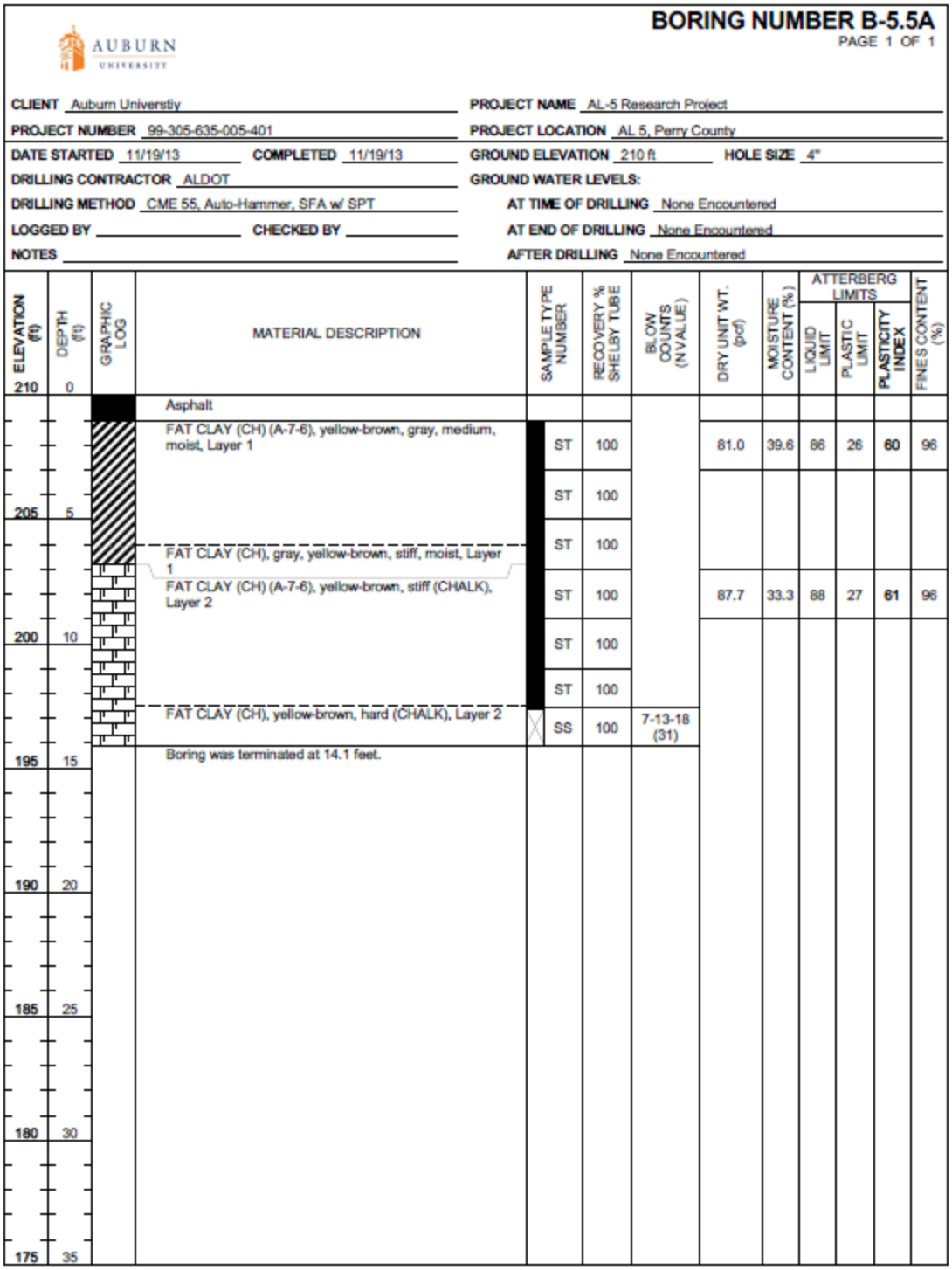

BORING NUMBER B-5.5A
PAGE 1 OF 1

AUBURN UNIVERSITY

CLIENT Auburn Universtiy
PROJECT NAME AL-5 Research Project
PROJECT NUMBER 99-305-635-005-401
PROJECT LOCATION AL 5, Perry County
DATE STARTED 11/19/13 COMPLETED 11/19/13
GROUND ELEVATION 210 ft HOLE SIZE 4"
DRILLING CONTRACTOR ALDOT
GROUND WATER LEVELS:
DRILLING METHOD CME 55, Auto-Hammer, SFA w/ SPT
AT TIME OF DRILLING None Encountered
LOGGED BY CHECKED BY
AT END OF DRILLING None Encountered
NOTES
AFTER DRILLING None Encountered

ELEVATION (ft)	DEPTH (ft)	GRAPHIC LOG	MATERIAL DESCRIPTION	SAMPLE TYPE NUMBER	RECOVERY % SHELBY TUBE	BLOW COUNTS (N VALUE)	DRY UNIT WT. (pcf)	MOISTURE CONTENT (%)	ATTERBERG LIMITS: LIQUID LIMIT	ATTERBERG LIMITS: PLASTIC LIMIT	ATTERBERG LIMITS: PLASTICITY INDEX	FINES CONTENT (%)
210	0		Asphalt									
			FAT CLAY (CH) (A-7-6), yellow-brown, gray, medium, moist, Layer 1	ST	100		81.0	39.6	86	26	60	96
205	5			ST	100							
				ST	100							
			FAT CLAY (CH), gray, yellow-brown, stiff, moist, Layer 1									
			FAT CLAY (CH) (A-7-6), yellow-brown, stiff (CHALK), Layer 2	ST	100		87.7	33.3	88	27	61	96
200	10			ST	100							
				ST	100							
			FAT CLAY (CH), yellow-brown, hard (CHALK), Layer 2	SS	100	7-13-18 (31)						
195	15		Boring was terminated at 14.1 feet.									
190	20											
185	25											
180	30											
175	35											

Figure 162: Boring Logs for Edge Drains (B5.5)

APPENDIX B: RAW DATA

Sand Blankets

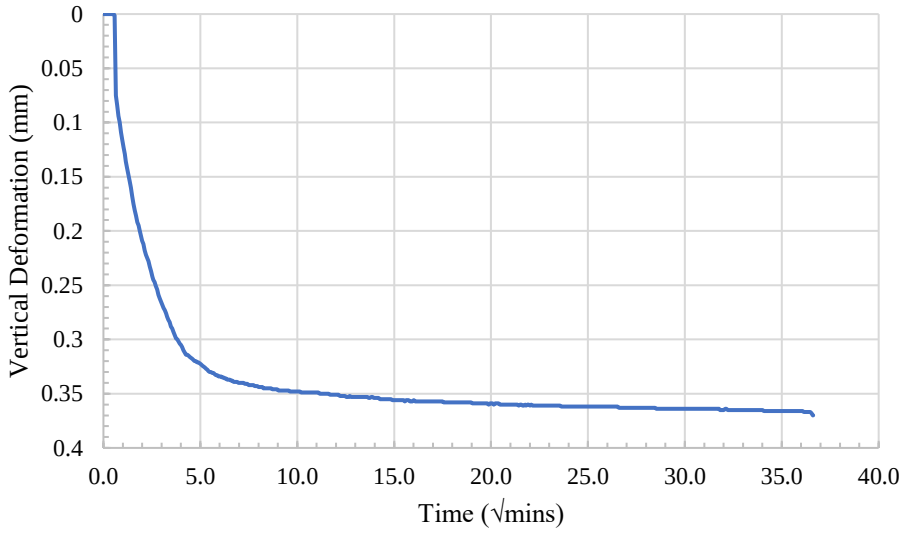

Figure 163: Consolidation Plot for Sand Blanket (B1.5) Stress Level #1

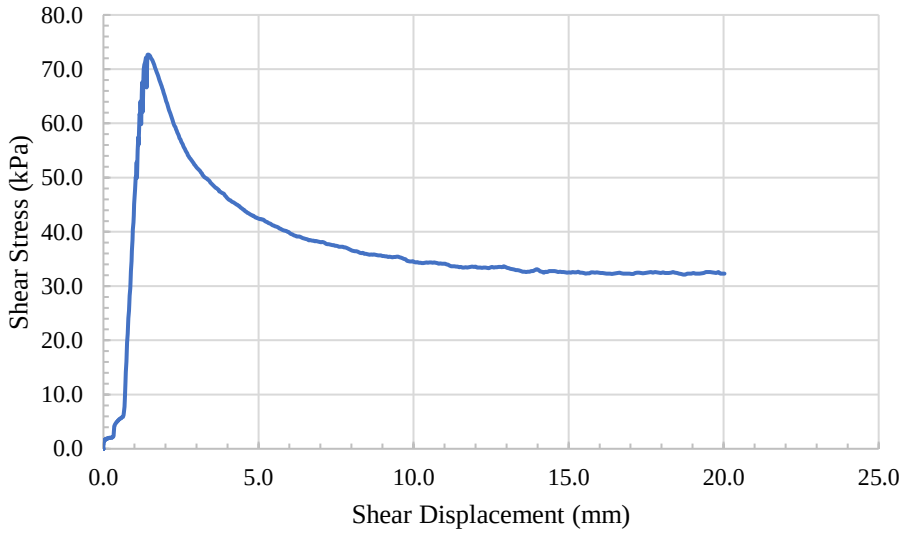

Figure 164: Shear Stress versus Shear Displacement for Sand Blanket (B1.5) Stress Level #1

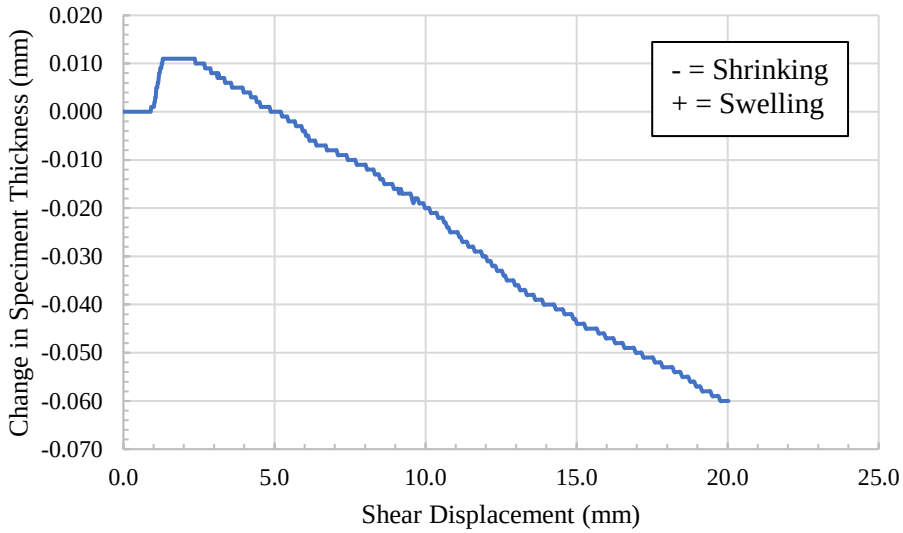

Figure 165: Change in Specimen Thickness versus Shear Displacement for Sand Blanket (B1.5) Stress Level #1

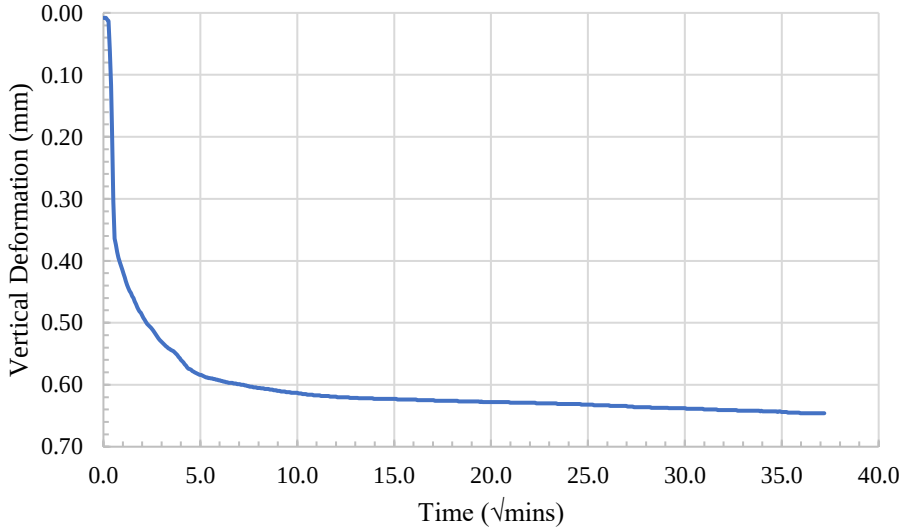

Figure 166: Consolidation Plot for Sand Blanket (B1.5) Stress Level #2

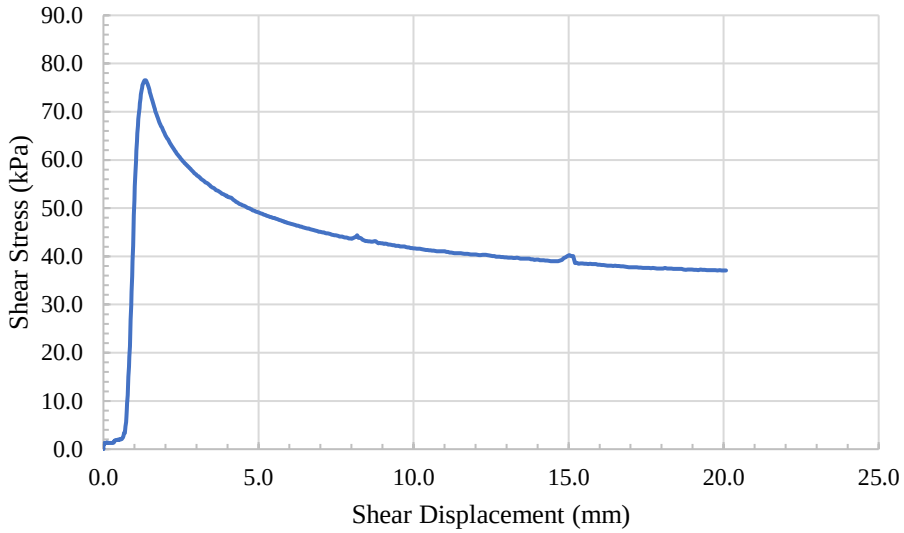

Figure 167: Shear Stress versus Shear Displacement for Sand Blanket (B1.5) Stress Level #2

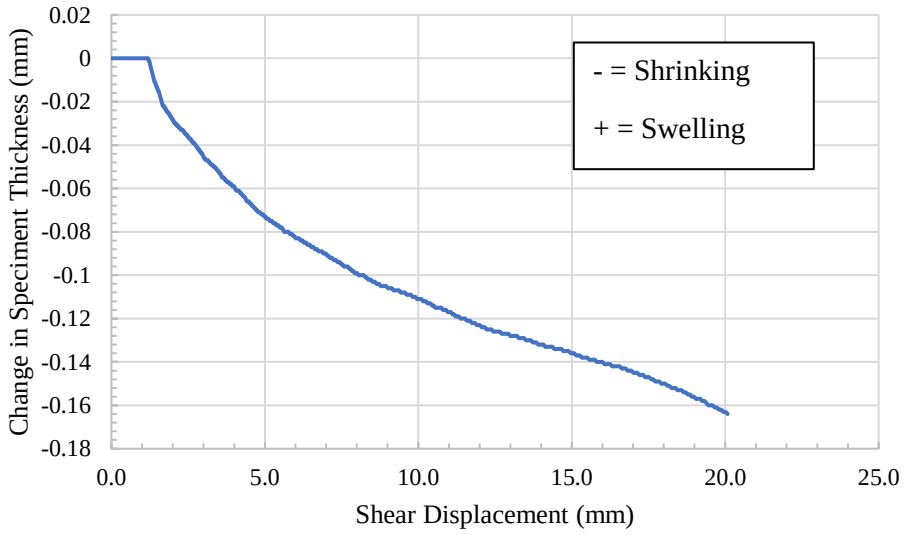

Figure 168: Change in Specimen Thickness versus Shear Displacement for Sand Blanket (B1.5) Stress Level #2

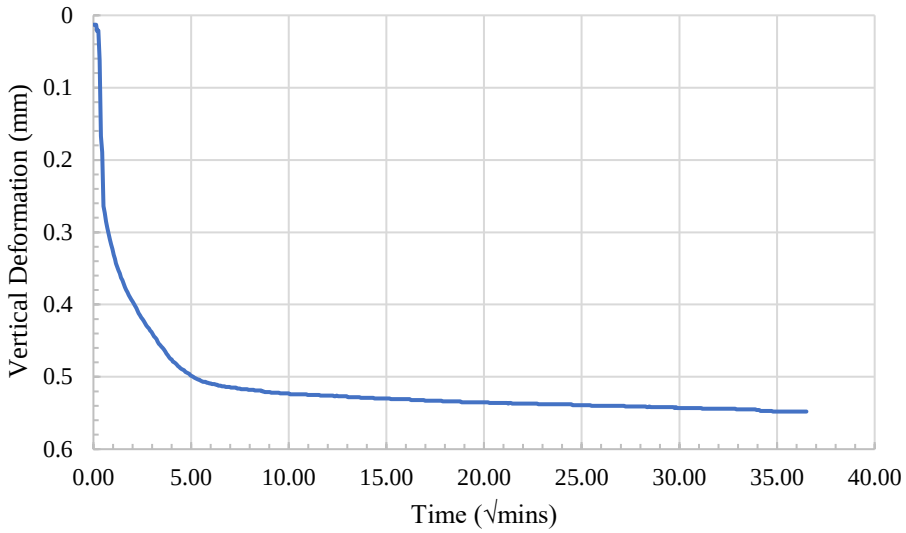

Figure 169: Consolidation Plot for Sand Blanket (B1.5) Stress Level #3

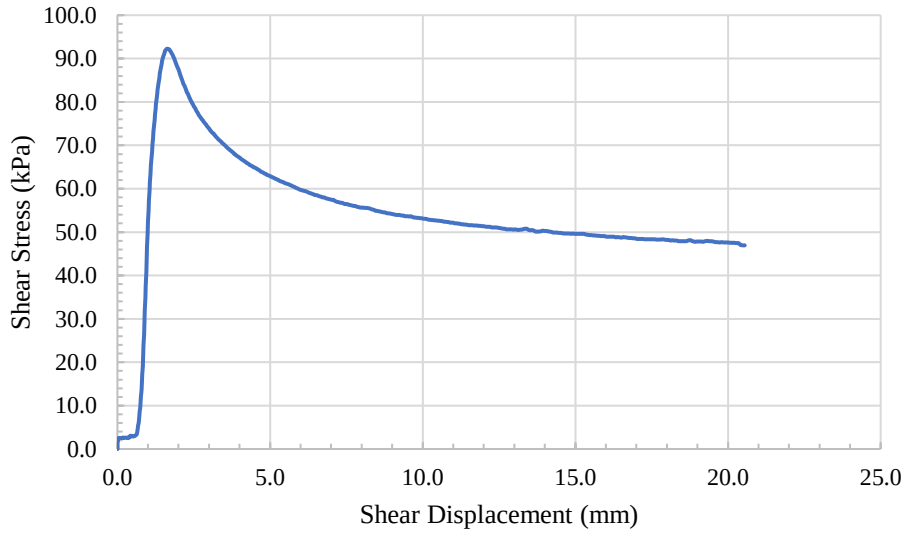

Figure 170: Shear Stress versus Shear Displacement for Sand Blanket (B1.5) Stress Level #3

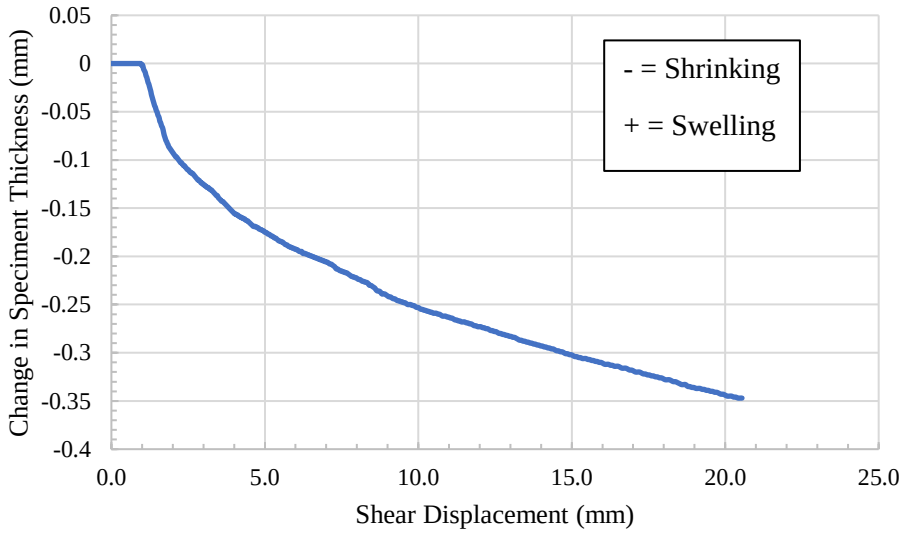

Figure 171: Change in Specimen Thickness versus Shear Displacement for Sand Blanket (B1.5) Stress Level #3

Vertical Barriers

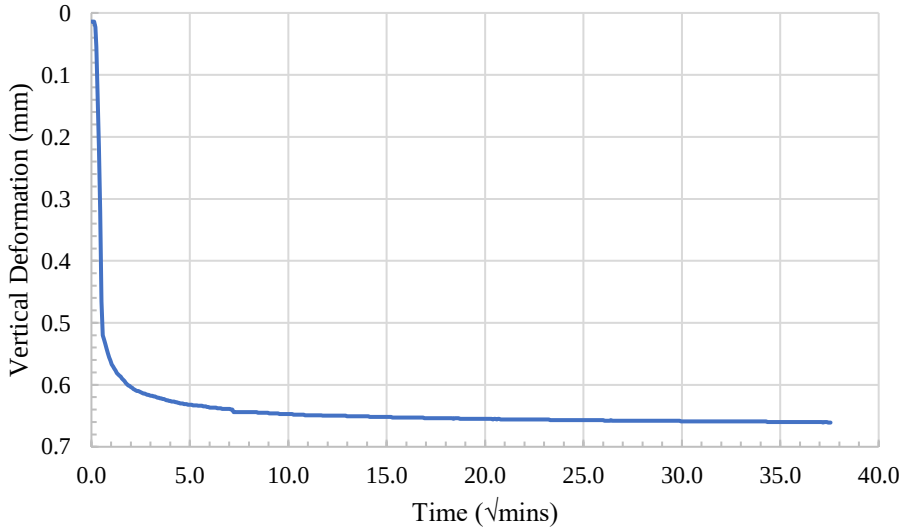

Figure 172: Consolidation Plot for Vertical Barriers (B2.5) Stress Level #1

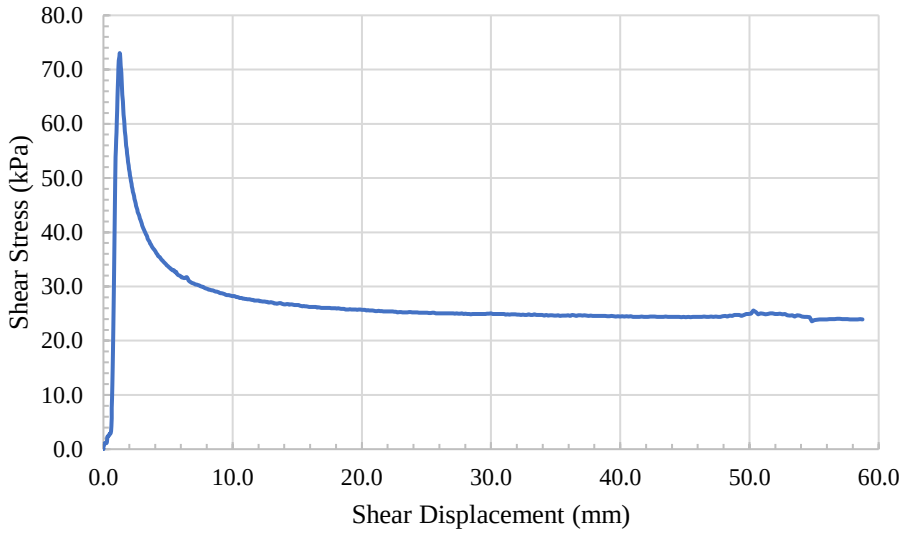

Figure 173: Shear Stress versus Shear Displacement for Vertical Barriers (B2.5) Stress Level #1

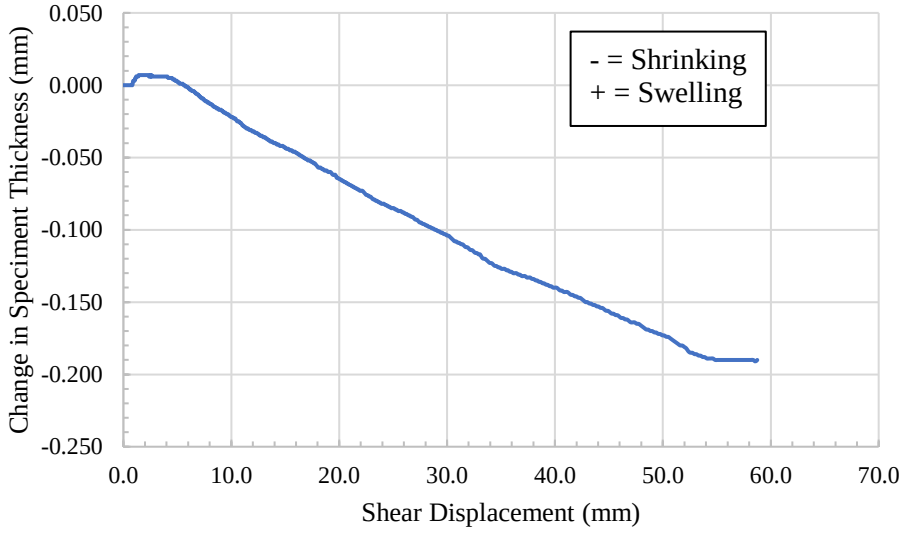

Figure 174: Change in Specimen Thickness versus Shear Displacement for Vertical Barriers (B2.5) Stress Level #1

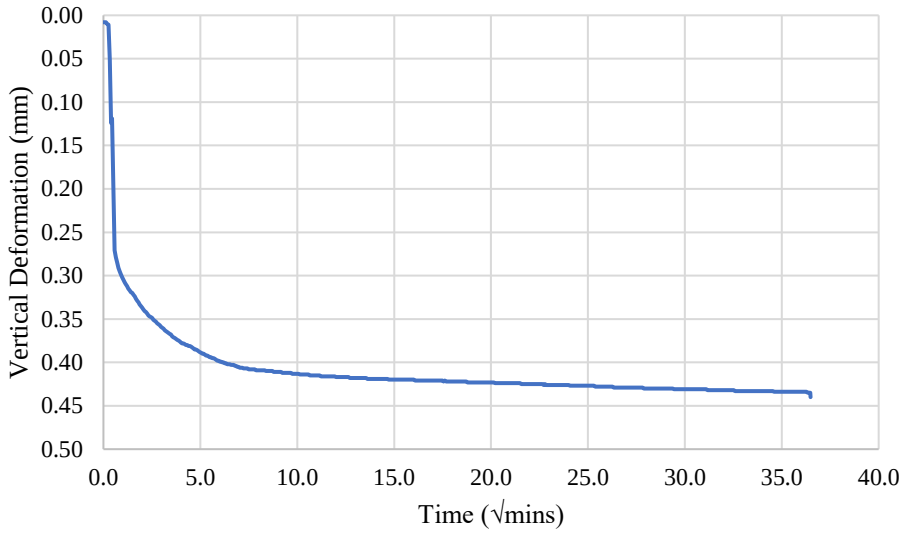

Figure 175: Consolidation Plot for Vertical Barriers (B2.5) Stress Level #2

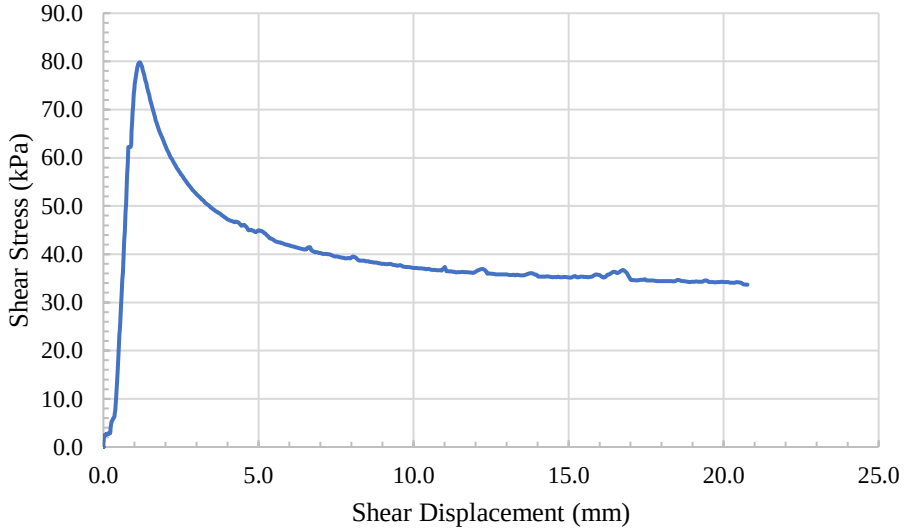

Figure 176: Shear Stress versus Shear Displacement for Vertical Barriers (B2.5) Stress Level #2

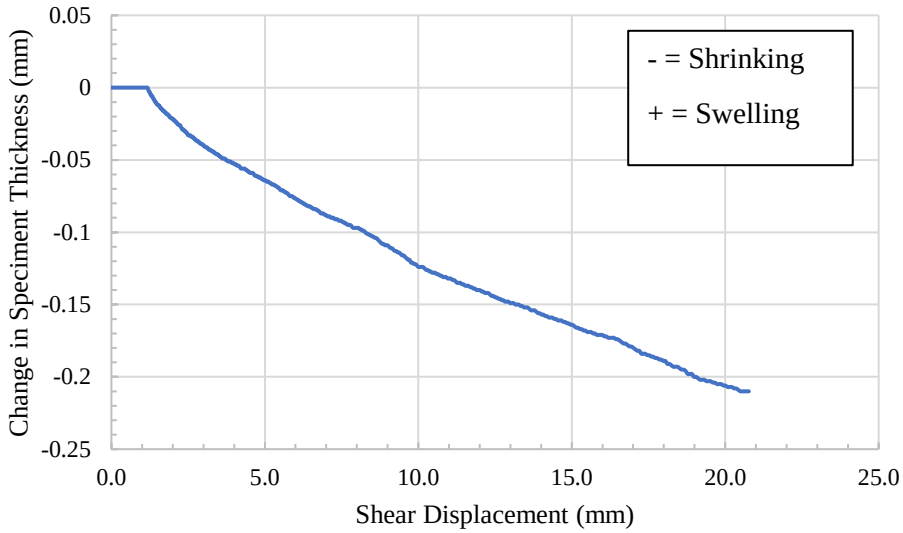

Figure 177: Change in Specimen Thickness versus Shear Displacement for Vertical Barriers (B2.5) Stress Level #2

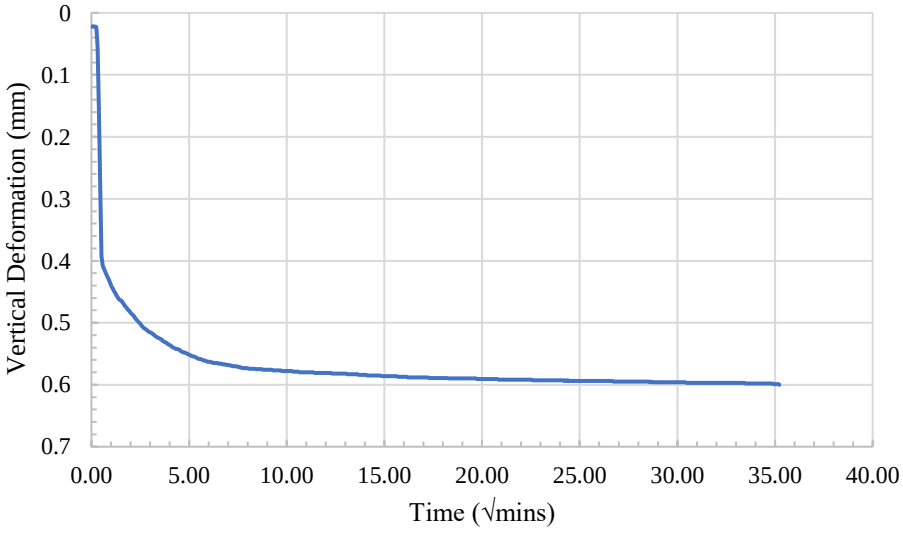

Figure 178: Consolidation Plot for Vertical Barriers (B2.5) Stress Level #3

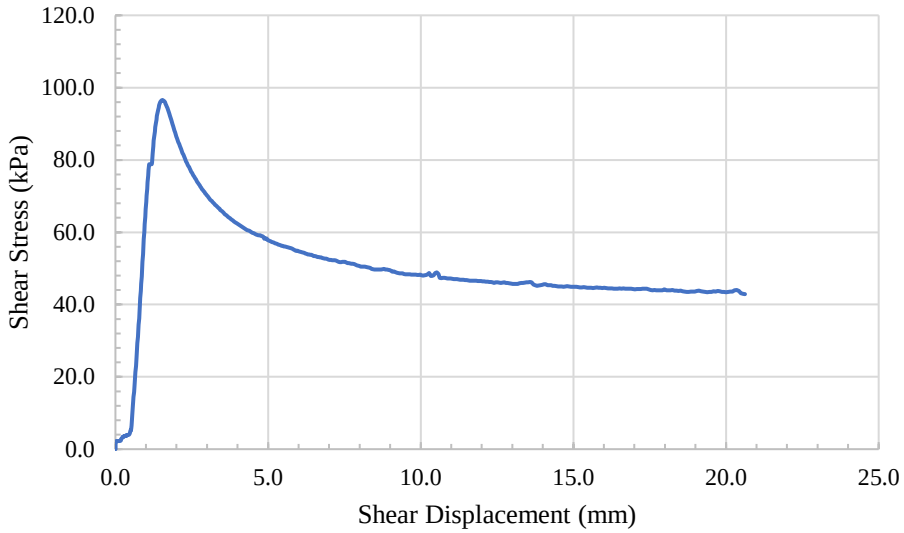

Figure 179: Shear Stress versus Shear Displacement for Vertical Barriers (B2.5) Stress Level #3

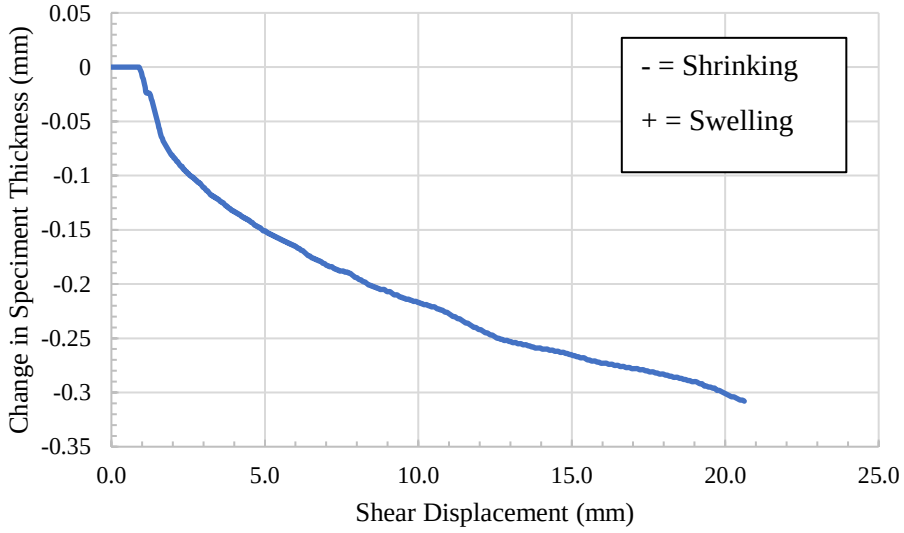

Figure 180: Change in Specimen Thickness versus Shear Displacement for Vertical Barriers (B2.5) Stress Level #3

Lime Columns

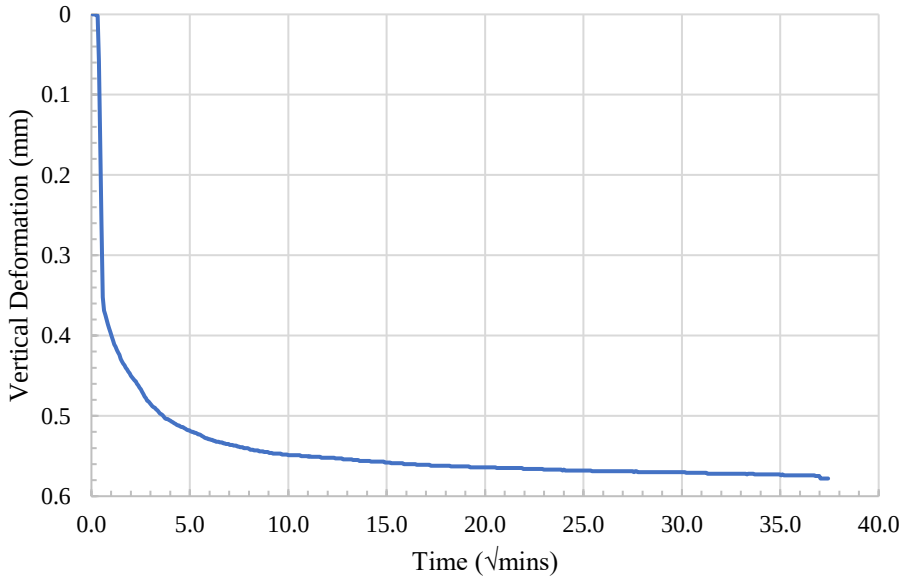

Figure 181: Consolidation Plot for Lime Columns (B3.5) Stress Level #1

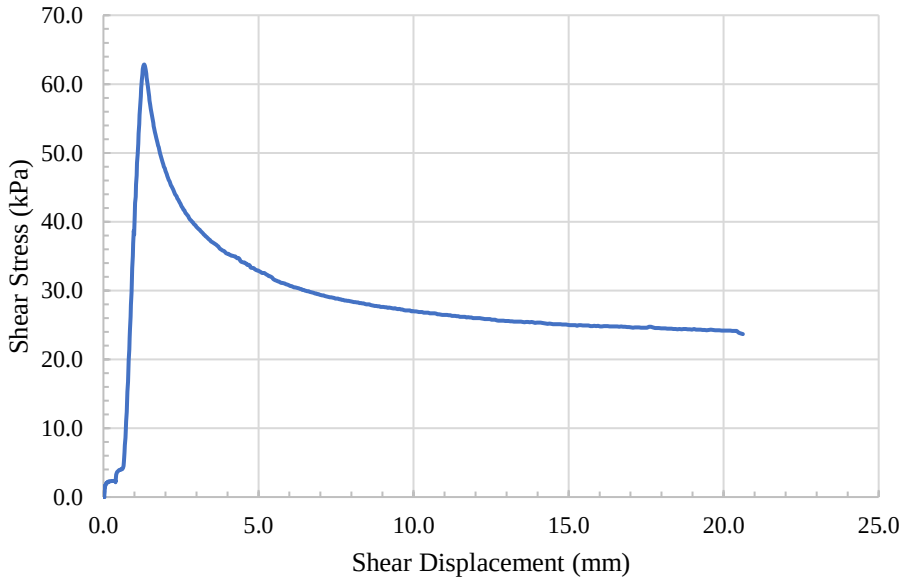

Figure 182: Shear Stress versus Shear Displacement for Lime Columns (B3.5) Stress Level #1

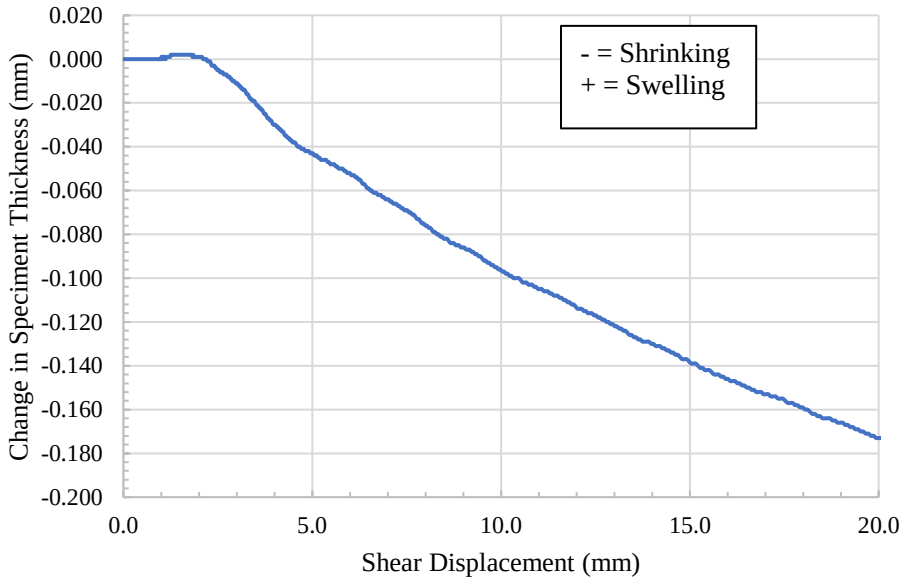

Figure 183: Change in Specimen Thickness versus Shear Displacement for Lime Columns (B3.5) Stress Level #1

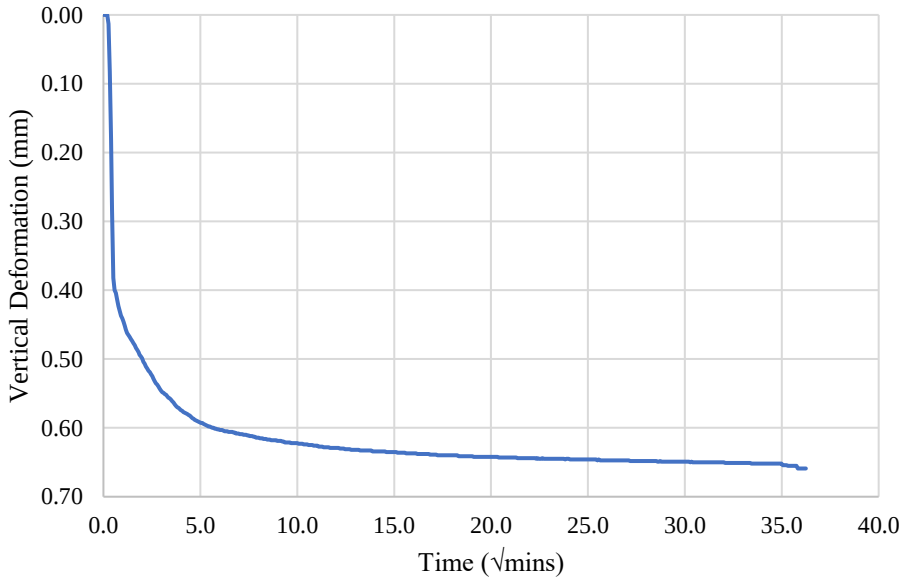

Figure 184: Consolidation Plot for Lime Columns (B3.5) Stress Level #2

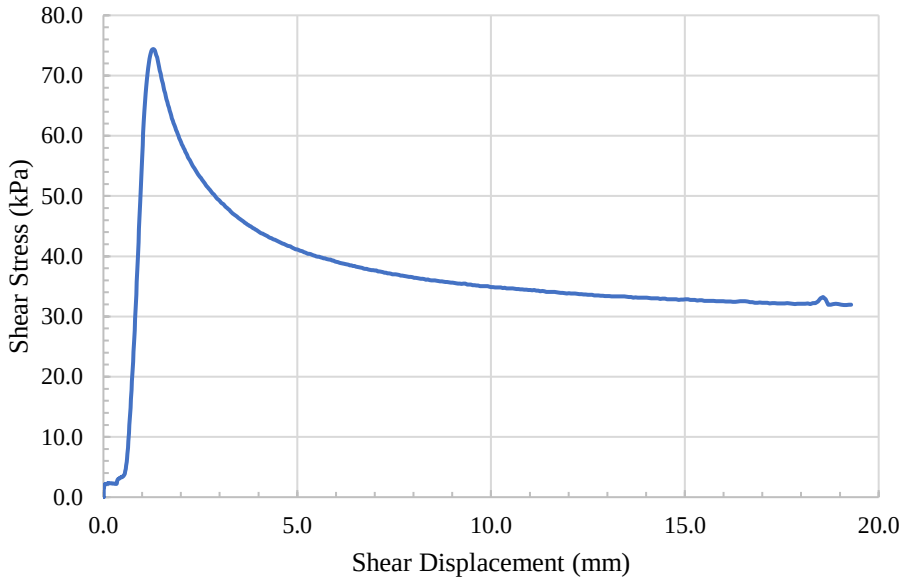

Figure 185: Shear Stress versus Shear Displacement for Lime Columns (B3.5) Stress Level #2

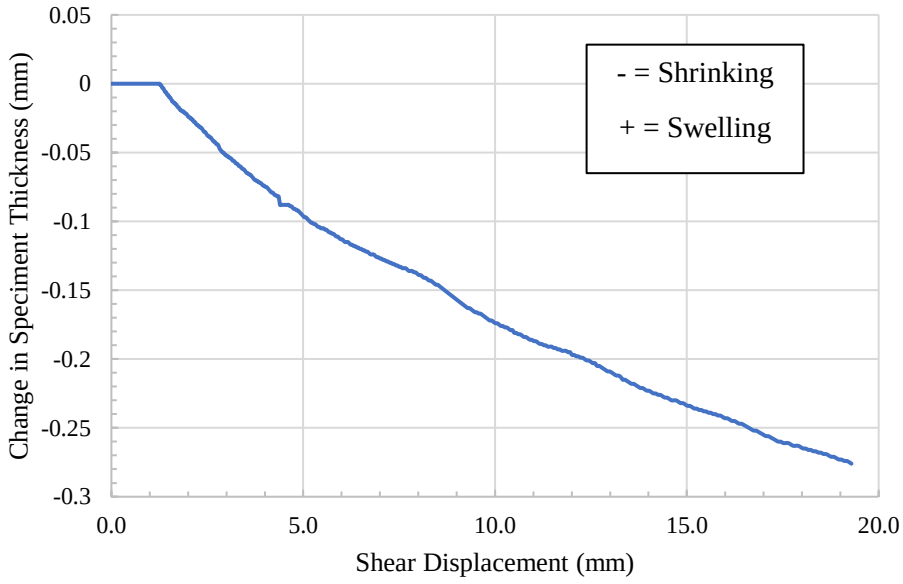

Figure 186: Change in Specimen Thickness versus Shear Displacement for Lime Columns (B3.5) Stress Level #2

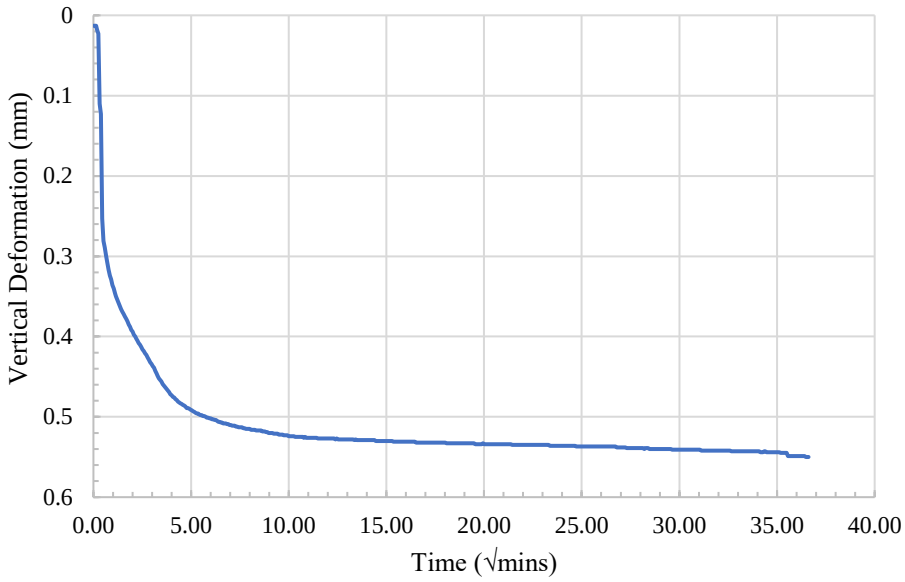

Figure 187: Consolidation Plot for Lime Columns (B3.5) Stress Level #3

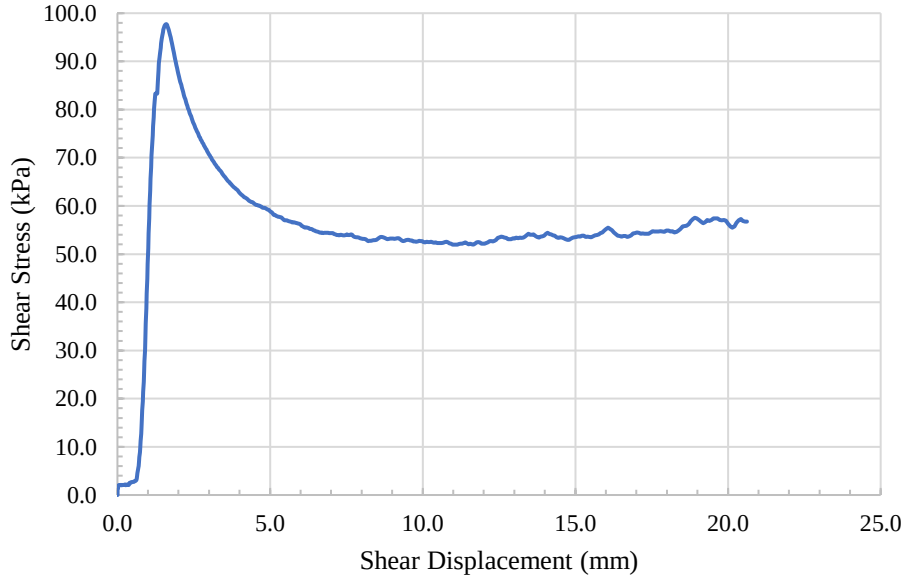

Figure 188: Shear Stress versus Shear Displacement for Lime Columns (B3.5) Stress Level #3

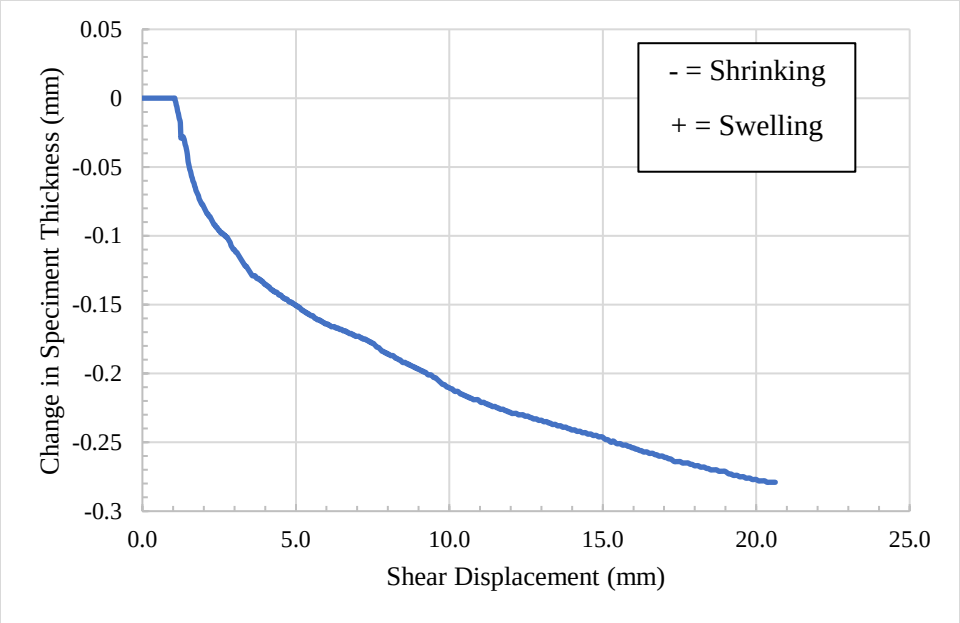

Figure 189: Change in Specimen Thickness versus Shear Displacement for Lime Columns (B3.5) Stress Level #3

Paved Shoulders

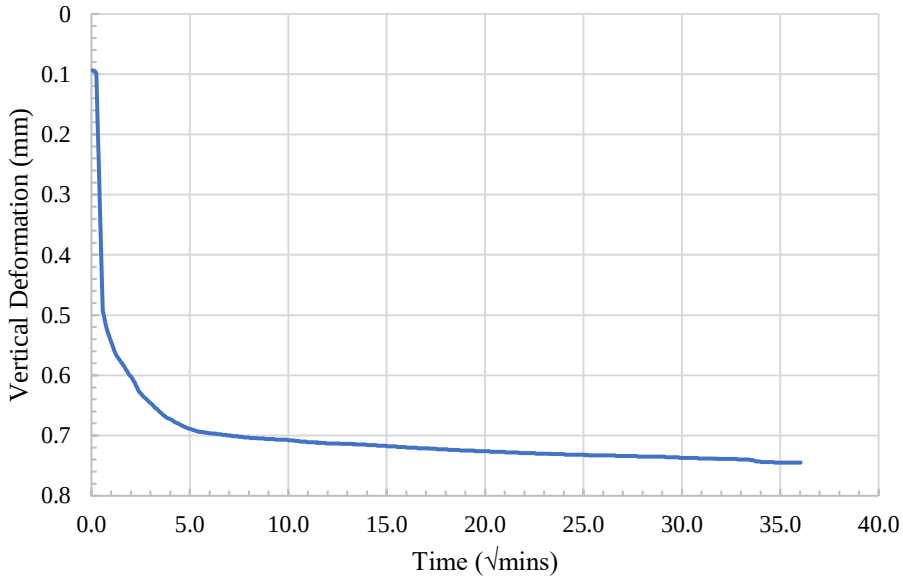

Figure 190: Consolidation Plot for Paved Shoulders (B4.5) Stress Level #1

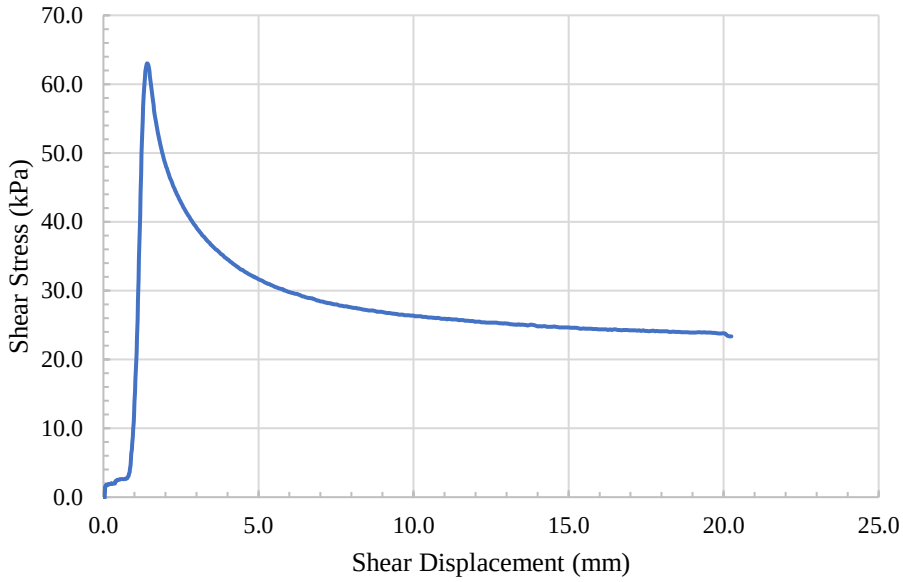

Figure 191: Shear Stress versus Shear Displacement for Paved Shoulders (B4.5) Stress Level #1

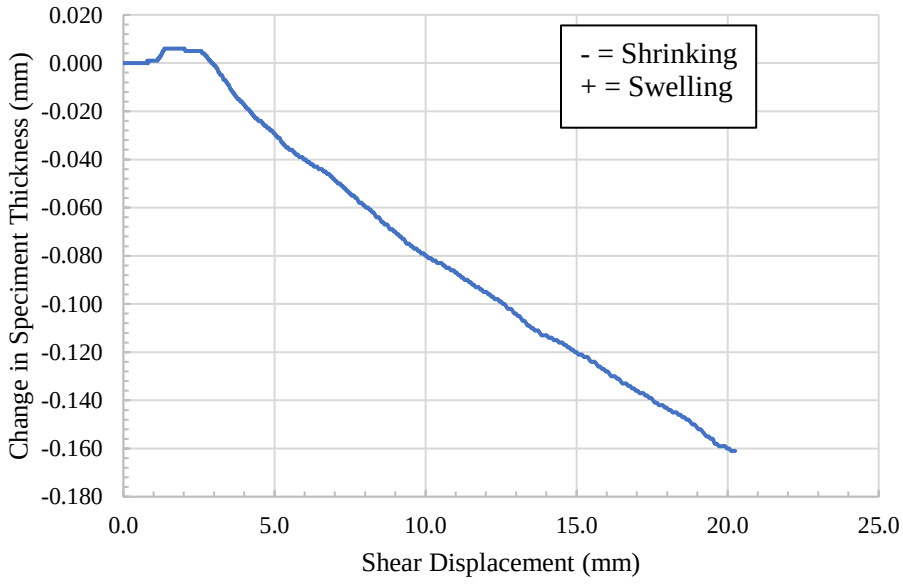

Figure 192: Change in Specimen Thickness versus Shear Displacement for Paved Shoulders (B4.5) Stress Level #1

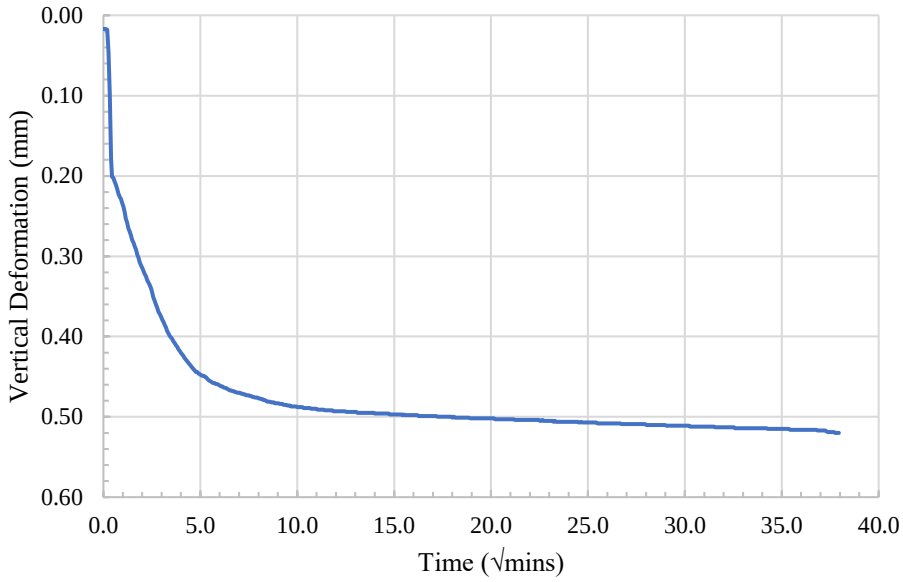

Figure 193: Consolidation Plot for Paved Shoulders (B4.5) Stress Level #2

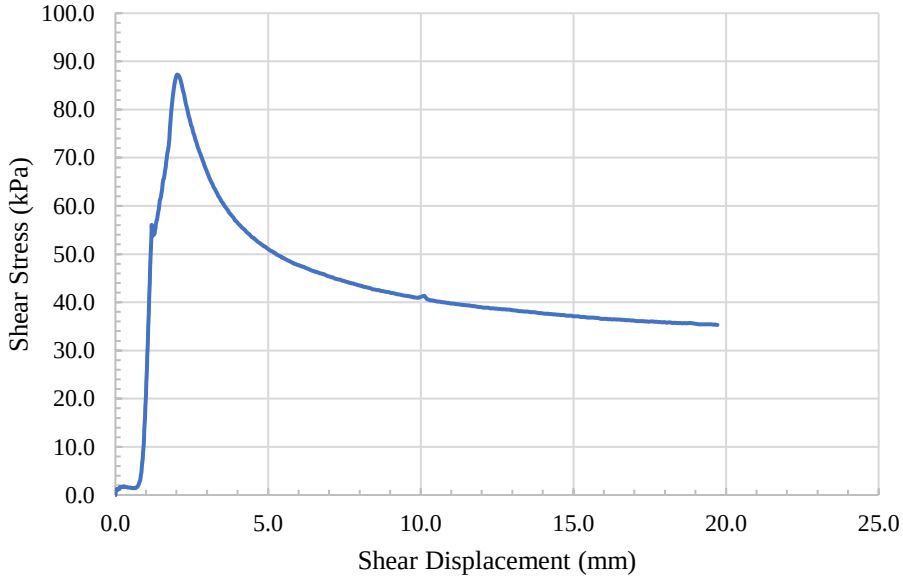

Figure 194: Shear Stress versus Shear Displacement for Paved Shoulders (B4.5) Stress Level #2

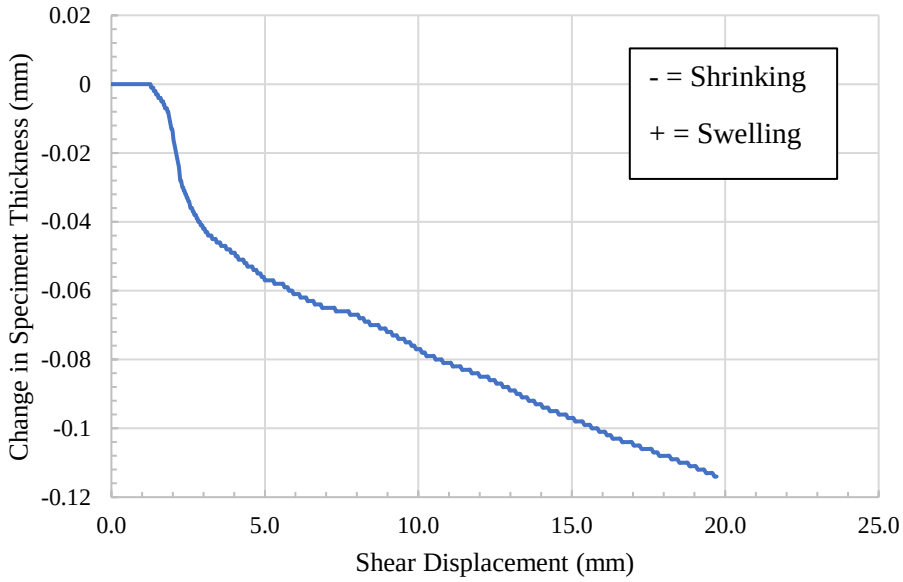

Figure 195: Change in Specimen Thickness versus Shear Displacement for Paved Shoulders (B4.5) Stress Level #2

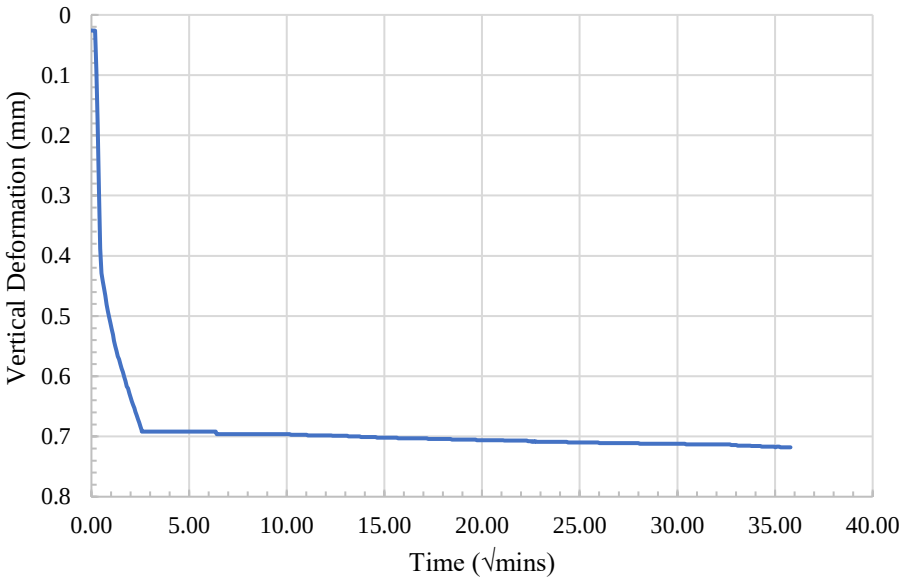

Figure 196: Consolidation Plot for Paved Shoulders (B4.5) Stress Level #3

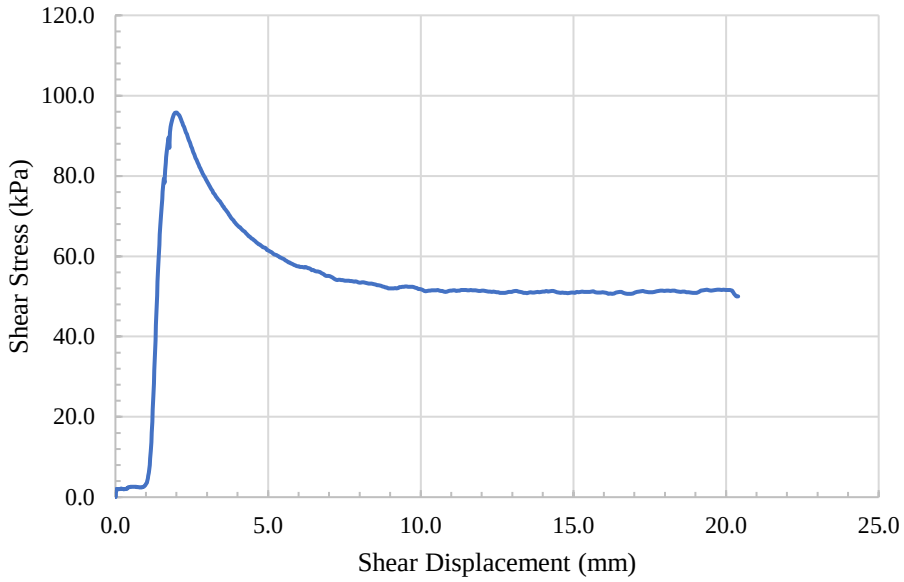

Figure 197: Shear Stress versus Shear Displacement for Paved Shoulders (B4.5) Stress Level #3

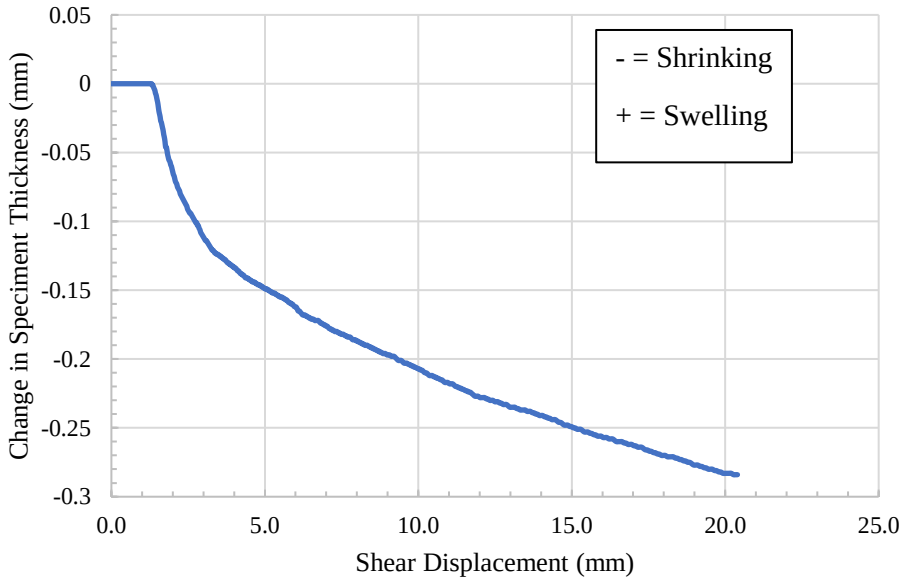

Figure 198: Change in Specimen Thickness versus Shear Displacement for Paved Shoulders (B4.5) Stress Level #3

Edge Drains

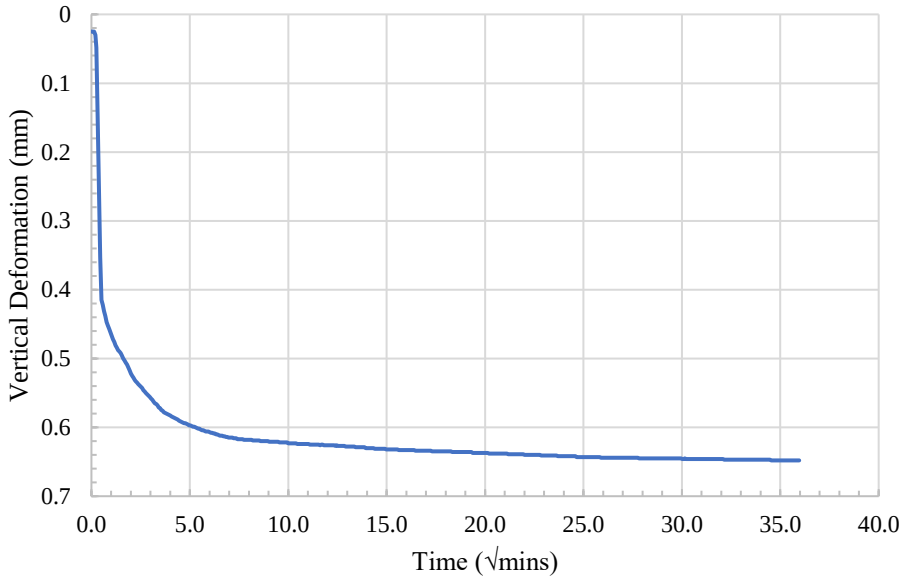

Figure 199: Consolidation Plot for Edge Drains (B5.5) Stress Level #1

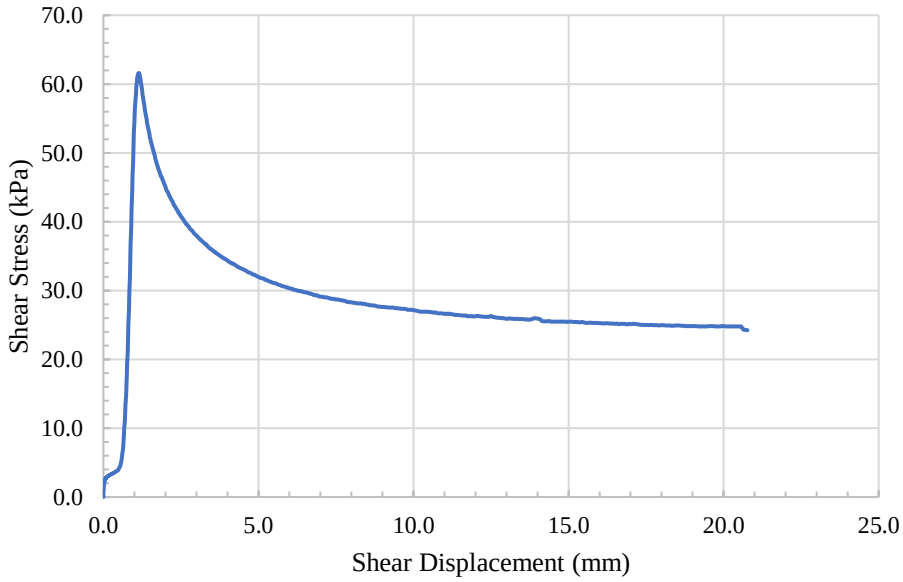

Figure 200: Shear Stress versus Shear Displacement for Edge Drains (B5.5) Stress Level #1

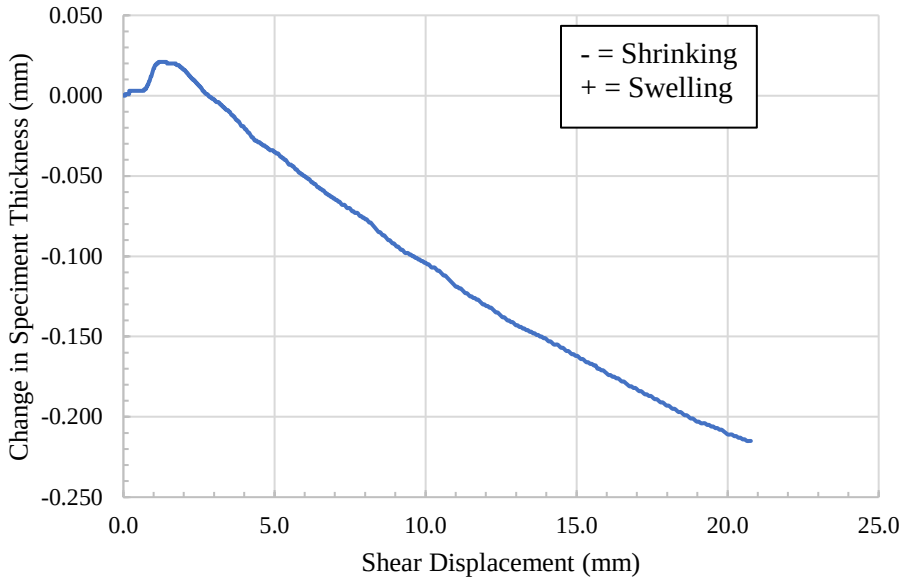

Figure 201: Change in Specimen Thickness versus Shear Displacement for Edge Drains (B5.5) Stress Level #1

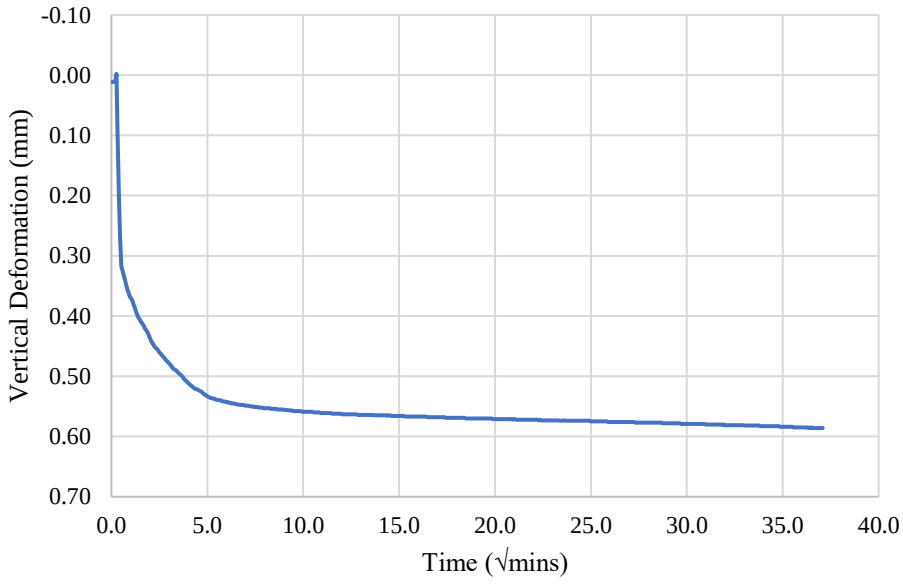

Figure 202: Consolidation Plot for Edge Drains (B5.5) Stress Level #2

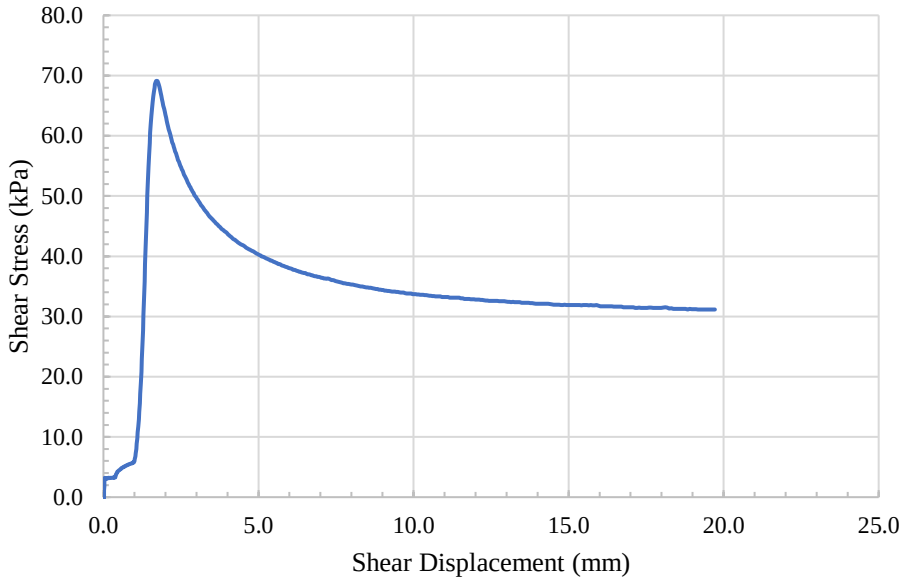

Figure 203: Shear Stress versus Shear Displacement for Edge Drains (B5.5) Stress Level #2

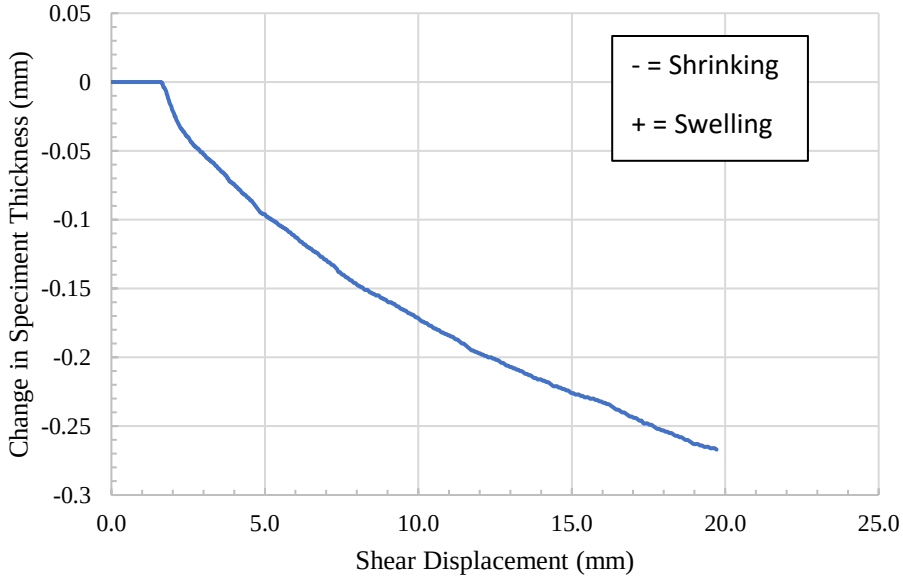

Figure 204: Change in Specimen Thickness versus Shear Displacement for Edge Drains (B5.5) Stress Level #2

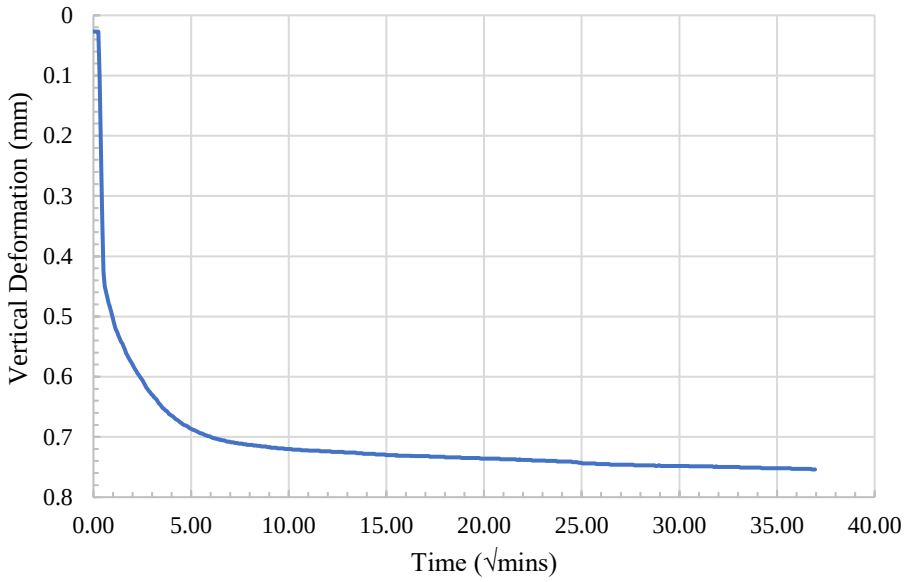

Figure 205: Consolidation Plot for Edge Drains (B5.5) Stress Level #3

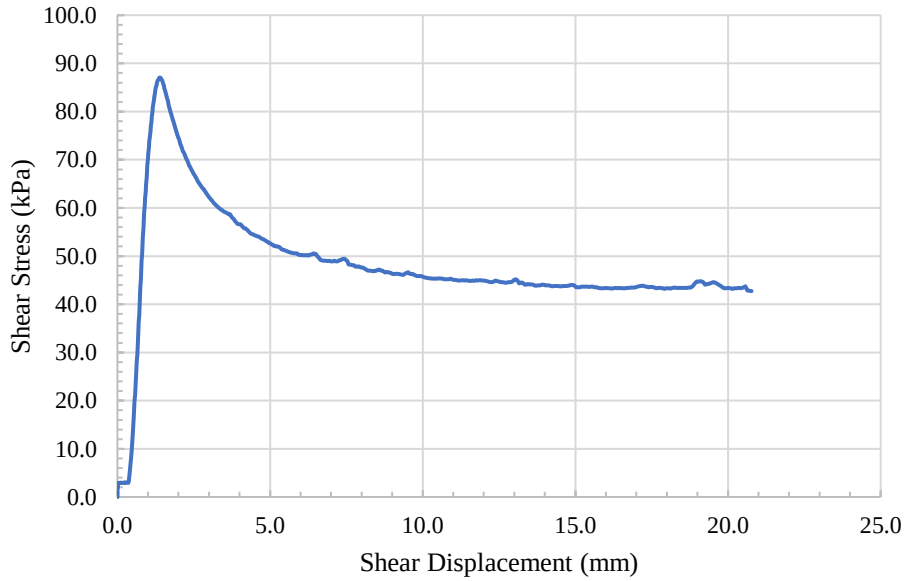

Figure 206: Shear Stress versus Shear Displacement for Edge Drains (B5.5) Stress Level #3

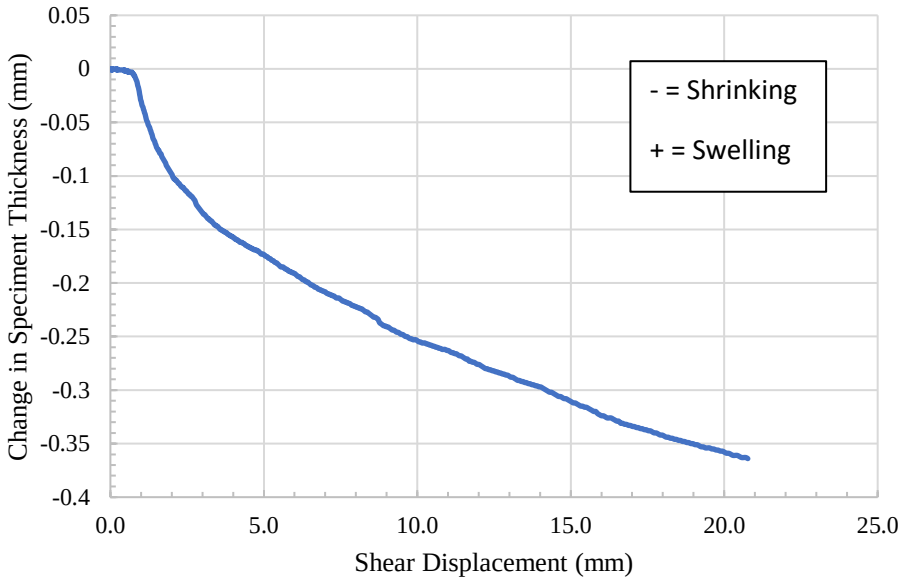

Figure 207: Change in Specimen Thickness versus Shear Displacement for Edge Drains (B5.5) Stress Level #3

Control

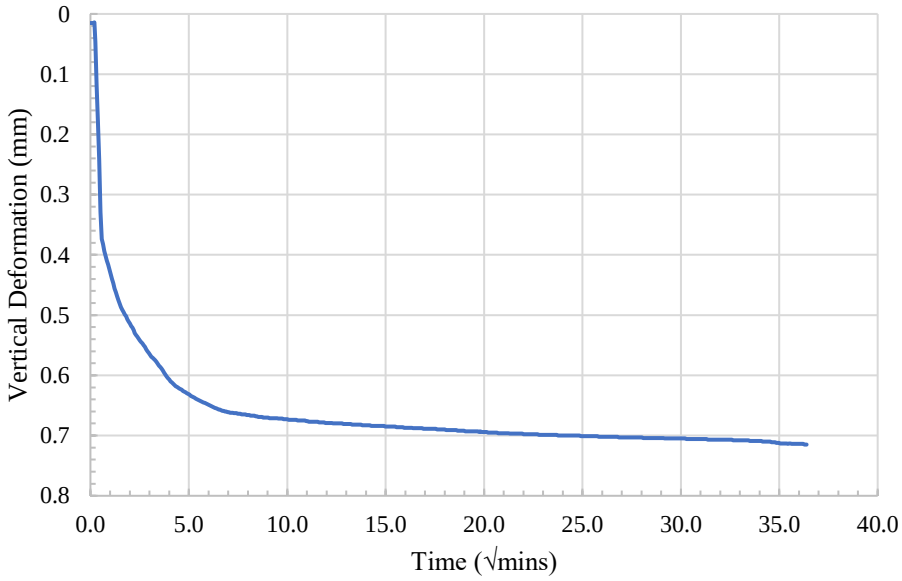

Figure 208: Consolidation Plot for Control Stress Level #1

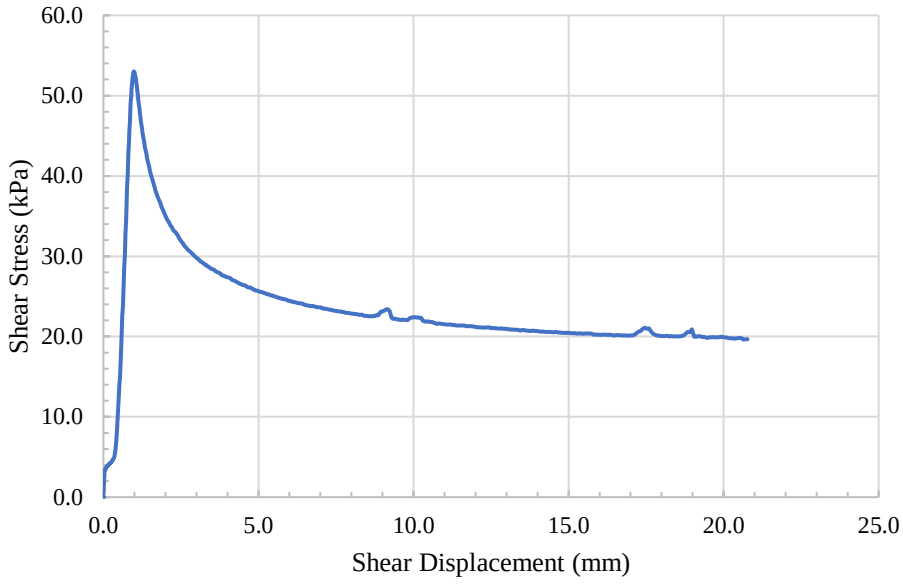

Figure 209: Shear Stress versus Shear Displacement for Control Stress Level #1

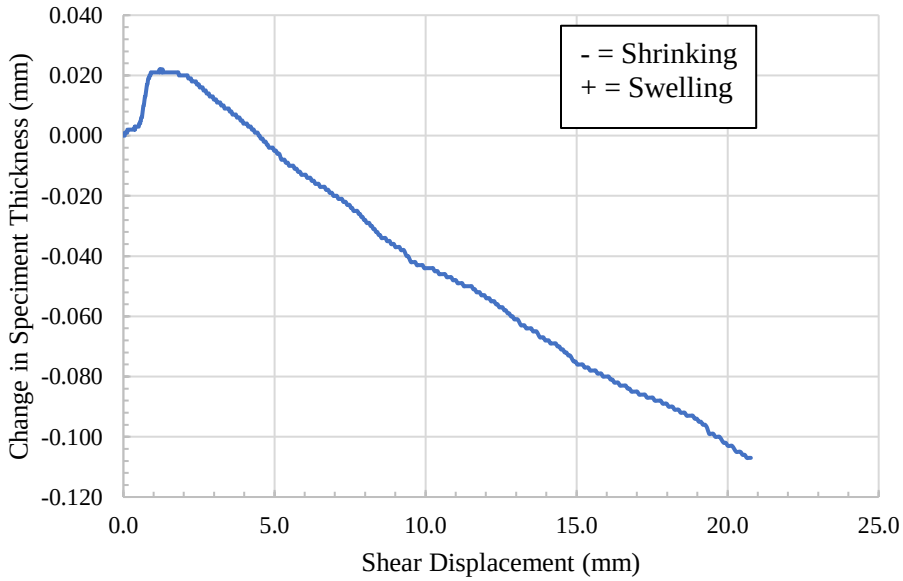

Figure 210: Change in Specimen Thickness versus Shear Displacement for Control Stress Level #1

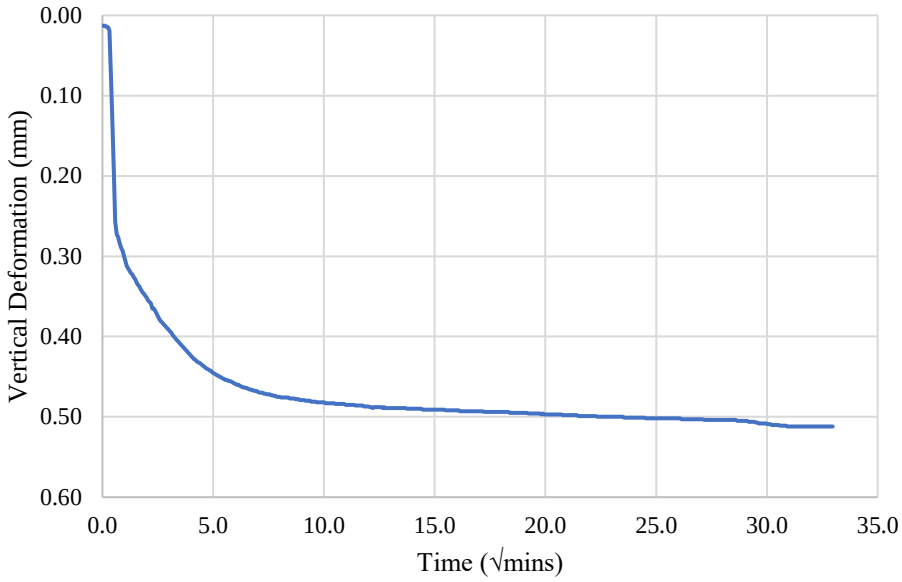

Figure 211: Consolidation Plot for Control Stress Level #2

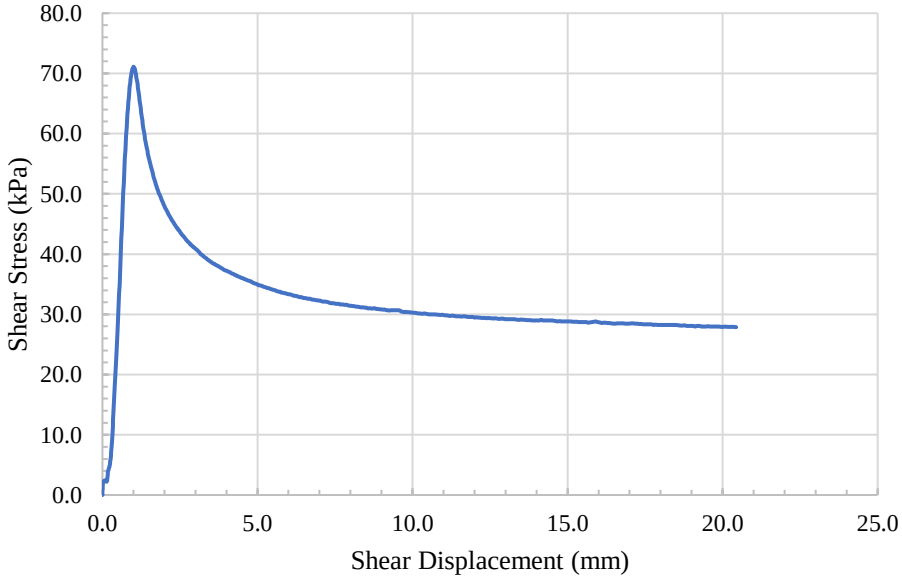

Figure 212: Shear Stress versus Shear Displacement for Control Stress Level #2

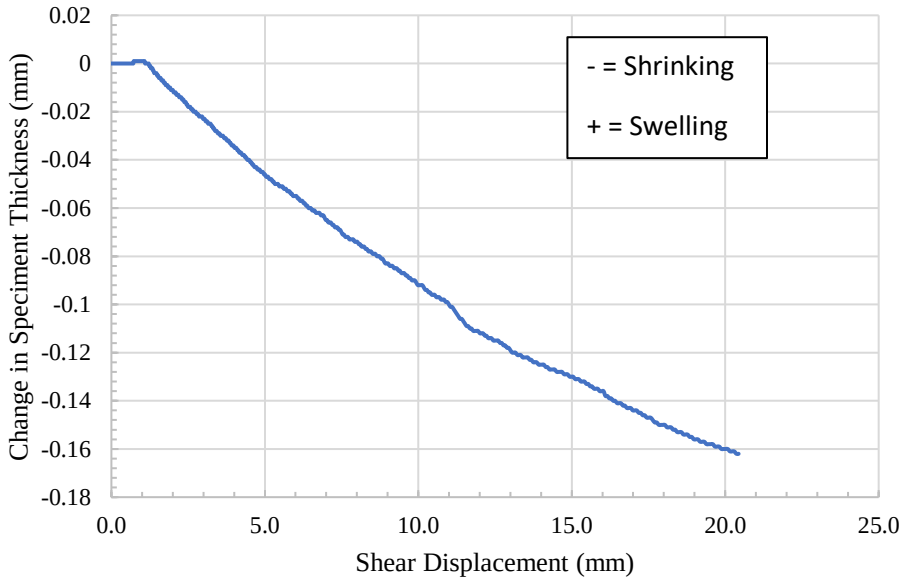

Figure 213: Change in Specimen Thickness versus Shear Displacement for Control Stress Level #2

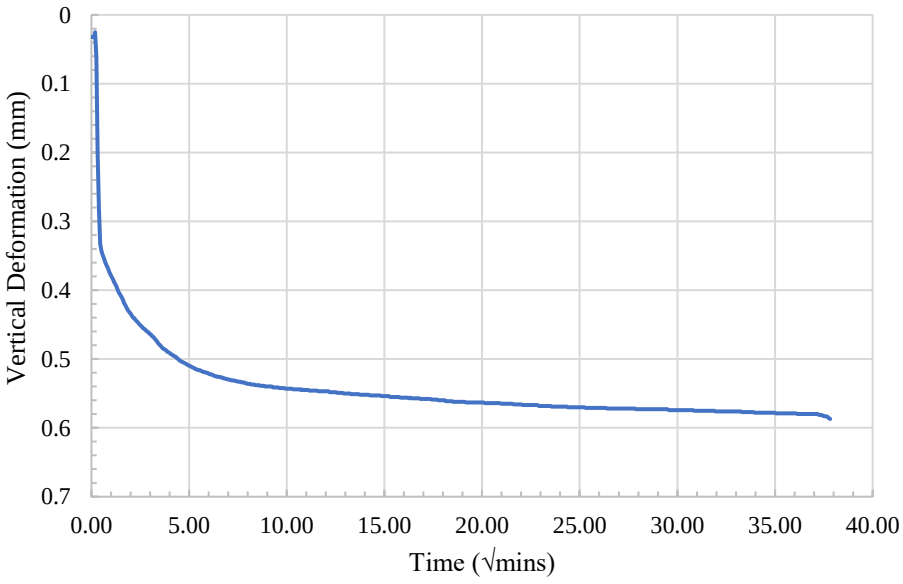

Figure 214: Consolidation Plot for Control Stress Level #3

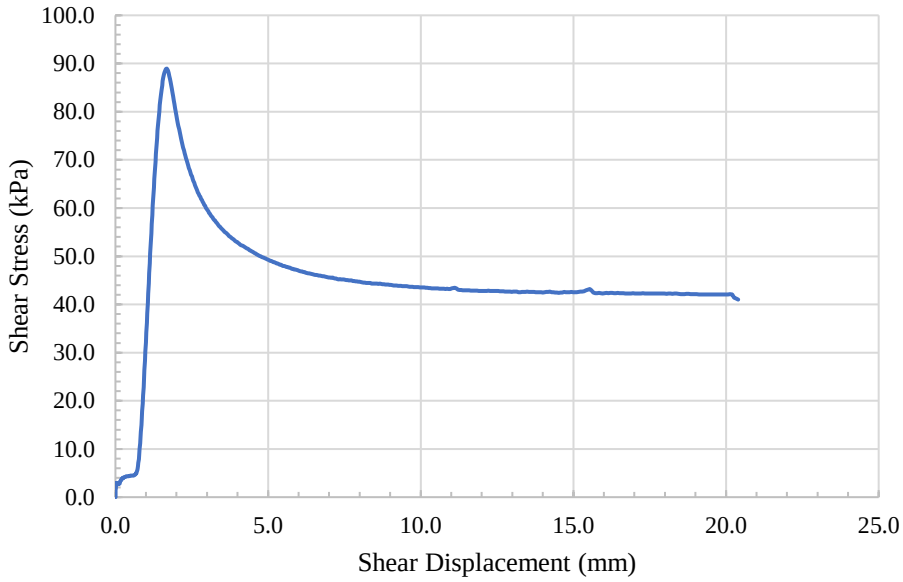

Figure 215: Shear Stress versus Shear Displacement for Control Stress Level #3

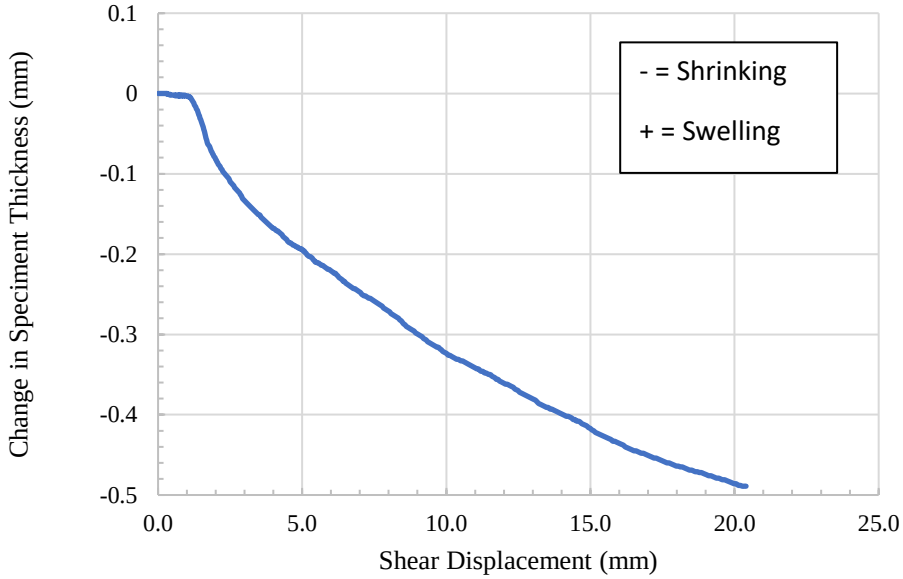

Figure 216: Change in Specimen Thickness versus Shear Displacement for Control Stress Level #3

APPENDIX C: LABORATORY PHOTOS

Sand Blanket

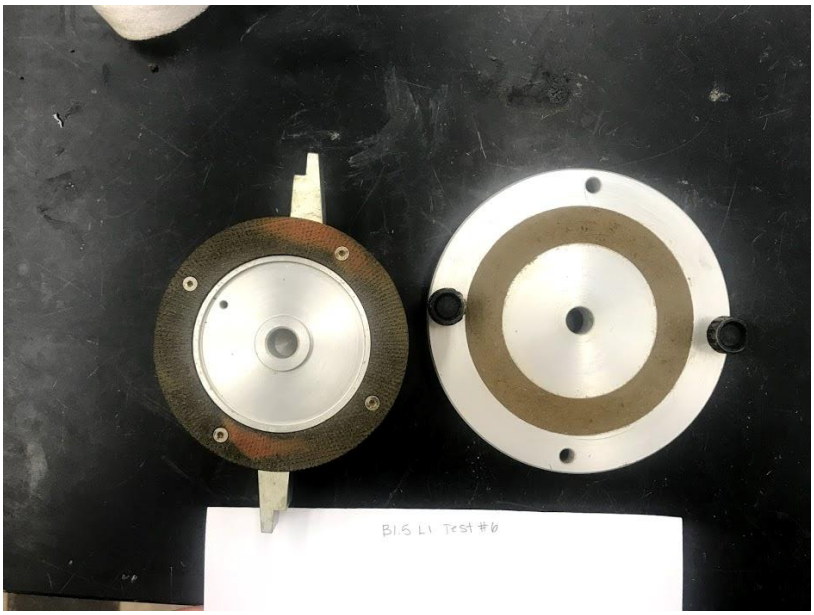

Figure 217: Stress Level #2 Specimen for Sand Blanket (B1.5)

Figure 218: Stress Level #2 Specimen After Shearing for Sand Blanket (B1.5)

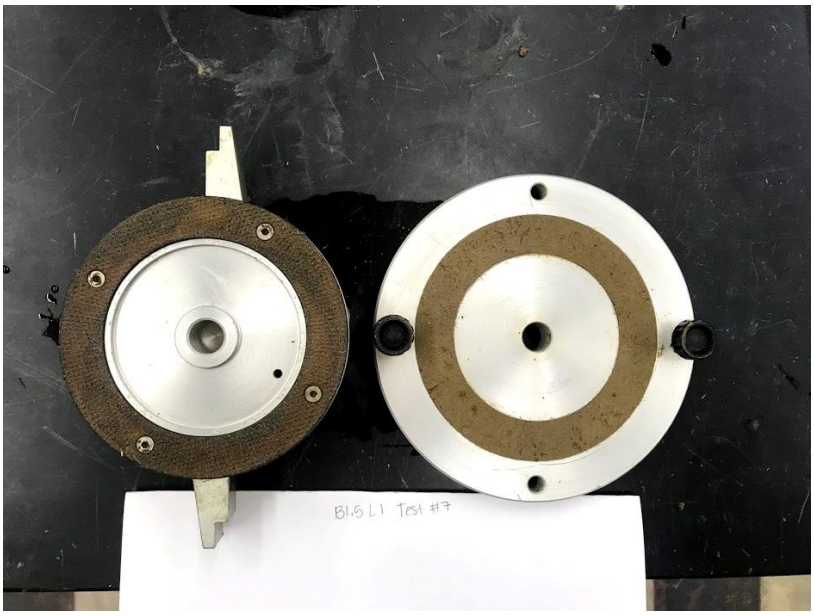

Figure 219: Stress Level #3 Specimen for Sand Blanket (B1.5)

Figure 220: Stress Level #3 Specimen After Shearing for Sand Blanket (B1.5)

Vertical Barriers

Figure 221: Stress Level #1 Specimen for Vertical Barriers (B2.5)

Figure 222: Stress Level #1 Specimen After Shearing for Vertical Barriers (B2.5)

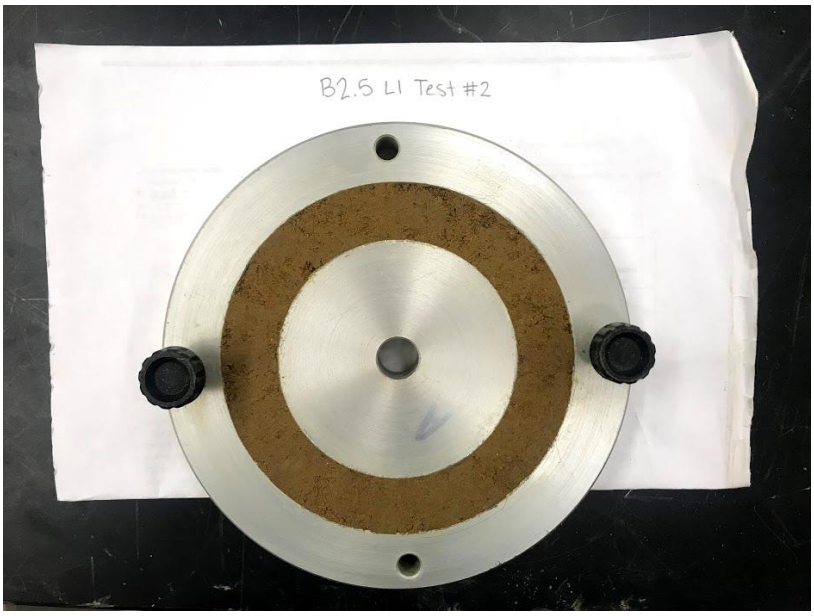

Figure 223: Stress Level #2 Specimen for Vertical Barriers (B2.5)

Figure 224: Stress Level #2 Specimen After Shearing for Vertical Barriers (B2.5)

Figure 225: Stress Level #3 Specimen for Vertical Barriers (B2.5)

Figure 226: Stress Level #3 Specimen After Shearing for Vertical Barriers (B2.5)

Lime Columns

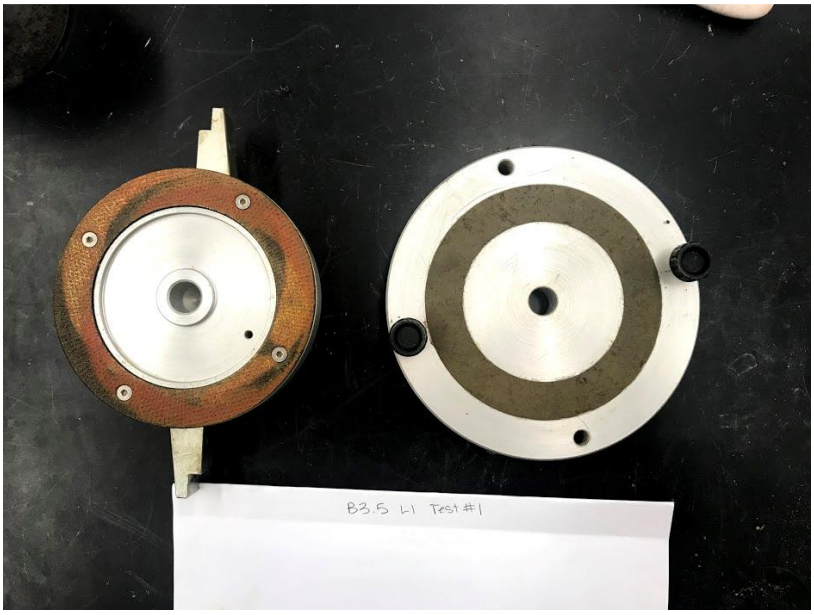

Figure 227: Stress Level #1 Specimen for Lime Columns (B3.5)

Figure 228: Stress Level #1 Specimen After Shearing for Lime Columns (B3.5)

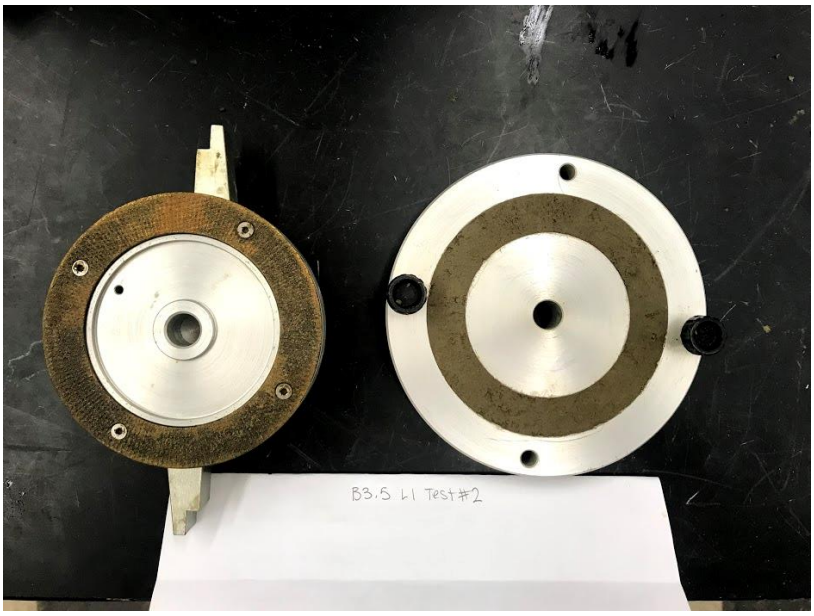

Figure 229: Stress Level #2 Specimen for Lime Columns (B3.5)

Figure 230: Stress Level #2 Specimen After Shearing for Lime Columns (B3.5)

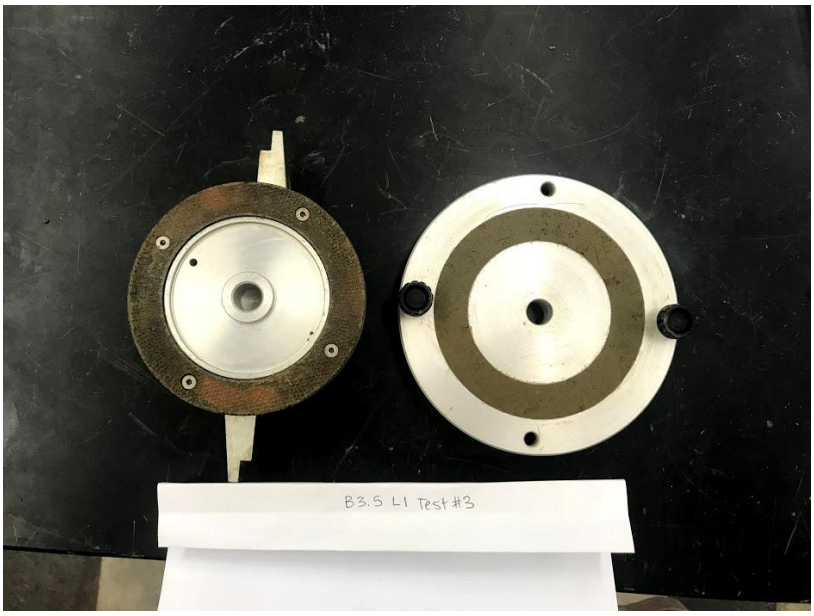

Figure 231: Stress Level #3 Specimen for Lime Columns (B3.5)

Figure 232: Stress Level #3 Specimen After Shearing for Lime Columns (B3.5)

Paved Shoulders

Figure 233: Stress Level #1 Specimen for Paved Shoulders (B4.5)

Figure 234: Stress Level #1 Specimen After Shearing for Paved Shoulders (B4.5)

Figure 235: Stress Level #2 Specimen for Paved Shoulders (B4.5)

Figure 236: Stress Level #2 Specimen After Shearing for Paved Shoulders (B4.5)

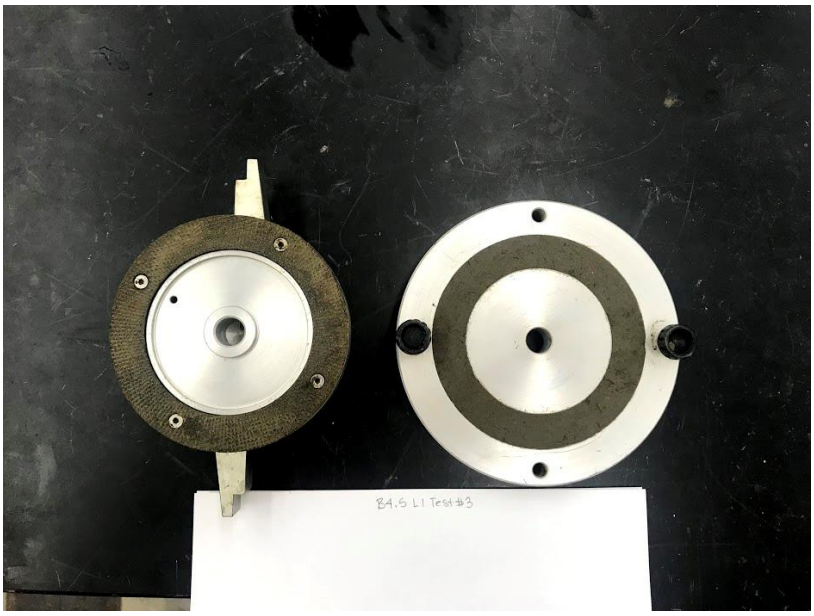

Figure 237: Stress Level #3 Specimen for Paved Shoulders (B4.5)

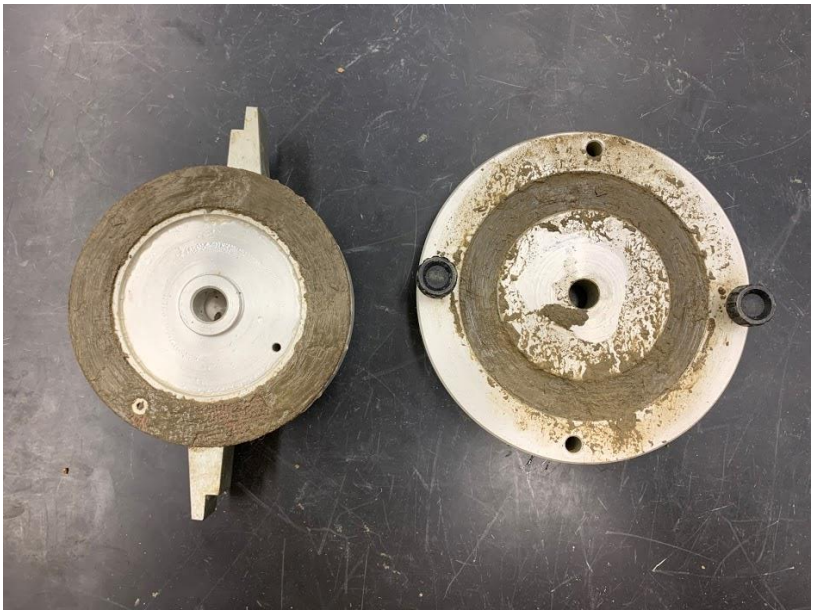

Figure 238: Stress Level #3 Specimen After Shearing for Paved Shoulders (B4.5)

Edge Drains

Figure 239: Stress Level #1 Specimen for Edge Drains (B5.5)

Figure 240: Stress Level #1 Specimen After Shearing for Edge Drains (B5.5)

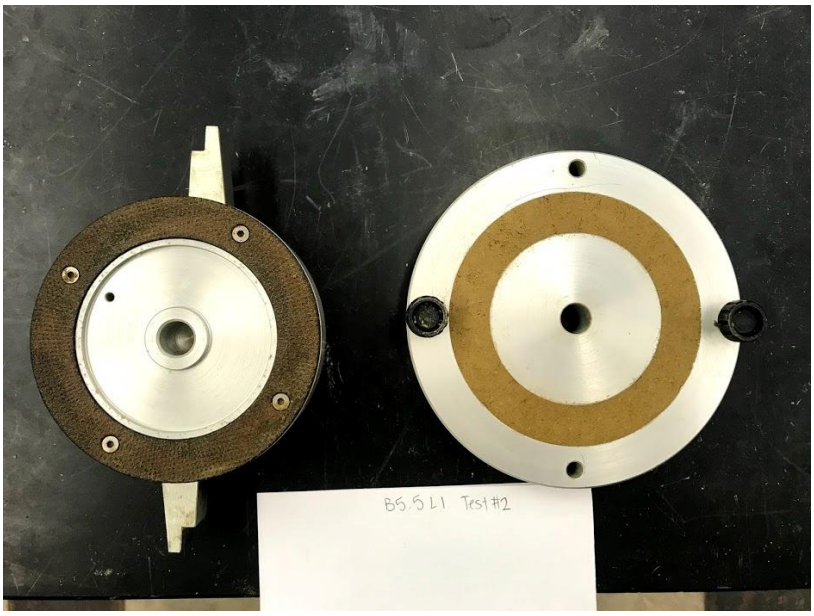

Figure 241: Stress Level #2 Specimen for Edge Drains (B5.5)

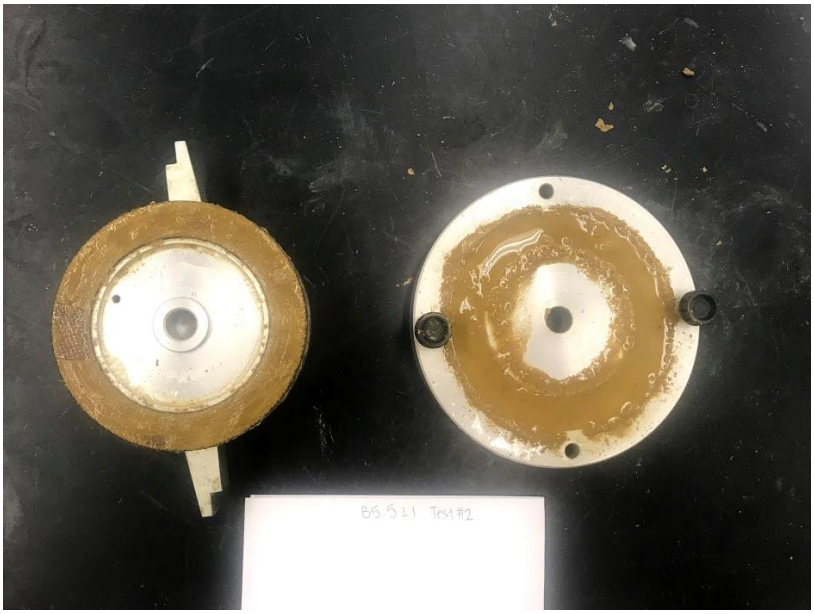

Figure 242: Stress Level #2 Specimen After Shearing for Edge Drains (B5.5)

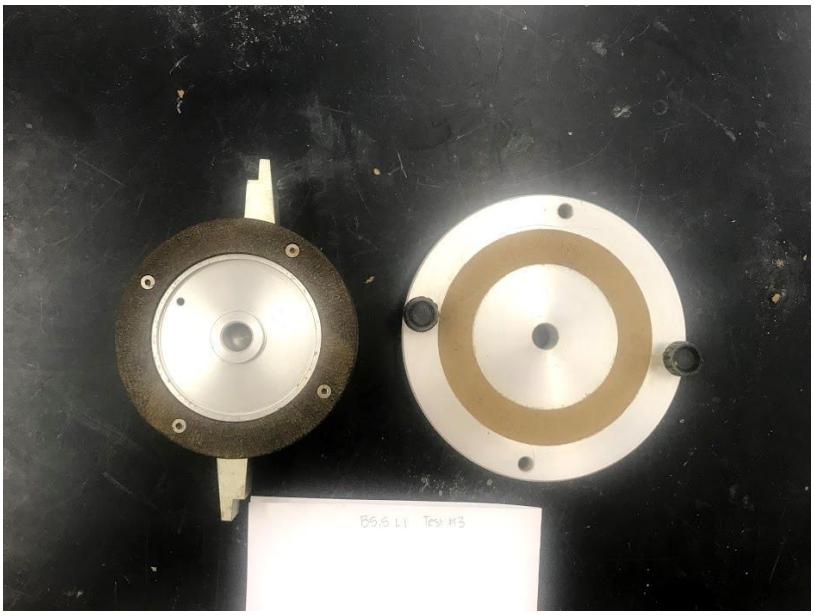

Figure 243: Stress Level #3 Specimen for Edge Drains (B5.5)

Figure 244: Stress Level #3 Specimen After Shearing for Edge Drains (B5.5)

Control

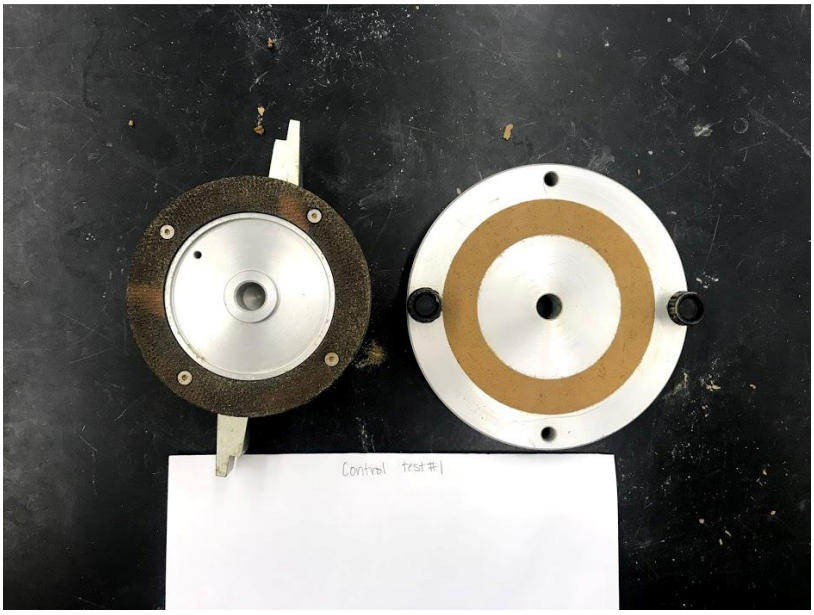

Figure 245: Stress Level #1 Specimen for Control

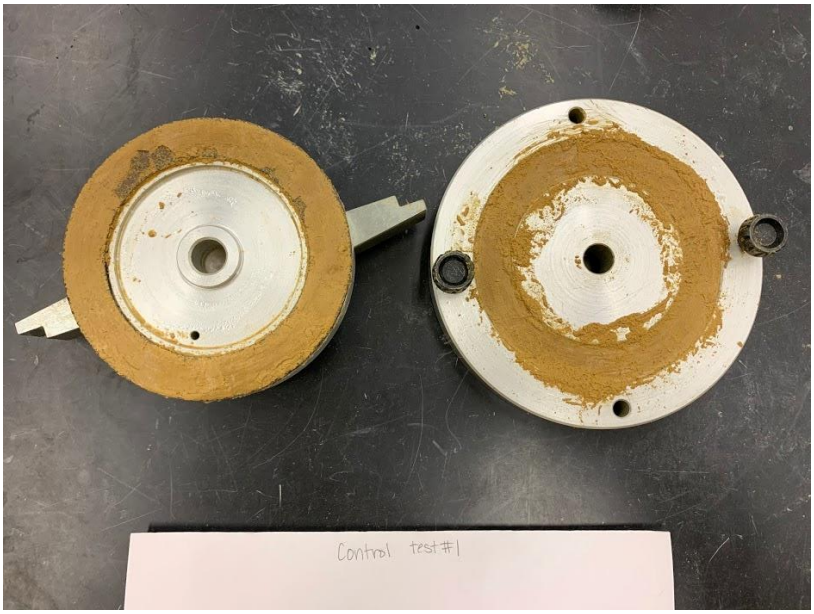

Figure 246: Stress Level #1 Specimen After Shearing for Control

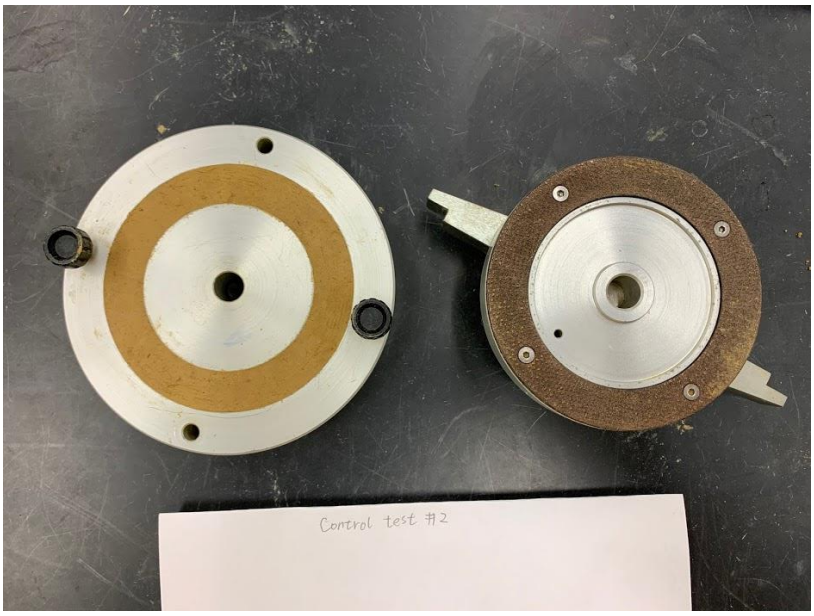

Figure 247: Stress Level #2 Specimen for Control

Figure 248: Stress Level #2 Specimen After Shearing for Control

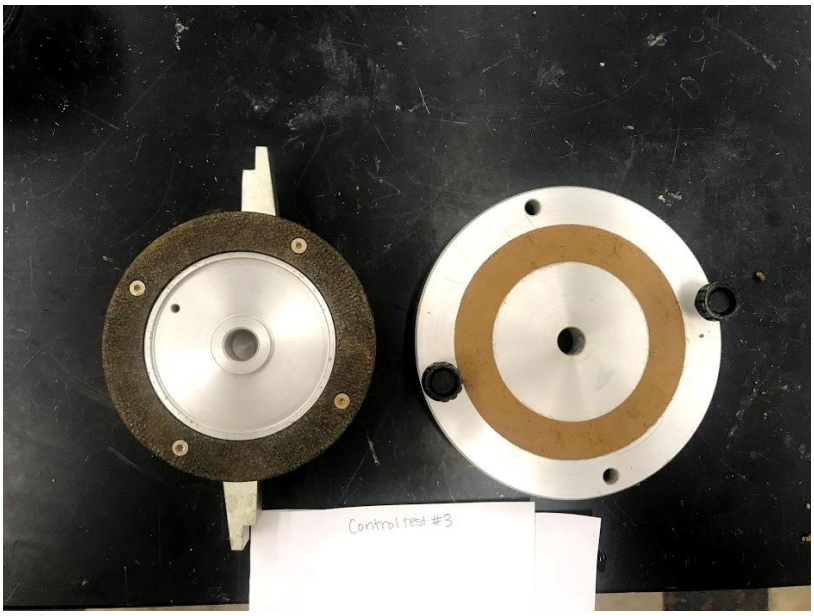

Figure 249: Stress Level #3 Specimen for Control

Figure 250: Stress Level #3 Specimen After Shearing for Control